Florida International University
FIU Digital Commons

FIU Electronic Theses and Dissertations | University Graduate School

7-16-2008

Development of Surface Flaw Thresholds for Pre-Cured Fiber Reinforced Polymer and Groove Size Tolerance for Near Surface Mounted Fiber Reinforced Polymer Retrofit Systems

Ahmet Serhat Kalayci
Florida International University

DOI: 10.25148/etd.FI08121907
Follow this and additional works at: https://digitalcommons.fiu.edu/etd

Recommended Citation
Kalayci, Ahmet Serhat, "Development of Surface Flaw Thresholds for Pre-Cured Fiber Reinforced Polymer and Groove Size Tolerance for Near Surface Mounted Fiber Reinforced Polymer Retrofit Systems" (2008). *FIU Electronic Theses and Dissertations*. 21.
https://digitalcommons.fiu.edu/etd/21

This work is brought to you for free and open access by the University Graduate School at FIU Digital Commons. It has been accepted for inclusion in FIU Electronic Theses and Dissertations by an authorized administrator of FIU Digital Commons. For more information, please contact dcc@fiu.edu.

FLORIDA INTERNATIONAL UNIVERSITY

Miami, Florida

DEVELOPMENT OF SURFACE FLAW THRESHOLDS FOR PRE-CURED FIBER REINFORCED POLYMER AND GROOVE SIZE TOLERANCE FOR NEAR SURFACE MOUNTED FIBER REINFORCED POLYMER RETROFIT SYSTEMS

A dissertation submitted in partial fulfillment of the

requirements for the degree of

DOCTOR OF PHILOSOPHY

in

CIVIL ENGINEERING

by

Ahmet Serhat Kalayci

2008

To: Interim Dean Amir Mirmiran
College of Engineering and Computing

This dissertation, written by Ahmet Serhat Kalayci, and entitled Development of Surface Flaw Thresholds for Pre-Cured Fiber Reinforced Polymer and Groove Size Tolerance for Near Surface Mounted Fiber Reinforced Polymer Retrofit Systems, having been approved in respect to style and intellectual content, is referred to you for judgment.

We have read this dissertation and recommend that it be approved.

Ton-Lo Wang

Nakin Suksawang

Zhenmin Chen

Amir Mirmiran, Major Professor

Date of Defense: July 16, 2008

The dissertation of Ahmet Serhat Kalayci is approved.

Interim Dean Amir Mirmiran
College of Engineering and Computing

Dean George Walker
University Graduate School

Florida International University, 2008

© Copyright 2008 by Ahmet Serhat Kalayci

All rights reserved.

DEDICATION

I dedicate this dissertation to my family.

ACKNOWLEDGMENTS

I would like thank to the American Association of State Highway and Transportation Officials in cooperation with the Federal Highway Administration and the Transportation Research Board of the National Research Council for sponsoring the project NCHRP 10-59.

I am grateful to Dr. Amir Mirmiran, Interim Dean of College of Engineering and Computing of the Florida International University for his support and guidance throughout my studies.

I would like to recognize and thank Dr. Ton-Lo Wang, Dr. Nakin Suksawang and Dr. Zhenmin Chen for serving on my advisory committee.

I would like to thank to Dr. Baris Yalim together with all the personnel and graduate students at the Florida International University Structures and Construction Laboratory.

Finally at last but not the least, I would like to thank to my family in Turkey, for their endless support and encouragement.

ABSTRACT OF THE DISSERTATION

DEVELOPMENT OF SURFACE FLAW THRESHOLDS FOR PRE-CURED FIBER REINFORCED POLYMER AND GROOVE SIZE TOLERANCE FOR NEAR SURFACE MOUNTED FIBER REINFORCED POLYMER RETROFIT SYSTEMS

by

Ahmet Serhat Kalayci

Florida International University, 2008

Miami, Florida

Professor Amir Mirmiran, Major Professor

Since the introduction of fiber reinforced polymers (FRP) for the repair and retrofit of concrete structures in the 1980's, considerable research has been devoted to the feasibility of their application and predictive modeling of their performance. However, the effects of flaws present in the constitutive components and the practices in substrate preparation and treatment have not yet been thoroughly studied.

This research aims at investigating the effect of surface preparation and treatment for the pre-cured FRP systems and the groove size tolerance for near surface mounted (NSM) FRP systems; and to set thresholds for guaranteed system performance. This study was conducted as part of the National Cooperative Highway Research Program (NCHRP) Project 10-59B to develop construction specifications and process control manual for repair and retrofit of concrete structures using bonded FRP systems.

The research included both analytical and experimental components. The experimental program for the pre-cured FRP systems consisted of a total of twenty-four (24) reinforced concrete (RC) T-beams with various surface preparation parameters and surface flaws,

including roughness, flatness, voids and cracks (cuts). For the NSM FRP systems, a total of twelve (12) additional RC T-beams were tested with different grooves sizes for FRP bars and strips. The analytical program included developing an elaborate nonlinear finite element model using the general purpose software ANSYS. The bond interface between FRP and concrete was modeled by a series of nonlinear springs. The model was validated against test data from the present study as well as those available from the literature. The model was subsequently used to extend the experimental range of parameters for surface flatness in pre-cured FRP systems and for groove size study in the NSM FRP systems.

Test results, confirmed by further analyses, indicated that contrary to the general belief in the industry, the impact of surface roughness on the global performance of pre-cured FRP systems was negligible. The study also verified that threshold limits set for wet lay-up FRP systems can be extended to pre-cured systems. The study showed that larger surface voids and cracks (cuts) can adversely impact both the strength and ductility of pre-cured FRP systems. On the other hand, frequency (or spacing) of surface cracks (cuts) may only affect system ductility rather than its strength. Finally, within the range studied, groove size tolerance of $\pm$1/8 in. does not appear to have an adverse effect on the performance of NSM FRP systems.

TABLE OF CONTENTS

LIST OF TABLES

TABLE PAGE

LIST OF FIGURES

FIGURE PAGE

CHAPTER 1

INTRODUCTION

1.1 General

Aged and deteriorated infrastructure around the world requires rapid and economical means of repair and retrofitting. Traditional repair and retrofitting techniques such as concrete or steel jacketing of columns and section restoration are often costly and time consuming as the operation of the retrofitted structure often needs to be shut down during the procedure. However, the introduction of fiber reinforced polymers (FRP) into the construction industry in the last two decades has helped engineers to overcome such problems. Retrofitting concrete structures with FRP composites is rapid and efficient. In addition to handling and installation advantages, FRP materials are light, strong, stiff and resistant to aggressive environment, as compared to steel.

FRPs are composite materials made of reinforcing fibers bundled in a polymer matrix. The role of the matrix is to distribute the stresses among the fibers and to protect the fibers from environmental and mechanical factors (ACI 440R 1996). Carbon, glass or aramid are the most commonly used fibers. According to the fiber type used, these materials are named as CFRP (carbon fibers), GFRP (glass fibers) and AFRP (aramid fibers). Fibers are generally unidirectionally or bi-directionally oriented in the polymer matrix. The strength of the FRP composites basically depends on the volume fraction of the fibers. Higher fiber volumes result in higher strengths. Typical dry fiber properties are shown in Table 1.1. Epoxy resins and pastes are often used to bond the FRP materials to

the reinforced concrete members. Generally being superior to steel from the durability point of view, there are several factors that affect the mechanical properties of the composites: fire and ultraviolet radiation. Both factors tend to damage the resin and degrade the properties of FRP.

Table 1.1 Typical Dry Fiber Properties (TR -55 2004)

Fiber	Tensile strength (ksi)	Modulus of Elasticity (ksi)	Elongation (%)
Carbon: high strength	624 - 711	33,359 - 34,810	1.9 - 2.1
Carbon: high modulus	397 - 796	42,641 - 47,717	0.7 - 1.9
Carbon: ultra high modulus	377 - 583	78,320 - 92,824	0.4 - 0.8
Aramid: high strength and high modulus	464 - 522	17,985 - 18,855	2.4
Glass	348 - 508	10,153 - 12,328	3.5 - 4.7

FRP applications used for structural retrofitting are in the form of either externally bonded (EB) or near-surface mounted (NSM) systems. EB systems can be wet lay-up sheets or pre-cured laminates. Wet lay-up systems consists of dry FRP fabrics of unidirectional or bidirectional fibers; wetted, bonded and cured in place using epoxy resin. Pre-cured systems, on the other hand, are previously cured strips or laminates; where epoxy is used only for their bonding onto the structural member. Due to the fabrication process of the pre-cured laminates, a very high proportion of fibers can be incorporated in the cross section resulting in less number of plies as compared to the wet lay-up systems. However, the amount of fiber is often lower in the transverse direction due to fabrication issues. NSM systems consist of bars or strips placed inside a groove made in a concrete member, which is then filled with epoxy paste.

As mentioned in TR-55 (2004), pre-cured laminates are more commonly used because of the following advantages:

1. Minor unevenness on the substrate surface can be easily bridged by the proper use of the adhesive epoxy;
2. Less surface preparation is required;
3. Installation is easer; and
4. Less material is generally needed..

On the other hand, wet lay-up systems are more advantageous when:

1. Substrate material is of low quality;
2. Special anchorage configurations are needed, as fabrics can be easily cut into the desired shape;
3. Strengthening is needed around a corner; or
4. The materials need to be transported to a distant site.

NSM systems are preferred when:

1. The strengthened surface is susceptible to traffic;
2. Substrate surface is uneven and of poor quality; or
3. Structure needs to be strengthened in the negative moment region.

There is considerable amount of research completed or is in progress in on the structural retrofitting with FRPs. Most of the early studies in the field has focused on the feasibility of various strengthening techniques with composites. Scientific community and industry both have gradually welcomed the introduction of the new materials, making FRP retrofitting now a common practice. Recent studies, however have focused more on the investigation of geometric and material properties and modeling issues, such as development lengths, bond issues and failure modes.

Long-term performance of FRP-strengthened systems depends not only on the material characteristics of the components, but also on the construction process. There is a lack of generally accepted construction specifications and standard procedures to ensure quality control. The users often depend solely on the information supplied by the manufacturers. With the growing use of FRP composites in the construction industry, the need for specifications and quality control of the constituent materials and the construction processes has become extremely crucial.

This study included an experimental program as part of the research sponsored by the American Association of State Highway and Transportation Officials (AASHTO) in cooperation with Federal Highway Administration (FHWA). The work has was conducted as part of the National Cooperative Highway Research Program (NCHRP) Project 10-59, which is administered by the Transportation Research Board (TRB) of the National Research Council (NRC).

Within the scope of the first phase of the NCHRP Project 10-59, upon review of the current construction practices, research findings and technical literature and manufacturer data, "NCHRP REPORT 514: Bonded Repair and Retrofit of Concrete Structures Using FRP Composites – Recommended Construction Specifications and Process Control Manual" was published in 2004. The second phase of the project consisted of the development of thresholds for surface irregularities and crack widths for FRP bonded concrete structures. This phase resulted in "NCHRP Report 609: Recommended Construction Specifications and Process Control Manual for Repair and Retrofit of Concrete Structures Using Bonded FRP Composites" which was published in 2008. The work in second phase was subdivided into two parts; tests related to EB wet

lay-up systems and EB pre-cured systems. Tests related to EB wet lay-up systems became part of the dissertation by Yalim (2008).

The second part of this phase, which forms the basis for this dissertation consists of the tests related to the EB pre-cured FRP reinforcement, for which surface roughness, flatness, voids and cracks (cuts) were investigated. For the NSM FRP systems, main research interest was the effect of groove size tolerance.

In addition to the experimental program, a thorough analytical study was conducted for both the pre-cured and the NSM FRP systems in order to address the effect of important parameters on the performance of such systems.

1.2 Objectives and Scope

The primary objective of this study was to develop tolerances and thresholds for repair and strengthening of concrete structures using composites focusing mainly on pre-cured and NSM FRP systems. Secondary objective was to assess the impact of various geometric and physical parameters. Research objectives for this study can be listed as follows:

1. Determine the optimum surface roughness profile; and thresholds of voids and bug holes on concrete surface, surface cracks (cuts) and surface out-of-flatness for the EB pre-cured FRP systems.
2. Determine the effect of groove size tolerance on NSM FRP repair and strengthening systems; and
3. Determine the effects of other geometric and material parameters on the behavior of pre-cured and NSM systems.

1.3 Organization of the Dissertation

Body of this dissertation is composed of four chapters, including this introductory chapter. Chapter 2 is dedicated to past studies. Available research on the historical development of the strengthening technique, analytical models for strength prediction and bond issues are presented both for the pre-cured and the NSM FRP systems. In addition previous studies related to the effect of surface flaws on the pre-cured systems and the effect of groove size tolerance on the NSM FRP systems are discussed.

Chapter 3 presents the experimental program conducted within the scope of this dissertation. Test specimens, program and setup are explained in detail. Load-deflection and load-strain plots as well as summary test data including peak responses for individual test specimens are provided.

Analytical studies are summarized in Chapter 4. ANSYS Finite Element (FE) software was used for modeling.

Chapter 5 contains a summary of the experimental program and the analytical work. Based on the findings from the experimental and analytical work, conclusions and recommendations for future work are also provided.

CHAPTER 2

BACKGROUND

2.1 Pre-cured Systems

2.1.1 General

According to ACI 4402R.02 (2002) the experimental work on the use of FRP materials as EB retrofitting reinforcement in concrete structures started in the late 1970's in Germany (Wolf and Meisler 1989). In the early years, Swiss and Japanese researchers contributed to the development of the technique (Meier 1987). First studies on the topic focused on the feasibility of the method. Ritchie et al. (1991) tested series of under-reinforced concrete beams strengthened with different EB FRP and anchorage configurations. Carbon, glass and aramid FRP plates were used with and without, half- and full-end anchorages. Test results showed significant increases in stiffness and strength. An analytical procedure was also proposed to predict the behavior of the strengthened system which involved slicing the section and computing the forces for the materials within the slice utilizing non-linear material models and employing equilibrium of forces within the cross section. The predicted and actual behaviors were pretty close although in some specimens premature failures were observed. Reported failure modes were concrete cover seperation, concrete crushing, FRP rupture and end anchorage failure. In addition, Smith and Teng (2002) identified shear failure, plate end interfacial debonding and intermediate crack-induced debonding modes. The failure modes are depicted in Figure 2.1.

Saadatmanesh and Ehsani (1991) proposed a simple analytical model similar to that of Ritchie et al. (1991) based on equilibrium of forces and compatibility of deformations. Neither model could effectively predict the debonding loads for lack of correlation with physical behavior.

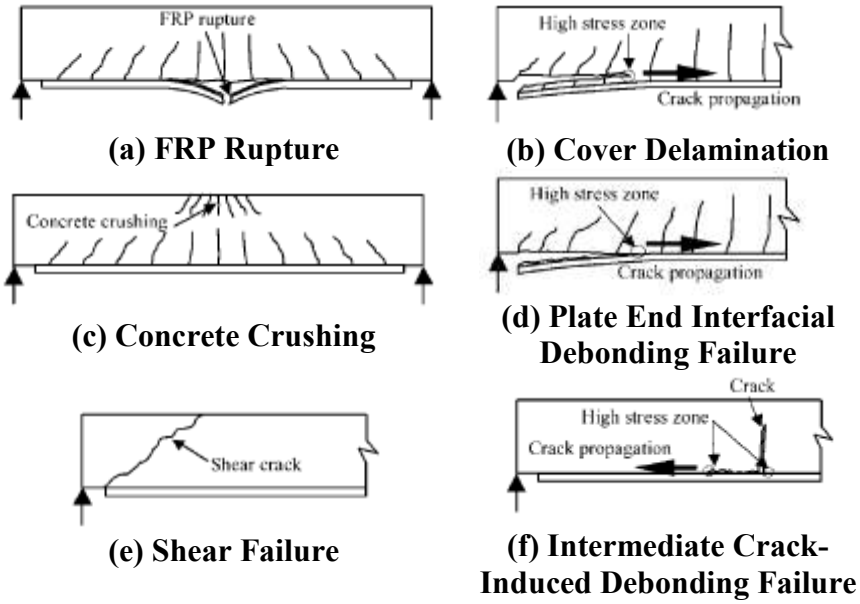

Figure 2.1 Failure Modes of FRP-Strengthened RC Beams (Smith and Teng 2002)

Studies by Meier (1995), Shahawy et al. (1996) and Arduini and Nanni (1997) and many others proved the effectiveness of the FRP retrofitting technique. Recent research on FRP has shifted to the prediction of the failure mechanisms, modeling and bond issues.

Among the identified failure modes, the most commonly reported one is the debonding failure. It is also the most undesired one, because it leads to the loss of composite action between concrete and FRP, preventing the full utilization of the material and it is quite brittle. In ACI 4402R.02 (2002) controlling failure modes were

identified in reference to the study by GangaRao and Vijay (1998) similar to those shown in Figure 2.1. In ACI 4402R.02 (2002) a bond-dependent coefficient denoted by κ_m was introduced in order to prevent cover delamination and FRP debonding failures by limiting the maximum strain in the FRP laminate. The expression for κ_m is shown as:

$$\kappa_m = \begin{cases} \frac{1}{60\varepsilon_{fu}}(1-\frac{nE_f t_f}{2{,}000{,}000}) \le 0.90 \; for \; nE_f t_f \le 1{,}000{,}000 \\ \frac{1}{60\varepsilon_{fu}}(\frac{500{,}000}{nE_f t_f}) \le 0.90 \; for \; nE_f t_f > 1{,}000{,}000 \end{cases} \quad \textbf{(2.1)}$$

where ε_{fu} is the rupture strain of the FRP plate, n is the number of the plies used and E_f and t_f are the Young's Modulus and the thickness of the FRP, respectively. Usable strain in FRP while avoiding the debonding failure is calculated by multiplying ε_{fu} by κ_m. The ACI 4402R.02 (2002) approach of limiting the strain is opposed by FIB Bulletin 14 (2001) as it may lead to an uneconomical use of FRP materials especially in large spans (Saxena et al. 2008).

Considering the intermediate flexure/shear cracks only, Teng (2004) proposed the following equation to limit the strain in the FRP plate in order to prevent debonding failures;

$$\varepsilon_f^{IC} = 0.114(4.32-\alpha)\tau_{\max} / \sqrt{E_f t_f} \quad \textbf{(2.2)}$$

where, $\tau_{\max}$ is the maximum bond stress and α is a geometric parameter calculated respectively as

$$\tau_{\max} = 1.5\beta_w f_t \quad \textbf{(2.3)}$$

$$\alpha = 3.32 L_{ee} / L_d \quad \textbf{(2.4)}$$

where f_t is the tensile strength of the concrete, L_d is the distance between the loaded section and the plate end, L_{ee} is the effective bond length and β_w is a geometric parameter as calculated respectively, as

$$L_{ee} = 0.228\sqrt{E_f t_f} \quad \textbf{(2.5)}$$

$$\beta_w = \sqrt{(2.25 - b_f / b_c)/(1.25 + b_f / b_c)} \quad \textbf{(2.6)}$$

where b_f and b_c are the width of the FRP plate and concrete soffit, respectively. Strain limiting factor (bond-dependent coefficient), κ_m, is then defined as

$$\kappa_m = \varepsilon_f^{IC} / \varepsilon_{fu} \quad \textbf{(2.7)}$$

El-Mihilmy and Tedesco (2000) and Ross et al. (1999) proposed analytical procedures and tools for the design and analysis of retrofitted members considering the amount of steel and FRP, and the degree of bond between the concrete and the plate.

Another important area which has been studied by other researchers and also an integral component of this study is the effects of surface anomalies and surface conditions on the performance of FRP-concrete system. Commonly identified anomalies are surface flatness, and voids and cracks (cuts). The degree of roughness is also believed to have a significant impact. NCHRP Report 514 (Mirmiran et al. 2004) reported thresholds for guaranteed system performance, and this study aimed at verifying those thresholds for the pre-cured FRP systems.

2.1.2 Bond Issues

Bond mechanism is important in understanding the failure modes in FRP retrofitted concrete structures. Of all possible failure modes, three are related the to bond

phenomena, as shown in Figure 2.1 b, d and f namely; concrete cover delamination, plate-end interfacial debonding and intermediate crack-induced debonding failures. Smith and Teng (2002) reported that concrete cover delamination (separation) and plate end debonding failures can be evaluated similarly as both are caused by high interfacial stresses near the ends where the laminate is terminated abruptly. Due to this high stress concentration, a crack forms near the end of the laminate, which then propagates to the level of the internal steel reinforcement in the case of cover separation. Progressive concrete cover separation follows towards the mid-span as the load increases (Figure 2.2). On the other hand, debonding occurs as soon as the cracks form in the loose concrete surface.

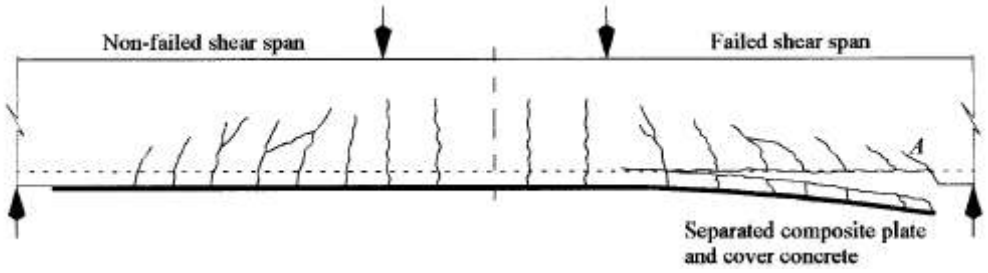

Figure 2.2 Concrete Cover Delamination (Garden and Halloway 1998)

The mechanism of intermediate crack-induced debonding failure is discussed in detail by Garden and Halloway (1998). This failure mode is initiated with the formation of a flexure-shear crack in the mid-span. The relative movement of the crack lips with respect to each other causes the loss of the bond between the concrete and the FRP in the vertical direction thus generating debonding which travels towards the ends accompanied by a significant load drop (see Figure 2.3).

Use of side straps (U-jacketing) near the ends and the mid-span solely for anchorage purposes or for the intention of shear strengthening helps prevent debonding failures (Buyukozturk et al. 2004).

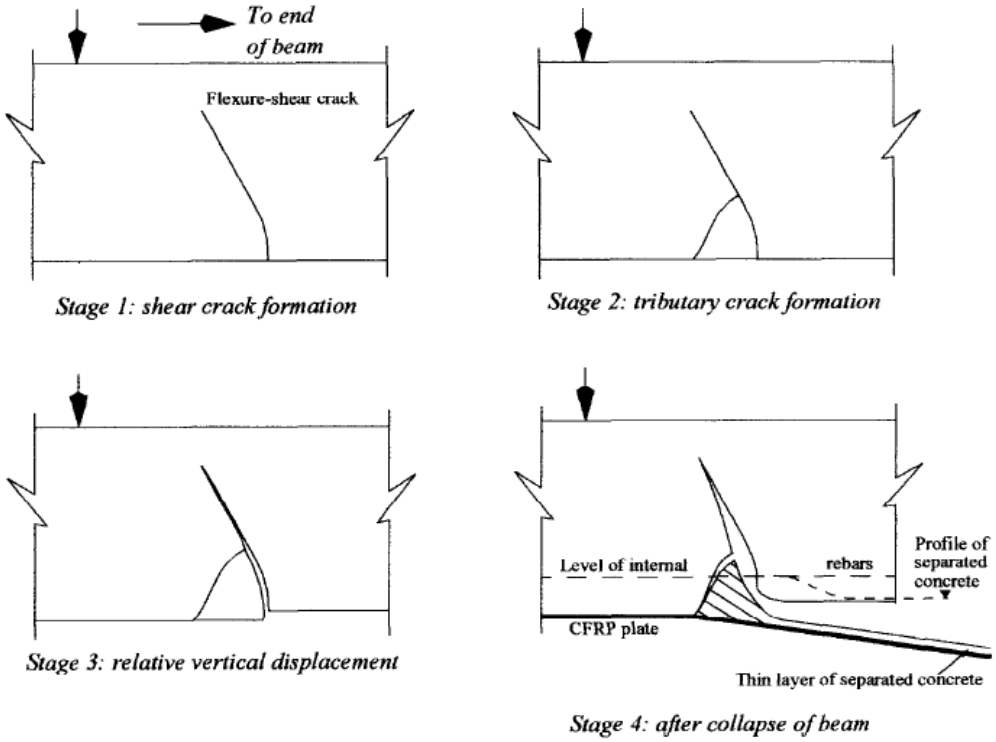

Figure 2.3 Intermediate Crack-Induced Debonding (Garden and Halloway 1998)

In order to understand the mechanism of debonding failures, researchers have developed models to predict the bond behavior. These studies can be classified as strength-based, fracture-mechanics based empirical or semi-empirical approaches (Buyukozturk et al. 2004). The strength-based method includes calculating the interfacial stress distributions using linear material models (stress analysis), comparing them against the ultimate strength (section analysis) and predicting debonding loads and mechanisms. Examples of such models can be found in Khalifa et al. (1998), Shen and Teng (2001) and El-Mihilmy and Tedesco (2001). Buyukozturk et al. (2004) and Smith and Teng

(2002) provided critical reviews for these methods. Strength-based models are not based on fracture mechanics. This may be somewhat misleading because debonding failures are actually initiated by small cracks, which then develop into larger cracks and initiate debonding in the form of crack propagation. In order to incorporate the principles of fracture mechanics into bond modeling, researchers have come up with fracture-mechanics-based models of bond behavior. Such models develop local bond-slip relationships that basically include an ascending and a descending branch. Key parameters defining the bond-slip curve are the maximum bond stress (τ_{max}), slip at the maximum bond stress (s_0), and slip at which bond stress approaches to zero (s_f). The curve ascends until τ_{max}, followed by the descending branch until failure. A schematic representation of such curves is shown in Figure 2.4.

Various researchers have developed bond-slip models for the FRP-concrete interface. Descriptions of the models by Neubauer and Sostasy (1999), Nakaba et al. (2001), Monti et al. (2003), Saviova et al. (2003) and Lu et al. (2005) are shown in Table 2.1 (after Lu et al. 2005). Models by Nakaba et al. (2001) and Saviova et al. (2003) are single continuous curves, whereas models by Neubauer and Rostasy (1999), Monti et al. (2003) and Lu et al. (2005) propose different equations to define the ascending and descending branches. Most of the bond-slip models do not take into account the mechanical properties of the adhesive, mainly because experiments have shown that the weakest link in the concrete-adhesive-FRP system is the concrete cover. In cases where soft epoxies are used, the validity of such models will be in question. Therefore, it is relevant to state that FRP-concrete bond strength does not depend on the strength of adhesives, as long as the bond between epoxy and FRP is stronger than the bond between

epoxy and concrete. In this table β_w is a geometrical factor depending on the width of the FRP plate, b_f, and concrete, b_c. t_a, E_a E_c are the thickness of the adhesive, Young's modulus of the adhesive and Young's Modulus of concrete, respectively. G_f is the fracture energy of the concrete.

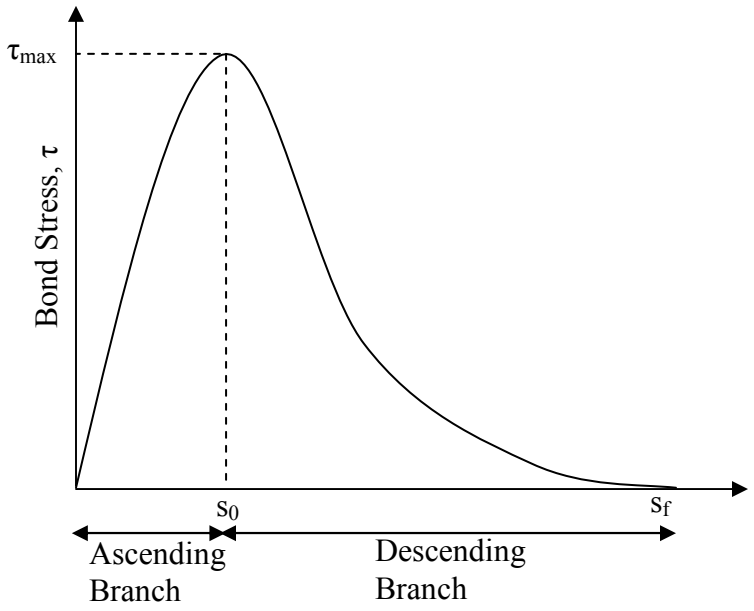

Figure 2.4 Two-Branch Bond-Slip Models

Lu et al. (2005) evaluated the validity of various bond slip models. They compiled a database of 253 bond test specimens. Using the tests results in the database and different bond-strength and bond-slip models, average predicted-to-measured bond strength ratios were calculated. The calculated ratios were in the range of 0.996 to 4.470, and 1.001 to 1.330 for the bond-strength and bon-slip models, respectively. The coefficients of variation (COV) and the coefficients of correlation (CC) for the bond-strength models were in the range of 0.156 to 0.975, and 0.908 to -0.028, respectively.

The COV and CC for the bond-slip models were in the ranges of 0.155 to 0.231 and 0.910 to 0.846, respectively. The study showed that the bond-slip models predict the bond behavior much better than the bond-strength models.

Abdel Baky et al. (2007) and Alemu and Bhargava (2007) used the bond-slip model proposed by Lu et al. (2005) for the finite element (FE) simulations. Bond between the concrete and the epoxy was modeled using discrete interface elements in both of these studies. Abdel Baky (2007) developed 2D and 3D finite element models using ADINA FE package. The 2D and 3D models were both sufficiently accurate in predicting the test results. Alemu and Bhargawa (2007) used ANSYS FE package to model some selected tests referenced from the literature. Bond was modeled with three orthogonal non-linear spring elements. The analysis showed good agreement with the test data. Additional information regarding modeling will be discussed later in Chapter 4.

2.1.3 Analysis and Design of FRP Strengthened Concrete Beams

Most of the published studies on the analysis of FRP-strengthened concrete beams compute the ultimate flexural strength of the section based on the two principals of equilibrium of forces and compatibility of strains. The basic assumptions of this common approach include:

1. Strain distribution is linear across the depth of the section, i.e., plane sections remain plane after bending;
2. Deformations are small;
3. Tensile strength of concrete is negligible;
4. Shear deformations are neglected; and

Bond-slip Model	Ascending Branch	Descending Branch	τ_{max}	s_0	β_w	G_f
Neubauer and Sostasy (1999)	$\tau_{\max}(\frac{s}{s_0})$	0	$1.8\beta_w f_t$	$0.202\beta_w$	$\sqrt{1.125\frac{2-b_f/b_c}{1+b_f/400}}$	-
Nakaba et al. (2001)	$\tau_{\max}(\frac{s}{s_0})\left[3/\left(2+\left(\frac{s}{s_0}\right)^3\right)\right]$		$3.5f_c^{'0.19}$	0.065	-	-
Monti et al. (2003)	$\tau_{\max}\frac{s}{s_0}$	$\tau_{\max}\frac{s_f-s}{s_f-s_0}$	$1.8\beta_w f_t$	$2.5\tau_{\max}\left(\frac{t_a}{E_a}+\frac{50}{E_c}\right)$	$\sqrt{\frac{1.5(2-b_f/b_c)}{1+b_f/100}}$	-
Saviova et al. (2003)	$\tau_{\max}\left(\frac{s}{s_0}\right)\left[2.86/\left(1.86+\left(\frac{s}{s_0}\right)^{2.86}\right)\right]$		$3.5f_c^{'0.19}$	0.051	-	-
Lu et al. (2005)	$\tau_{\max}\sqrt{\frac{s}{s_0}}$	$\tau_{\max}e^{-\alpha\left(\frac{s}{s_0}-1\right)}$	$\alpha_1\beta_w f_t$	$0.0195\beta_w f_t$	$\sqrt{\frac{2.25-b_f/b_c}{1.25+b_f/b_c}}$	$0.308\beta_w^2\sqrt{f_t}$ $\alpha=\frac{1}{\frac{G_f}{\tau_{\max}}-\frac{2}{3}}$

Table 2.1 Bond-Slip Models (Lu et al. 2005)

5. No slip occurs between concrete and FRP; i.e., perfect bond is assumed.

An et al. (1991) proposed a methodology to compute the ultimate strength of such members. Non-linear material properties were used in the analysis. Steel was modeled as elastoplastic material, FRP as linear elastic until failure, and concrete using Hognestad's model as shown in Figure 2.5.

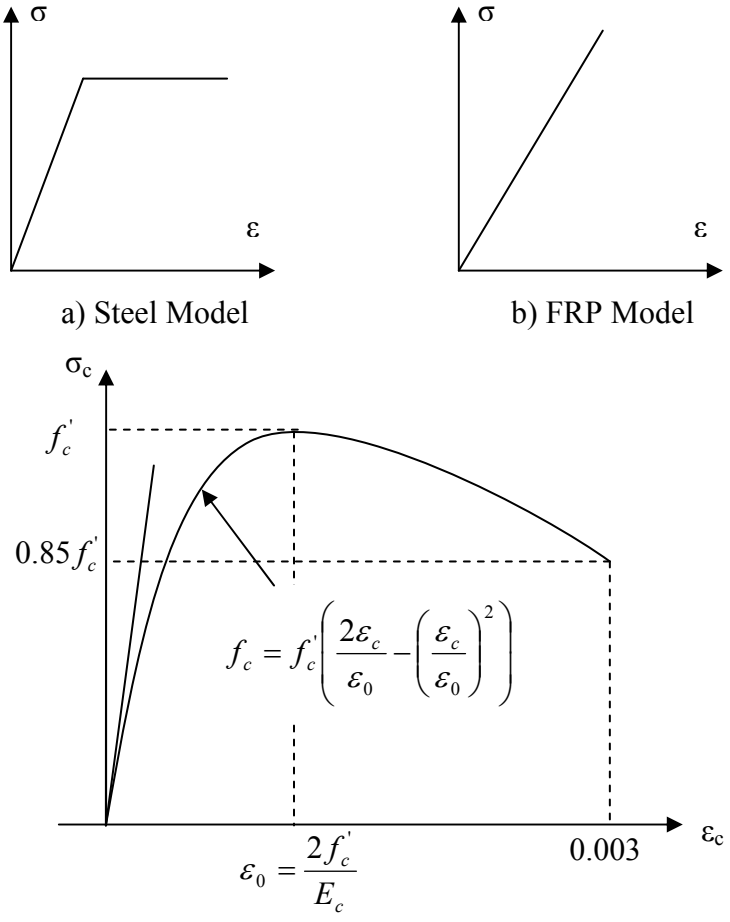

a) Steel Model b) FRP Model

c) Hognestad's Concrete Model

Figure 2.5 Material Models

Stresses in FRP, steel and concrete are calculated directly from the material models. Strain in the extreme concrete fiber is progressively increased until failure occurs

at a concrete crushing strain of 0.003 or until the FRP ruptures. Strains in FRP and steel are calculated accordingly. Compressive force in a rectangular concrete section is given by:

$$C_c = \alpha f_c' bc \tag{2.8}$$

where α is the parameter used to convert the non-linear stress-strain relationship for concrete into a rectangular stress block, f_c' is the concrete strength, b is the width of the section, and c is the depth of neutral axis. α is obtained by equating the area under the stress-strain curve to an equivalent area given by:

$$\alpha = \frac{\int_0^{\varepsilon_{cf}} f_c d\varepsilon_c}{f_c' \varepsilon_{cf}} \tag{2.9}$$

where f_c is the stress obtained from the Hognestad's model, and ε_{cf} is the strain in the extreme fiber of the concrete section. The location of the concrete compressive force, d_c, measured from the top is given by:

$$d_c = \gamma c \tag{2.10}$$

where γ is the centroid factor, obtained from the first moment of the area under the concrete stress-strain diagram as given by:

$$\gamma = \frac{\frac{1}{3} - \frac{\varepsilon_{cf}}{12\varepsilon_0}}{1 - \frac{\varepsilon_{cf}}{3\varepsilon_0}} \text{ , if } 0 \le \varepsilon_{cf} < \varepsilon_0 \tag{2.11a}$$

$$\gamma = 1 - \frac{\left(\varepsilon_{cf}^3 - 5.1\varepsilon_0\varepsilon_{cf}^2 - 0.004\varepsilon_0^2 + 0.024\varepsilon_{cf}^2\right)}{\varepsilon_{cf}\left(3.925\varepsilon_0^2 - 10.2\varepsilon_0\varepsilon_{cf} - 0.9\varepsilon_{cf}^2 - 0.016\varepsilon_0 + 0.048\varepsilon_{cf}\right)}, \tag{2.11b}$$

$$\text{if } \varepsilon_0 \le \varepsilon_{cf} < 0.003$$

The depth of neutral axis, c is obtained by iterative solution of the following:

$$\alpha f_c^{'} bc + \sum_{i=1}^{n} f_{si} A_{si} + f_{FRP} A_{FRP} = 0 \qquad \textbf{(2.12)}$$

where f_{si} and A_{si} and are the stress and cross-sectional area of the ith layer of steel, respectively, and f_{FRP} and A_{FRP} are the stress and the cross-sectional area of FRP laminate, respectively. The flexural strength of the section is then given by:

$$M = \alpha f_c^{'} bc\left(\frac{h}{2} - \gamma c\right) + \sum_{i=1}^{n} f_{si} A_{si}\left(\frac{h}{2} - d_i\right) + f_{FRP} A_{FRP}\left(\frac{h}{2} - d_{FRP}\right) \qquad \textbf{(2.13)}$$

where d_i is the distance from the top to the centroid of the ith layer of steel, h is the depth of the section and d_{FRP} is the distance from the top to the centroid of the FRP laminate. Stress, strain and force diagrams for the cross section are shown in Figure 2.6.

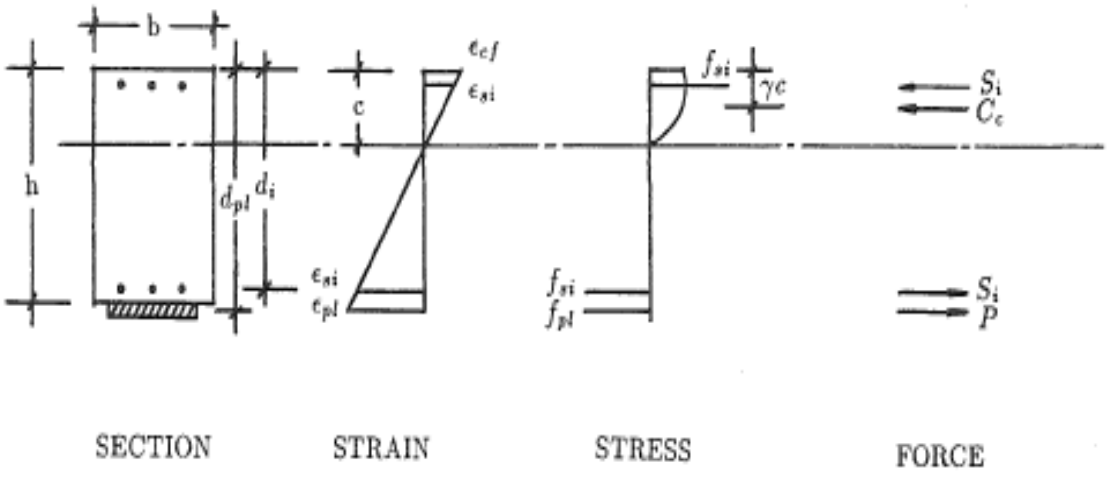

Figure 2.6 Cross-Section, Strain, Stress and Force Diagrams (An et al. 1991)

An et al. (1991) conducted a parametric study using the above method. The selected parameters were internal steel reinforcement ratio, FRP area, FRP ultimate strength, FRP stiffness and concrete compressive strength. They reported that the efficiency of the technique increases for beams with low reinforcement ratios. The increase in the concrete compressive strength did not significantly enhance the flexural

strength. This method, however, only considered concrete crushing and FRP rupture failure modes, but did not include debonding failures

Ross et al. (1999) identified four distinct regions between these points on the load-displacement response of FRP-strengthened concrete beams between concrete cracking, steel yielding, concrete compressive strength and CFRP failure as shown in Figure 2.7.

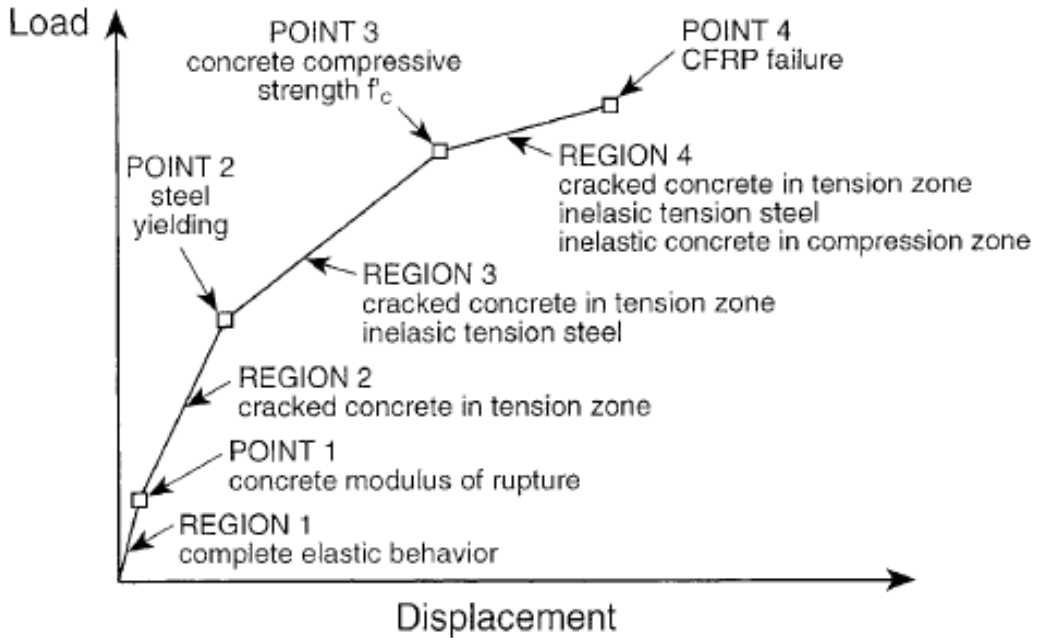

Figure 2.7 Load-Displacement Response of FRP-Strengthened Concrete Beam (Ross et al. 1999)

Elastic material properties are used in Regions 1 and 2, whereas post yielding modulus (E_{cy}) is used for concrete in Region 3, after steel yields and before concrete reaches its full strength. In Region 4 concrete has reached its full strength, using the rectangular stress block assumptions. Ross et al. (1999) were successful in simplifying the procedures for calculating the flexural strength of the FRP-strengthened concrete

beams but the issue of system behavior in the presence of debonding failures was not addressed.

El-Mihilmy and Tedesco (2000) used a similar approach to develop design nomographs as shown in Figure 2.8. Steel and FRP reinforcement indices are calculated as:

$$\omega = \frac{f_y}{f_c^{'}}\rho\,,\ \rho = \frac{A_s}{bd} \tag{2.14a}$$

$$\omega_f = \frac{E_f}{f_c^{'}}\rho_f\,,\ \rho_f = \frac{A_f}{bd} \tag{2.14b}$$

where f_y is steel yield strength and ω and ω_f are the reinforcement index for steel and FRP, respectively. A_f and d are cross-sectional area of FRP and effective depth respectively. ρ and ρ_f stand for steel and FRP reinforcement ratio, respectively.

ACI 4402R.02 (2002) requires limiting the ultimate strain in FRP to prevent debonding failures for the ultimate strength calculations. Bond-dependent coefficient, κ_m (See Equation 2.1) is devised for this purpose. In addition an environmental reduction factor, denoted by C_E is applied to the ultimate strain of FRP to account for the deteriorating effects of the environment, as:

$$f_{fu} = C_E f_{fu}^{*} \tag{2.15a}$$

$$\varepsilon_{fu} = C_E \varepsilon_{fu}^{*} \tag{2.15b}$$

$$E_f = \frac{f_{fu}}{\varepsilon_{fu}} \tag{2.15c}$$

where f_{fu}^{*} and ε_{fu}^{*} are the ultimate strength and strain reported by the manufacturer, f_{fu} and ε_{fu} are the design strength and strain, and E_f is the modulus of elasticity of FRP. The strain in FRP at anytime during loading is then given by:

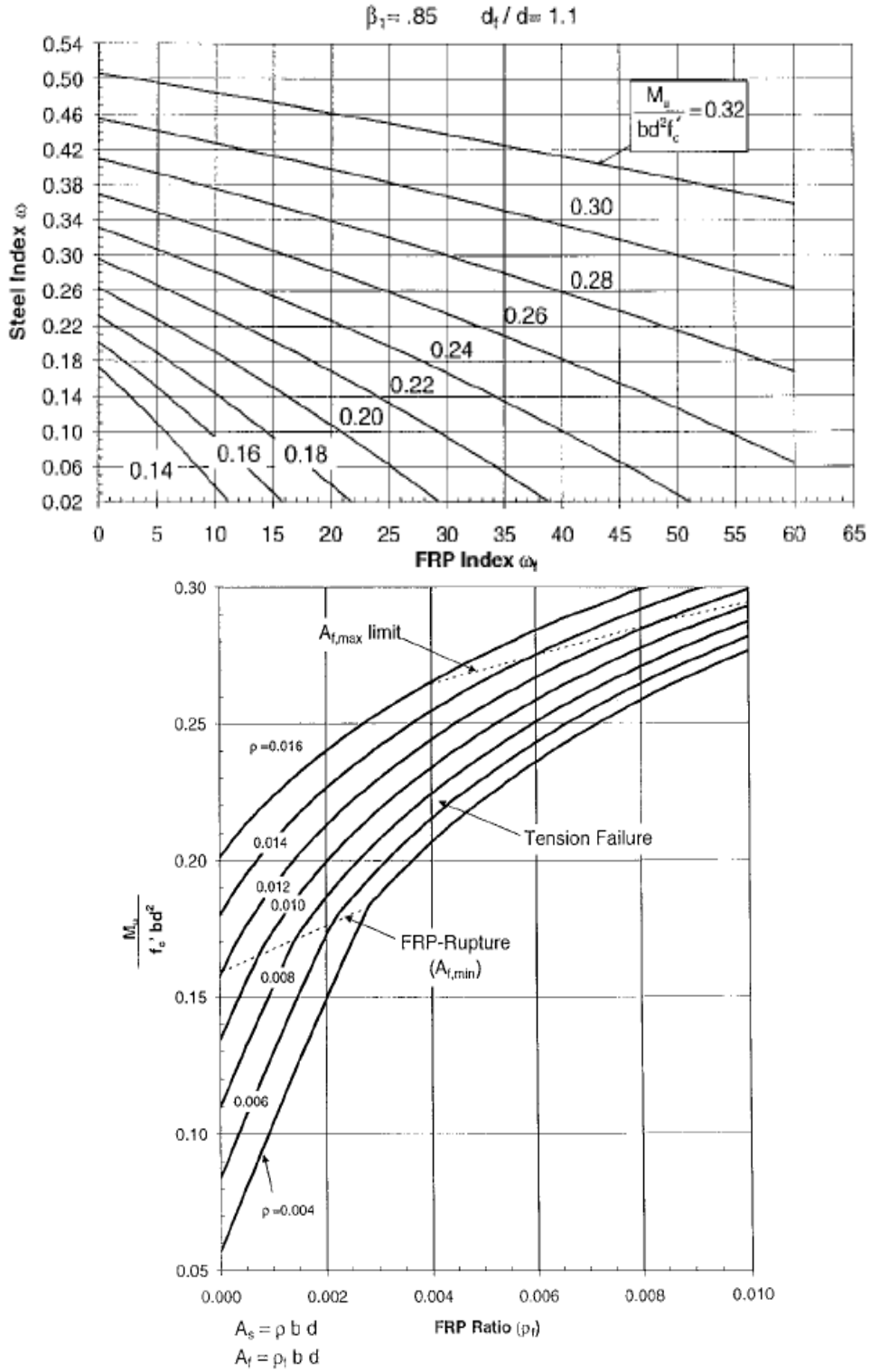

(For f_y = 60 ksi, 17400 ksi, $f_c^{'}$=3.6 ksi, ε_U =0.01 and $d_f / d = 1.2$)

Figure 2.8 Typical Design Nomographs

$$\varepsilon_{fe} = \varepsilon_{cu}\left(\frac{h-c}{c}\right) - \varepsilon_{bi} \le \kappa_m \varepsilon_{fu} \quad \textbf{(2.16)}$$

where; ε_{fe} is the effective strain, and ε_{bi} is the initial strain which may be present in FRP because of the construction forces or application practices. Effective stress f_{fe} is given by:

$$f_{fe} = E_f \varepsilon_{fe} \quad \textbf{(2.17)}$$

The ductility of FRP-strengthened concrete beam is ensured by the use of appropriate strength reduction factors as:

$$\phi = \begin{cases} 0.90 \quad for \quad \varepsilon_s \ge 0.005 \\ 0.70 + \dfrac{0.20(\varepsilon_s - \varepsilon_{sy})}{0.005 - \varepsilon_{sy}} \quad for \quad \varepsilon_{sy} < \varepsilon_s < 0.005 \\ 0.70 \quad for \quad \varepsilon_s \le \varepsilon_{sy} \end{cases} \quad \textbf{(2.18)}$$

2.1.4 Effects of Surface Irregularities

Surface irregularities that may affect the performance of FRP-strengthened concrete members are identified as surface roughness, flatness, voids and cracks (cuts), each described in the following sections.

2.1.4.1 Surface Roughness

The state of concrete surface plays an important role in the performance of FRP-strengthened concrete members. The degree of surface roughness is measured based on the recommendations by ICRI/ACI (1999) and ACI 546 (1996), where by nine (9) distinct concrete surface profiles (CSP) were identified, as shown in Figure 2.9. The profiles range from 1 for the smoothest to 9 for the roughest surface. Recommended methods to obtain the desired CSP level are also described in the figure. The profile

images shown were obtained by video density imaging techniques at the University of Illinois, Urbana-Champaign.

There is significant difficulty in replicating the desired CSP level, even when ICRI/ACI (1999) guidelines are strictly followed, by the same person and using same equipment. Quality control and practice are necessary for consistency. Ueda and Dai (2005) reported significant scatter in the data for bond strengths with different surface conditions without repeatability.

Figure 2.9 Concrete Surface Profiles (ICRI/ACI 1999)

In the literature, there is a general agreement that surface roughness plays an important role on the bonding strength of the FRP materials onto concrete surface (Maerz et al. 2001). De Lorenzis et al. (2001) studied the factors affecting the bond of FRP laminates to concrete surface, and reported that FRP system with the roughened surface

performed better than the one with the sandblasted surface. Toutanji and Orthiz (2001) reported that surface treatment by water jetting produced better bond strength than sand blasting.

Chepur (1996) studied the effect of various factors such as surface roughness, concrete strength and adhesive type on the FRP-concrete bond strength, and concluded that interfacial bond strength would increase with increasing mechanical abrasion.

Shen et al. (2002) used laser profilometry to categorize different levels of concrete surface roughness, and concluded that sufficient bond strength could be developed using intermediate CSPs, which were rougher than those recommended by ICRI/ACI (1999). It was also reported that optimum CSP varies for different FRP systems. Jeffries (2004) showed that surface grinding does not improve the bond between FRP and concrete, and may even adversely affect by inducing micro-cracks. Chepur (2002), on the other hand, stated that surface roughness did not affect the flexural strength of FRP-strengthened beams with concrete strength smaller than 3 ksi as at that time failure is controlled by the weak concrete. The inconsistency among the results of different studies may be attributed to the differences in the workmanship and the difficulties in duplicating specimens together with lack of objective means of categorizing different surface roughness levels.

Most FRP design and/or construction guidelines recommend surface preparation methods for effective applications. ACI 4402R.02 (2002) and NCHRP Report 514 (Mirmiran et al. 2004) both refer to the recommendations by ICRI/ACI (1999) and ACI 546 (1996) for surface profiling of bond-critical applications. ACI 4402R.02 (2002) suggests abrasive or water blasting techniques for surface preparation to a minimum

concrete surface profile CSP 3, as defined by ICRI/ACI (1999). NCHRP Report 514 (Mirmiran et al. 2004) does not specify any CSP number for bonded repair using FRP composites. FIB Bulletin 14 (2001) recommends surface grinding as the most appropriate method for wet lay-up FRP systems, but does not require a specific surface profile.

Yalim (2008) conducted both flexural and double bond shear tests to investigate surface roughness as part of the research project NCHRP 10-59B for wet lay-up FRP systems. Flexural specimens were strengthened with a single layer of wet lay-up carbon FRP sheet, and side U-straps were used as anchorage. Test parameters included surface roughness level and the quantity of side straps. Three different levels of surface profiles were utilized, corresponding to CSP 1, CSP 2-3 and CSP 6-9, as defined by ICRI/ACI (1999). The anchorage level ranged from no straps to full continuous straps. High-pressure water washing and grinding were used to achieve desired levels of surface roughness. Bond specimens were also prepared using the same grades of surface roughness with zero, four and full side straps arrangements. Flexural tests resulted in generally similar responses regardless of the degree of roughness. However, the slight difference among surface profiles was magnified with higher levels of anchorage. Flexural strength and ductility were also enhanced and the mode of failure changed from FRP debonding to FRP rupture, with the additional side straps. The results of bond tests were in general agreement with the flexural tests. Finally, a CSP level of 2-3 was recommended as a conservative measure, although CSP 1 proved to be sufficient for most of the cases. The results of this study were published in NCHRP Report 609 (Mirmiran et al. 2008).

2.1.4.2 Surface Flatness

Surface out-of-flatness is a term which refers to a depression or a bump over a given length. The presence of such irregularities has pronounced effect on the bond strength and overall system performance. There have been very limited studies on this subject. However, similar studies focusing on the FRP-strengthened members with curved soffit do exist. The analogy between these studies and the idealized surface out-of-flatness as a flaw can be beneficial in understanding the influence of such irregularities.

De Lorenzis et al. (2006) proposed an analytical model for the interfacial stress in curved members bonded with a thin plate, and showed that in the elastic range, the concentration of transverse and normal stress at plate ends decreased with the increasing radius of curvature. This implies that plate-end debonding is less critical for curved members than for straight members.

Eshwar et al. (2004) showed that the transverse stresses resulting from the straightening of the FRP plate under tensile stresses may lead to premature debonding at high curvatures. In order to prevent such failures, limitations on curvatures were recommended by researchers and design/construction guidelines. Porter (2003) suggested a limit of 0.2 in over 40 in. length. Eshwar et al. (2004) showed that the curvature limit of $1x10^{-1}$ set by TR-55 (2004) is acceptable, provided that it does not extend over a length of 40 in. FIB Bulletin 14 (2001) proposes a limit of $4.5x10^{-3}$ for wet lay-up systems. NCHRP Report 514 (Mirmiran et al. 2004), on the other hand, recommends filling of any depressions deeper than 1/8 in. over a length of 12 in.

Yalim (2008) tested 10 specimens with out-of-flatness levels of control, 1/16 in. and 1/8 in. over a length of 12 in. in the form of both depressions (valley) and bumps (peak). The test specimens were similar to those explained in Section 2.1.4.1. The overall behavior of the peak specimens were similar to that of the control specimens, and the failure mode was FRP debonding initiated at the edge of the peak region and propagating towards the ends. The failure in the 1/8 in. valley specimens initiated much sooner than the control and 1/16 in. valley specimens, which were characterized by a plateau at a load level of about 19% less than the average load capacity of control specimens. No such behavior was observed in the 1/16 in. specimens, which in fact behaved similar to the control specimens. The failure mode for all valley specimens was FRP debonding similar to those of the peak specimens. A database consisting of the test results from similar studies was compiled, and it was concluded that the FRP debonding stress decreases with the increasing out-of-flatness level.

2.1.4.3 Surface Voids

Voids may be present on the concrete surface either due to the initial placement and/or environmental conditions. They may also develop at the interface between the resin and the FRP due to air entrapment. Bug holes on the concrete surface are similar to voids, as they generate disbonds between concrete and the FRP. This kind of concrete flaw occurs due to poor compaction of the concrete or defective formwork. In addition to surface voids and bug holes, defective FRP may also cause bond failures. Disbonds can be simulated in the laboratory by intentionally altered formworks, by drilling holes after

casting on the cured specimens, or simply by placing Teflon sheets between concrete and the FRP.

Untreated voids/disbonds may lead to debonding failure due to reduced bond area. A study by Ekenel and Myers (2004) showed that such defects weaken the structural integrity and performance of the FRP system. Size, shape and the location of the disbond are the main parameters involved in the study of surface voids. Kaiser (2002) studied the effects of disbonded regions through fracture mechanics, and showed the adversity on the bond. In contrast to this, Puliyadi (2001) reported that disbonds of up to 6 in. have no significant effect on the structural performance of the FRP system.

Delaney and Karbhari (2006) conducted a comprehensive study on FRP defects. Disbond width, length, shape and location were the main parameters of interest. Rectangular and circular disbonds were generated using Teflon sheets. Several 6.6 ft long, 5.9 in. wide and 7.9 in. deep rectangular concrete beams were strengthened by two layers of CFRP. Disbonds were located at a distance from 0 to 26 in. from the mid-span of size varied from 1 to 9.8 in. and located both at the concrete-resin interface and in the interlaminar adhesive. According to the test results, the recommendations of the present guidelines such as NCHRP Report 514 (Mirmiran et al. 2004) and ACI 4402R.02 (2002) were conservative. Disbonds smaller than 2 in. had no significant impact on performance. Even very large disbonds of size 9.8 x 5.9 in. (rectangular) or 5.9 in. diameter circular defects, although comprised 15% and 7% of the total bond area, respectively, had little influence on the system performance, reducing the load capacity by less than 5% each.

Voids may be present between the layers in multi-layer FRP applications such as FRP bridge decks. In NCHRP Report 564 (Telang et al. 2004), the effects of these types

of voids were addressed. If the void is large enough and grows progressively, it may turn into a crack when it reaches the surface, and may lead to delamination.

NCHRP Report 514 (Mirmiran et al. 2004), although not based on experimental data, recommended to fill any void with a diameter larger than 1/2 in. or a depth greater than 1/8 in. The same study recommended epoxy injection for FRP defects of size between ¼ in. and 1 ¼ in., patching for those between 1¼ and 6 in. provided that the number of such defects is less than 5 per any unit surface area of 10-ft length or width and finally full replacement for larger defects. ACI 4402R.02 (2002) set limits for disbonds as follows: disbonds of 2 $in.^2$ are considered small, provided that the total disbond area is less than 5% of the total bond area and the number of such defects does not exceed 10 within 10 ft^2. Otherwise, the system must be repaired either by resin injection or ply replacement. For medium disbonds between 2 and 25 in^2, resin injection or ply replacement is recommended. Treatment method for larger disbonds involves removing the defective portion and applying an equivalent amount of FRP.

Yalim (2008) tested a total of 14 concrete beam specimens to study the effects of voids on FRP-concrete system performace. Void frequency was kept constant, but void diameter and depth were varied: 1/2 in., 3/8 in. and 1/4 in. diameter circular voids drilled at 1/8 in., 3/16 in. and 1/4 in. depths on the concrete surface. Both 4 and 11 strap specimens were utilized. Specimen properties were identical to those explained in Section 2.1.4.1. The void depth appeared to have little or no effect on the structural performance of the FRP system. The 1/2 in. void diameter limit set by NCHRP Report 514 (Mirmiran et al. 2004) turned out to be conservative. Dominant failure modes were FRP debonding

and FRP rupture for the 4 strap and 11 strap specimens, respectively. It was reported that debonding initiated at the mid-span and propagated towards the support until failure.

2.1.4.4 Surface Cracks (Cuts)

Researchers have often used pre-cracked reinforced concrete beams to the study the effects of such flaws on the FRP system. Arduini and Nanni (1997) reported that the performance of specimens was so slightly affected by pre-cracking that they were comparable with the uncracked beams. Studies by Shahawy et al. (1996) and Thannoon et al. (2005) showed that FRPs could be successfully used to restore and further enhance the flexural capacity of the pre-cracked concrete members. Bizindavyi and Neale (1999) reported through single lap shear tests that concrete cracks might increase stress transfer length. In a study by Kaiser and Karbhari (2003), it was showen that FRPs could provide resistance to crack opening. However, crack widths wider than 1/100 in. seemed to cause local delamination, which may later lead to failure. Epoxy injection was recommended to fix this problem. Delaney and Karbhari (2006) preloaded several specimens to residual cracks widths of 0.008, 0.025, 0.04 and 0.06 in., and then strengthened them with FRPs. The beams were then loaded until failure. Test results showed no significant difference in terms of ultimate loads and deflections.

Both NCHRP Report 514 (Mirmiran et al. 2004) and ACI 4402R.02 (2002) recommended that cracks narrower than 0.01 in. may be left untreated or epoxy injected, whereas cracks wider than 0.01 in. must be cut and filled with epoxy. None of these guidelines recommend any thresholds for crack spacing or depth.

Within the scope of this study, surface cracks generated by a geometric cut in the concrete surface were investigated. Using this approach the size and distribution of such defects were better controlled. This study focused on the effects of cracks as discontinuities and disbonds, but not as individual.

Yalim (2008) tested a total of 14 beam specimens with various cut widths, spacing and side-strap configurations to study the effects of such defects. Specimen geometry was identical to those explained in Section 2.1.4.1. The 1/16, 3/32 and 1/8 in. wide cuts were induced at 1, 1.5 and 2 in. spacing. Also 4 and 11 straps were provided to simulate different anchorage levels. Based on the test results, it was reported that the NCHRP Report 514 (Mirmiran et al.) crack width limit of 0.01 in. for epoxy filling was too conservative. A threshold value of 1/32 in. was recommended primarily for durability rather than structural requirements. Crack depth appeared to have no significant impact on FRP system performance. It was reported that the 4-strap specimens failed by FRP debonding, whereas the 11-strap specimens failed by FRP rupture.

2.2 NSM FRP Systems

2.2.1 General

The use of near surface mounted steel rebars inserted into pre-cut grooves can be traced back to the late 1940's, on a deficient bridge in Sweden (Asplund 1949). However, the use of NSM FRP reinforcement with epoxy and adhesive is quite new (De Lorenzis et al. 2000). The NSM FRP application offers several advantages over external bonding of FRP, as follows: (a) the reinforcement can be anchored into adjacent members; (b) the members can be strengthened in their negative moment regions; (c) the members do not

require as much surface preparation (e.g., grinding, treating cracks and voids) as in external bonding applications; and (d) the procedure requires minimal installation time once the groove is cut (Paretti and Nanni 2004). Nevertheless, research on NSM FRP is limited, as compared to external bonding, and it still lacks design and construction guides (De Lorenzis and Teng, 2007).

CFRP has been used in most of the existing experimental work due to its superior strength and stiffness, with very few GFRP and almost no ARFP reinforcement. FRP bars can be manufactured in a variety of shapes such as round, square, rectangular, or oval; with smooth, sand-blasted, sand-coated, sprirally-wound or ribbed surface texture (De Lorenzis and Teng, 2007).

The effects of groove geometry on NSM FRP systems have been studied by various researchers. The most frequently studied parameters are shown in Figure 1, where W is the groove width, H is the groove depth, w is the FRP strip width, h is the FRP strip height, d_b is the FRP bar diameter, d_e is the distance from the groove edge to the member surface, d_g is the clear spacing between the grooves, and d_s is the distance from the centroid of the FRP reinforcement to the centroid of the tension steel. Paretti and Nanni (2004) suggested that the groove width (W) and depth (H) should be at least 1.5w and 3h for FRP strips, respectively, or $1.5d_b$ for FRP bars. De Lorenzis and Nanni (2002) recommended that the groove dimensions for the #3 and #4 bars should be at least 3/4 and 1 in., respectively.

Hassan and Rizkalla (2004) proposed that the clear spacing between the grooves should be at least twice the bar diameter, regardless of the groove width. They also suggested a minimum edge distance of four times the bar diameter to avoid excessive

stress concentrations near the edge. Using a finite element model, they further showed that the stresses in concrete decreased with the increasing groove width. The effect of epoxy type was also studied, but negligible differences in the ultimate loads were reported. In an earlier study by Hassan and Rizkalla (2003), it was noted that larger groove widths would result in larger debonding loads due to the increase in the interfacial area between the epoxy and concrete. The debonding loads would also increase for concretes with higher compressive strengths.

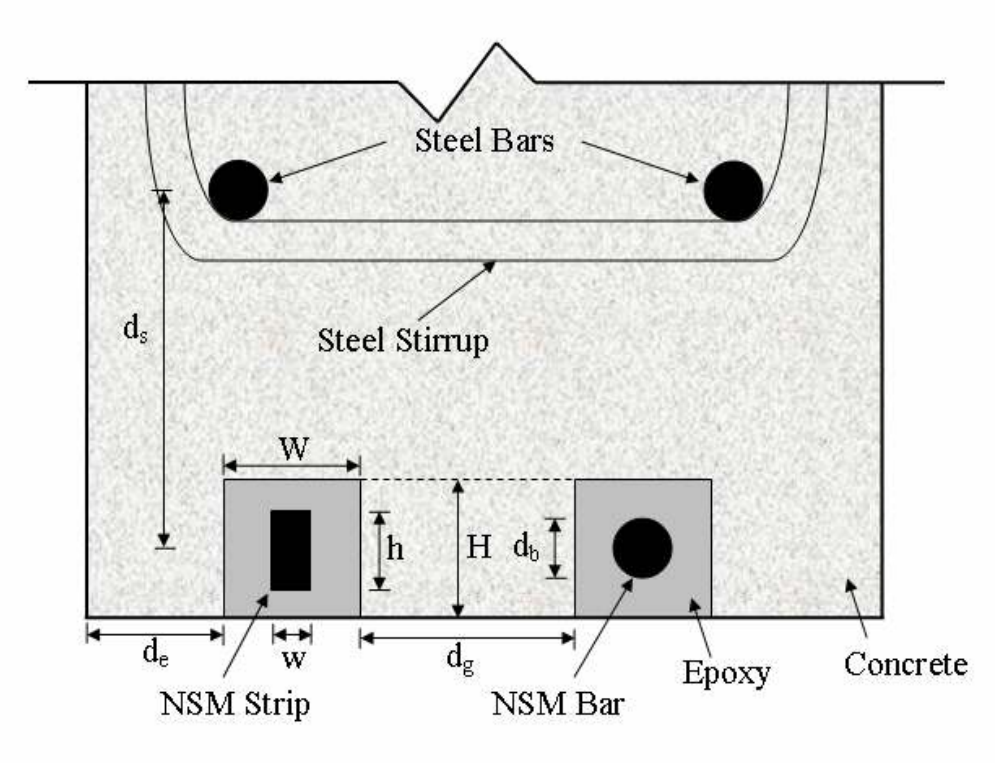

Figure 2.10 Groove Geometry

Novidis and Pantazopoulou (2007) observed an increase in the flexural strength for deeper grooves. Their study also showed that for the same area of NSM FRP reinforcement, flexural strength increases with the number of FRP strips.

Testing specimens with different amounts of NSM FRP, Barros et al. (2007) reported that strengthening efficacy, a measure of improved flexural strength, has an inverse relation with the FRP reinforcement ratio (ρ_f). Analyzing the available research data, they also reported that the ratio of the maximum to ultimate strains in FRP ($\varepsilon_{max}/\varepsilon_u$), increased with decreasing ρ_f and increasing d_g and d_e.

Kotynia (2007) reported that using high modulus NSM FRP increased the flexural strength, but reduced the $\varepsilon_{max}/\varepsilon_u$ ratio.

Although there is significant research data on bond characteristics of NSM FRP systems, the effect of groove size tolerance on the overall structural performance of retrofitted beams has not yet been studied.

2.2.2 Analysis of NSM FRP Systems

Prediction of flexural strength and the load-deflection response of a concrete beam strengthened with NSM FRP reinforcement follows the same procedure (ACI 440R2.02 2002), which was explained for EB FRP systems in Section 2.1.3. Basic assumptions include linear strain distribution through the cross-section, perfect bond between steel, FRP and concrete, and Whitney's rectangular stress block approximation of nonlinear compressive stress distribution in concrete. Yost et al. (2007) reported a simple approximate closed-form solution to predict the ultimate strength of singly reinforced concrete beams strengthened with NSM FRP for FRP rupture and concrete crushing failure modes. Stress-strain profiles are shown in Figure 2.11. Balanced FRP area was defined as the total amount of FRP, which must be provided for the simultaneous rupture in FRP and compression failure in concrete, as calculated by:

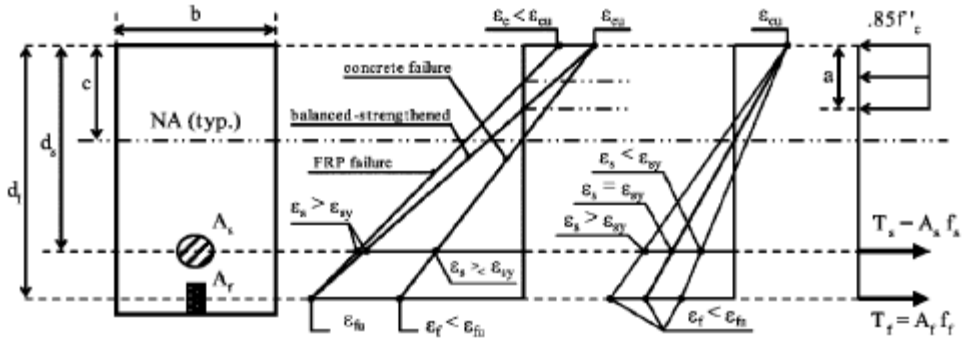

a) Cross Section **b) Strain Distribution** **c)Strain Distribution for Concrete failure** **d)Internal Forces**

Figure 2.11 Model Parameters

$$A_{fb} = \frac{0.85 f_c^{'} b \beta_1 d_f \left\{ \frac{\varepsilon_{cu}}{\varepsilon_{cu} + \varepsilon_{fu}} \right\} - A_S f_y}{f_{fu}} \tag{2.19}$$

where A_{fb} is the balanced FRP area, and d_f is the distance from the top fiber to the centroid of the NSM FRP.

For FRP rupture failure mode ($A_f < A_{fb}$), the depth of the rectangular stress block and the flexural strength are given by:

$$a = \frac{A_f f_{fu} + A_s f_y}{0.85 f_c^{'} b} \tag{2.20}$$

$$M_n = A_f f_{fu} (d_f - \frac{a}{2}) + A_s f_y (d_s - \frac{a}{2}) \tag{2.21}$$

For concrete crushing failure, steel and concrete strains were set to ε_{sy}, yield strain of steel, and ε_{cu}, respectively, and A_{sy} is given by:

$$A_{sy} = \frac{0.85 f_c^{'} b \beta_1 d_s \left(\frac{\varepsilon_{cu}}{\varepsilon_{cu} + \varepsilon_{sy}} \right) - A_f E_f \varepsilon_{sy} \left(\frac{d_f}{d_s} \right)}{f_y} \tag{2.22}$$

If $A_s < A_{sy}$, the assumption is valid, and a and M_n are then calculated by:

$$a = \frac{\sqrt{\left(A_f E_f \varepsilon_{cu} - A_s f_y\right)^2 + 4(0.85) f_c^{'} b \beta_1 A_f E_f \varepsilon_{cu} d_f} - (A_f E_f \varepsilon_{cu} - A_s f_y)}{(2)0.85 f_c^{'} b} \quad \textbf{(2.23)}$$

$$M_n = A_f f_f (d_f - \frac{a}{2}) + A_s f_y (d_s - \frac{a}{2}) \quad \textbf{(2.24)}$$

Otherwise, steel stress needs to be determined by trial and error. In either case, stress in FRP, f_f, is calculated from the strain compatibility.

2.2.3 Bond Issues

Local bond-slip behavior of FRP rebars in concrete has been studied by many researchers. Larralde and Silva-Rodriguez (1993) conducted a series of pull-out tests using spirally wound GFRP rebars in concrete blocks. Test results showed that bond strength of FRP bars was lower than that of identical steel bars, and the slip at failure was greater. An analytical study was carried out by Focacci et al. (2000) in order to determine model parameters for bond-slip relationships reported in the literature.

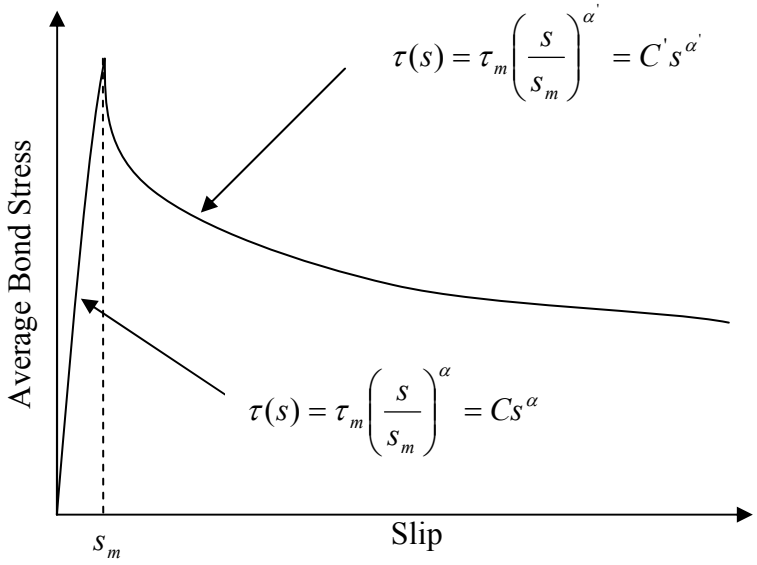

Figure 2.12 Typical Average Bond-Slip Curve

De Lorenzis et al. (2002) proposed the bond-slip relationship shown in Figure 2.12 for NSM FRP bars. In this model, τ_m is the maximum bond stress at the corresponding slip s_m, s is the slip, α, α', C and C' are the constants. Unlike the EB FRP, no explicit relationship exists to calculate the model parameters and constants for NSM FRP. Reported values for selected test cases of spriral wound bars from the study by De Lorenzis et al, (2002) are given in Table 2.2.

Table 2.2 Bond-Slip Parameters

Specimen	Bar diameter To groove width Ratio	τ_m (ksi)	s_m (mili in.)	α	α'	Embedment Length (x bar diameter)
SW/k1.25	1.25	1.38	9.69	0.58	-0.22	47
SW/k1.50	1.50	1.55	8.19	0.54	-0.25	34
SW/k2.00	2.00	1.19	7.40	0.69	-0.25	52
SW/k2.50	2.50	1.06	14.49	0.50	-0.24	42

CHAPTER 3

EXPERIMENTAL PROGRAM

The experimental program consisted of testing of reinforced concrete beam specimens retrofitted with pre-cured externally bonded (EB) or near surface mounted (NSM) FRP reinforcements. A total of 6 specimens were prepared for each of the four surface anomalies, namely: surface roughness, flatness, voids and cracks (cuts). For the groove size study in the NSM FRP systems 12 specimens were tested half with strips and the other half with bars. Experimental program was carried out in parallel with the study by Yalim (2008) within the scope of NCHRP Project 10-59B. Unless otherwise stated all beams were prepared with CSP 1 surface profile, as will be explained in Section 3.2.3.1.

3.1 Pre-Cured Systems

3.1.1 Specimen Details

A total of 7-ft long 12-in deep reinforced concrete T-beams were cost with a net flexural span of 6.5 ft. Longitudinal reinforcement consisted of 2 #5 bars at the top and 2 #3 bars at the bottom. Transverse reinforcement included #3 bars at 5 in. on center. Details of the cross sections are shown in Figure 3.1. Flexural span was selected such that shear failure would be prevented. Pre-cured CFRP was used for flexural strengthening, whereas wet lay-up CFRP laminate was used to provide anchorage in the form of U-straps. Flexural FRP was 67.5 in long and 2 in. wide. U-straps were 4 in. wide, and were

wrapped around the web with a total length of 24 in. Two U-straps were provided in each shear span. Schematics of the strengthened beams are shown in Figure 3.2.

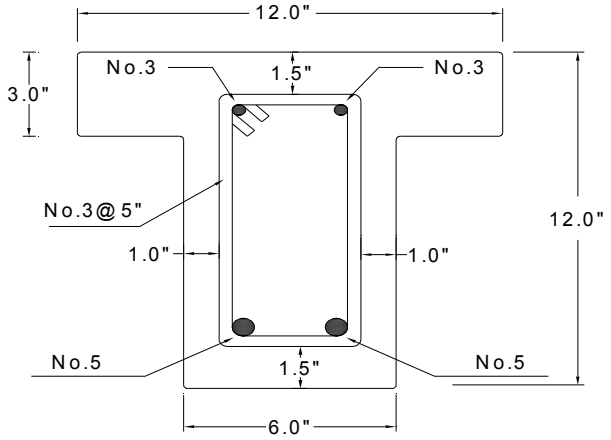

Figure 3.1 Specimen Cross Section

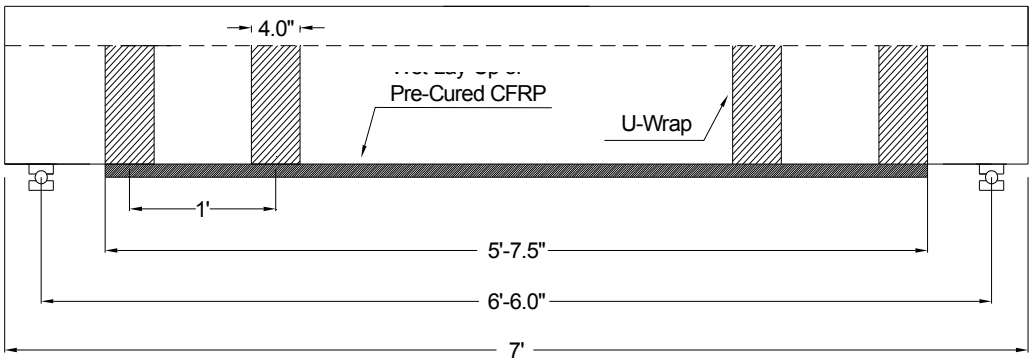

Figure 3.2 FRP-Strengthened Beam

Target concrete compressive strength was 5 ksi, and steel yield strength was 60 ksi. Cylinder tests were conducted to measure the actual concrete strength. All pre-cured specimens were made from two different batches of concrete. Beams for surface roughness and voids were made from the batch with measured a concrete strength of 5.03 ksi, whereas surface cracks and flatness specimens were cast from the batch with a measured concrete strength of 3.61. Different epoxies were used for the pre-cured and the

wet lay-up FRP systems, as required by the application guidelines provided by the manufacturers. A sand-based two-part epoxy was used for the pre-cured system. For the wet lay-up U-straps, a resin-based two-part epoxy adhesive was used. The epoxy resin for the wet lay-up U-straps acted as a binding and curing agent, unlike the pre-cured system for which the epoxy paste was only for binding. Unidirectional carbon FRP fabrics and laminates were used for the U-straps and the flexural pre-cured systems, respectively. Mechanical properties of the FRP and the epoxy used for the tests are shown in Table 3.1, as reported by their respective manufacturers.

Table 3.1 Mechanical Properties of the FRP and Epoxy

	FRP		Epoxy	
	Wet Lay-Up	**Pre-Cured**	**Wet Lay-Up**	**Pre-Cured**
Tensile Strength (ksi)	123.2	350	8	3.6
Tensile Modulus (ksi)	10,240	19,000	250	650
Elongation at Break (%)	1.12	1.87	3	1
Unit Tensile Strength (lb/in.)	4,928	-	-	-
Width (in.)	-	2	-	-
Thickness (in.)	0.040	0.055	-	-

3.1.2 Test Setup and Instrumentation

Test setup and instrumentation for all pre-cured specimens were same. The FRP-strengthened beams were tested in 3-point flexure. A 60-kip capacity self-reacting frame was designed for the tests. Load was applied using a 10,000 psi capacity hydraulic jack at the mid-span, and was monitored using a 50-kip capacity load cell. Three 1.5 in.-stroke string potentiometers were placed at quarter points for deflection measurement. A single electrical resistance foil type strain gage was attached at the mid-span on the main flexural FRP. Load was applied using a hand pump. Test setup and instrumentation are shown in Figure 3.3.

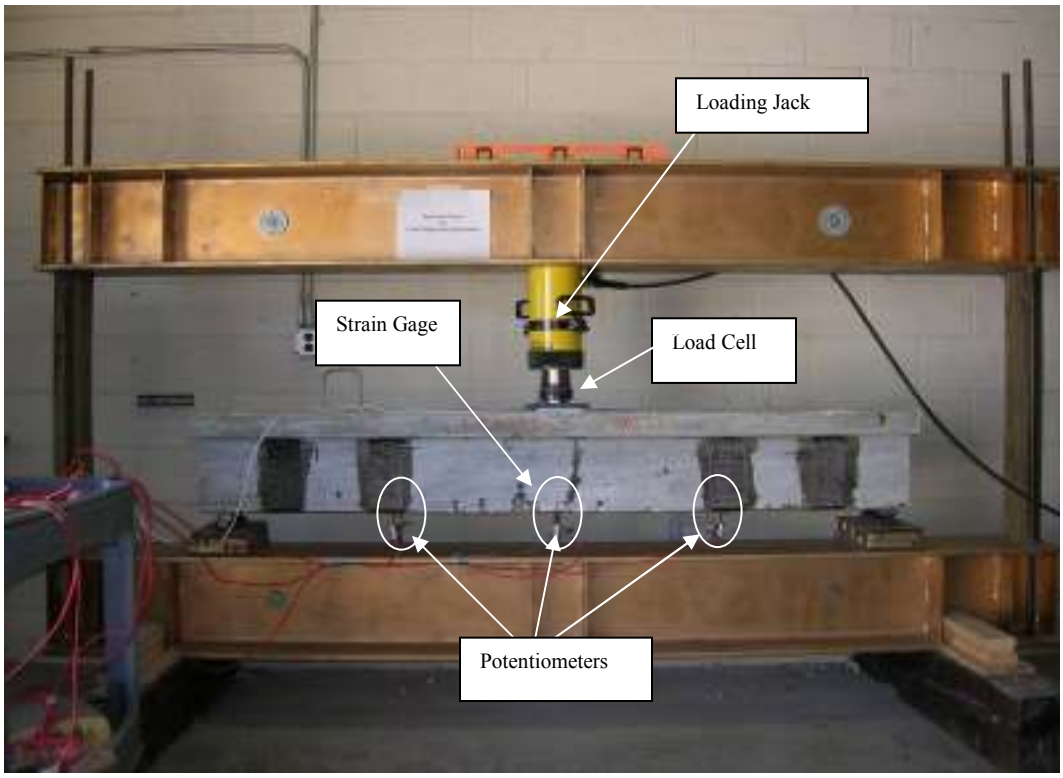

Figure 3.3 Test Setup and Instrumentation for the Pre-Cured Specimens

3.1.3 Specimen Preparation

3.1.3.1 Surface Roughness

Cross sectional details of the formwork used for the test specimens are shown in Figure 3.4. Formwork was made using 3/4 in. thick plywood and 2 in. x 4 in. timber for support. The inside of the forms were covered by 1/16 in. thick metal sheets to provide smooth concrete surface and easy formwork removal. Final assembly of the steel cages was carried out in the lab. The formwork with the steel cage is shown in Figure 3.5. A total of 12 beams were cast from each batch of concrete delivered in ready-mix truck. After casting, all beams were covered with plastic sheets, and were allowed to cure for 7 days in the outside environment.

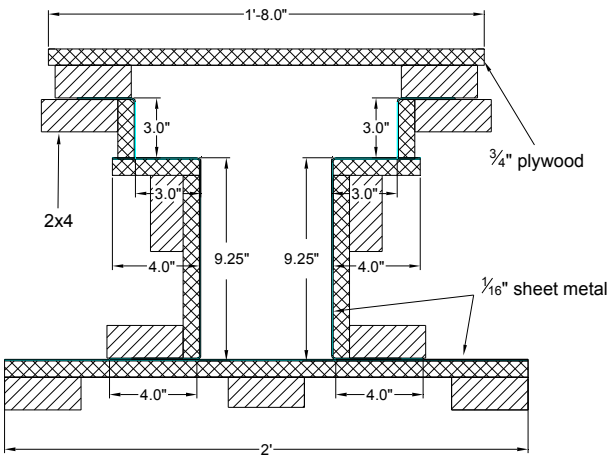

Figure 3.4 Formwork Cross Section

Figure 3.5 Formwork and Steel Cage

A total of 6 specimens were tested for the surface roughness study with the test matrix shown in Table 3.2. Three different levels of surface roughness were introduced in the specimens. Concrete surface profiles utilized for this study are shown in Figure 3.6. ICRI 2-3 represents a range between CSP 2 and 3, and ICRI 6-9 represents a range between CSP 6 to 9.

The major challenge in preparing the specimens was to concrete surface profiles using a consistent application procedure. The ICRI 1 and ICRI 2-3 surface profiles were produced using a 4-in. angle grinder, whereas the ICRI 6-9 surface profile was produced using a 3.5 ksi pressure washer applied at a distance of 2 in. and at an angle of 45^{o}.

Table 3.2 Test Matrix for Surface Roughness

Concrete Surface Profile (ICRI)	Number of Specimens
ICRI 1	2
ICRI 2-3	2
ICRI 6-9	2
Total	**6**

a) ICRI 1

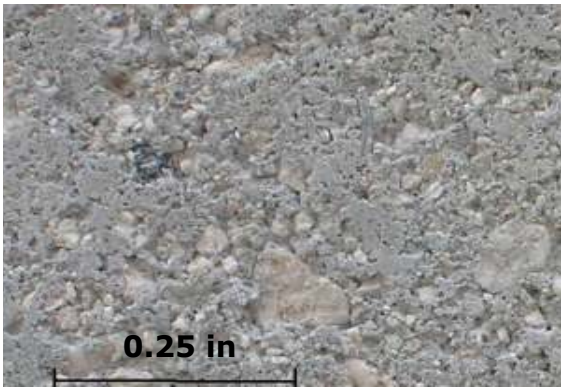

b) ICRI 2-3

c) ICRI 6-9

Figure 3.6 Concrete Surface Profiles used in Present Study

Following surface preparation to the desired level of roughness, exact locations for the pre-cured laminates were marked. The boundaries of the marked lines were taped. A thin layer of epoxy was applied on the beam surface. Using an in-house built special equipment, as shown in Figure 3.7 (e), a thin layer of epoxy was applied onto one face of the pre-cured laminate. The laminate was then placed onto the beam, and a roller was used to ensure its proper bond. The tapes were then removed. More epoxy was applied to taper the surface at the locations of U-straps. The next day after the epoxy was cured, U-straps were applied using the respective epoxy resin. The step-by-step procedure is shown in Figure 3.7.

3.1.3.2 Surface Flatness

Previous research on the effect of surface flatness on wet lay-up FRP systems showed that the NCHRP Report 514 (Mirmiran et al. 2004) limit of 1/8 in. for the depressions to be filled was unconservative and was needed to be revised as 1/16 in. (Yalim 2008). Having this information, it was decided to verify the 1/16 in. out-of-flatness for the pre-cured FRP specimens. The test matrix is shown in Table 3.3.

Table 3.3 Test Matrix for Surface Flatness

Type of out-of-flatness	Number of Specimens
1/16 in. (Valley)	2
1/16 in. (Peak)	2
0 (level) - Control	2
Total	**6**

a) Marking

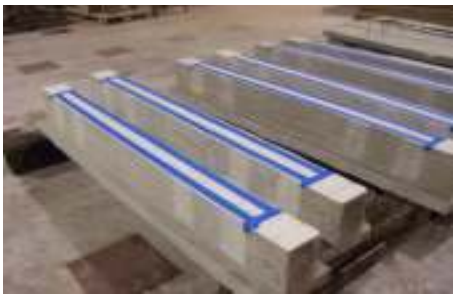

b) Taping

c) Epoxy Mixing

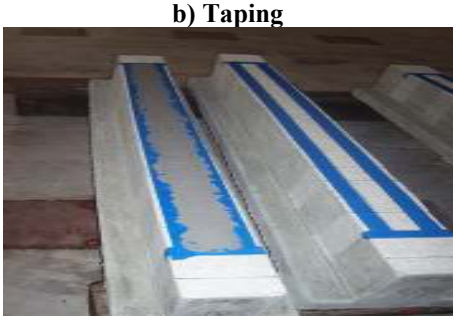

d) Epoxy Applied on the Beams

e) Epoxy Applied on the Laminate

f) Laminate Placed and Tapes Removed

g) Rolling to Ensure No Air Entrapment

h) Tapering for the U-Straps

i) Close-up of U-Strap Taper

j) U-Strap Application

Figure 3.7 Pre-cured FRP Application Procedure

A total of 6 specimens were tested for surface flatness, of which two were control (level), two with valleys and two with peaks of 1/16 in., each. Sketches of valley and peak specimens are shown in Figure 3.8. Shaded portions represent the removed concrete. The FRP-strengthened beam with surface out-of-flatness is shown schematically in Figure 3.9.

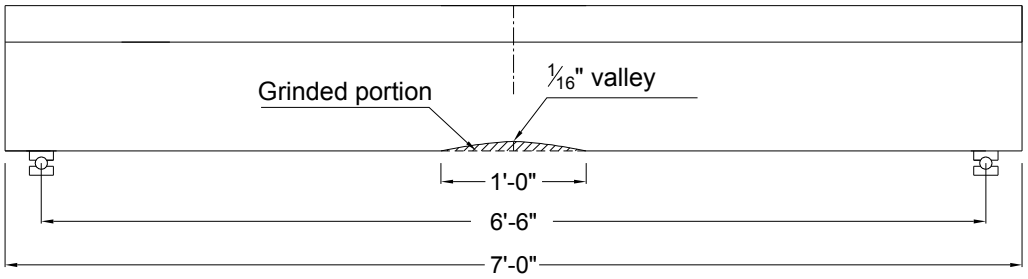

(a) Valley Specimen

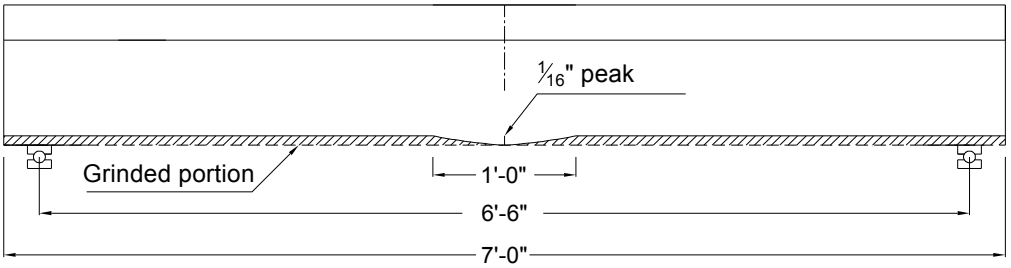

(b) Peak Specimen

Figure 3.8 Surface Flatness Specimens

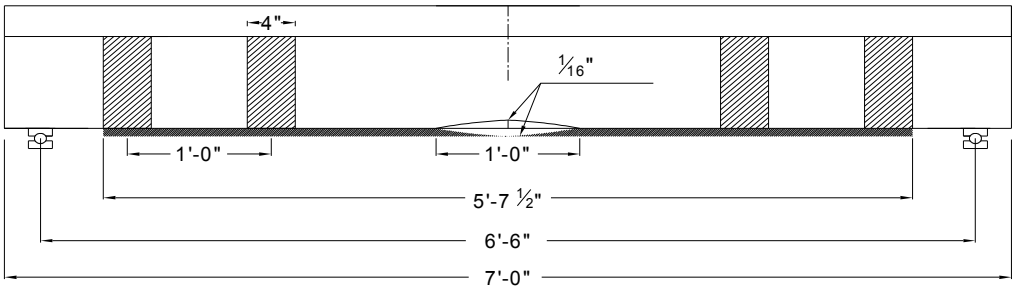

Figure 3.9 FRP-Strengthened Beam with Surface Out-of-Flatness

Concrete surface profile generated for all surface flatness specimens was CSP 1, using a 4 in. diameter angle grinder. First, a 12 in. long section was marked in the middle of the beam. Then, using the angle grinders the excess concrete was removed to obtain the desired level of out-of-flatness in the form of valley or peak. This procedure is shown in Figure 3.10.

Figure 3.10 Surface Flatness Preparation by Grinding

Two side views of the beams with valley and peak are shown in Figure 3.11.

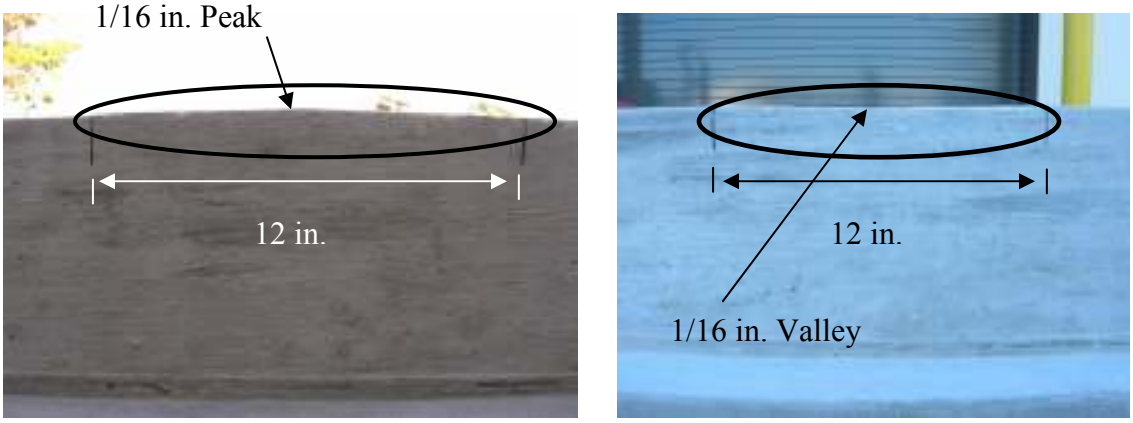

(a) 1/16 in. Peak **(b) 1/16 in. Valley**

Figure 3.11 Concrete Surface Peaks and Valleys

After the desired out-of-fatness was generated on the concrete surface, the FRP system was installed following the same procedure outlined in Section 3.2.3.1.

3.1.3.3 Surface Voids

The test matrix for surface voids is shown in Table 3.4. All voids were drilled with circular section. Three parameters were identified; depth, diameter and frequency. The void frequency was kept constant at 5% as the trial study by Yalim (2008) showed that any frequency above 5% is not viable for testing and requires section restoration. The 2.5, 5 and 10% frequency void patterns for the 12 in. long section are shown in Figure 3.12. Void depth was also identified to be insignificant based on the test results from the study by Yalim (2008). Void diameter was therefore the major focus of the study.

(a) 2.5% Frequency

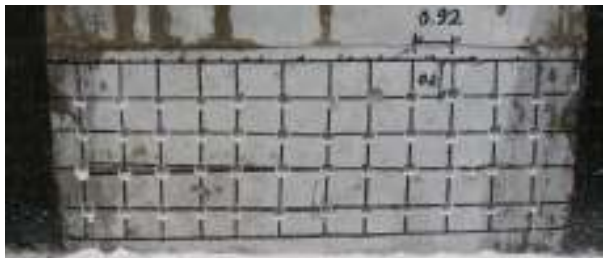

(b) 5% Frequency

(c) 10% Frequency

Figure 3.12 Different Void Frequencies

Table 3.4 Test Matrix for Surface Voids

Void Diameter (in.)	Number of Specimens
1/4	2
3/8	2
1/2	2
Total	**6**

Voids were drilled on the beam soffit using the appropriate drill size over the area where the pre-cured laminate would be placed. Void patterns for a 12-in. long segment of the beam with different diameters are shown in Figure 3.13. Criteria for the void pattern formation was to avoid weak paths which may lead to cracking and cover delaminations.

After the voids were drilled in the pre-determined pattern, the surface was cleaned from dust and loose particles, and the FRP application procedure explained in Section 3.2.3.1 was followed.

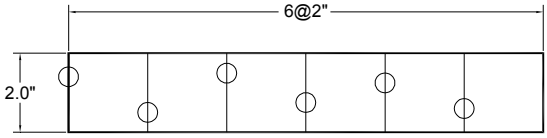

a) 1/2 in. Diameter

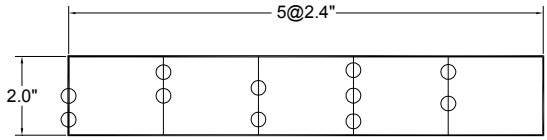

b) 3/8 in. Diameter

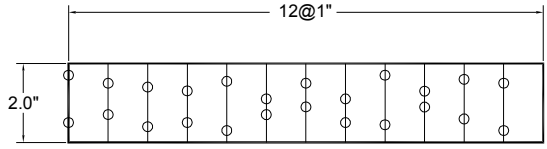

c) 1/4 in. Diameter

Figure 3.13 Void Patterns for 12 in.-Length

3.1.3.4 Surface Cracks (Cuts)

For the surface crack study, crack width, the major parameters were identified as; depth and frequency. Yalim (2008) reported that crack width and depth were not as

dominant as the frequency. The present study, therefore, focused on crack frequency for pre-cured FRP systems, using the test matrix shown in Table 3.5.

Table 3.5 Test Matrix for Surface Cracks

Crack Spacing (in.)	Number of Specimens
1	2
1.5	2
2	2
Total	**6**

The crack depth and width for all specimens were 1/4 in. and 1/16 in., respectively. A hand saw with 4 in. diameter and 1/16 in. thick masonry blade was used to generate cuts on the beam surface. Figure 3.14 shows a view of a beam with the intentional surface cracks.

Figure 3.14 Typical Crack Profile with 1 in. Spacing

Figure 3.15 Surface Crack Beams Prior to Testing

After the cracks were made, the typical procedure for FRP application was followed, as described in Section 3.2.3.1. Two of the beams are shown in Figure 3.15.

3.1.4 Test Results

3.1.4.1 Surface Roughness

Test results for the surface roughness specimens are presented in the order of the smoothest to the roughest surface. Figures 3.16-3.21 show the load-deflection and load-strain responses for CSP 1, CSP 2-3 and CSP 6-9 specimens. The average response curve for each group of specimens is also shown in each figure. Figures 3.22 and 3.23 show the load-deflection and load-strain responses, respectively for all specimens. In all figures, loads were normalized with respect to the target concrete compressive strength of 5 ksi, and based on the flexural strength of the section.

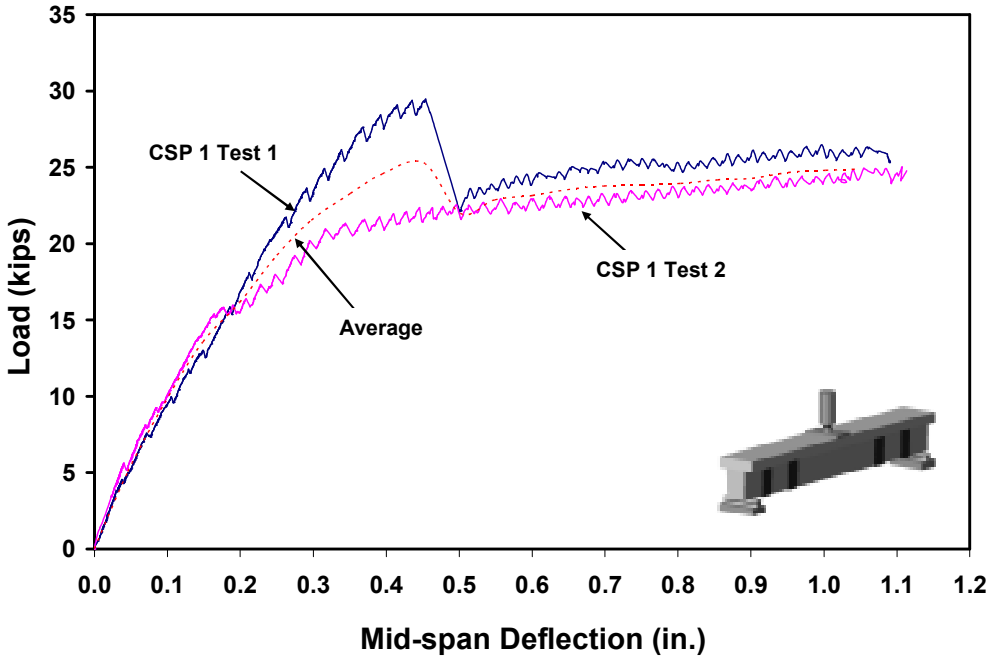

Figure 3.16 Load-Deflection Responses for Pre-Cured FRP Specimens with CSP 1

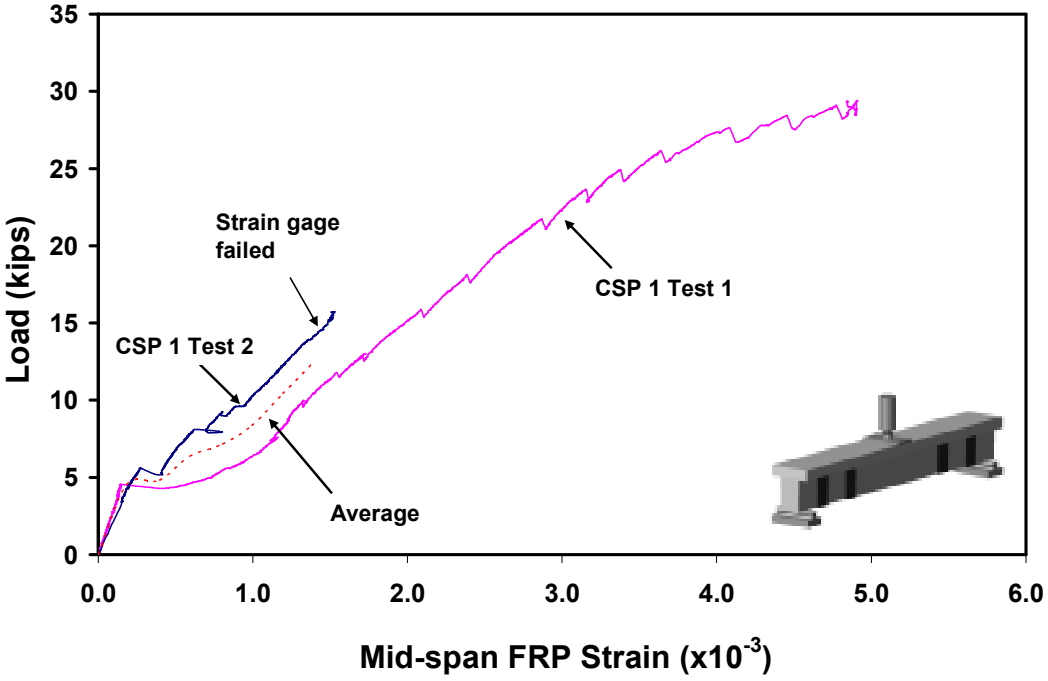

Figure 3.17 Load-Strain Responses for Pre-Cured FRP Specimens with CSP 1

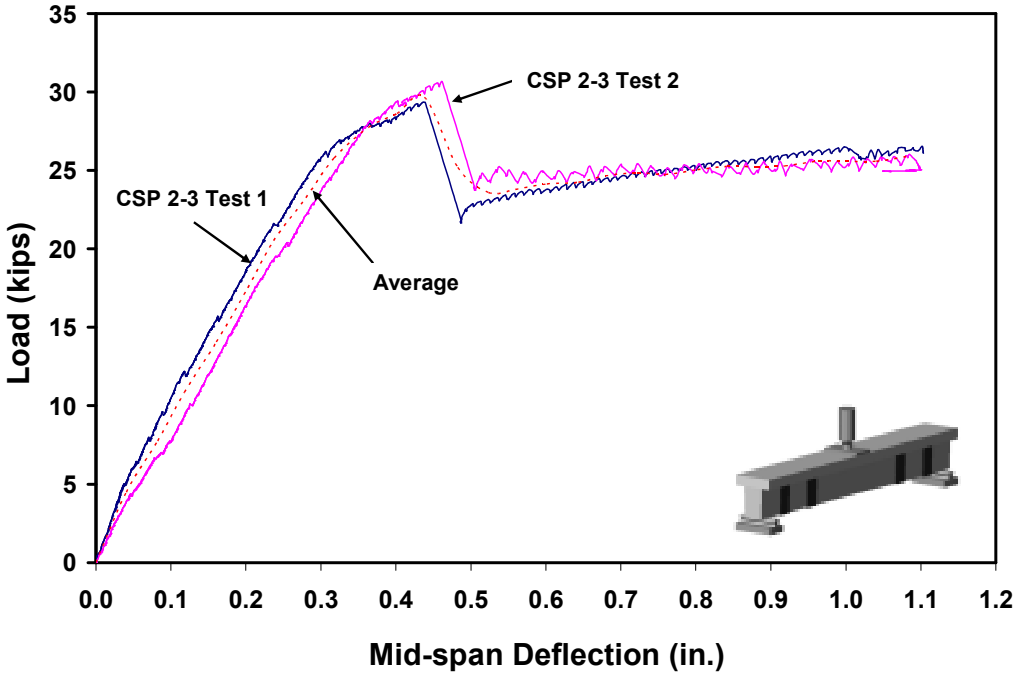

Figure 3.18 Load-Deflection Responses for Pre-Cured FRP Specimens with CSP 2-3

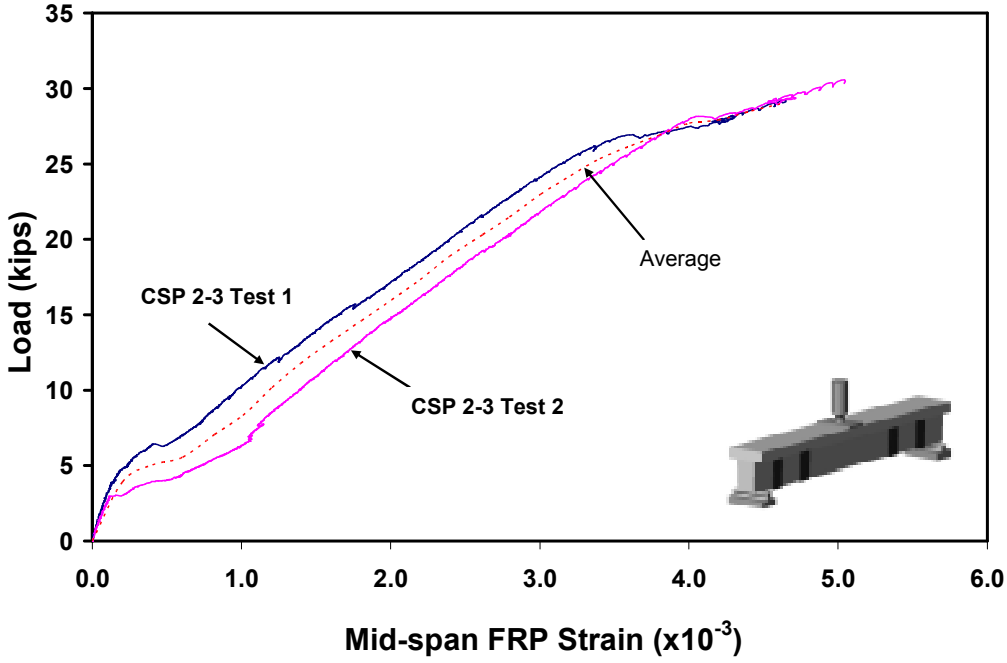

Figure 3.19 Load-Strain Responses for Pre-Cured FRP Specimens with CSP 2-3

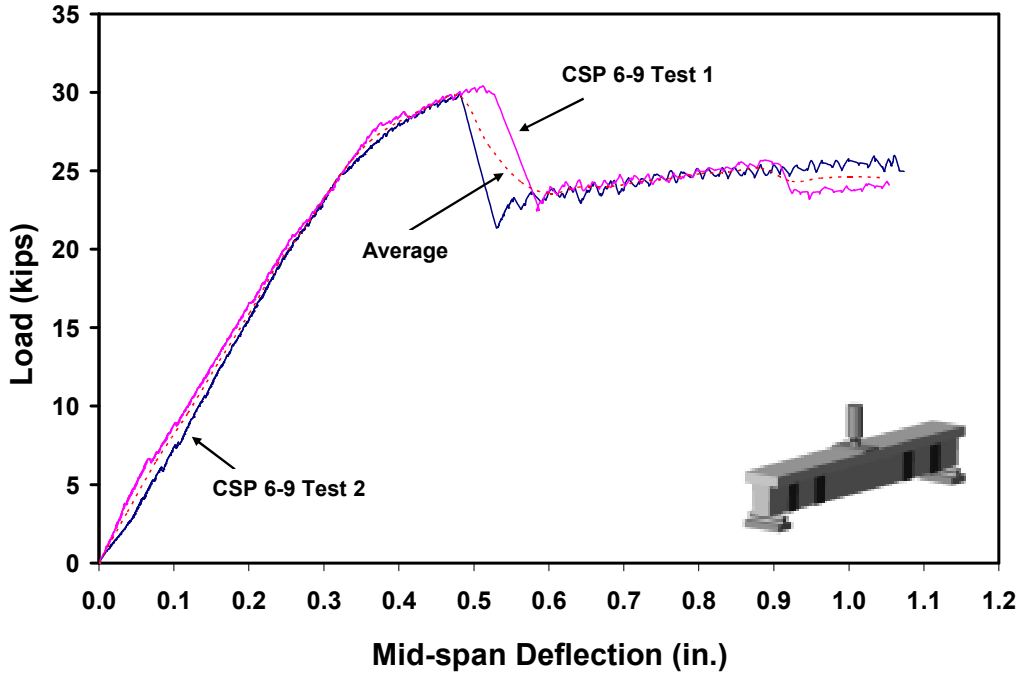

Figure 3.20 Load-Deflection Responses for Pre-Cured FRP Specimens with CSP 6-9

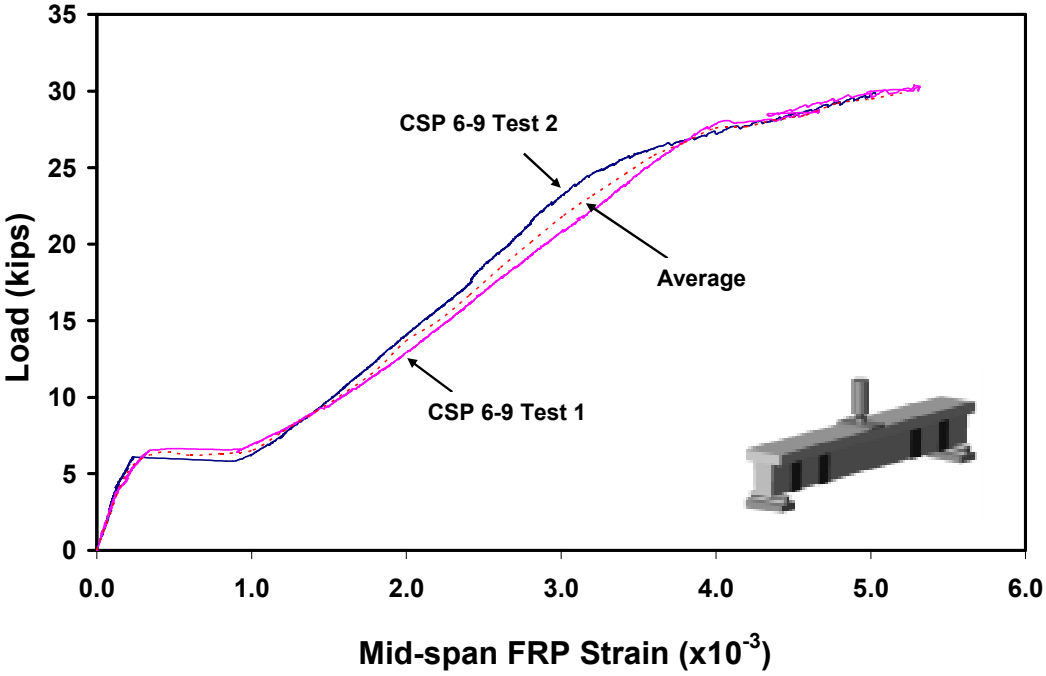

Figure 3.21 Load-Strain Responses for Pre-Cured FRP Specimens with CSP 6-9

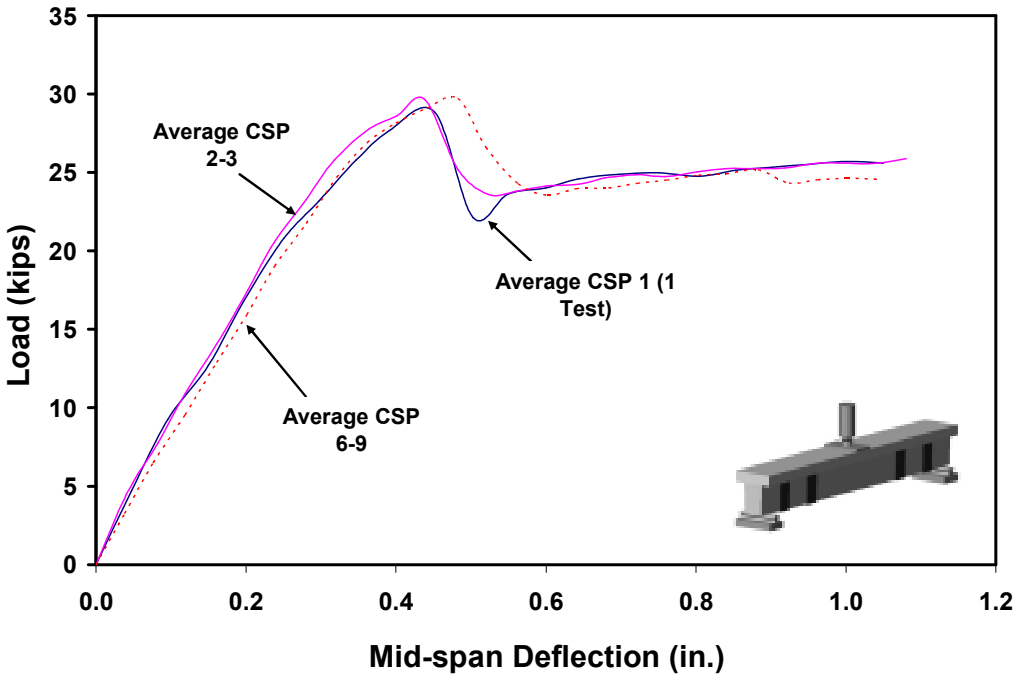

Figure 3.22 Load-Deflection Responses for Pre-Cured FRP Specimens with Different Surface Roughness

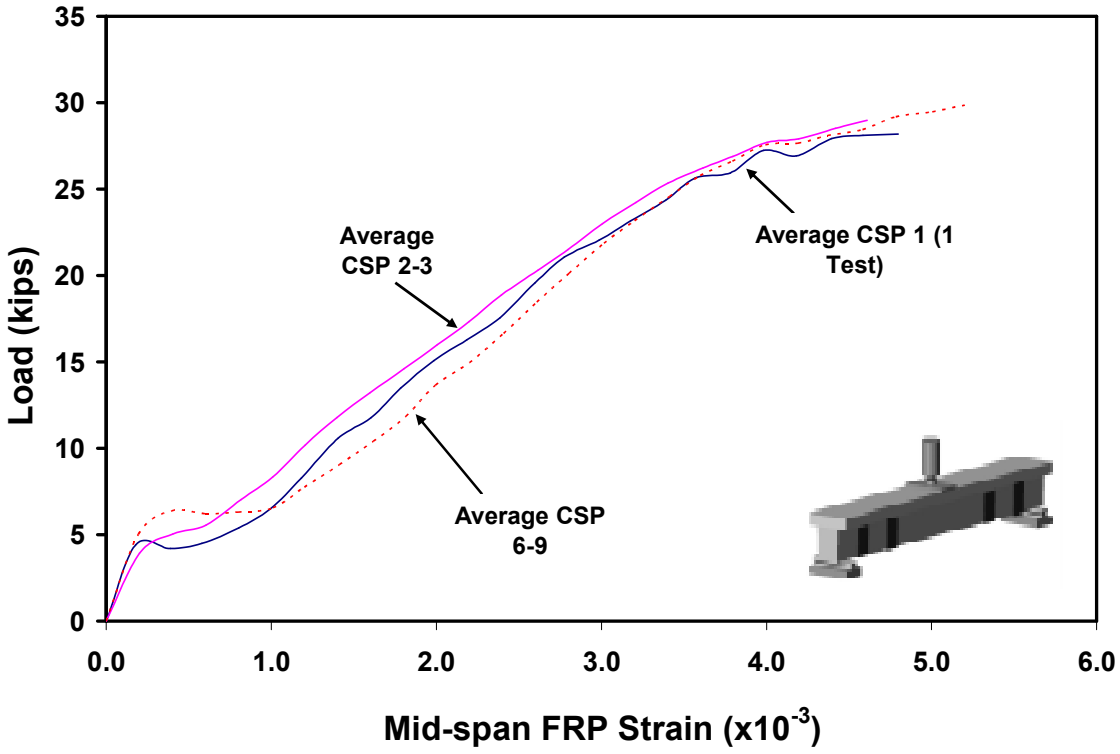

Figure 3.23 Load-Strain Responses for Pre-Cured FRP Specimens with Different Surface Roughness

From Figures 3.22 and 3.23, it is clear that load-deflection and load-strain responses for all pre-cured FRP specimens were quite similar, regardless of the surface roughness level. It should be noted that results were shown for only one CSP 1 test, because of gage failure during the other test. All specimens had a peak at around 30 kips, which is then followed by a sudden drop. This is due to delamination of the main flexural FRP strip, which initiates at the mid-span and propagates towards the supports. U-straps, however, stopped the propagation, before complete delamination occured. Anchored at both ends by the U-straps, the pre-cured FRP then acted as a tension member and still sustained limited load, with the beam acting as a tied arch. Post delamination behavior is

not studied within the scope of this study. Test results for the surface roughness specimens are also listed in Table 3.6.

Table 3.6 Test Results for Surface Roughness Specimens

Concrete Surface Profile (CSP)	Specimen No.	Normalized Peak Load (kips)	Displacement at Peak Load (in.)	FRP Strain at Peak Load ($x10^{-3}$)
1	1	29.5	0.454	4.842
	2	26.6	N/A	Gage Failed
2-3	1	29.3	0.437	4.598
	2	30.7	0.462	5.076
6-9	1	29.9	0.482	5.027
	2	30.4	0.512	5.281

The FRP strain at the peak load for all specimens was about 5 mili-strains. Although some difference can be seen when the mid-span displacement at peak load values are compared, no apparent trend could be identified. Overall, Table 3.7 shows no strong relationship between the surface roughness level and the performance of pre-cured FRP specimens. The common failure mode for all surface roughness specimens was FRP debonding, as shown in Figure 3.24.

Figure 3.24 Typical Failure Mode for the Pre-Cured FRP Specimens with Different Surface Roughness

3.1.4.2 Surface Flatness

Load-deflection and load-strain responses for control (flat or level) specimens are shown in Figures 3.25 and 3.26, respectively. Failure mode for control specimens is shown in Figure 3.27.

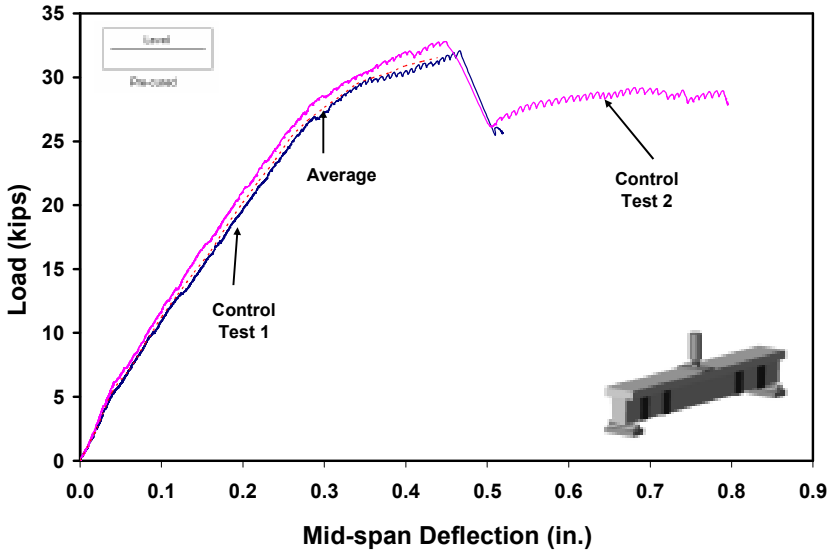

Figure 3.25 Load-Deflection Responses for Control (Level) Specimens

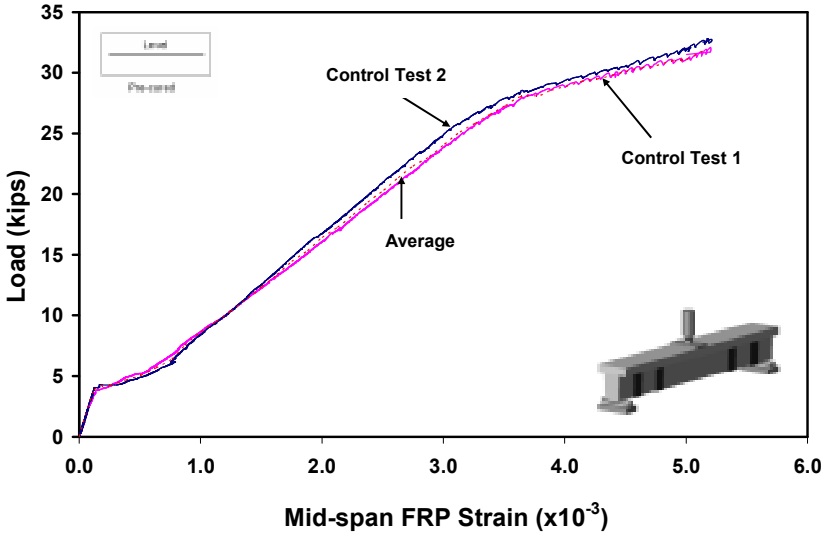

Figure 3.26 Load-Strain Responses for Control (Level) Specimens

As shown in Figures 3.25 and 3.26, behavior of control specimens is quite repeatable. The failure mode for both control beams was FRP debonding at the bond line, as shown in Figure 3.27. Debonding initiated at the mid-span and propagated to the ends as a result of flexure-shear cracks. As the load increased, these cracks opened wider, and led to a relative vertical displacement between the faces of the crack. This developed some force on the laminate, which eventually led to loss of bond between the concrete and the laminate at the concrete-FRP bond line. Debonding was stopped by the U-straps, however, only after a significant load drop was observed. A thin layer of concrete adhered to FRP when debonding occurred. Load-deflection and load-strain graphs for the peak specimens are shown in Figures 3.28 and 3.29, respectively. The averages for peak specimens are compared to their control counterparts in Figures 3.30 and 3.31. Representative failure modes for peak specimens are shown in Figure 3.32.

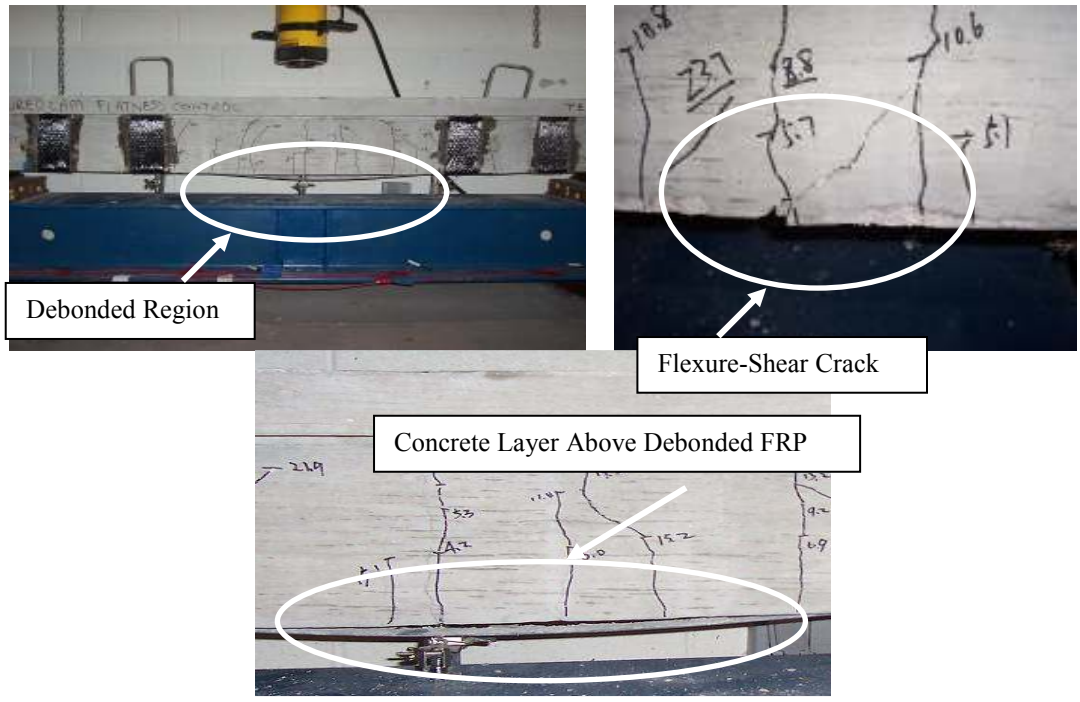

Figure 3.27 Failure Mode of Pre-Cured Control (Level) Specimens

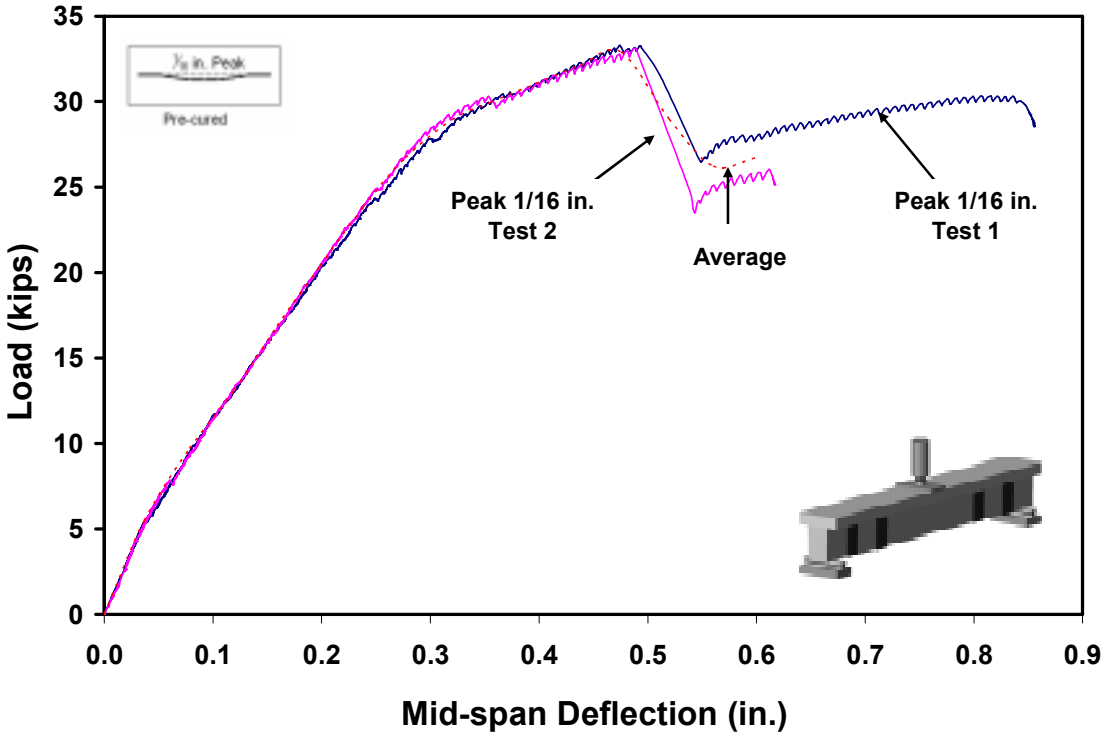

Figure 3.28 Load-Deflection Responses for Peak Specimens

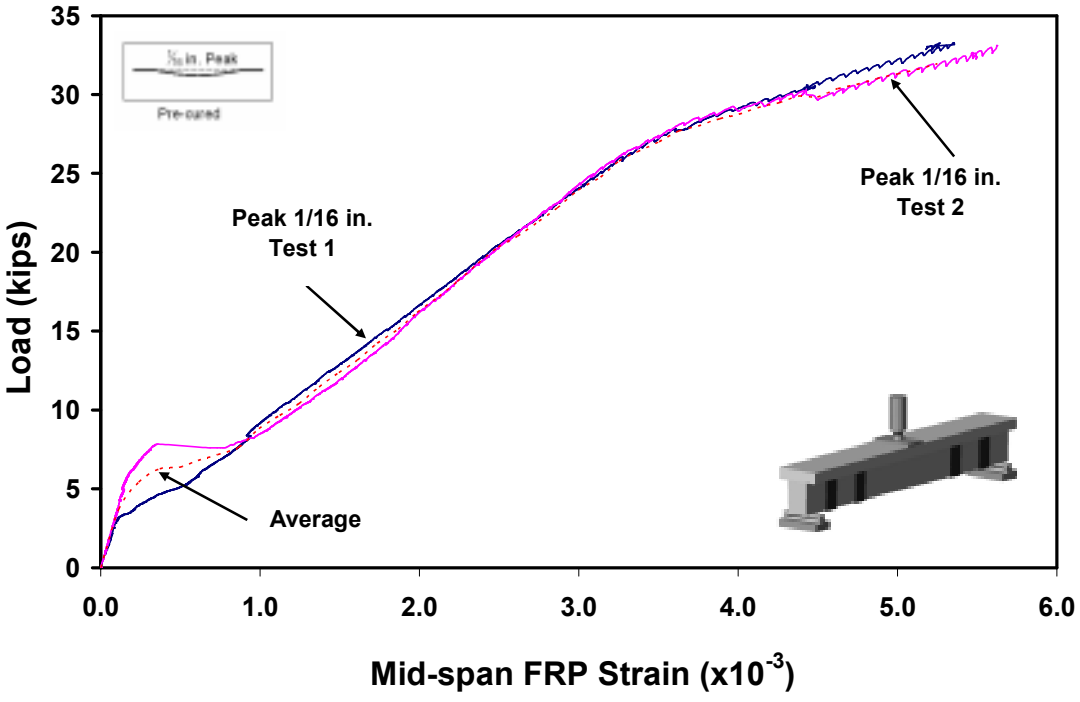

Figure 3.29 Load-Strain Responses for Peak Specimens

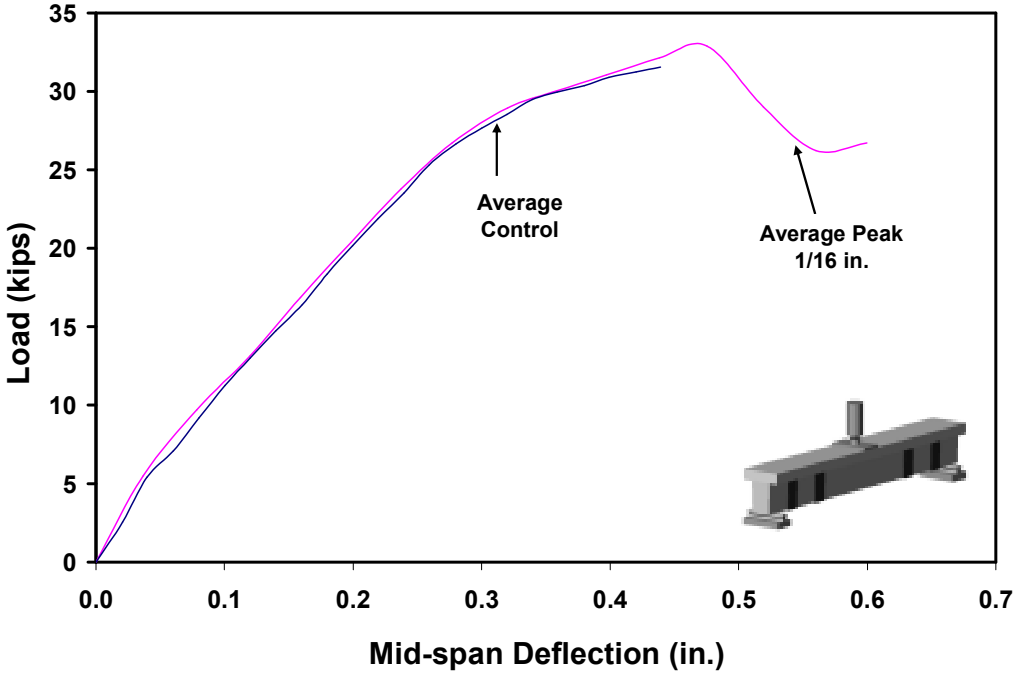

Figure 3.30 Load-Deflection Responses for Control and Peak Specimens

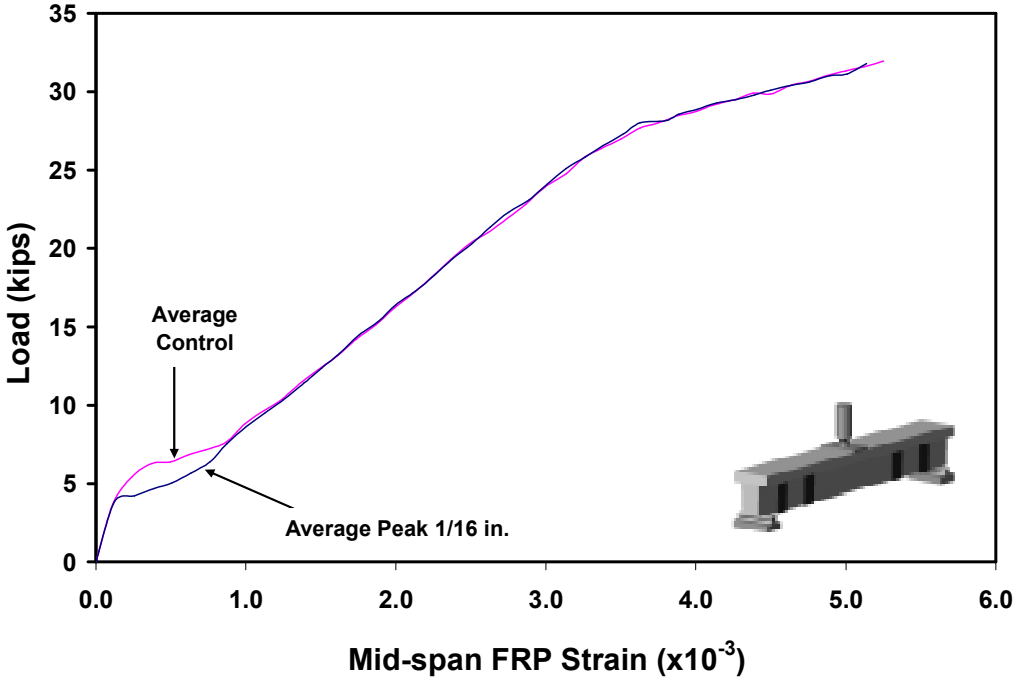

Figure 3.31 Load-Strain Responses for Control and Peak Specimens

(a) General View (b) Debonded Laminate and Beam Soffit

Figure 3.32 Failure Mode of Peak Specimens

Load-deflection diagrams for the 1/16 in. peak specimens are almost identical to the control specimens. Test results for the control and peak specimens are summarized in Table 3.7. Loads were normalized with respect to the target concrete compressive strength of 5 ksi (35 MPa), based on the flexural strength of the section.

Table 3.7 Summary Results for Control and Peak Specimens

Out-of-Flatness Level	Specimen No.	Normalized Peak Load (kips)	Displacement at Peak Load (in.)	FRP Strain at Peak Load ($x10^{-3}$)
1/16 in. Peak	1	33.3	0.475	5.355
	2	33.1	0.488	5.623
Control	1	32.1	0.466	5.202
	2	32.8	0.448	5.175

Load-deflection and load-strain graphs for valley specimens are shown in Figures 3.33 and 3.34, respectively. The averages for valley specimens are compared to their control counterparts in Figures 3.35 and 3.36.

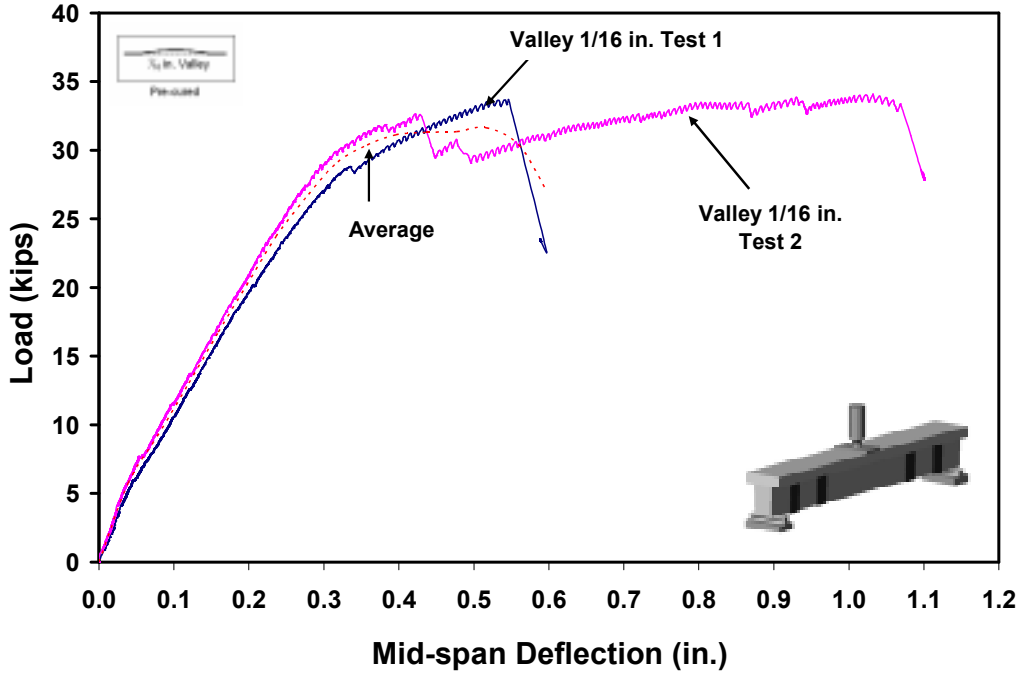

Figure 3.33 Load-Deflection Responses for Valley Specimens

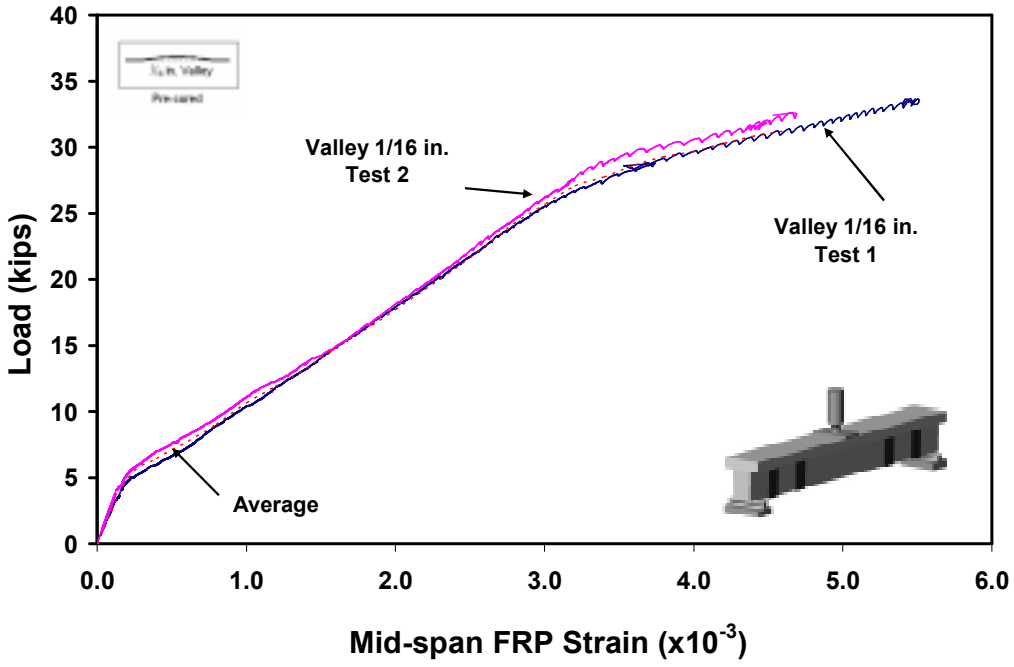

Figure 3.34 Load-Strain Responses for Valley Specimens

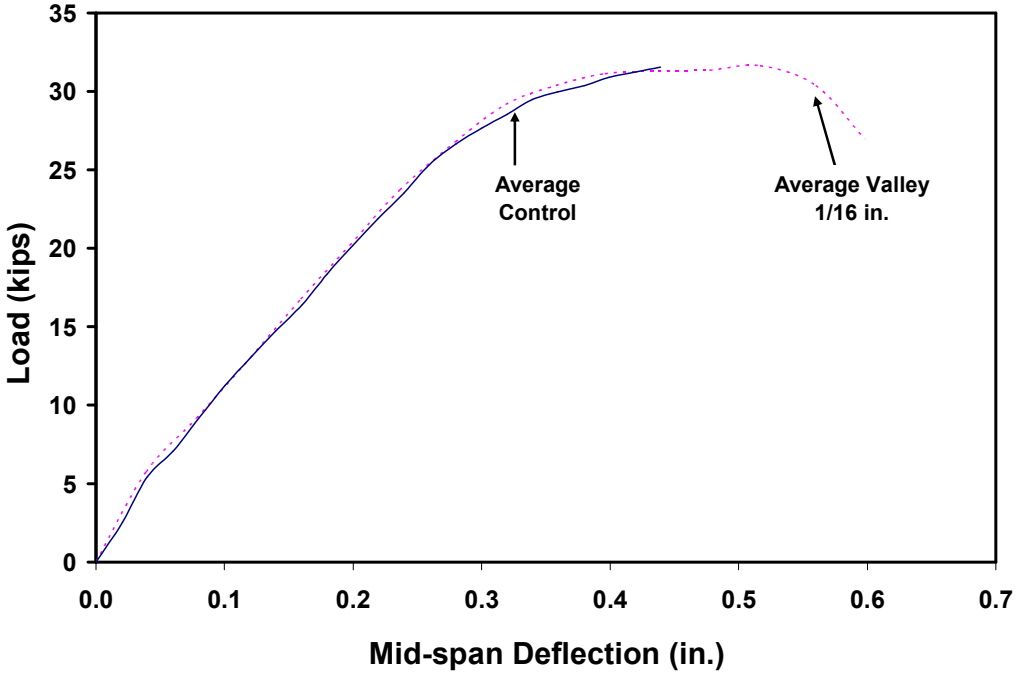

Figure 3.35 Load-Deflection Responses for Control and Valley Specimens

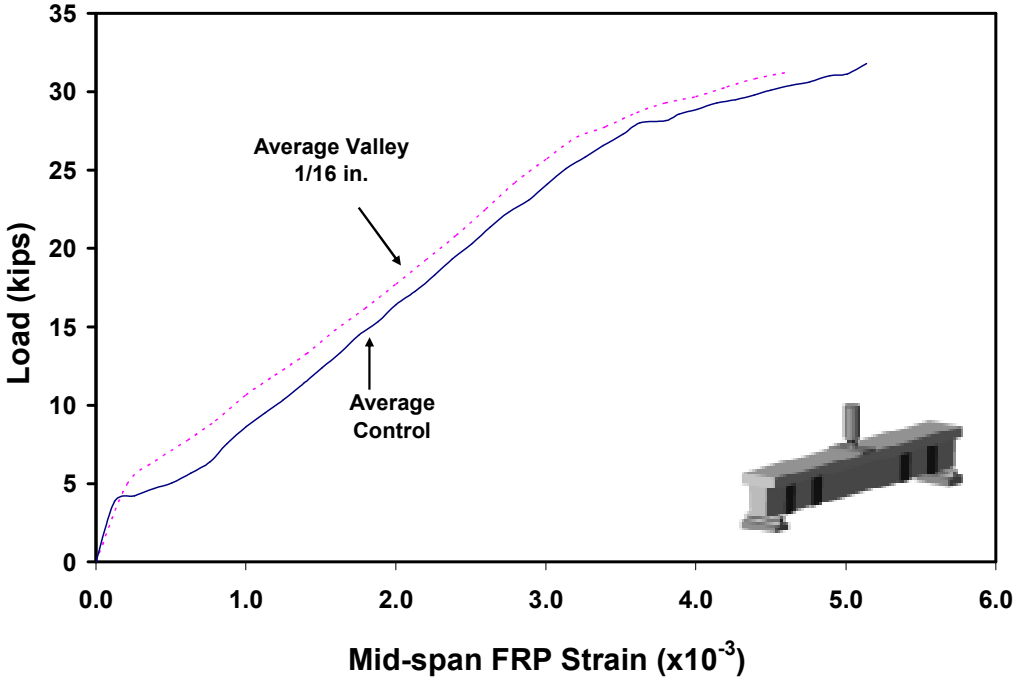

Figure 3.36 Load-Strain Responses for Control and Valley Specimens

Failure mode in both valley specimens was FRP debonding, similar to the control specimens, as shown in Figure 3.37.

Figure 3.37 Failure Mode of Valley Specimens

Test results for the control and valley specimens are summarized in Table 3.8. In general, load-strain responses for all six pre-cured FRP specimens were quite similar, regardless of the type of out of flatness. Valley specimens showed slightly lower FRP strains than those for the peak and control specimens at the same load level, perhaps because the curvature of the valley is opposite of the bending curvature of the beam.

Table 3.8 Summary Results for Control and Valley Specimens

Out-of-Flatness Level	Specimen No.	Normalized Peak Load (kips)	Displacement at Peak Load (in.)	FRP Strain at Peak Load ($x10^{-3}$)
1/16 in. Valley	1	33.7	0.546	5.486
	2	34.1	0.422	4.690
Control	1	32.1	0.466	5.202
	2	32.8	0.448	5.175

3.1.4.3 Surface Voids

Tests results are presented in the order of the smallest void diameter to the largest. The void depth was kept at 1/8 in. for all specimens. Load-deflection and load-strain

responses for the 1/4, 3/8 and 1/2 in. void diameter specimens are shown in Figures 3.38-3.43, respectively. The figures show that the stiffness of the similar specimens are generally the same, while their ultimate loads are slightly different. The average load-deflection and load-strain responses for each group of specimens are shown in Figures 3.44 and 3.45, respectively. From these two figures, it can be seen that all six specimens behaved quite similarly, regardless of their different void diameters. Table 3.9 summarizes the peak responses for the pre-cured specimens with voids. For comparison, the peak responses are averaged in Table 3.10.

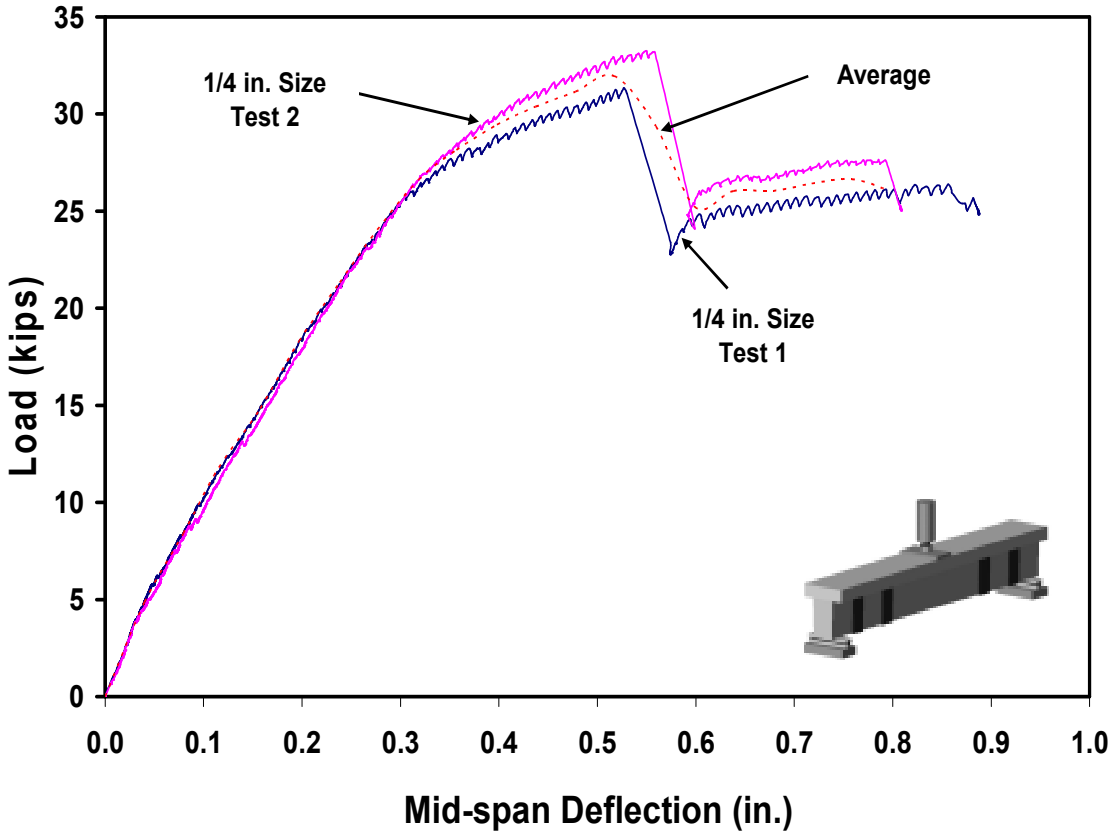

Figure 3.38 Load-Deflection Responses for 1/4 in. Void Diameter Specimens

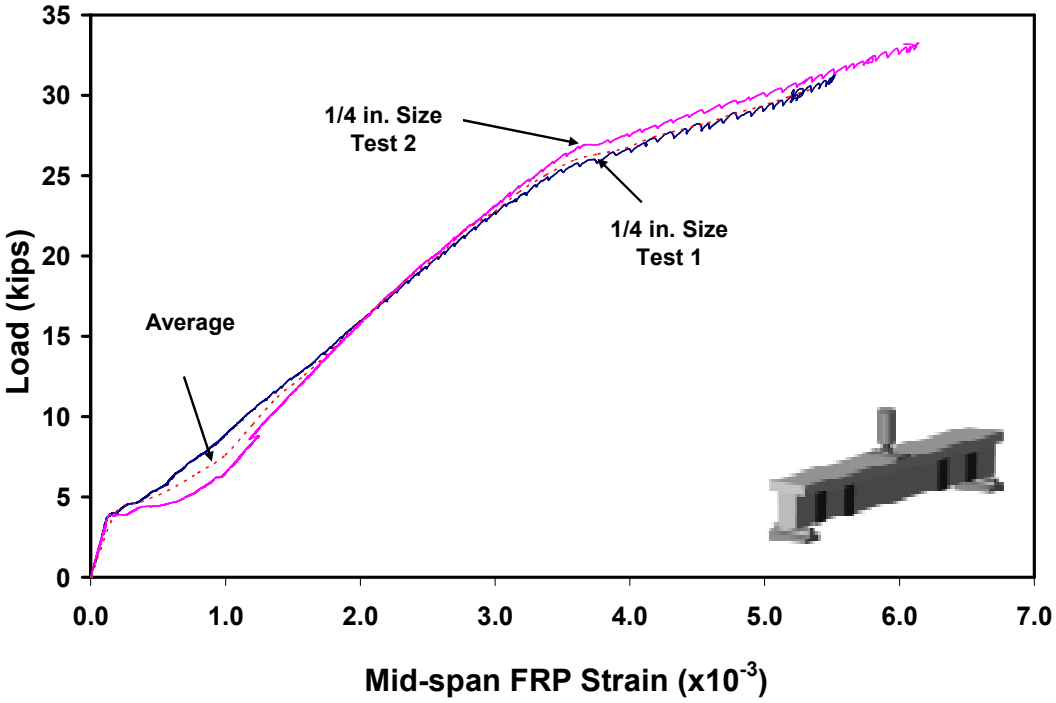

Figure 3.39 Load-Strain Responses for 1/4 in. Void Diameter Specimens

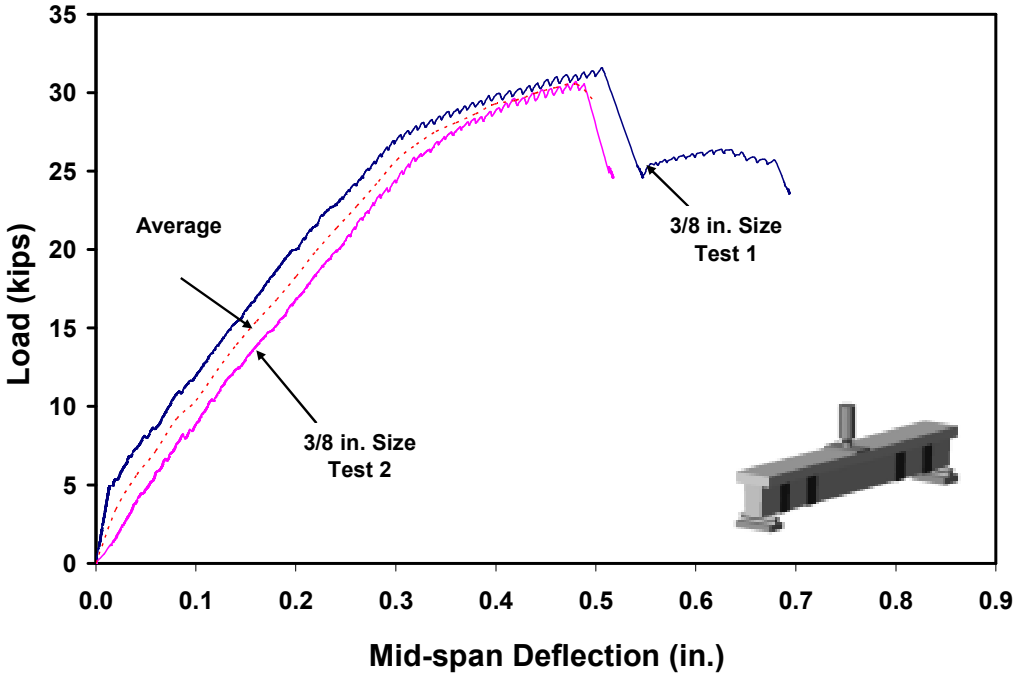

Figure 3.40 Load-Deflection Responses for 3/8 in. Void Diameter Specimens

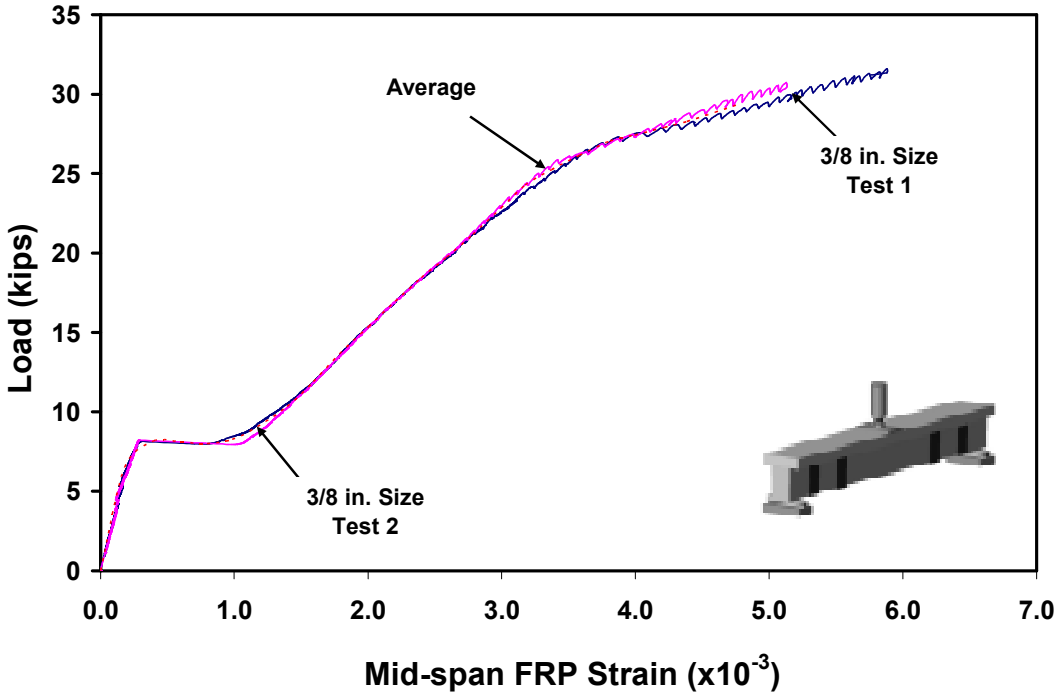

Figure 3.41 Load-Strain Responses for 3/8 in. Void Diameter Specimens

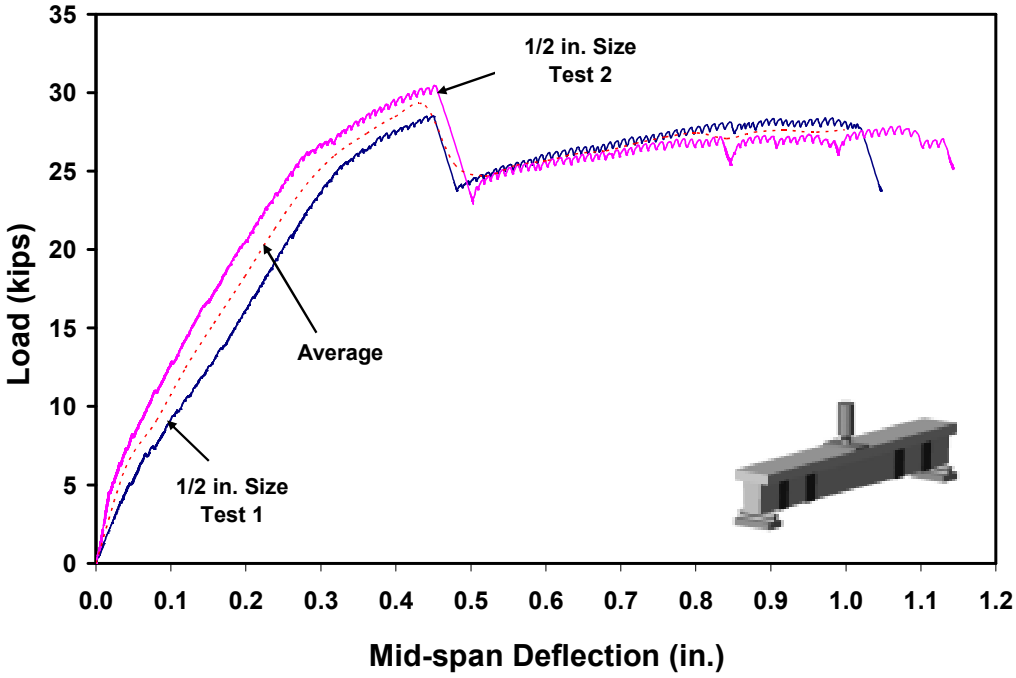

Figure 3.42 Load-Deflection Responses for 1/2 in. Void Diameter Specimens

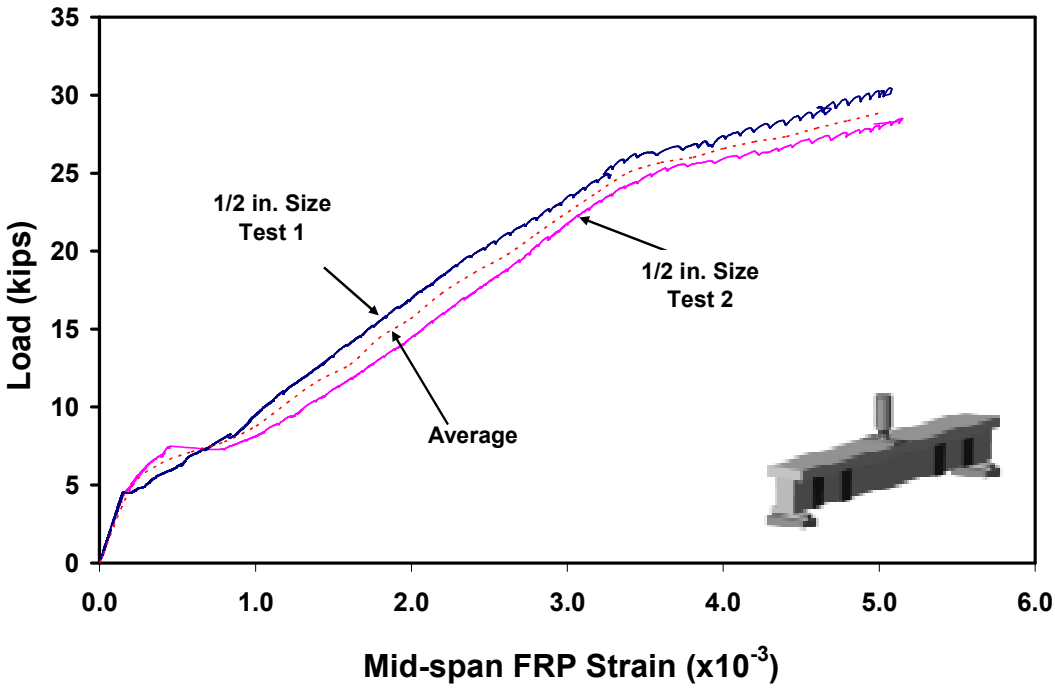

Figure 3.43 Load-Strain Responses for 1/2 in. Void Diameter Specimens

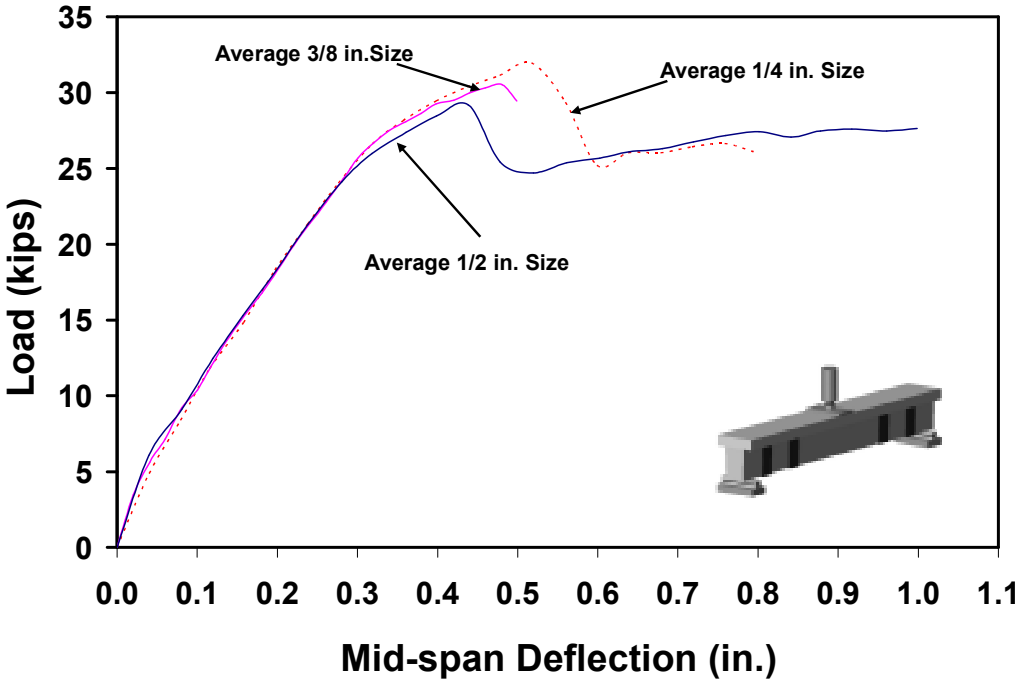

Figure 3.44 Load-Deflection Responses for Specimens with Surface Voids

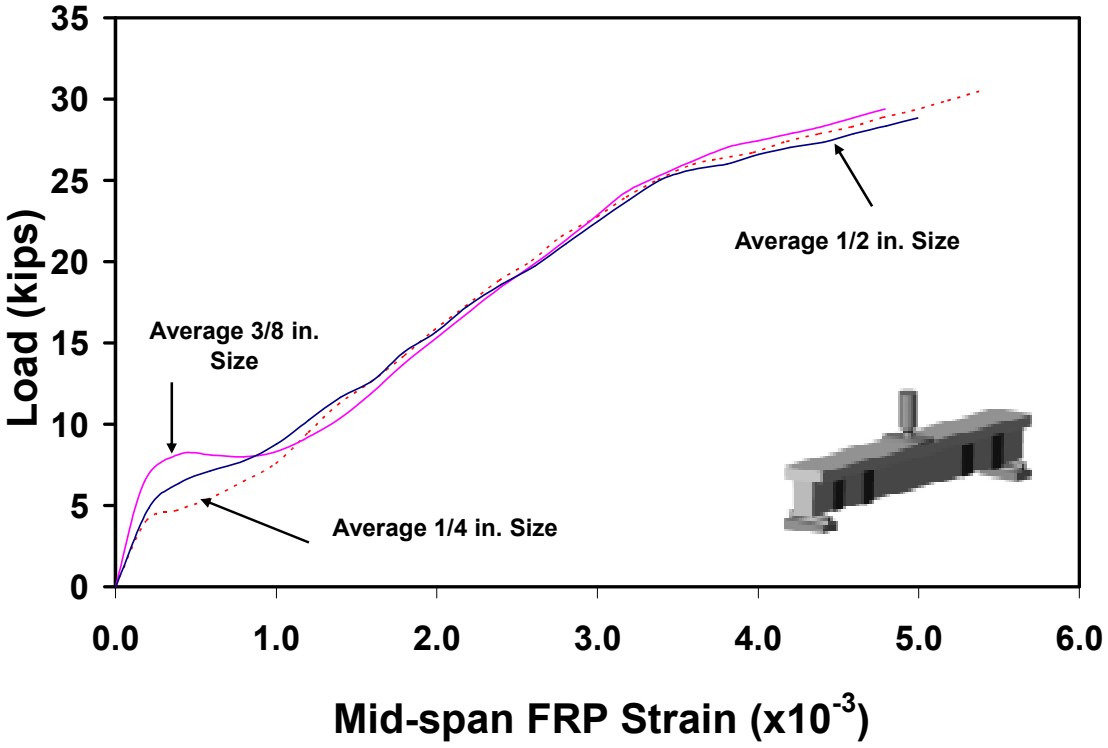

Figure 3.45 Load-Strain Responses for Specimens with Surface Voids

Table 3.9 Test Results for Specimens with Surface Voids

Void Diameter	Specimen No.	Peak Load (kips)	Displacement at Peak Load (in.)	FRP Strain at Peak Load ($x10^{-3}$)
1/4 in.	1	31.3	0.527	5.523
	2	33.3	0.549	6.135
3/8 in.	1	31.6	0.506	5.885
	2	30.7	0.480	5.135
1/2 in.	1	28.5	0.448	5.146
	2	30.5	0.451	5.080

Table 3.10 Average Peak Responses Specimens with Surface Voids

Void Diameter	Peak Load (kips)	Displacement at Peak Load (in.)	FRP Strain at Peak Load ($x10^{-3}$)
1/4 in.	32.3	0.538	5.829
3/8 in.	31.2	0.493	5.510
1/2 in.	29.5	0.450	5.113

From Table 3.11, it can be concluded that for the same void frequency, the peak load, mid-span deflection and FRP strain decrease with the increased void size. Although there is only 8.7% decrease in the peak load from 1/4 in. diameter to 1/2 in. diameter, displacement at peak drops by 16.4%, and the corresponding FRP strain by 12.2%. As the void diameter gets larger, ductility of the retrofitted beam is reduced within the void diameter range investigated in this study.

Failure mode in all pre-cured specimens was by FRP debonding for all void diameters investigated. Debonding initiated by a major flexural or flexure-shear crack close to mid-span, and then propagated to both ends causing a major drop in the load capacity. Figure 3.46 shows modes of failure for specimens with surface voids.

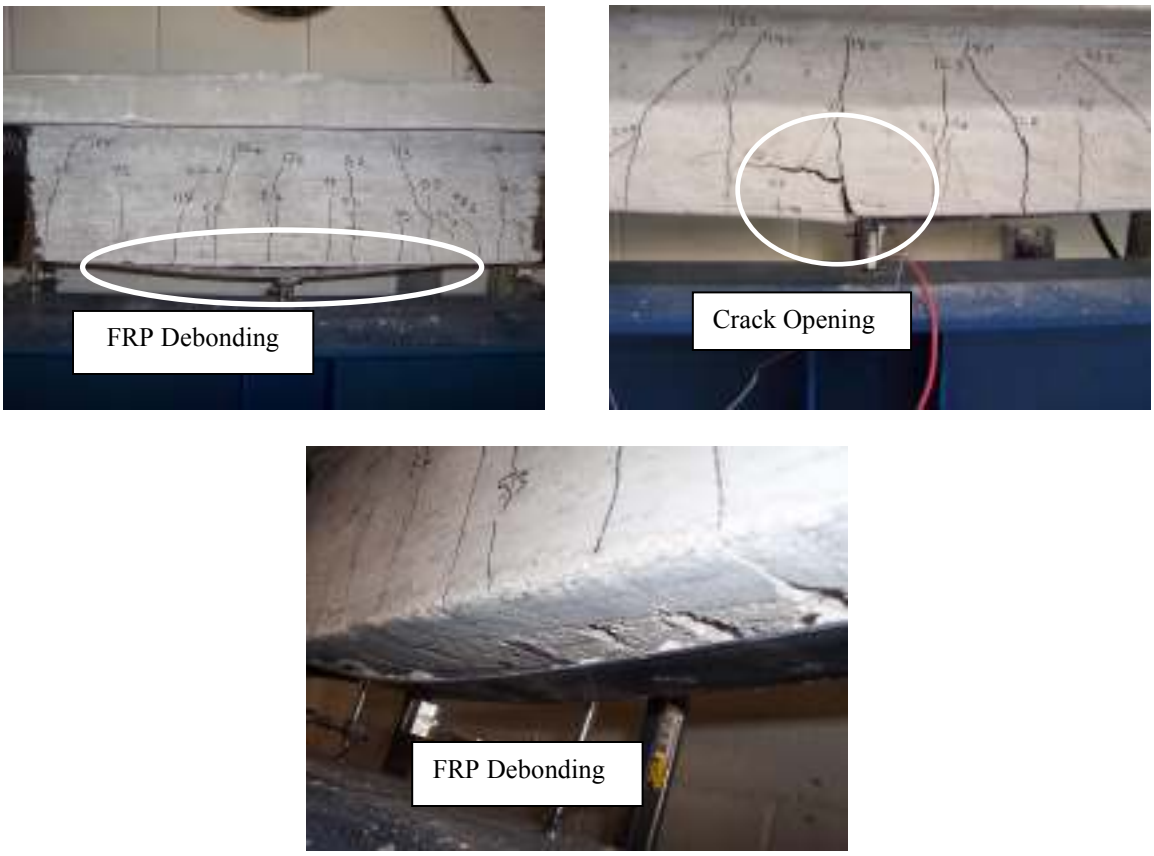

Figure 3.46 Failure Mode for Specimens with Surface Voids

3.1.4.4 Surface Cracks (Cuts)

Test results for the surface crack (cut) specimens are presented in the order of the smallest crack spacing (i.e., largest frequency) to the largest crack spacing (i.e., smallest frequency). Intentional cracks (cuts) were made on beam soffits for pre-cured FRP systems with 1/16 in. thick masonry blades. The only parameter studied was the cut frequency, because wet lay-up tests of Yalim (2008) had identified cut spacing as the major controlling parameter. A constant cut width of 1/16 in., a constant cut depth of 1/4 in. and three cut spacing of 1, 1.5 and 2 in. were made in the pre-cured specimens. Load-deflection and load-strain response responses for the specimens with 1, 1.5 and 2 in. spacing are shown in Figures 3.47 through 3.54.

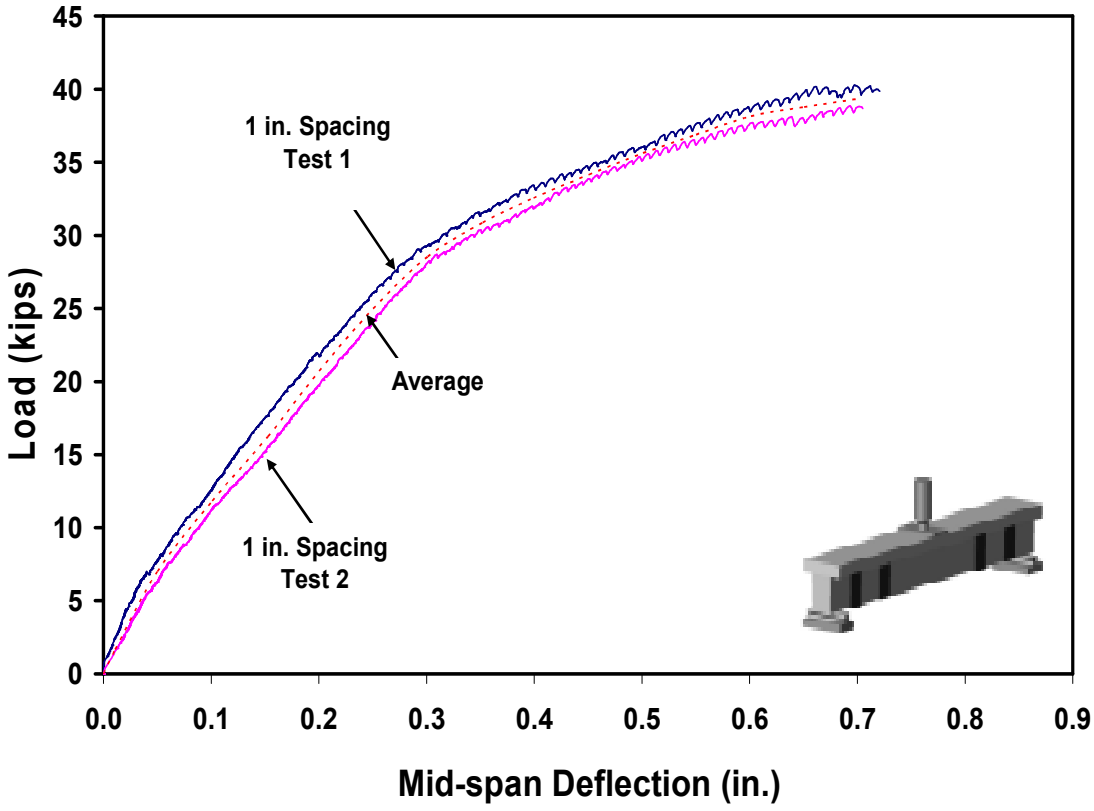

Figure 3.47 Load-Deflection Responses for Specimens with 1 in. Cut Spacing

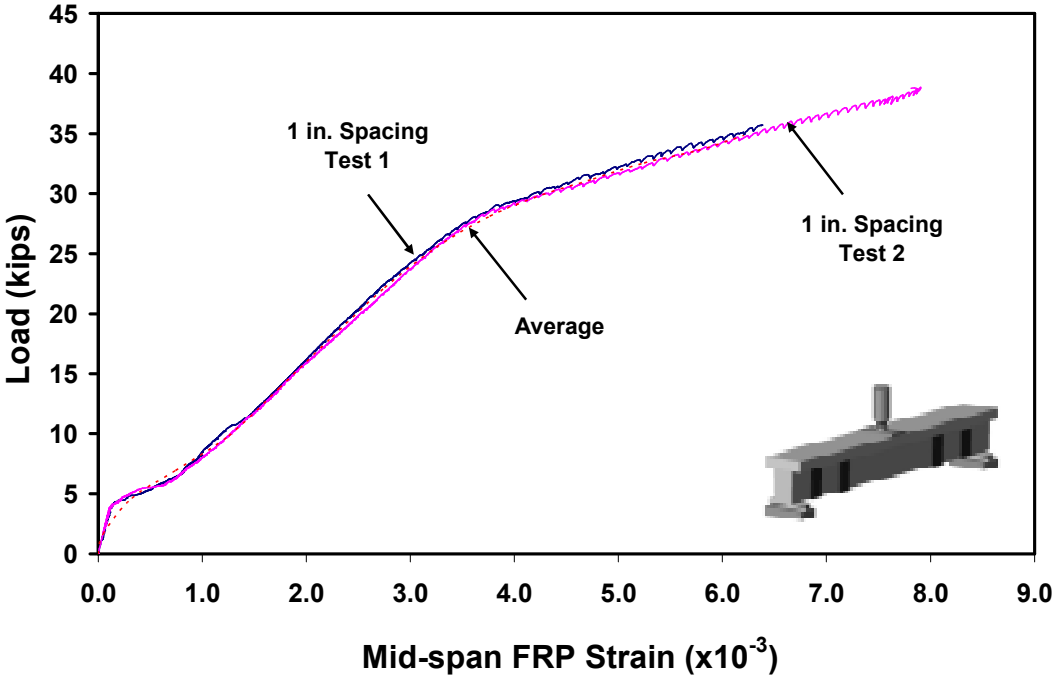

Figure 3.48 Load-Strain Responses for Specimens with 1 in. Cut Spacing

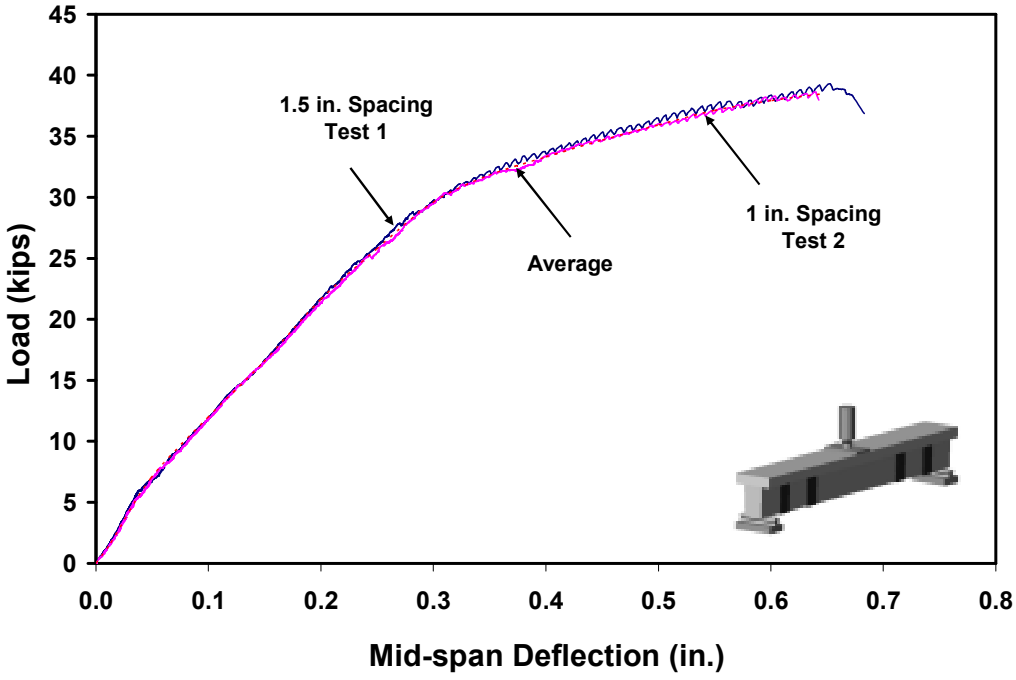

Figure 3.49 Load-Deflection Responses for Specimens with 1.5 in. Cut Spacing

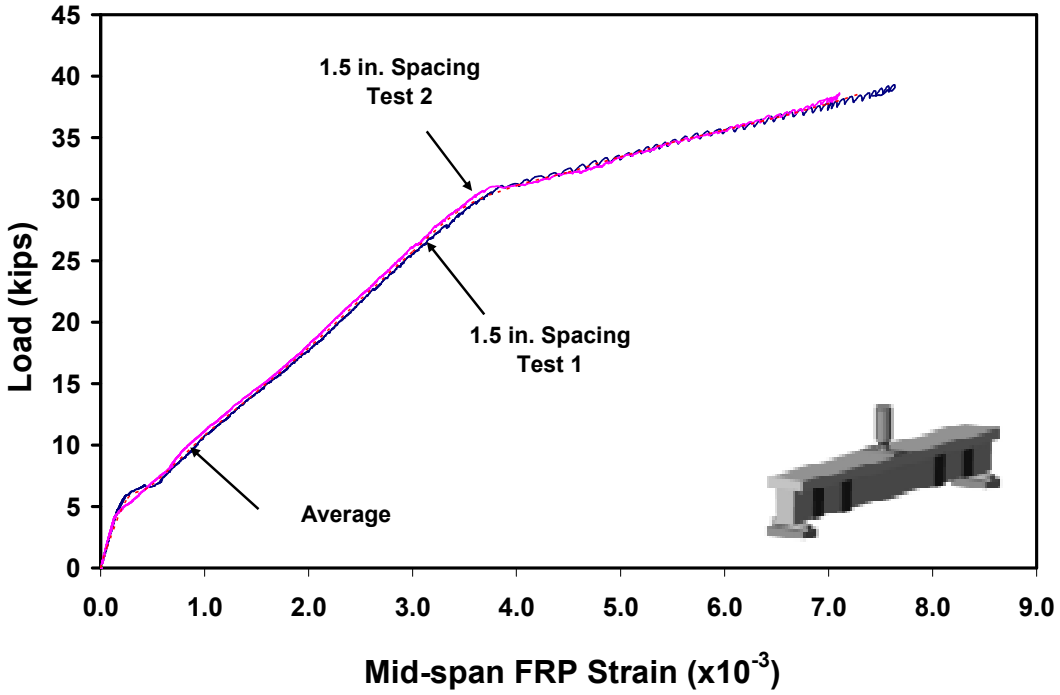

Figure 3.50 Load-Strain Responses for Specimens with 1.5 in. Cut Spacing

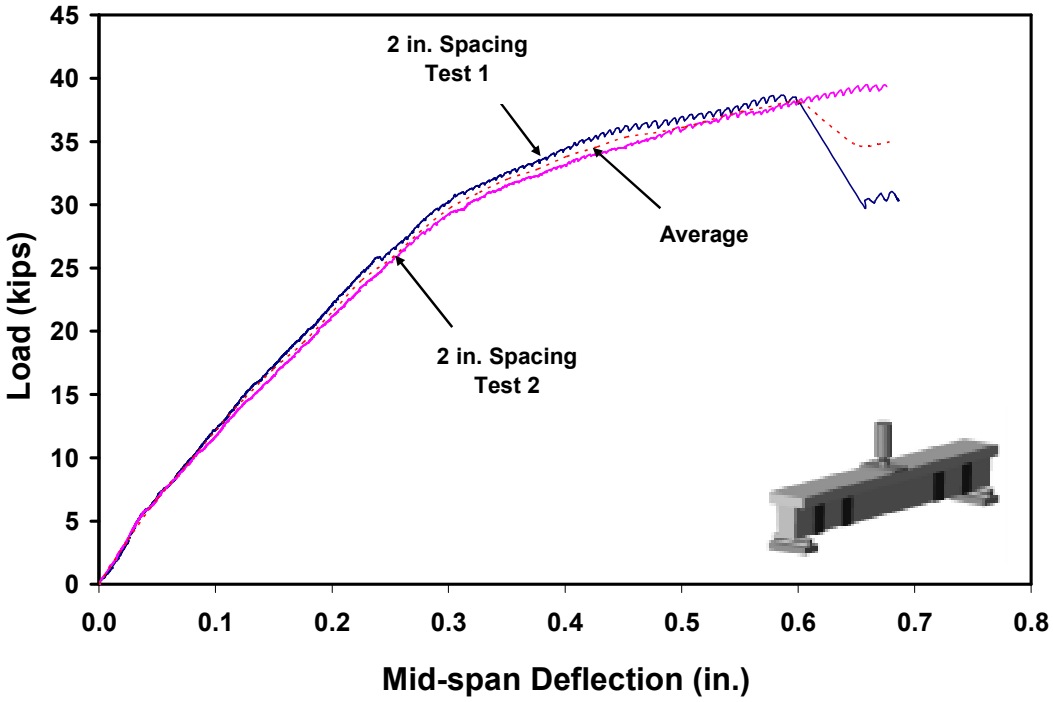

Figure 3.51 Load-Deflection Responses for Specimens with 2 in. Cut Spacing

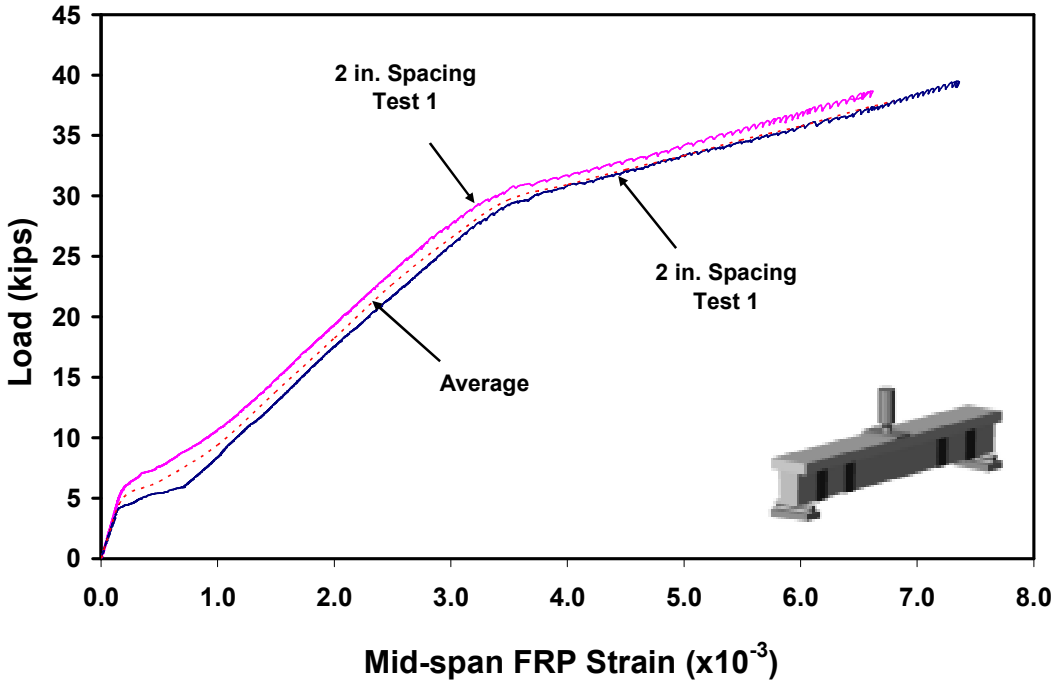

Figure 3.52 Load-Strain Responses for Specimens with 2 in. Cut Spacing

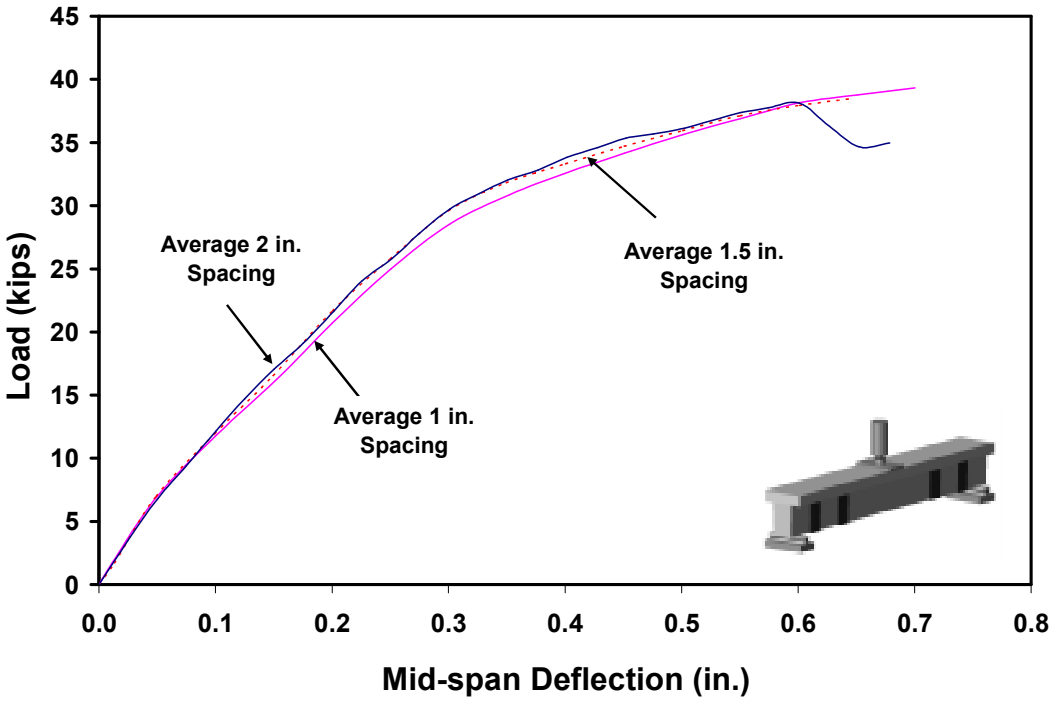

Figure 3.53 Load-Deflection Responses for Specimens with Surface Cuts

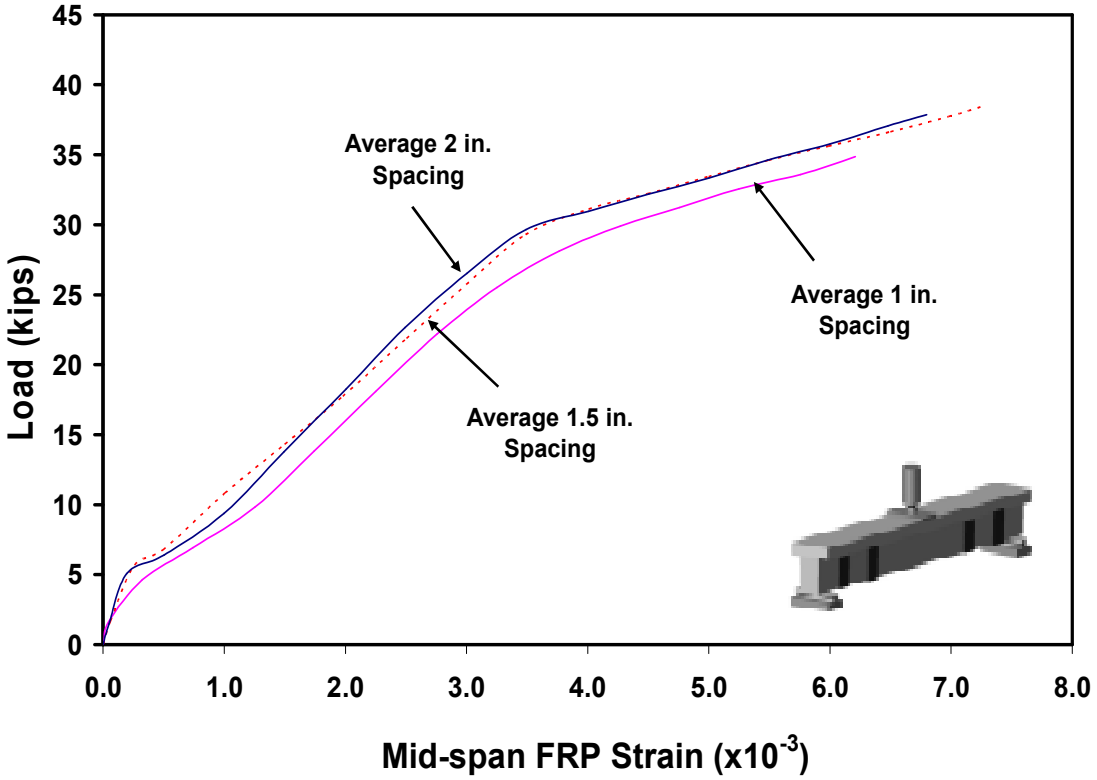

Figure 3.54 Load-Strain Responses for Specimens with Surface Cuts

Generally, three segments can be delineated in each load-deflection response curve: pre-cracking, post-cracking and post-yielding. Test results are summarized in Table 3.11. The average peak responses are listed in Table 3.12.

Table 3.11 Test Results for Specimens with Surface Cuts

Crack Spacing	Specimen No.	Normalized Peak Load (kips)	Displacement at Peak Load (in.)	Strain at Peak Load (x 10^{-3})
1 in.	1	40.3	0.698	N/A
	2	38.9	0.693	7.907
1.5 in.	1	39.3	0.653	7.633
	2	38.6	0.640	7.107
2 in.	1	38.7	0.587	6.601
	2	39.5	0.658	7.345

The data shown in Table 3.12 indicates that with closer cut spacing (i.e., higher cut frequency), deflections and FRP strains corresponding to the first peak load are increased, while the peak loads remain unchanged. Therefore, cut spacing or frequency seems to affect ductility rather than strength.

Table 3.12 Average Peak Responses for Specimens with Surface Cuts

Crack Spacing	Normalized Peak Load (kips)	Displacement at Peak Load (in.)	FRP Strain at Peak Load ($\times 10^{-3}$)
1 in.	39.6	0.700	7.907 (1 test)
1.5 in.	39.0	0.646	7.370
2 in.	39.1	0.623	6.973

Similar to the other pre-cured FRP specimens, failure mode for the specimens with surface cuts was by FRP debonding, which initiated close to the mid-span and then propagated toward the supports. The presence of intentional cracks (cuts) on the beam soffits helped develop wider and more frequent shear-flexure cracks. Figure 3.55 shows typical modes of failure for pre-cured specimens with surface cuts.

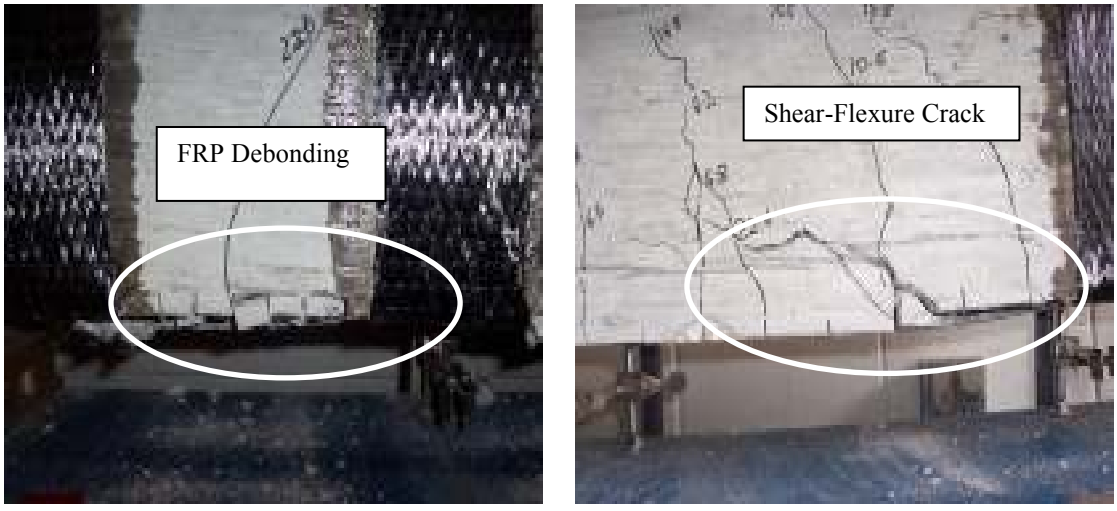

Figure 3.55 Typical Failure Mode for Specimens with Surface Cracks

3.2 NSM FRP Systems

3.2.1 Specimen Details, Materials, Test Setup and Instrumentation

Specimen geometry and internal steel reinforcement configuration for NSM FRP specimens are identical to the externally bonded pre-cured FRP specimens. Cross sectional details are shown in Figure 3.56.

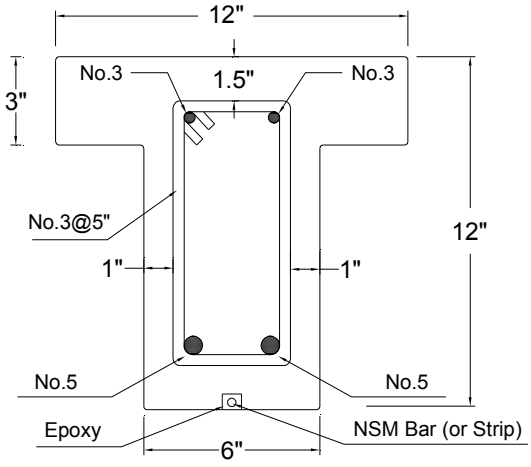

Figure 3.56 NSM FRP Specimen Cross Section

A single NSM FRP strip or bar was used for flexural strengthening of each specimen. Rectangular grooves were utilized for the strips and square grooves were cut for the bars. Since groove depth is easier to control, this study focused only on the groove width tolerance. No wet lay-up side straps were provided for any of the specimens. The length of the FRP reinforcement was 67.5 in. The concrete used for the specimens had a compressive strength of 4.3 ksi measured as the average of 9 concrete cylinders. The steel reinforcements had a yield strength of 60 ksi, as provided by the fabricator. Geometric and mechanical properties of the FRP reinforcement used in this study are provided in Table 3.13. The bonding agent used in this study was a two-part structural epoxy paste

with an average modulus of elasticity of 435 ksi and an average tensile strength of 9 ksi, as reported by the manufacturer.

Table 3.13 Properties of the FRP Reinforcement for NSM Grooves

Type	CFRP #3 Strip	CFRP #3 Bar
Diameter (in.)	-	0.362
Width (in.)	0.177	-
Depth (in.)	0.63	-
Tensile Strength (ksi)	300	300
Tensile Modulus (ksi)	18,000	18,000

Test setup and instrumentation (Figure 3.57) were also identical to the externally bonded pre-cured FRP specimens except for two additional PI gages at the mid-span at the top and bottom. The PI gages generally provide an average strain more reliably than bonded strain gages, and are less likely to fail due to cracks.

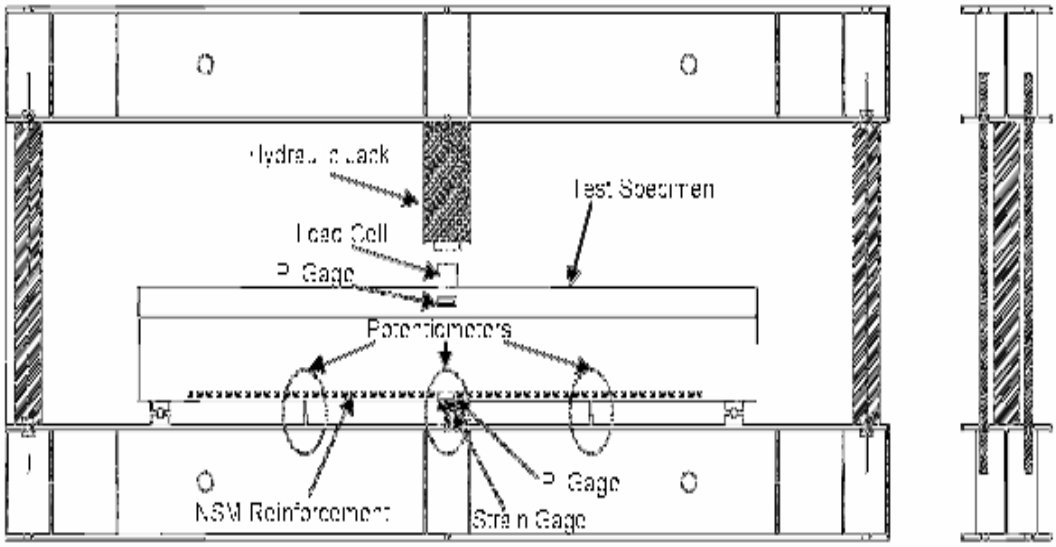

Figure 3.57 Test Setup and Instrumentation for NSM FRP Specimens

3.2.2 Specimen Preparation and Test Matrix

Once the specimens were cast as described in Section 3.1.3.1 and after curing for at least 28 days, grooves of desired dimensions were cut end to end on the soffits of the beams using a diamond blade hand saw. A metallic guide was used to ensure the

straightness and the accuracy of the dimensions of the grooves. Figure 3.58 shows the NSM groove in one of the specimens, laid upside down.

Figure 3.58 NSM Groove

The grooves were then cleaned of dust and other loose particles using a vacuum. The ends of the grooves were sealed to prevent epoxy leakage. The epoxy was mixed in the proportions specified by the manufacturer. The grooves were first filled half way with epoxy. Then, the NSM reinforcement (strip or bar) was placed into each groove, and lightly pressed into the epoxy. The grooves were then completely filled with epoxy and the surface was leveled. The specimens were kept for at least 7 days for curing before load testing. Preparation steps are shown in Figure 3.59. No U-strap was used for these specimens.

(a) Epoxy Mixing

(b) Grooves Filled Half-way

(c) FRP Placement

(d) Surface Leveled

Figure 3.59 NSM FRP Specimen Preparation Steps

Table 3.14 summarizes the test matrix. For each type of reinforcement (strip or bar), a mid-size groove was chosen as control. The undersized and oversized grooves were provided with ±1/8 in. tolerance.

Table 3.14 Test Matrix for NSM Grooves

Reinforcement Type	Groove Size (depth x width) (in.)	Groove Type	Number of Specimens
NSM Strip	1 x 7/16	Undersized	2
	1 x 9/16	Control	2
	1 x 11/16	Oversized	2
NSM Bar	7/16 x 7/16	Undersized	2
	9/16 x 9/16	Control	2
	11/16 x 11/16	Oversized	2

All NSM reinforcement were cut 67.5 in. long to provide development length of 33.75 in. on either side of mid-span. The selection of the groove size and the development length followed earlier studies by Paretti and Nanni (2004) and Hassan and Rizkalla (2004).

3.2.3 Test Results

3.2.3.1 NSM Strips

The results are presented in the order of mid-size (control) specimens, undersize and oversize specimens, respectively. For NSM strips, the 9/16 in. wide groove was selected as the control case, and the groove depth was kept constant at 1 in. Using a tolerance of ±1/8 in., the undersized and oversized grooves were 7/16 in. and 11/16 in., respectively. Load-deflection and load-strain responses for the 9/16 in. groove size (control) specimens are shown in Figures 3.60 and 3.61, respectively.

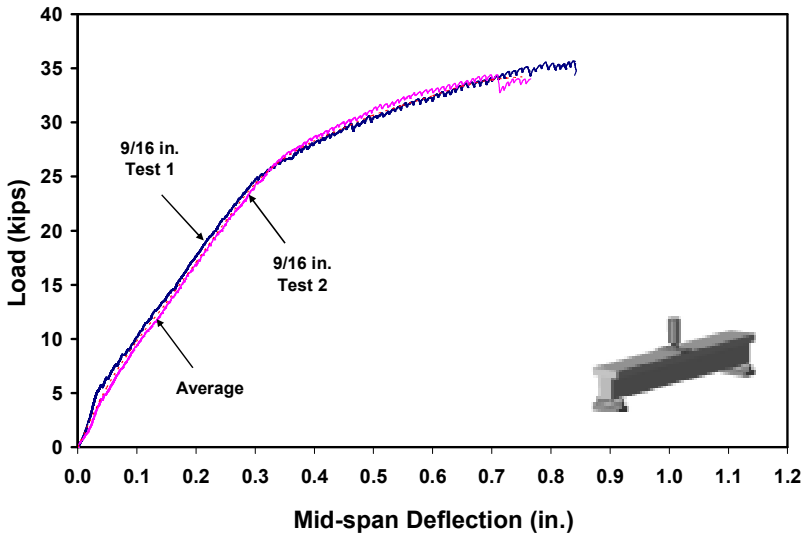

Figure 3.60 Load-Deflection Responses for 9/16 in. Groove Size Specimens (NSM Strip)

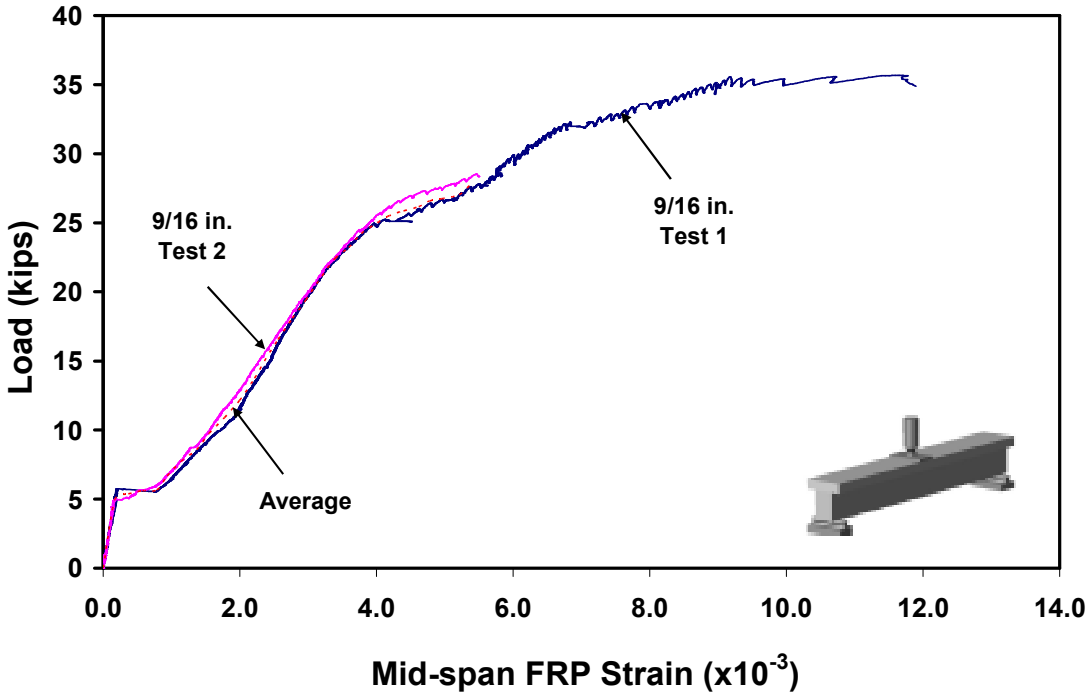

Figure 3.61 Load-Strain Responses for 9/16 in. Groove Size Specimens (NSM Strip)

The figures clearly show that both control specimens behaved quite similarly with a tri-linear response. There was no strain reading beyond 5.5×10^{-3} for Control Specimen 2, because the gage failed due to cracking of epoxy. However, both specimens show a plateau at a load of about 5 kips due to cracking of concrete.

Two different failure modes were observed for the control specimens; epoxy splitting and concrete splitting. Epoxy splitting failure occurred as a result of excessive deformation and cracking, which caused the loss of bond between the NSM strip and epoxy, accompanied by a sudden load drop. Concrete splitting failure, on the other hand, was developed when epoxy remained intact. Failure mode for Control Specimen 1 was epoxy splitting, while the failure mode for Control Specimen 2 was concrete splitting, as shown in Figure 3.62.

(a) **Epoxy Splitting** **(b) Concrete Splitting**

Figure 3.62 Failure Modes of Control Specimens (NSM Strip)

Load-deflection and load-strain graphs for undersized specimens with 7/16 in. groove width are shown in Figures 3.63 and 3.64, respectively. Similar to the control specimens, response curve for undersized specimens was tri-linear. Although the ultimate loads were similar, mid-span deflections were slightly lower than those for the control specimens. A similar plateau was noted at a load of about 5 kips, when concrete cracked. Strains as high as $9x10^{-3}$ were recorded at the ultimate load.

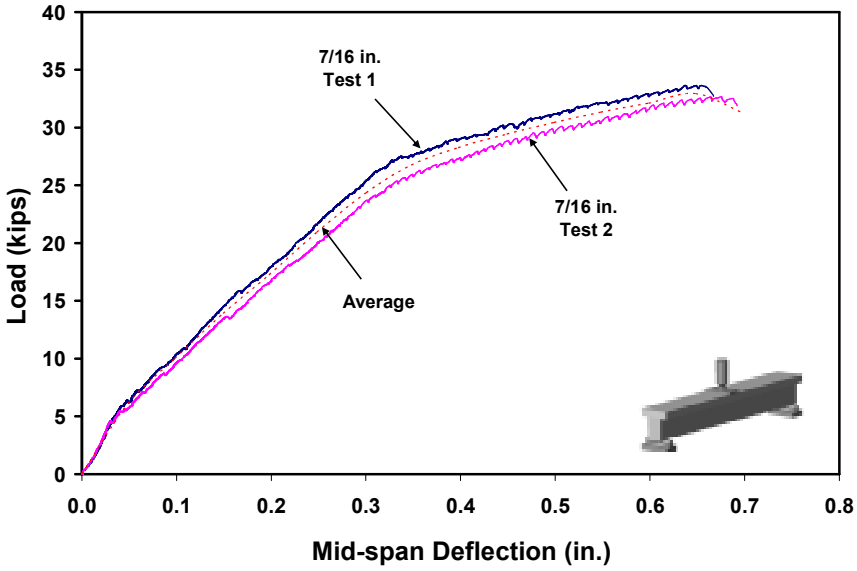

Figure 3.63 Load-Deflection Responses for 7/16 in. Groove Size Specimens (NSM Strip)

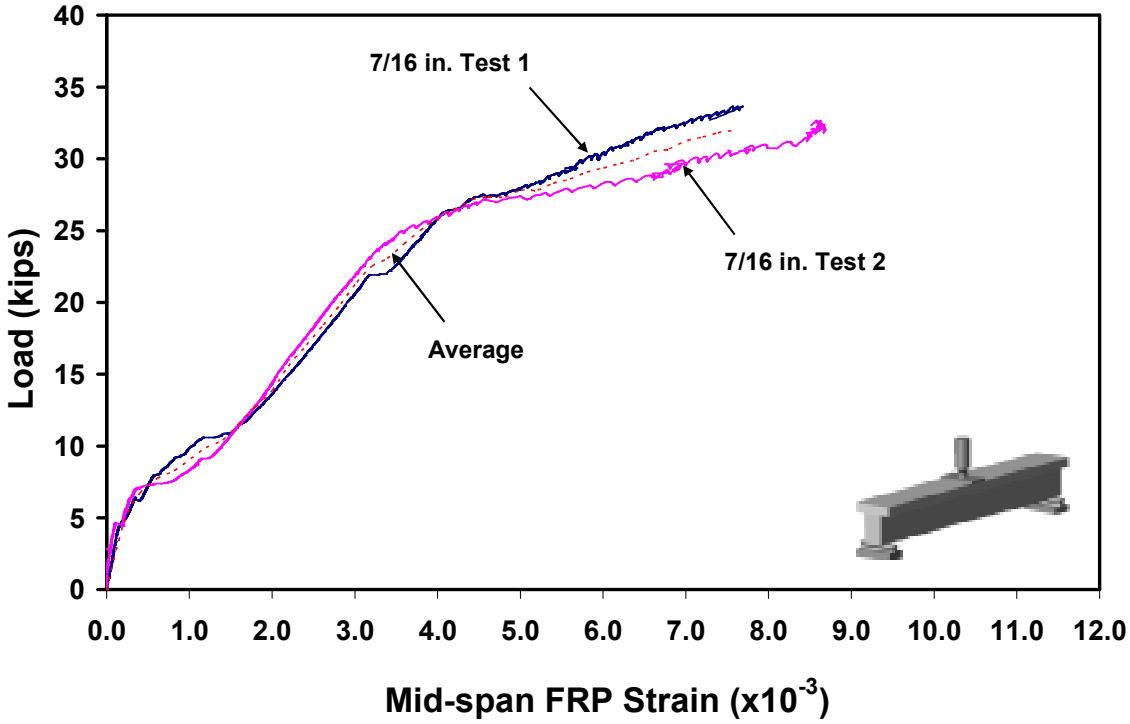

Figure 3.64 Load-Strain Responses for 7/16 in. Groove Size Specimens (NSM Strip)

Both failure modes of concrete and epoxy splitting were also observed in the undersized specimens, as shown in Figure 3.65.

(a) **Concrete Splitting** (b) **Epoxy Splitting**

Figure 3.65 Failure Mode of Undersized Groove Specimens (NSM Strip)

Load-deflection and load-strain responses for the oversized specimens with 11/16 in. groove width are shown in Figures 3.66 and 3.67, respectively. Only one of the two load-strain curves is shown in Figure 3.67, due to gage failure in the other one. The

failure mode observed in the oversized specimens was only concrete splitting failure, as shown in Figure 3.68.

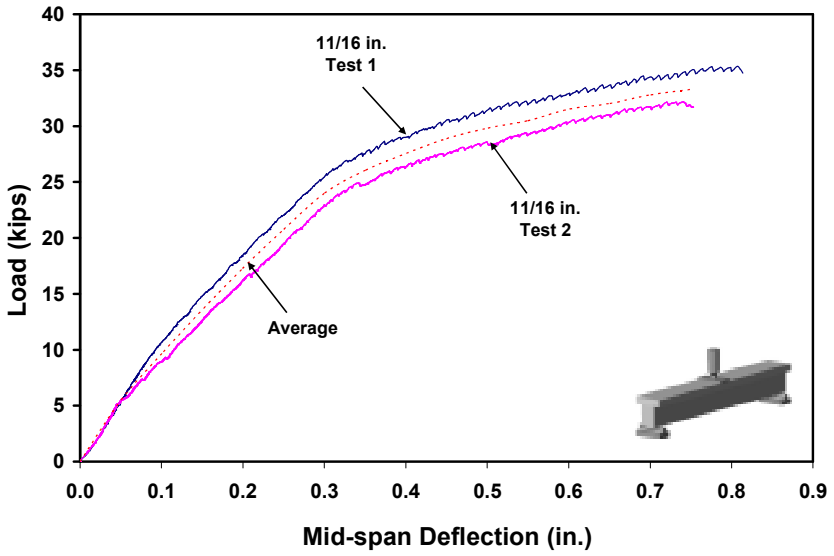

Figure 3.66 Load-Deflection Responses for 11/16 in. Groove Size Specimens (NSM Strip)

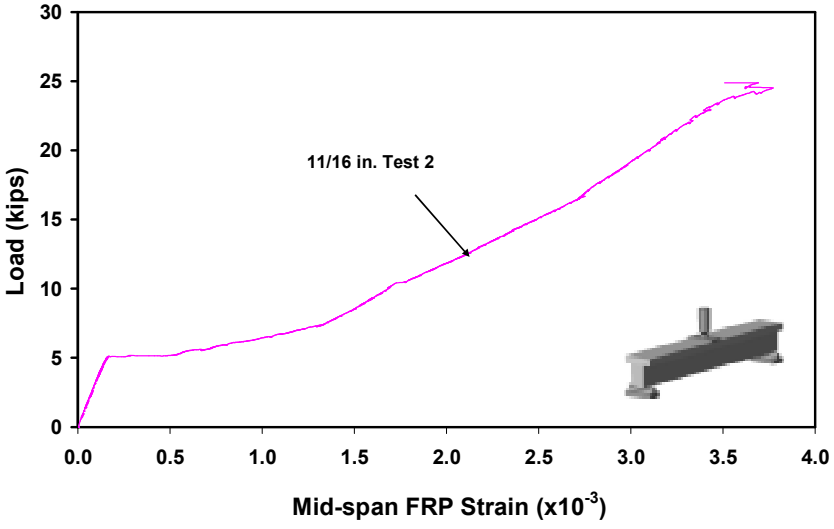

Figure 3.67 Load-Strain Responses for 11/16 in. Groove Size Specimens (NSM Strip)

Figure 3.68 Failure Mode of Oversized Specimens (NSM Strip)

The averages for each group of specimens (control, undersized and oversized grooves) are compared with each other in Figures 3.69 and 3.70. Test results are also summarized in Table 3.15.

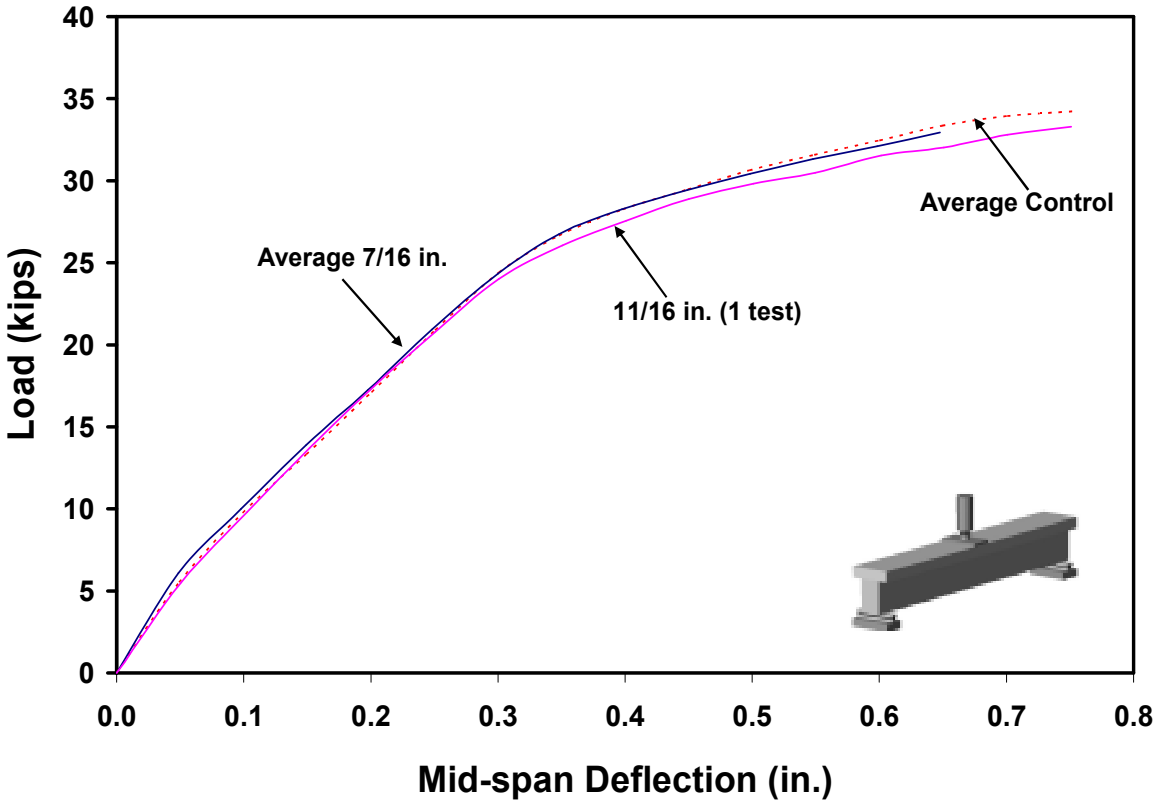

Figure 3.69 Load-Deflection Responses for NSM Strip Specimens

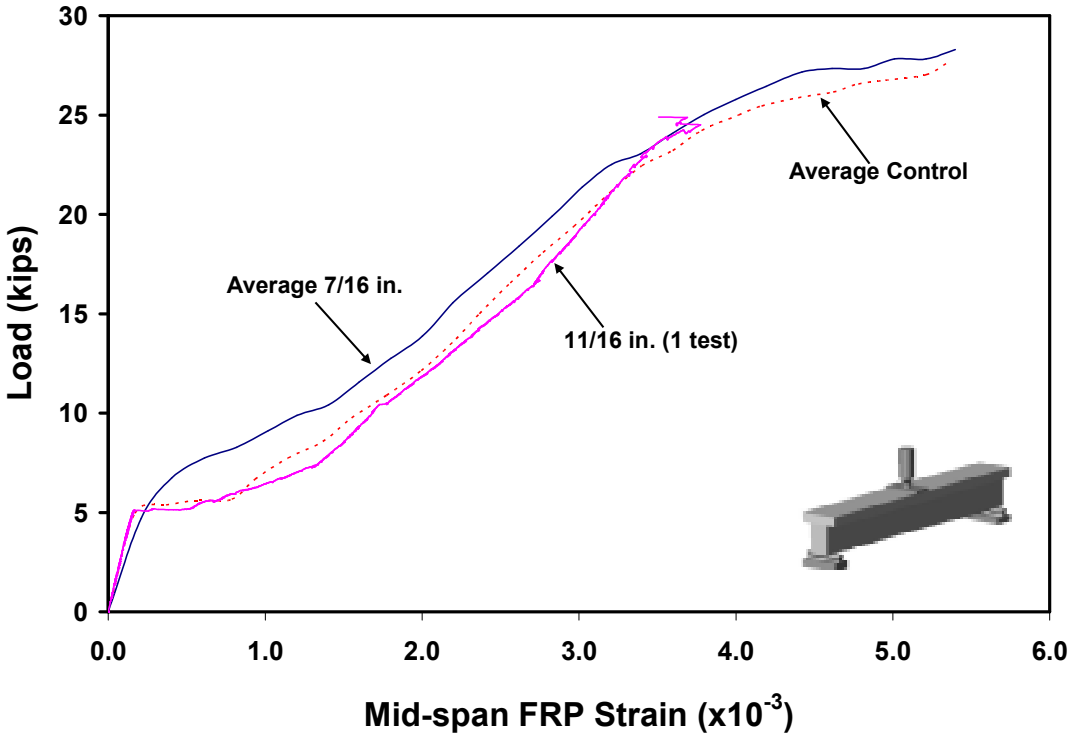

Figure 3.70 Load-Strain Responses for NSM Strip Specimens

It is clear that the groove width tolerance of ±1/8 in. does not significantly affect the behavior of NSM strip specimens in the range of groove size studied.

Table 3.15 Summary Results for NSM Strip Specimens

Specimen	Specimen No.	Peak Load (kips)	Displacement at Peak Load (in.)	FRP Strain at Peak Load ($x10^{-3}$)
NSM Strip, 7/16 in. Groove	1	33.7	0.654	7.680
	2	32.7	0.676	9.000
NSM Strip, 9/16 in. Groove	1	35.7	0.838	11.566
	2	34.4	0.690	Gage Failed
NSM Strip, 11/16 in. Groove	1	35.3	0.808	Gage Failed
	2	32.2	0.740	Gage Failed

3.2.3.2 NSM Bars

For NSM bars, the 9/16 in. square groove size was chosen as the control case. With a tolerance of ±1/8 in., the undersized and oversized grooves were 7/16 in. and 11/16 in. square, respectively. Load-deflection and load-strain graphs for the 9/16 in.

groove size (control) specimens are shown in Figures 3.71 and 3.72, respectively. These figures show a response similar to that seen for the NSM strips. Both specimens failed by concrete splitting, as shown in Figure 3.73.

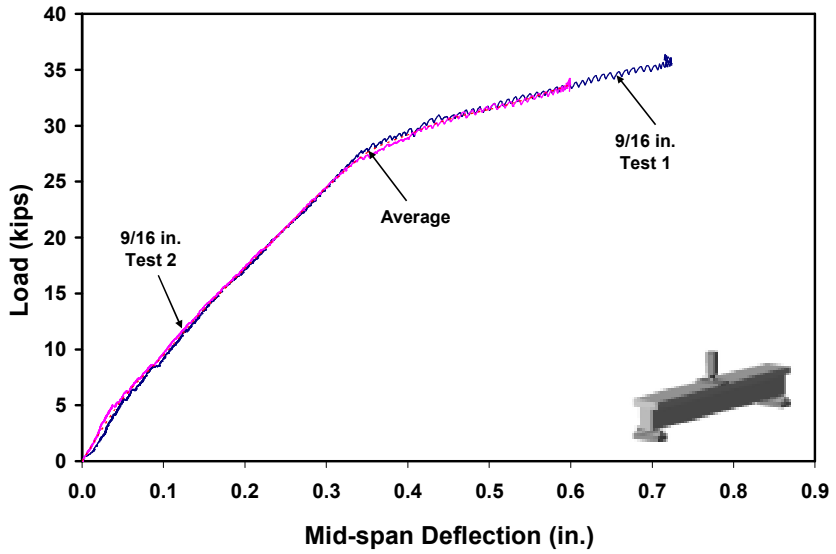

Figure 3.71 Load-Deflection Responses for 9/16 in. Groove Size Specimens (NSM Bar)

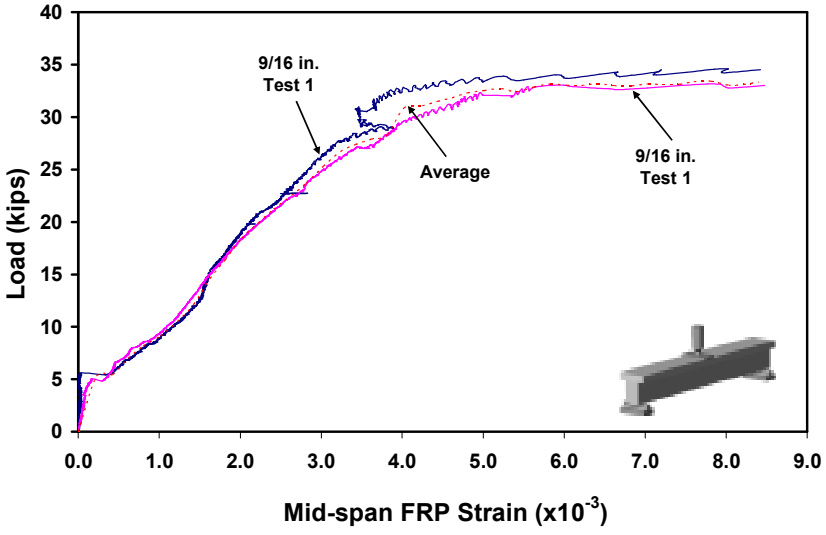

Figure 3.72 Load-Strain Responses for 9/16 in. Groove Size Specimens (NSM Bar)

Figure 3.73 Failure Mode of Control Specimens (NSM Bar)

Load-deflection and load-strain graphs for undersized groove specimens with 7/16 in. groove size are shown in Figures 3.74 and 3.75, respectively. The response is quite similar to the control specimens. Strains as high as $10x10^{-3}$ were measured. Primarily, epoxy splitting was observed for the undersized specimens, as shown in Figure 3.76.

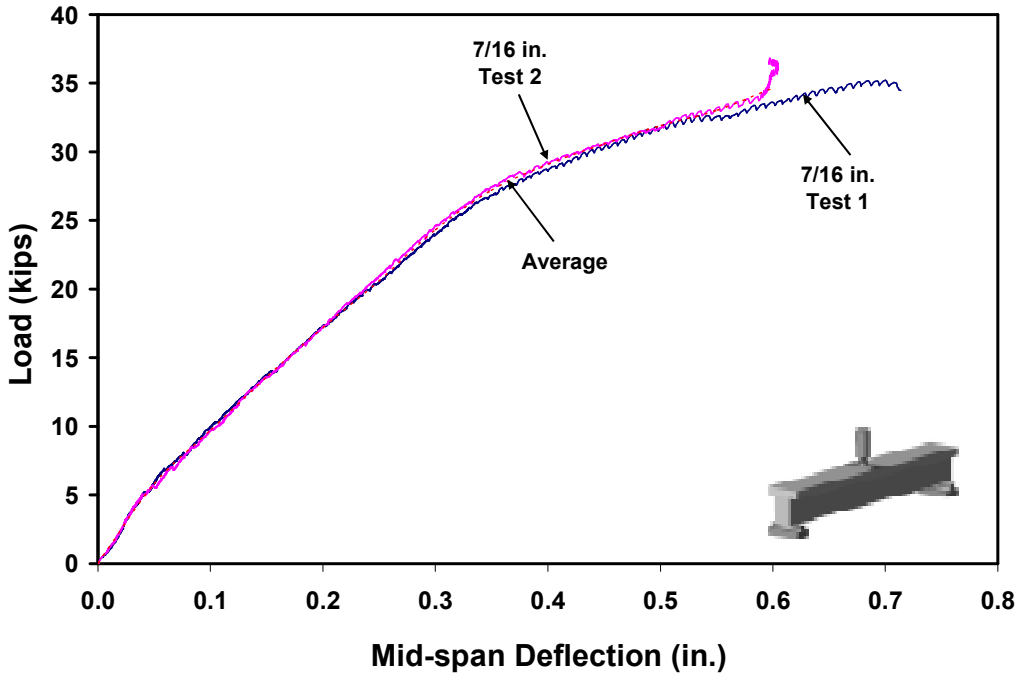

Figure 3.74 Load-Deflection Responses for 7/16 in. Groove Size Specimens (NSM Bar)

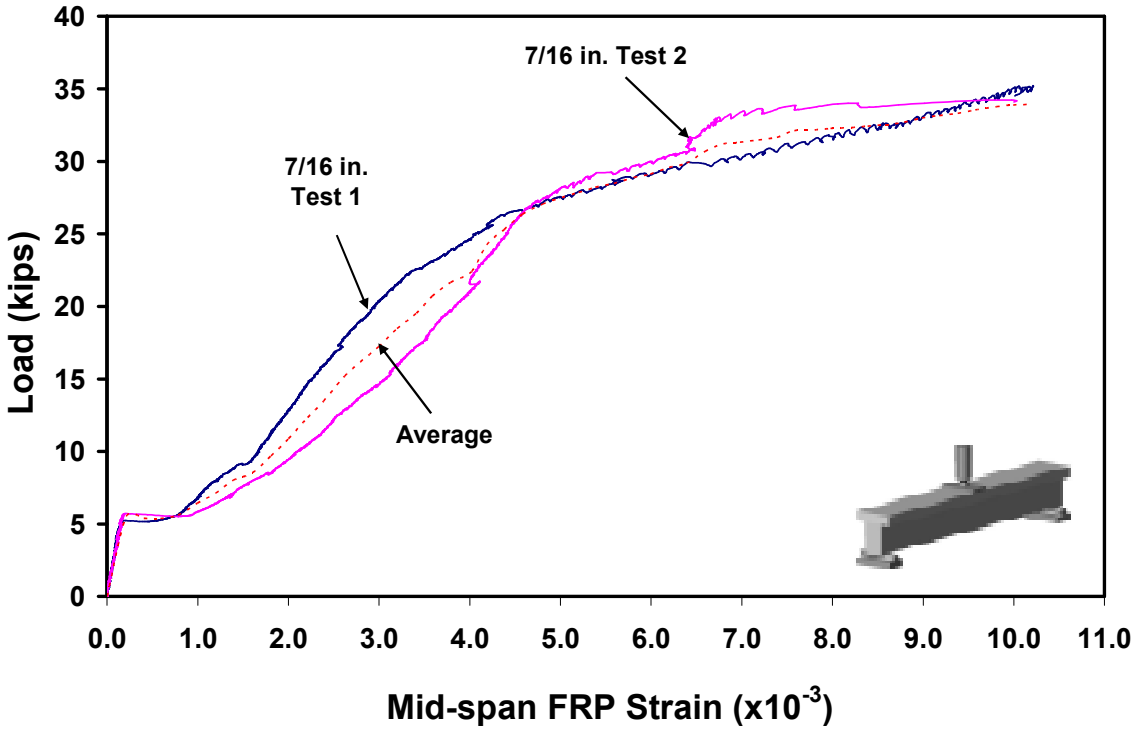

Figure 3.75 Load-Strain Responses for 7/16 in. Groove Size Specimens (NSM Bar)

Figure 3.76 Failure Mode of Undersized Specimens (NSM Bar)

Load-deflection and load-strain responses for oversized groove specimens with 11/16 in. groove size are shown in Figures 3.77 and 3.78, respectively.

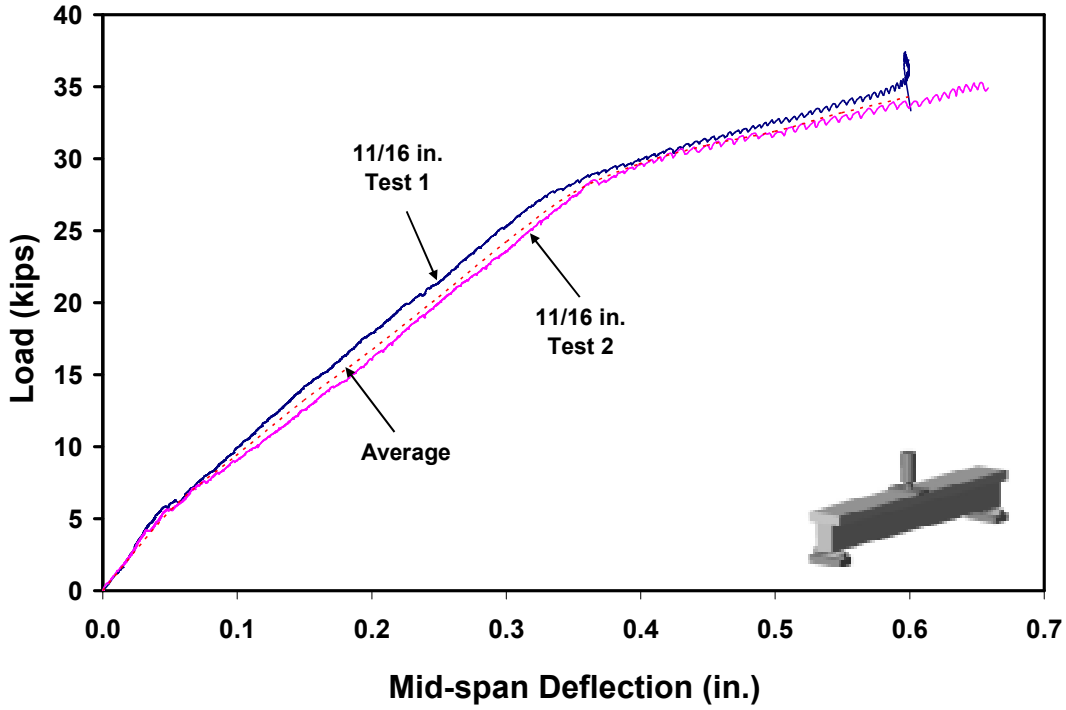

Figure 3.77 Load-Deflection Responses for 11/16 in. Groove Size Specimens (NSM Bar)

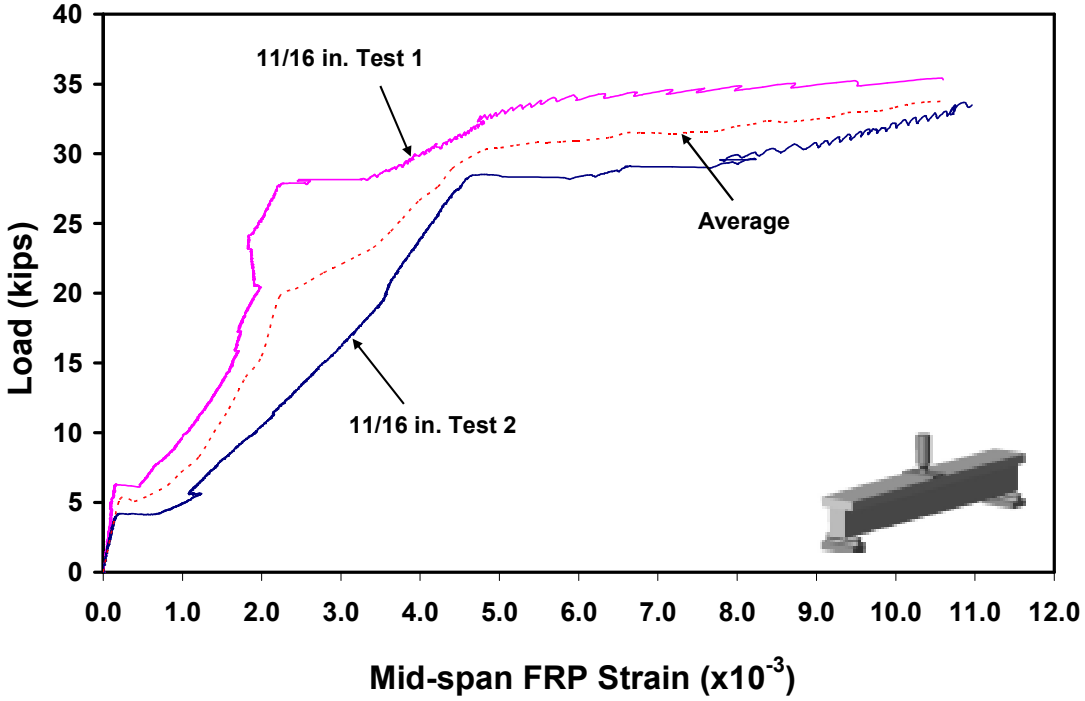

Figure 3.78 Load-Strain Responses for 11/16 in. Groove Size Specimens (NSM Bar)

One of the two oversized groove specimens failed by epoxy splitting and the other failed by concrete splitting, as shown in Figure 3.79.

(a) Epoxy Splitting (b) Concrete Splitting

Figure 3.79 Failure Modes of Oversized Groove Specimens (NSM Bar)

The averages for each group of specimens (control, undersized and oversized grooves) are compared with each other in Figures 3.80 and 3.81 for the load-deflections and load-strains, respectively. Test results are also summarized in Table 3.16.

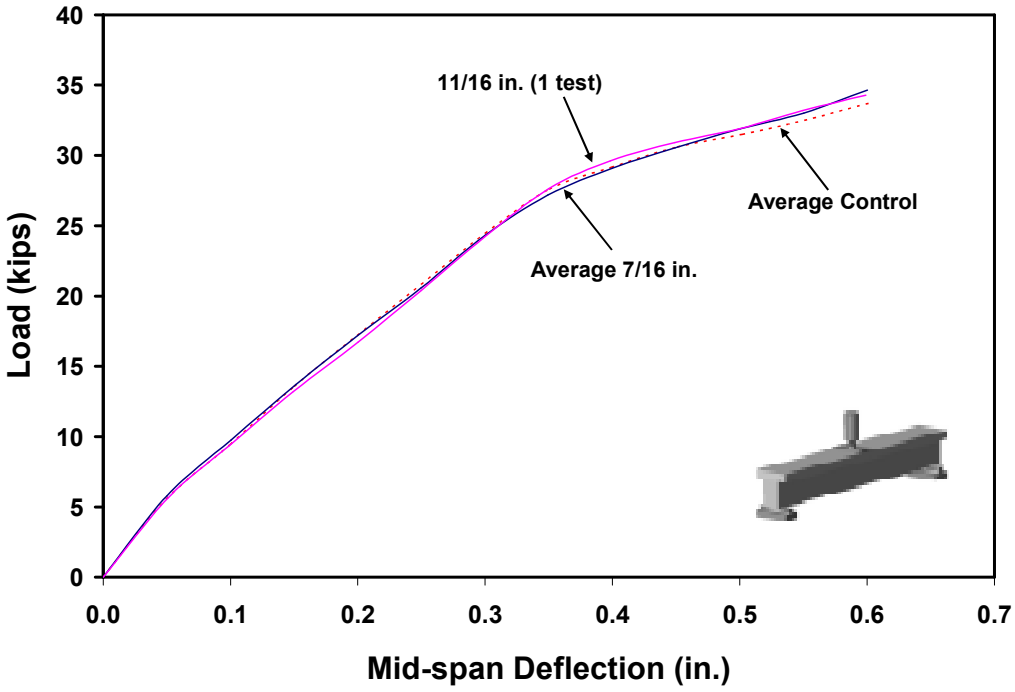

Figure 3.80 Load-Deflection Responses for NSM Bar Specimens

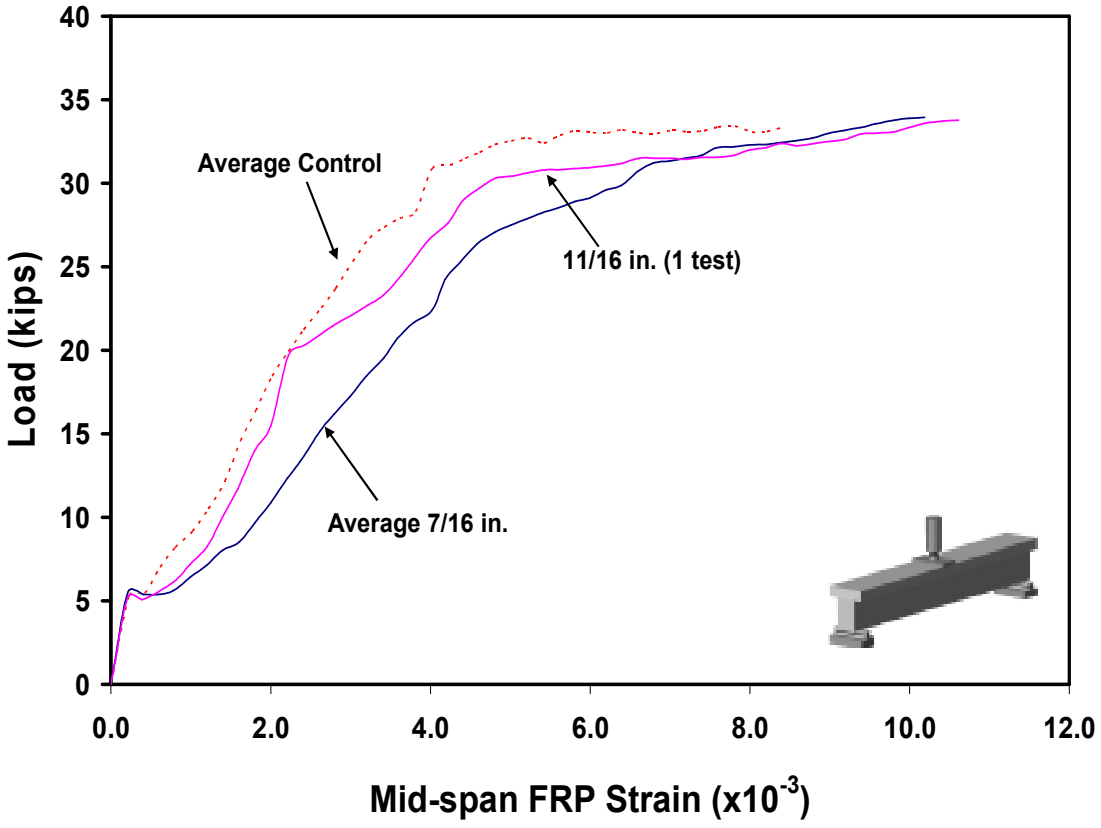

Figure 3.81 Load-Strain Responses for NSM Bar Specimens

It is clear that similar to the test results for NSM strips, the ±1/8 in. tolerance for groove size does not significantly affect the performance. It does appear that, with some exceptions, smaller grooves lead to epoxy splitting failure, whereas larger grooves lead to concrete splitting failure, as discussed by Hassan and Rizkalla (2004).

Table 3.16 Peak Responses for NSM Bars

Specimen	Specimen No.	Peak Load (kips)	Displacement at Peak Load (in.)	FRP Strain at Peak Load ($x10^{-3}$)
NSM Bar, 7/16 in. Groove	1	35.2	0.700	6.024
	2	36.8	0.597	7.054
NSM Bar, 9/16 in. Groove	1	36.4	0.716	Gage failed
	2	34.2	0.599	8.412
NSM Bar, 11/16 in. Groove	1	37.4	0.597	Gage failed
	2	35.3	0.653	Gage failed

3.2.4 Comparison with Previous Studies

A comprehensive database was established from the literature on a total of 62 beam tests utilizing CFRP and GFRP bars or strips for flexural strengthening. Table 3.17 lists the studies comprising the database. Table 3.19 summarizes some geometric and physical parameters of all specimens in the database.

Table 3.17 Studies in the Database

Study	Number of Tests in the Database
This Study	7
Hassan and Rizkalla (2003)	8
Taljsten (2003)	2
El-Hacha and Rizkalla (2004)	3
Hassan and Rizkalla (2004)	7
Barros and Fortes (2005)	4
Barros et al. (2006)	3
Teng et al. (2006)	4
Castro et al. (2007)	6
Katynia (2007)	7
Yost et al. (2007)	6
Novidis and Pantazopoulou (2007)	5
Total	62

Test data from the literature was normalized to allow for comparisons. The normalized dependent variable was selected to be the strain efficacy. Strain efficacy ($\varepsilon_{max}/\varepsilon_u$) can be defined as the ratio of the maximum measured strain to the ultimate strain in the FRP. Normalized independent variables were the bonded length to FRP area (L_d/A_{FRP}) ratio, groove width to depth ratio (W/H), groove width to edge distance ratio (W/d_e), and groove depth to steel cover ratio (H/d_s). The parameters were described earlier in Section 2.2.1 and depicted in Figure 2.10. Most of the aforementioned variables are also depicted in Figure 3.82.

Table 3.18 Geometric and Physical Properties of Test Specimens in the Database

	Geometric Parameters					Physical Parameters			
	Section Geometry (in.)[1]	**Specimen Length (in.)**	**Total Length of FRP (in.)**	**FRP Type**	**Number of FRP Bars**	**Concrete Comp. Strength (ksi)**	**FRP Modulus (ksi)**	**FRP Tensile Strength (ksi)**	**Failure Mode[2]**
Present Study	T6x12,3x12	84.0	33.75	CFRP	1	4.3	18,000	300	es, cs
Hassan and Rizkalla [2003]	T9.8x5.9, 1x11.8	98.4	5.9 to 47.2	CFRP	1	7.0	21,755	290	cs
Taljsten [2003]	R7.9x11.8	141.7	39.4, 51.2	CFRP	2	8.8	16,679	600	es, fr
El-Hacha and Rizkalla [2004]	T11.8x5.9, 2x11.8	98.4	49.2	CFRP	1, 2	6.5	17,770 to 20,300	204 to 290	es, fr
Hassan and Rizkalla [2004]	R5.9x11.8	98.4	5.9 to 47.2	CFRP	1	7.0	16,100	278	cs
Barros and Fortes [2005]	R3.9x6.7 (6.9,7,7.1)	59.1	17.7	CFRP	1, 2, 3	6.7	23,032	397	ccd, cs
Barros et al. [2006]	R4.7x6.7	35.4	11.8	CFRP	1, 2, 3	6.4	23,032	397	ccd, cs
Teng et al. [2006]	R5.9x11.8	126	0, 5.9, 16.7	CFRP	1	6.4	21,900	300	ccd, cc
Castro et al. [2007]	T21.7x5.9, 3.9x15.8	157.5	59.1	CFRP GFRP	1, 2, 3	5.1 to 7.7	5,917 to 21,320	100 to 300	cs, fr
Kotynia [2007]	R7.1x14.2	165.4	52.2	CFRP	1, 2, 3	3.6 to 6.3	23,641 to 24,946	326 to 424	cc, cs
Yost et al. [2007]	R6(9,12)x7.5	108.0	48	CFRP	1, 2	5.4	23,931	239	cc, fr
Novidis and Pantazopoulou [2007]	R11.8x7.1	37.0	15.4	CFRP	1, 2	4.6	19,765	435	cs

[1]Cross-Section: T: T-section, R: Rectangular section, Taxb,cxd where a: flange width, b: web width, c: flange thickness, and d: beam height, values in parenthesis show the specimens with different dimensions.

[2] Failure Mode: cs: concrete splitting, es: epoxy splitting, fr: FRP rupture, ccd: concrete cover delamination, and cc: concrete crushing.

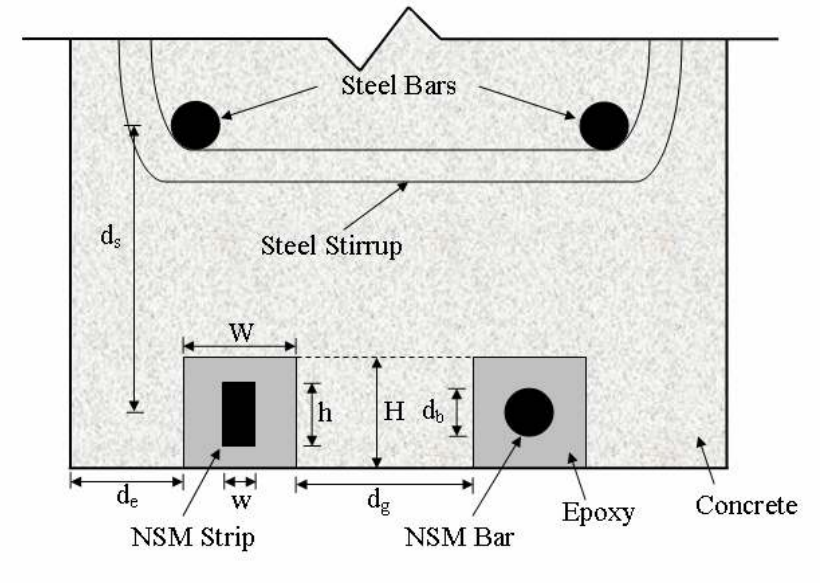

Figure 3.82 Geometric Parameters Related to NSM FRP

Figures 3.83 (a) – (d) show strain efficacy ($\varepsilon_{max}/\varepsilon_u$) vs. L_d/A_{FRP}, W/H, W/d_e and W/d_s ratios. Common legend is shown in Figure 3.83 (e).

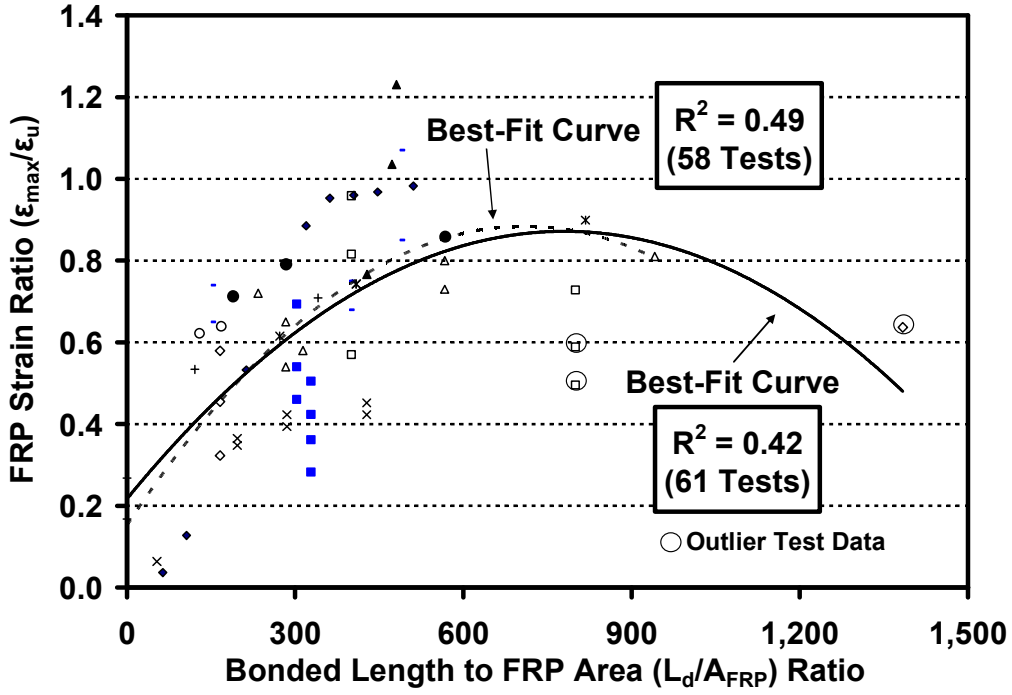

Figure 3.83 (a) Strain Efficacy Versus Bonded Length to FRP Area Ratio

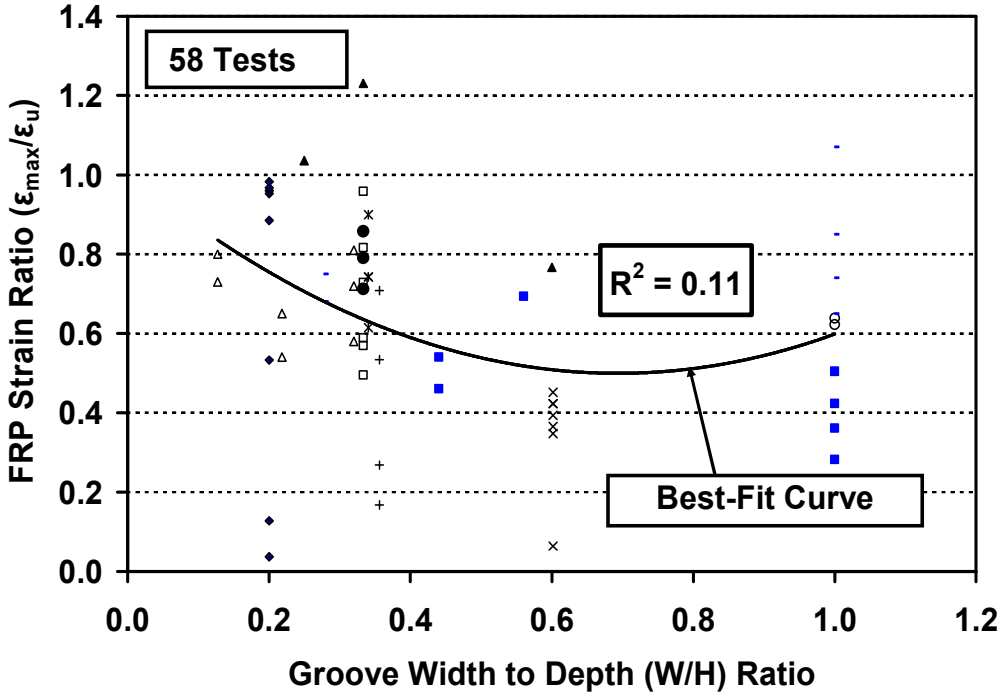

Figure 3.83 (b) Strain Efficacy Versus Groove Width to Depth Ratio

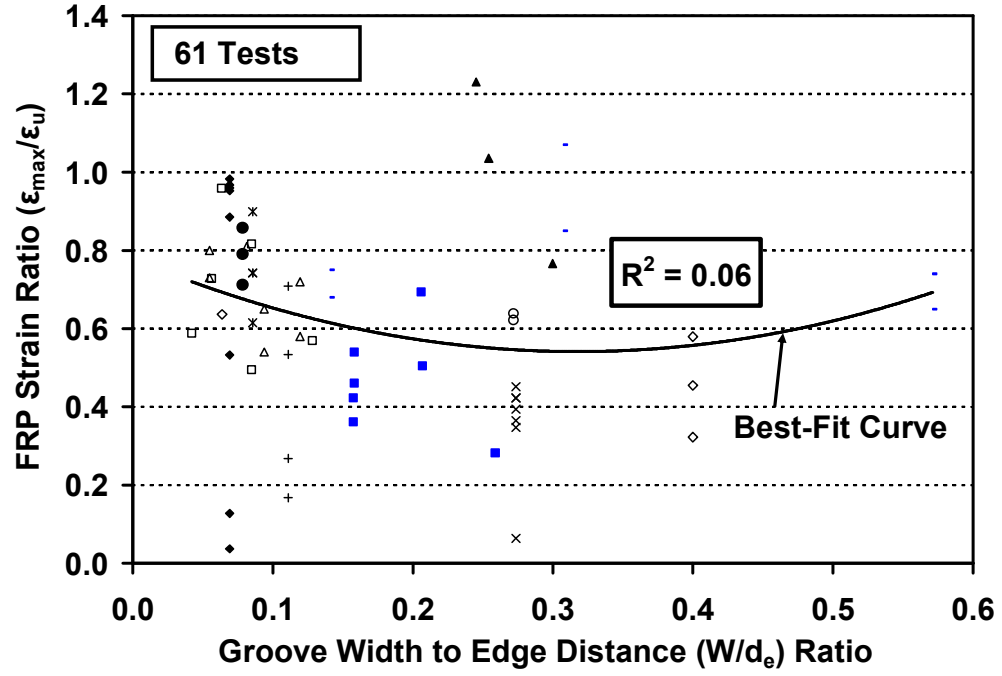

Figure 3.83 (c) Strain Efficacy Versus Groove Width to Edge Distance Ratio

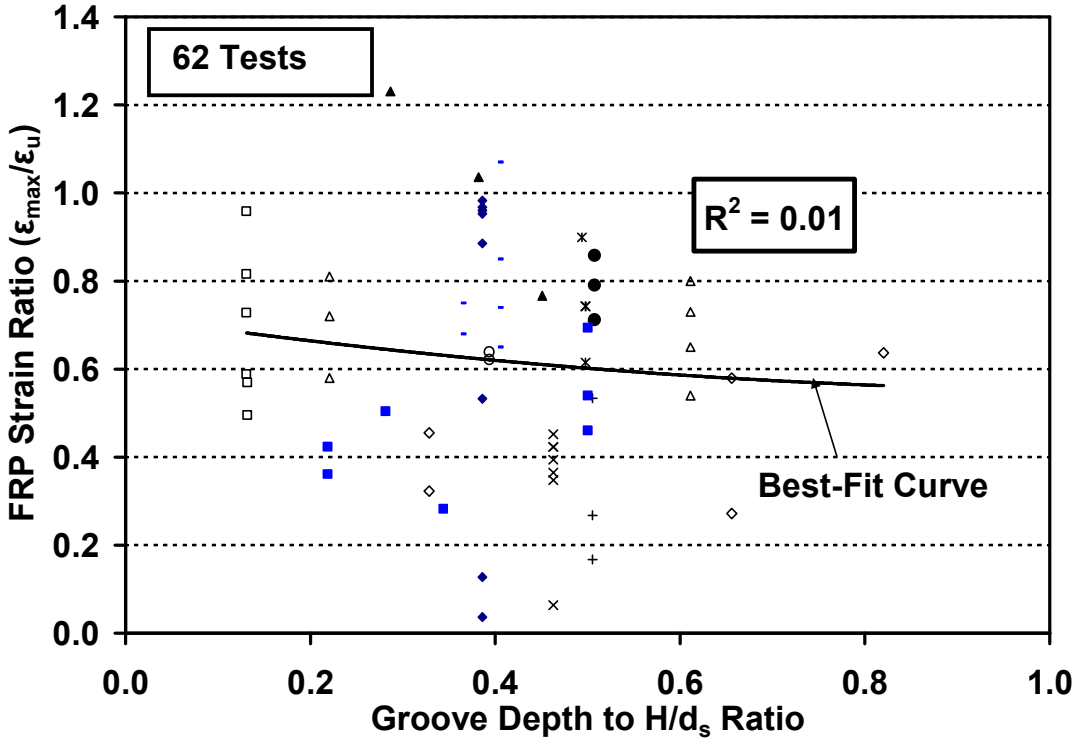

Figure 3.83 (d) Strain Efficacy Versus Groove Depth to Steel Cover Ratio

Figure 3.83 (e) Legend

In each of the above figures, the best-fit regression line and R^2, goodness of the fit are shown. There are two best-fit curves in Figure 3.83 (a). The solid and the dashed curves are for the data including and excluding the outliers, respectively. The outliers are also circled. From the best-fit curves it can be seen that, FRP strain efficacy increased relative to the L_d/A_{FRP} ratio, but peaked at about 0.85. Zero bonded length in the figure refers to arrangements in four-point bending, whereby FRP is provided only within the constant moment region. Removing the outlier test data, the best-fit curve improves considerably to an R^2 value of 0.49. This finding is in agreement with an earlier study by Hassan and Rizkalla (2003), where the authors reported dissipating effectiveness of the bond length beyond a threshold value. With the R^2 values of 0.11, 0.06 and 0.01, respectively, W/H, W/d_e and W/d_s ratios do not appear to have any significant impact on the strain efficacy.

CHAPTER 4

ANALYTICAL STUDY

4.1 Introduction

In order to verify the experimental program and to investigate a broader range of parameters, a 3-D finite element (FE) analysis was conducted using a general purpose FE software ANSYS® 11.0 (2007). ANSYS is a comprehensive FE package with special elements for concrete modeling. In this chapter, the results of the analyses for the pre-cured EB and NSM FRP systems will be presented. For the pre-cured EB FRP systems, tests on surface flatness were simulated by modeling the bond between concrete and FRP. For the NSM FRP systems, the test specimens for the groove size tolerance were modeled. Also, a parametric study on NSM FRP was conducted. Before presenting the analytical results, the element types used and the nonlinear algorithm of ANSYS are presented.

4.1.1 Element Types

In pre-cured EB FRP systems, the main components were concrete, steel rebars, FRP laminate and the bond interface between concrete and FRP. Concrete was modeled with SOLID65 elemenets, steel rebars with LINK8, FRP with SHELL63, and the bond interface with COMBIN39 elements. The latter element type does not simulate the behavior of concrete, epoxy or FRP laminate, but rather the interaction of the three components. In the NSM FRP systems, perfect bond was assumed so that no bond

modeling was required. Similar to the pre-cured EB FRP system, concrete and steel rebars were modeled with SOLID65 and LINK8 elements, respectively. NSM FRP reinforcement was also modeled with LINK8 elements. The epoxy was modeled using SOLID45 elements. The various elements used in the modeling are described below.

4.1.1.1 SOLID65

SOLID65 is an 8-noded solid element solely for concrete modeling. The element has cracking and crushing capabilities, as well as plastic deformation and creep. It allows the user to model steel rebars as smeared or discrete reinforcement. The element is defined by 8 nodes, with 3 translational degrees of freedom (DOF) at each node. It also includes isotropic material properties. Element geometry is shown in Figure 4.1.

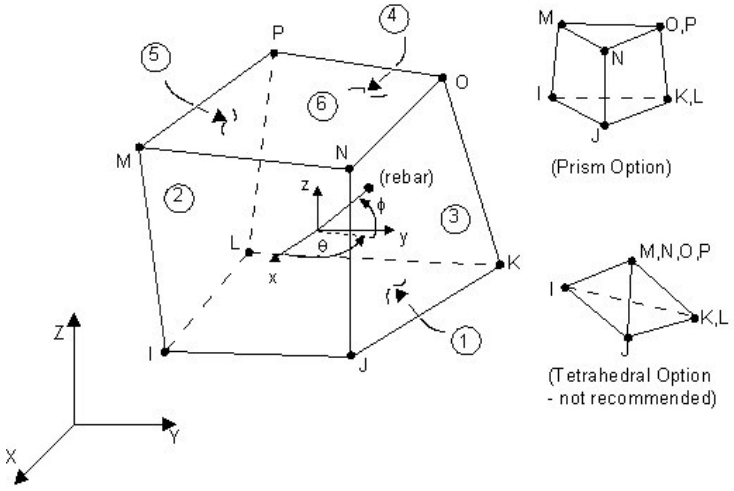

Figure 4.1 SOLID65 Geometry (ANSYS 2007)

4.1.1.2 LINK8

LINK8 is a 2-noded spar, as a uniaxial tension-compression element with three translational DOFs at each node. The element is capable of plasticity, creep, swelling, stress stiffening, and large deflections. Element geometry is shown in Figure 4.2.

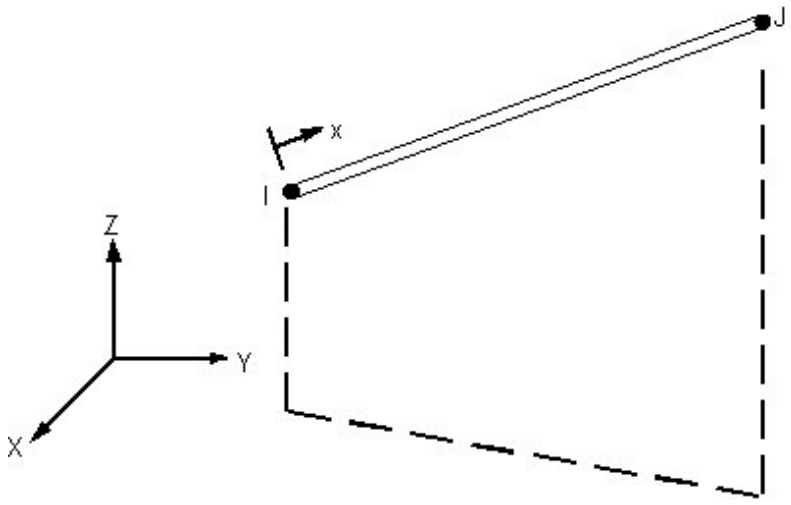

Figure 4.2 LINK8 Geometry (ANSYS 2003)

4.1.1.3 SHELL63

SHELL63 is a 4-noded elastic shell element with both bending and membrane capabilities. The element has 6 DOFS at each node; 3 translations and 3 rotations. It also includes orthotropic material properties. Although the element is capable of stress stiffening and large deflections, only its elastic capabilities were used. Element geometry is shown in Figure 4.3.

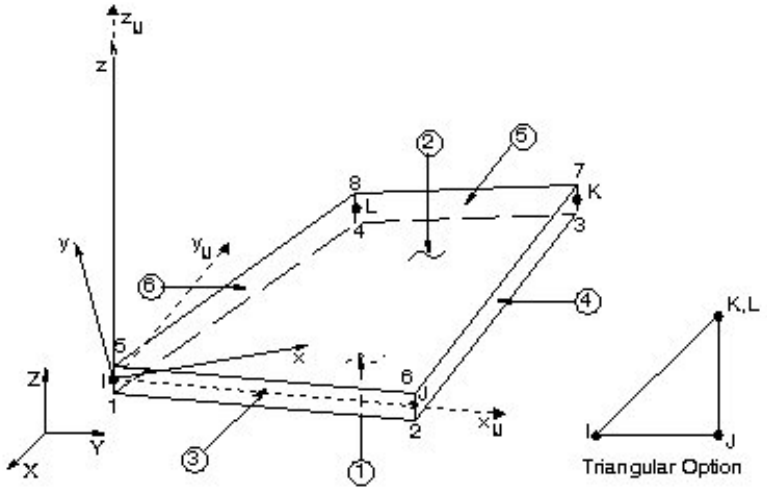

Figure 4.3. SHELL63 Geometry (ANSYS 2003)

4.1.1.4 COMBIN39

COMBIN 39 is a 2-noded unidirectional element with nonlinear generalized force-deflection capability which can be used in 1-D, 2-D or 3-D applications. In this study, the 1-D longitudinal option was used which is a uniaxial tension-compression element with 3 translational DOFs at each node. Element geometry is shown in Figure 4.4.

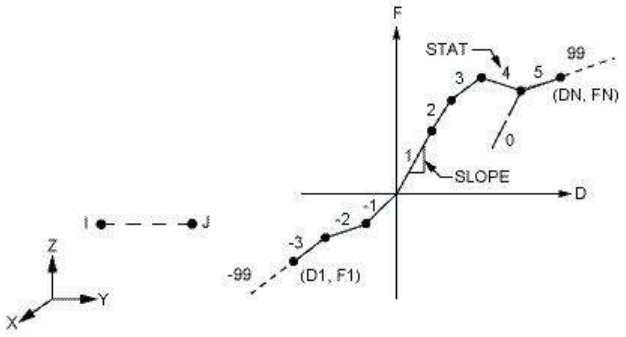

Figure 4.4 COMBIN39 Geometry (ANSYS 2003)

4.1.1.5 SOLID45

SOLID45 is identical to the SOLID65 element, except for its lack of cracking and crushing capabilities. The element also has orthotropic material properties. Element geometry is shown in Figure 4.5.

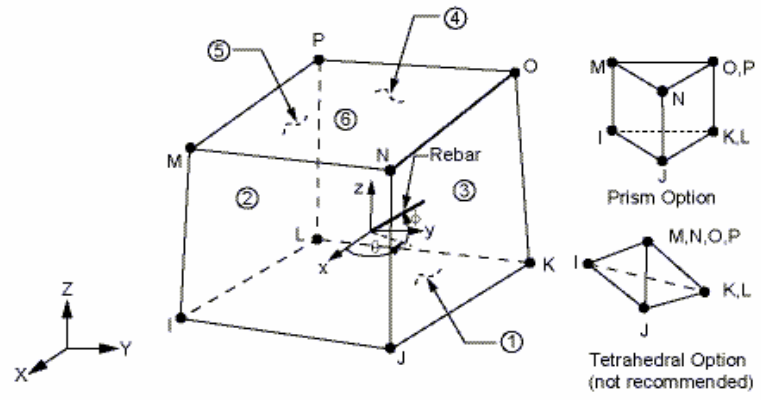

Figure 4.5 SOLID45 Geometry (ANSYS 2003)

4.1.2 Real Constants

Some elements in ANSYS require additional inputs, termed real constants, to define geometric or physical properties. Real constants for SOLID65 element define the smeared reinforcement details. Since the steel and FRP rebars were modeled separately using LINK8 elements, the real constants were entered as zero in SOLID65, except for the material type. Cross sectional area and thickness were entered for the LINK8 and. SHELL63 elements. SOLID45 requires no real constant, but for COMBIN39 all the force-displacement pairs are needed. Force-deformation relationship was based on the bond-slip model by Lu et al. (2005), which was explained in detail in Section 2.1.2. Table 4.1 shows a sample force-deformation input for COMBIN39 elements for a concrete compressive strength of 5 ksi, and a width ratio (b_f / b_c) of 1/3.

Table 4.1 Force-Deformation Input for COMBIN39 elements

Deformation (in.)	Force (kips)
0.0000	0.000
0.0004	0.179
0.0008	0.253
0.0016	0.358
0.0020	0.401
0.0024	0.439
0.0028	0.474
0.0035	0.537
0.0041	0.575
0.0043	0.530
0.0047	0.472
0.0075	0.211
0.0102	0.094
0.0130	0.042
0.0157	0.019
0.0185	0.008
0.0213	0.004
0.0240	0.002
0.0268	0.001
0.0295	0.000

4.1.3 Material Models

4.1.3.1 Concrete

Hognestad's stress-strain relationship was utilized for concrete. Multilinear isotropic hardening table (MIHT) was used to input stress-strain pairs for points on the curve. In addition to the nonlinear relationship, linear material properties were entered using the linear isotropic material properties table. These properties are the modulus of elasticity (E) and the Poisson's ratio (υ). Thirdly, a series of real constants are needed as follows: shear transfer coefficient for an open crack (STCOC), shear transfer coefficient for a closed crack (STCCC), uniaxial tension cracking stress (UTCS), uniaxial crushing stress (UCS), biaxial cracking stress (BCS), ambient hydrostatic stress state coefficient (AHSSC), biaxial crushing stress under ambient hydrostatic pressure (BCSH), uniaxial crushing stress under hydrostatic pressure (UCSH), and stiffness multiplier for cracked tensile condition (SMCTC). The range of values for STCOC is between 0 and 1, where 0 represents no shear transfer, and 1 represents full transfer of shear. STCCC is required only when cyclic loading is involved. UTCS in this study was calculated as the modulus of rupture for concrete. UCS was set to -1 to turn the crushing capability off. BCS, AHSSC, BCSH and UCSH were irrelevant to this study, and therefore were set to zero. SMCTC is used to define the effect of tension stiffening, where tensile strength drops after cracking. The range of values for this constant is between 0 and 1, where 0 denotes full loss of tensile strength and 1 denotes no loss (Wu 2006). Points defining the stress-strain relationship and constants used for concrete with a typical compressive strength of 5 ksi are listed in Table 4.2 and 4.3, respectively. In addition to 5 ksi, concretes with 4, 7

and 10 ksi compressive strengths were also modeled as will be explained in the parametric studies.

Table 4.2 Hognestad's Model for Concrete (f'_c = 5 ksi)

Stress (ksi)	Strain
0.0000	0.00000
0.7984	0.00021
1.5273	0.00041
2.1869	0.00062
2.7771	0.00083
3.2979	0.00103
3.7492	0.00124
4.1312	0.00145
4.4438	0.00165
4.6869	0.00186
4.8607	0.00207
4.9650	0.00227
5.0000	0.00248
4.9576	0.00257
4.9149	0.00265
4.8721	0.00274
4.8294	0.00283
4.7866	0.00291
4.7439	0.00300

Table 4.3 Constants for Concrete (f'_c = 5 ksi)

ShrCf-Op	0.2
ShrCf-Cl	0.5
UnTensSt (ksi)	0.53
UnCompSt	-1
BiCompSt	0
HydroPrs	0
BiCompSt	0
UnTensSt	0
TenCrFac	0.6

4.1.3.2 Steel

Bilinear isotropic hardening model and linear isotropic material properties were used to model steel. E and υ were taken as 29,000 ksi and 0.3, respectively. Yield stress and post-yielding tangent modulus were entered as 66 ksi and 0.1, respectively. A

relatively small value for tangent modulus was used to overcome convergence problems arising due to the zero slope.

4.1.3.3 Pre-cured and Wet Lay-up FRP

Both the pre-cured and the wet lay-up FRP were modeled with linear orthotropic material properties, with a major "strong" direction and weaker orthogonal directions. E, υ and shear modulus (G) for each of the three directions are entered as shown in sample inputs for pre-cured and wet lay-up FRPs used in the experimental program in Table 4.4.

Table 4.4 Linear Orthotropic Material Properties for Pre-Cured and Wet Lay-up FRP

	Pre-cured FRP	**Wet Layup FRP**
E_X (ksi)	19000	10240
E_Y (ksi)	1900	706
E_Z (ksi)	1900	706
υ_{XY}	0.2	0.2
υ_{YZ}	0.2	0.2
υ_{XZ}	0.2	0.2
G_{XY} (ksi)	1267	4231
G_{YZ} (ksi)	90	292
G_{XZ} (ksi)	90	292

4.1.3.4 NSM FRP and Epoxy

Linear isotropic material properties were used for both the NSM FRP and the epoxy with E and υ being 18,000 and 0.3 for the NSM FRP, and 435 and 0.3 for the epoxy for the typical benchmark model. In addition to the benchmark model different FRP and epoxy moduli were also used in the parametric studies as will be described in their respective sections.

4.1.3.5 Bond Modeling

In EB FRP systems, there are two approaches for modeling: one with perfect bond and no relative slippage between the concrete and FRP; while the other one includes a bond-slip model for the FRP-concrete interface. In the latter case what is modeled is not the epoxy but rather the overall behavior of the FRP-epoxy-concrete interface. In order to simulate such behavior, COMBIN39 nonlinear spring elements were used with the most common bond-slip model of Lu et al. (2005) as previously explained in Chapter 2. FRP was connected to concrete using 3 mutually orthogonal springs at each coinciding node. For the longitudinal springs, the nonlinear force-deflection relationship was obtained from the adopted bond-slip model. In the other two orthogonal directions, significantly stiffer springs were provided to prevent undesired deflections. Figure 4.6 shows a schematic representation of the interface model. In this figure, C represents the concrete node and F represents the FRP node which coincide. Although could not be shown, all three springs at the same node location are connected to the same concrete and FRP nodes. Similar approaches have been used by Abdel Baky et al. (2007) and Alemu and Bhargava (2007) in their numerical simulations. Perfect bond was assumed at the locations of wet lay-up U-straps.

Using the equations proposed by Lu et al. (2005) the bond-slip relationship for the test specimens were predicted. Calculated bond stress versus slip relationship was converted into force-deflection relationship, as required by the ANSYS program. A typical bond-slip relationship is shown in Figure 4.7.

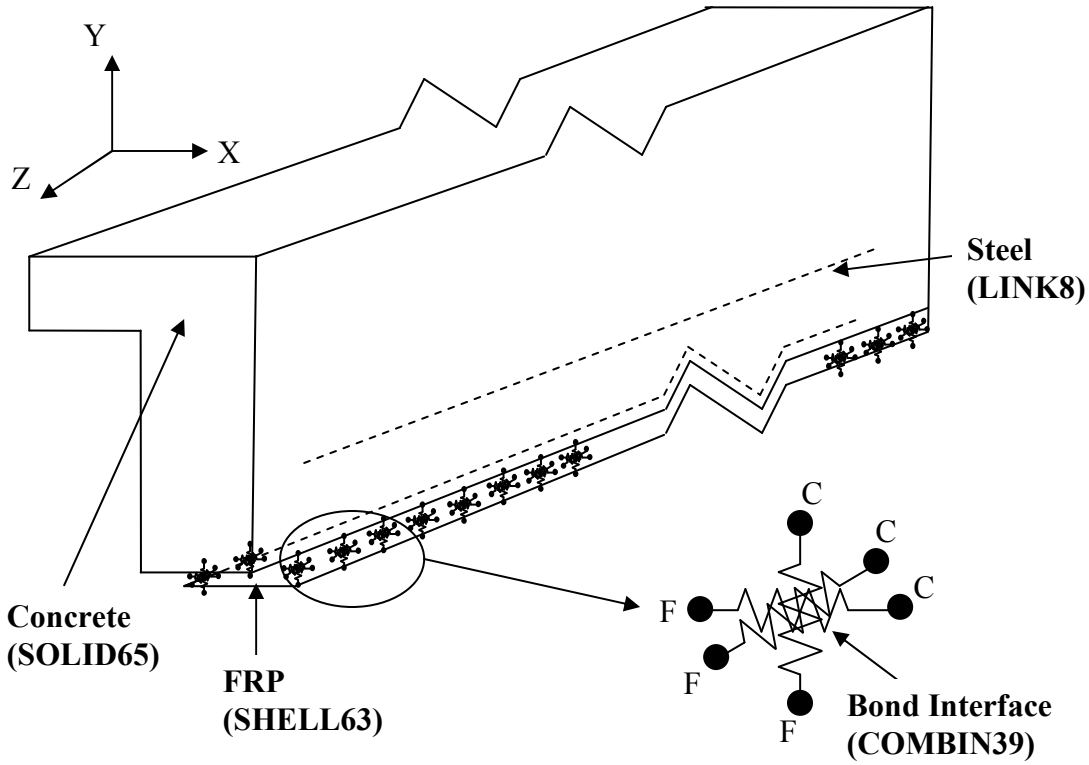

Figure 4.6 Bond Modeling (U-Straps are Not Shown)

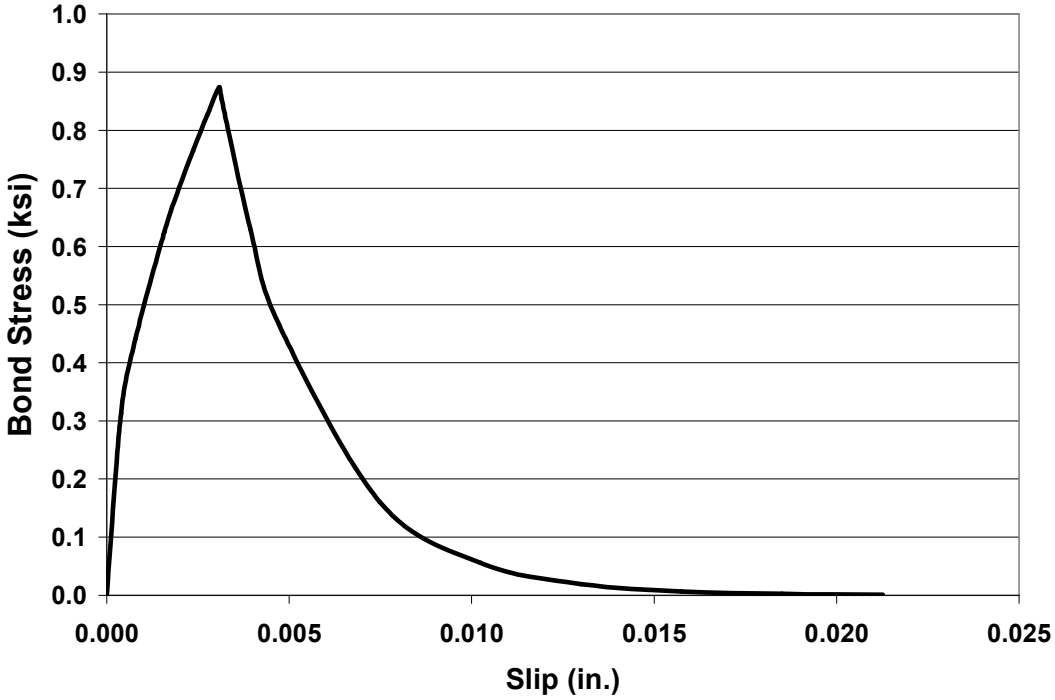

Figure 4.7 Typical Bond-Slip Relationship

4.1.4 Loading and Boundary Conditions

Loading was applied either in displacements or force control, the former producing better results for flexural models, while the latter and worked better for pull-off models, as will be explained later. Symmetry boundary conditions were applied whenever possible in order to save computational time and memory. Appropriate restraints were also applied at each support.

4.1.5 Analysis Algorithm and Solution Controls

ANSYS employs an iterative technique for nonlinear analysis, Newton-Rapson approach, whereby the load step is divided into substeps and is gradually applied. For each substep a separate linear analysis is carried out. Automatic time stepping was used, which increases load step size as long as converged solutions are obtained, and reduces it if necessary. The option helps save computational time. The minimum, maximum and total number of substeps specified, as follows: The minimum number of substeps ranged from 2,000 to 40,000, whereas the maximum number of substeps varied from 10,000 to 80,000. Throughout the analyses, depending on the requirements of each model, convergence tolerance values of 0.025 and 0.05 were used. Restart option was used when convergence difficulties were experienced. Using this option allows the user to relax the convergence tolerance in an attempt to proceed with the analysis. Line search was turned on as a convergence enhancement tool. The maximum number of iterations was set to 1,000, as the experience proved it to be the optimum value for convergence.

4.2 Pre-Cured FRP Systems

4.2.1 Model Validation for Pull-Off Tests by Yao et al. (2005)

In order to test the validity of the adopted bond-slip model of Lu et al. (2005), a representative test case among the near end supported single-shear pull tests conducted by Yao et al. (2005) was modeled using ANSYS. Bond-slip models are generally developed using the results from the bond pull-off tests. Therefore, it was decided to validate the ANSYS model using such test cases. Test setup and the imposed bond-slip relationship are shown in Figures 4.8 and 4.9, respectively.

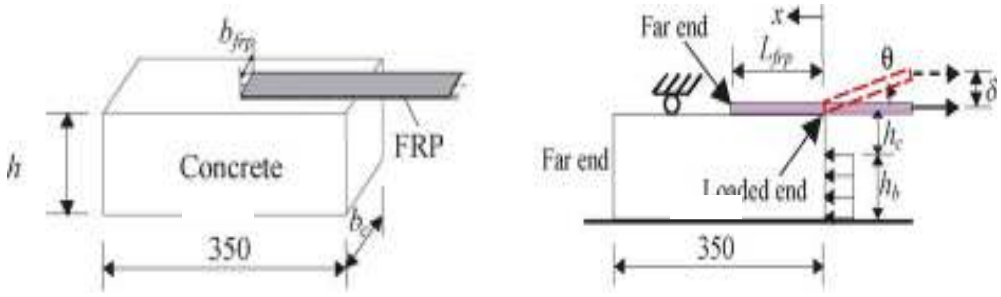

a) Perspective **b) Elevation**

Figure 4.8 Test Setup (Yao et al. 2005)

Test specimen I-11 of Yao et al. (2005) was modeled with parameters in Figure 4.8, $h, b_{frp}, b_c, h_b, L_{frp}$ and θ taken as 6, 1, 6, 1.2, 3 in and 0^o, respectively. The SOLID65, SHELL63 and COMBIN39 elements were used for modeling the concrete, the FRP plate and the interface, respectively. The failure load was found as 1.35 kips while the reported failure load was 1.29 kips with an error margin of only 4.65%. This validated the ANSYS adaptation of the bond-slip model.

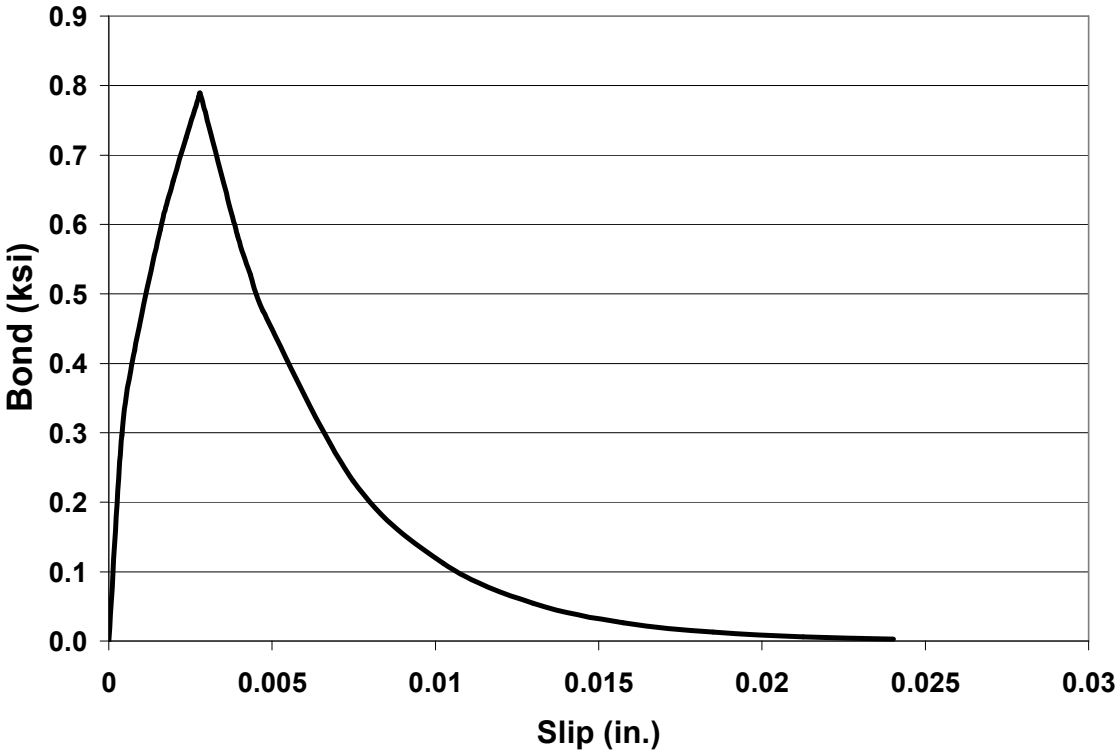

Figure 4.9 Bond-Slip Relationship for Bond Pull-Off Specimen

4.2.2 Pre-cured Beam Specimens

4.2.2.1 Model Verification for Previous Studies

In order to verify the proposed finite element model, a representative test case, namely specimen A1-II, from the study by Brena and Macri (2004) was modeled with ANSYS. Specimen details are shown in Figure 4.10.

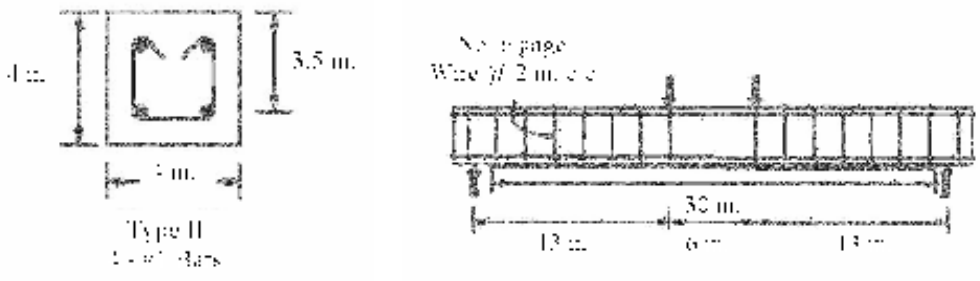

a) Cross-section b) Elevation

Figure 4.10 Specimen Details

Figure 4.11 compares the load-deflection diagram from the experiment and the predicted one using the model. As it can seen the proposed model was able to predict the actual response within an acceptable range. The model softens near the ultimate load, which is not observed during the test. The error in predicting the peak load, displacement at the peak load and post-cracking stiffness (i.e., between cracking and yielding points) were 16%, 11% and 8%, respectively.

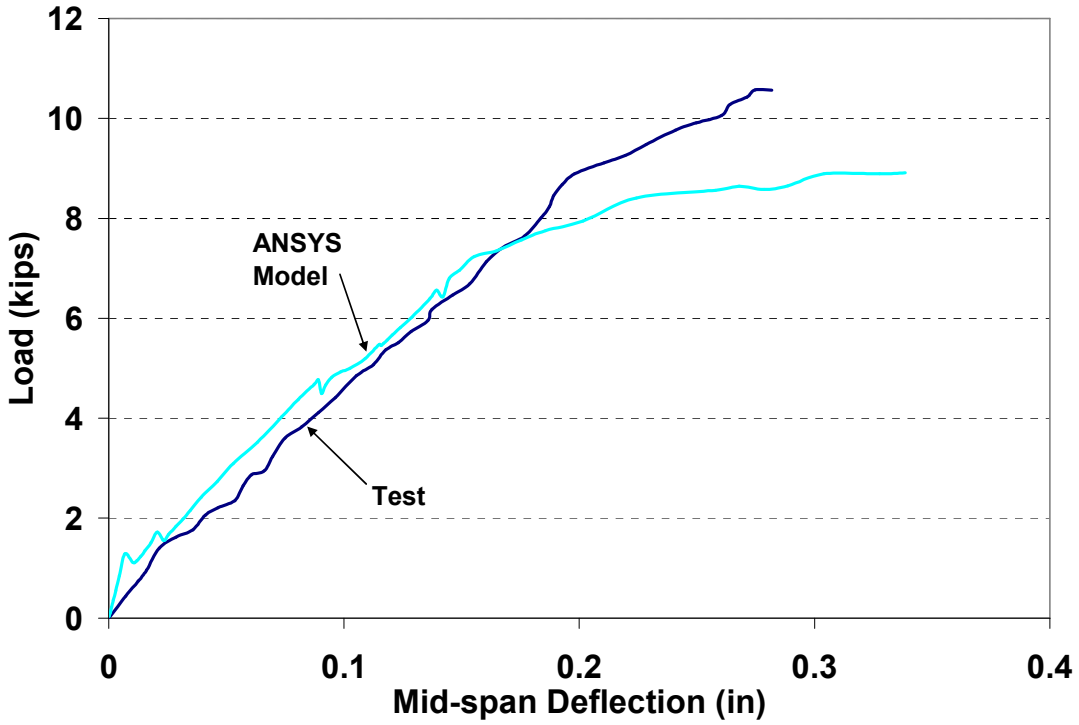

Figure 4.11 Comparison of the Measured and Predicted Load-Deflection Diagrams

4.2.2.2 Model Verification for Control Specimen

Before modeling specimens with surface flaws, the control specimen was modeled. While modeling the control specimen, three possible approaches for treating the bond between the concrete and FRP were utilized, as follows: perfect bond modeling,

perfect bond modeling with infinitely stiff springs, and bond modeling using spring elements with finite stiffness. In the perfect bond modeling, the coinciding nodes of the concrete and FRP are simply merged together. In the perfect bond modeling with infinitely stiff springs, the coinciding nodes are not merged but rather are connected with very stiff springs in three mutually orthogonal directions. Finally, bond can be modeled using springs with finite stiffness based on appropriate bond-slip relationships, as described in Section 4.1.3.4. Figure 4.12 shows the load-deflection diagrams obtained utilizing all three approaches in comparison the test result.

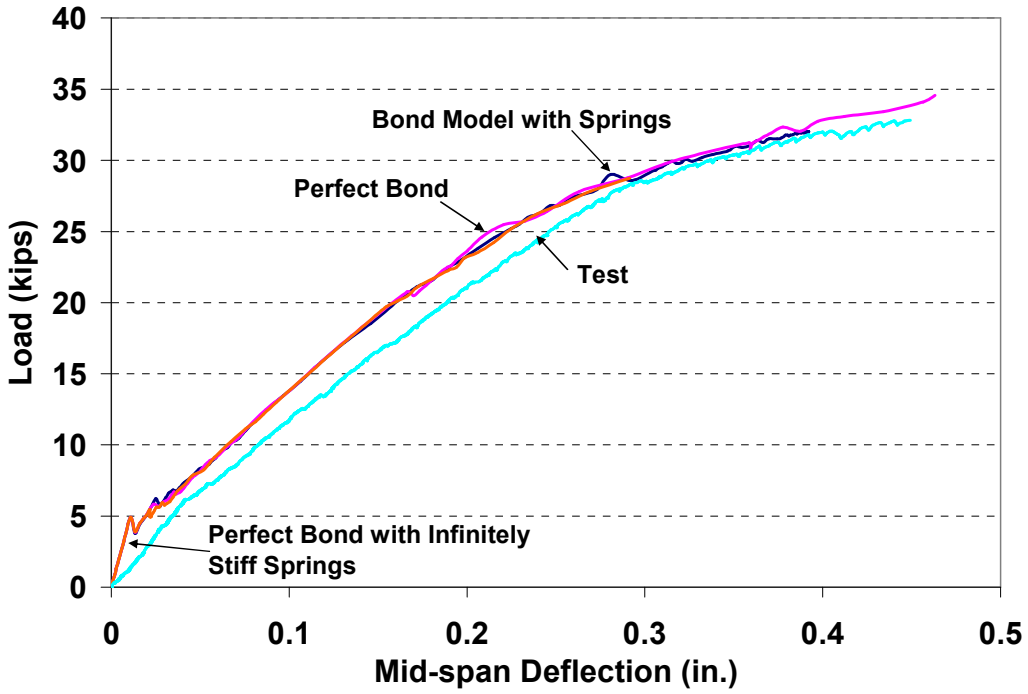

Figure 4.12 Load-Deflection Diagrams for the Control Specimen

As seen from the figure, all three approaches for bond modeling in the pre-cured FRP-strengthened concrete beams produced similar results generally agreeable with the test results. Similar conclusions were reported by Niu and Wu (2006) who used the

general purpose FE package DIANA for analyzing a carbon FRP-strengthened concrete beam tested under three point bending. Some of the parameters investigated in their study were interface stiffness, interfacial bond strength and the shape of the bond-slip curve. Interface stiffness refers to the initial stiffness of the bond-slip curve, and interfacial bond strength to the maximum bond strength. Interface stiffness ranging from 0.160 to 5.71 ksi were considered for this study and the reported load-deflection diagrams showed no significant difference. Likewise the value of the interface bond strength did not affect the load-deflection behavior, although values ranging from 0.073 to 2.32 ksi were considered for the simulation. Finally, the shape of the bond-slip curve did not show a significant impact on the response. Considering the case of bond model with springs the error in predicting the peak load, displacement at the peak load and post-cracking stiffness were 2%, 13% and 4%, respectively.

4.2.2.3 Modeling of Surface Flatness

Although only 1/16 in. of surface out-of-flatness was considered in the experimental program, it was decided to investigate this issue further through FE modeling. The models were developed for both valley and peak specimens with surface out-of-flatness levels of 1/2 in., 1.4 in., 1/8 in. and 1/16 in. The interface between the concrete and the pre-cured FRP was modeled, as described in Section 4.1.3.4, whereas perfect bond was assumed for wet lay-up U-straps. Figure 4.13 shows the FE mesh and the FRP configuration for the 1/2 in. valley model. Note the depression on the right hand side in Figure 4.13a. In Figure 4.13b wet lay-up U-straps and the main flexural reinforcement are shown.

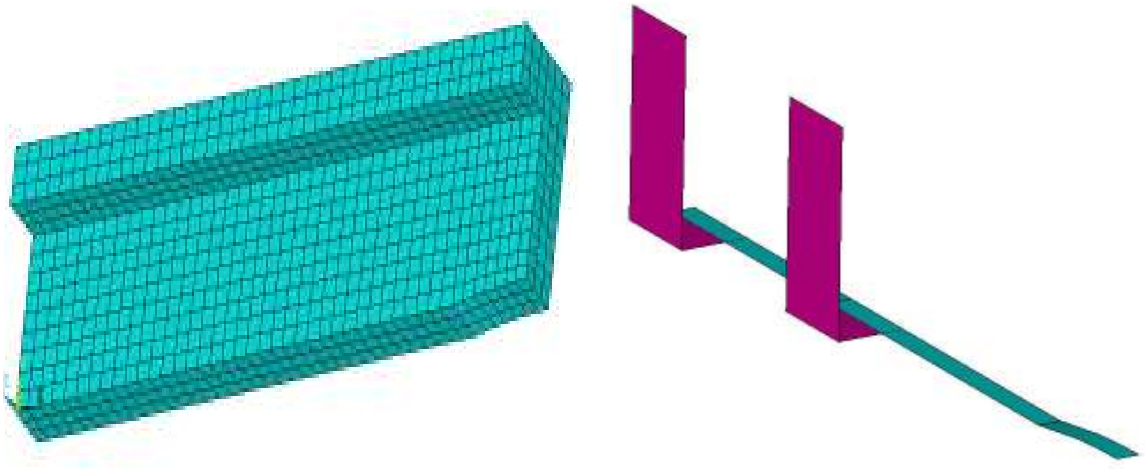

a) FE mesh b) FRP Configuration

Figure 4.13 FE Mesh and FRP Configuration for the 1/2 in. Valley Model

Figures 4.14 and 4.15 show the predicted and experimental load-deflection response for the 1/16 in. peak and valley specimens, respectively.

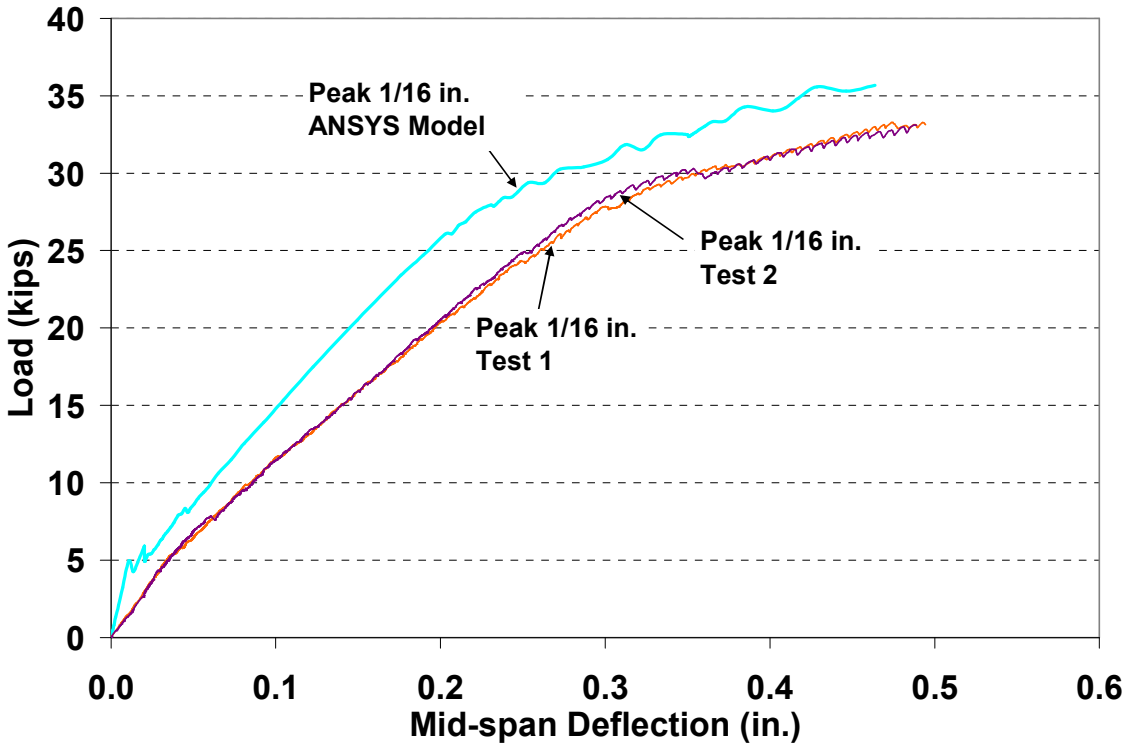

Figure 4.14 Load-Deflection Response for the 1/16 in. Peak Specimens

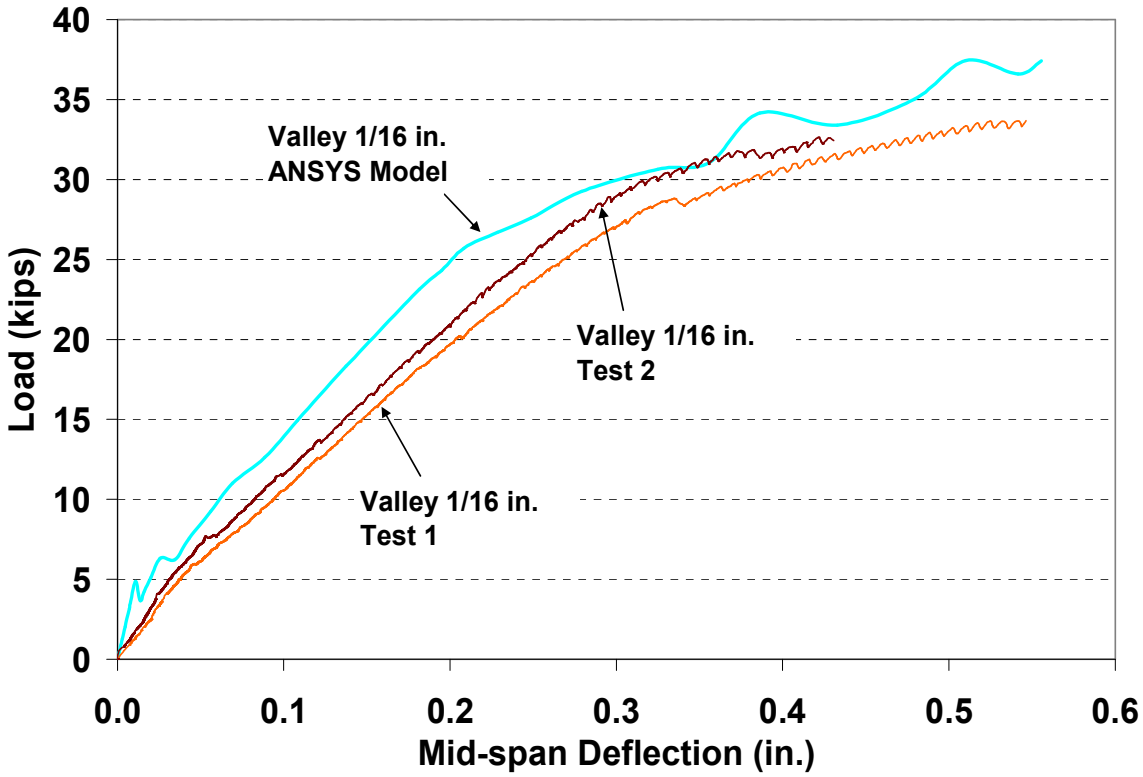

Figure 4.15 Load-Deflection Response for the 1/16 in. Valley Specimens

As seen from the above figures, both the peak and valley models were successful in predicting the actual response with an acceptable accuracy. The difference between the initial stiffness is due to the unintentional pre-cracking of the specimens. In Figure 4.14, for the Peak 1/16 in. specimen 1, the error in predicting the peak load, displacement at the peak load and post-cracking stiffness were 7%, 6% and 24%, respectively. Similarly in Figure 4.15, for the Valley 1/16 in. specimen 2, the error in predicting the peak load, displacement at the peak load and post-cracking stiffness were 15%, 30% and 17%, respectively. Figure 4.16 compares the predicted load-deflection response for all the peak and the valley models together with the control specimen.

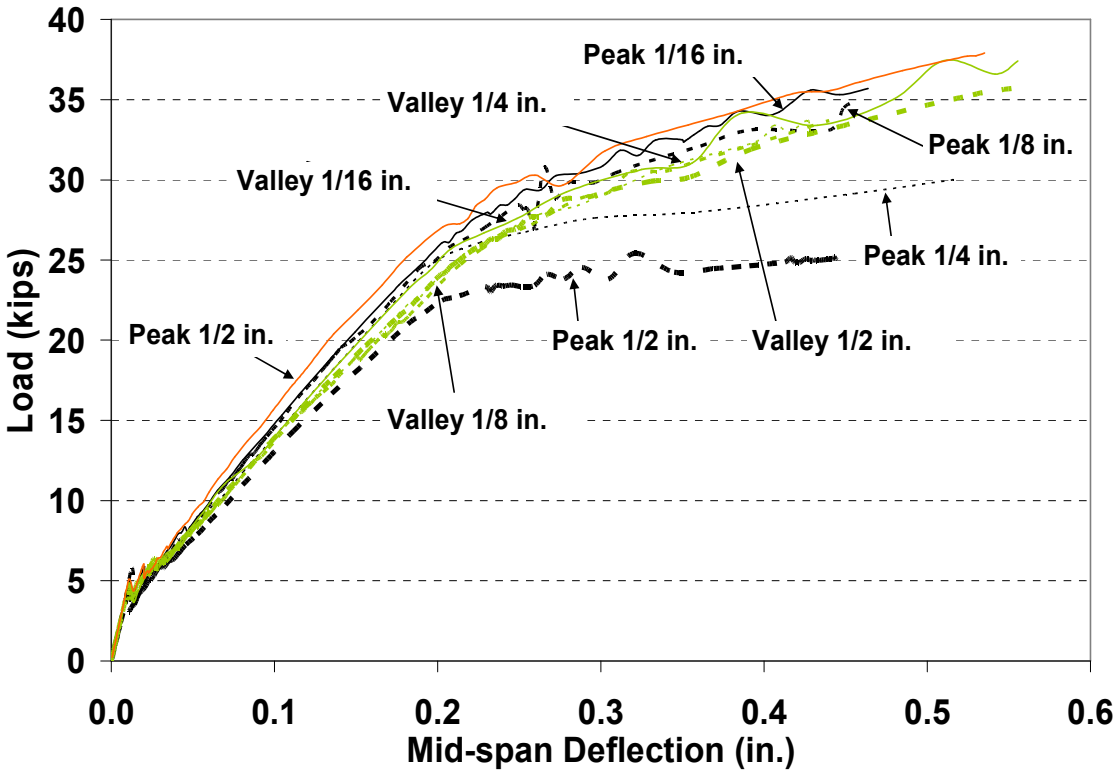

Figure 4.16 Load-Deflection Responses for Surface Flatness Models

Figure 4.16 shows that the control model and the 1/2 in. peak model were the upper and lower bounds for the load-deflection response. All flawed models showed lower stiffness than that of the control model along with a lower peak load. Figures 4.17 and 4.18 show the load-deflection response for all peak and valley models. It is clear from Figure 4.17 that the poorest performance was demonstrated by the 1/2 in. peak specimen, whereas the 1/16 in. and 1/8 in. specimens performed almost the same. Peak loads for the 1/2, 1/4, and 1/8 and 1/16 in. specimens were around 25, 30 and 35 kips, respectively at a mid-span deflection of approximately. No such trend could be seen for the valley models, as all peaked around 35 kips and 0.55 in. mid-span deflection with no significant difference in their load-deflection responses. From the load-deflection response for the surface flatness models, it can be concluded that 1/8 in. out-of-flatness is

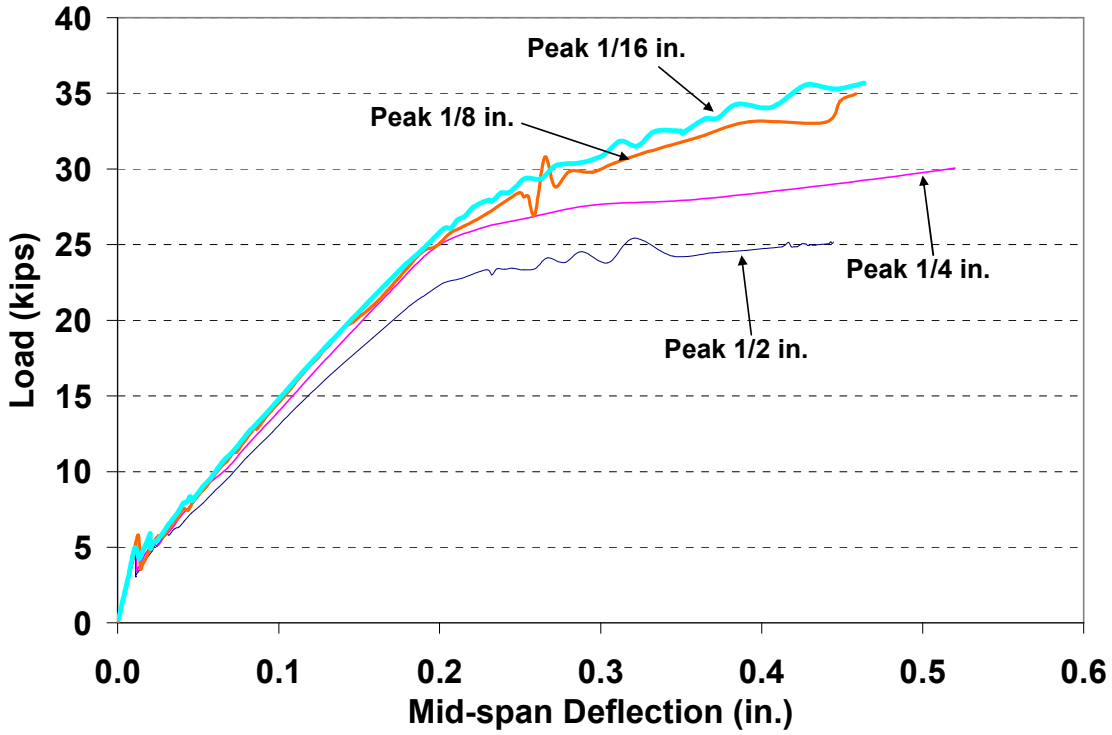

Figure 4.17 Load-Deflection Responses for Peak Models

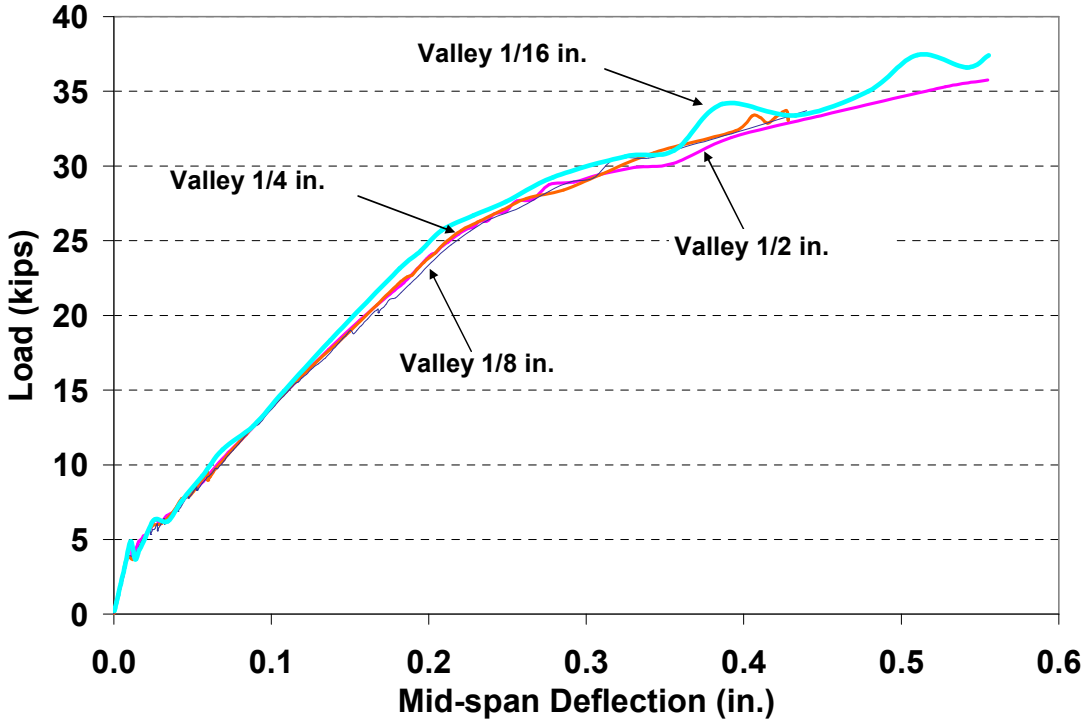

Figure 4.18 Load-Deflection Responses for Valley Models

the appropriate threshold limit for guaranteed system performance. Figure 4.19 shows the maximum stress in the pre-cured FRP for each model.

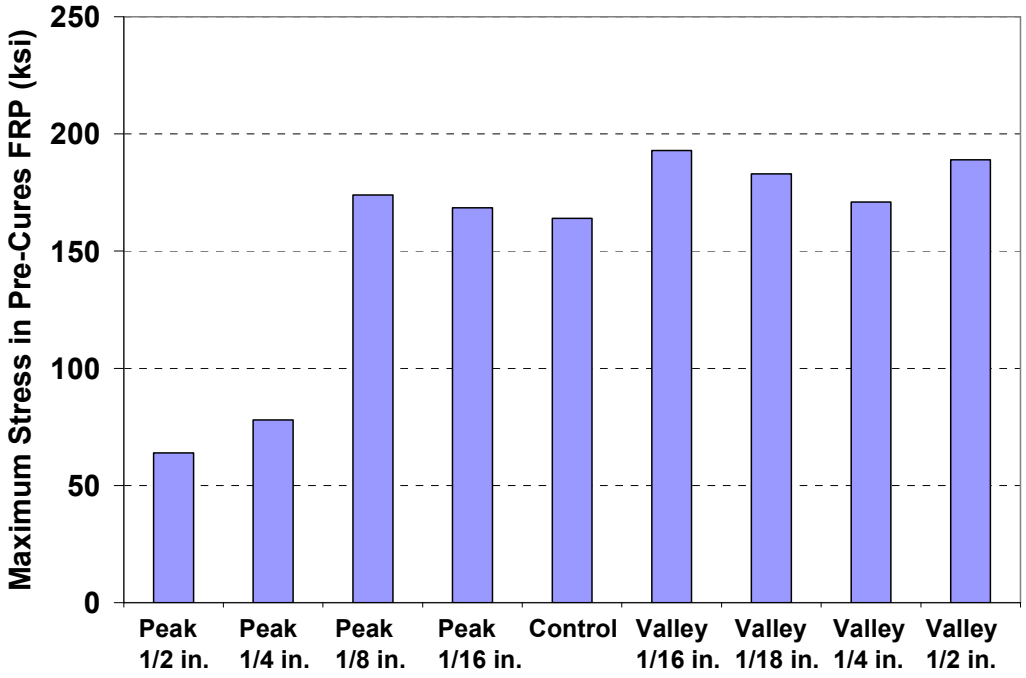

Figure 4.19 Maximum Stress in Pre-Cured FRP

Considering Figures 4.17 and 4.19 together, it can be concluded that as the out-of-flatness level increases for the peak specimens, the maximum stress in FRP decreases. This implies that the failure is premature and more brittle, as compared to the control and valley specimens. No such trend exists for the valley specimens. In valley specimens, the FRP in the curved region debonds, but debonding is arrested at the edges of the region and FRP begins to straighten itself. Once the FRP straightens, the out-of-flatness level no longer affects the behavior, which can be likened to a tied arch. After straightening, the FRP acts as a tension member, and the load capacity of the beam remains unaffected. In the case of peak specimens, however, once the load is applied, debonding initiates at the

edges of the bump. However, since the curvature is concave down, no FRP straightening occurs. Thus, the tensile capacity of the FRP remains limited. Figure 4.20 schematically shows this phenomenon.

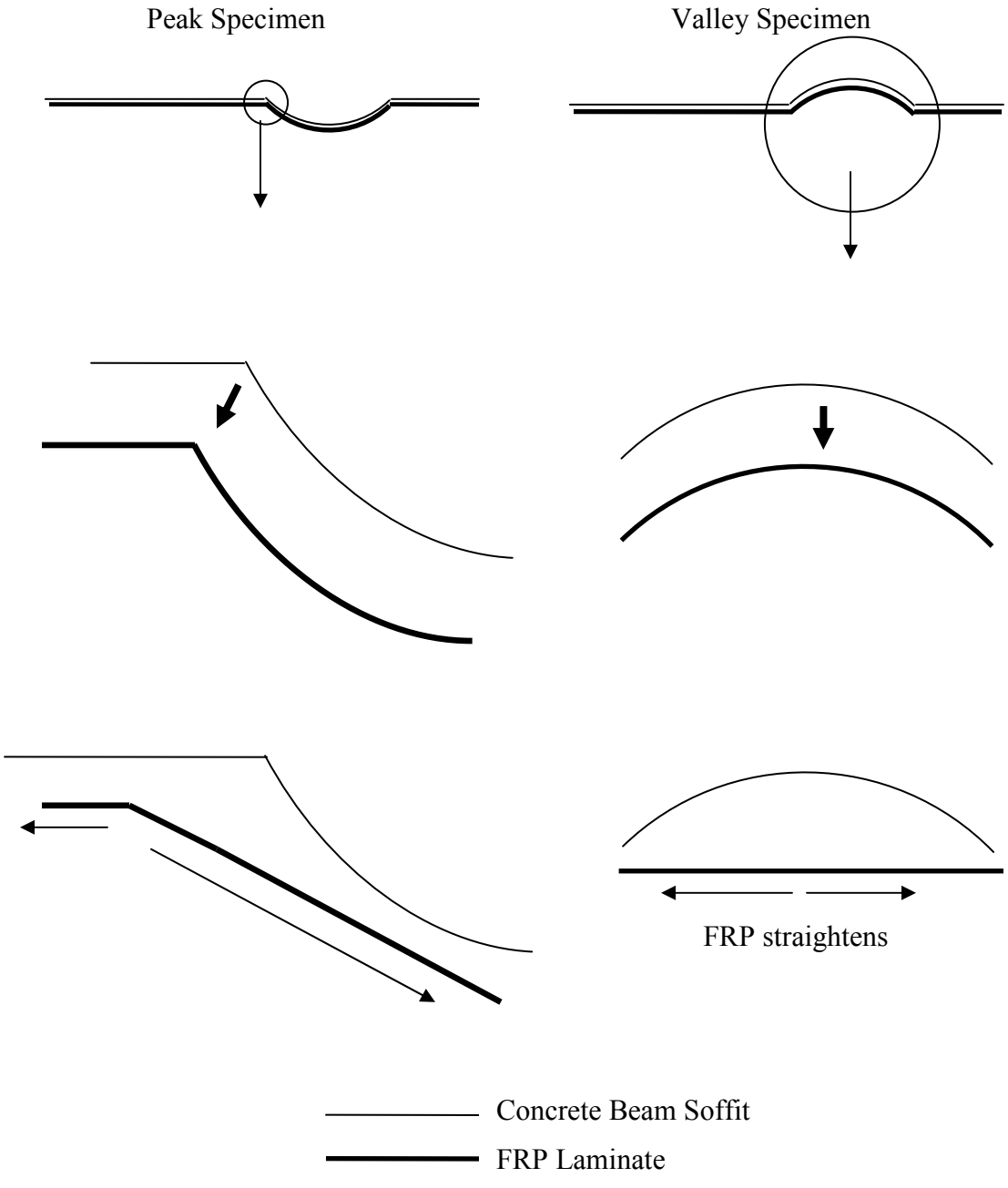

Figure 4.20 Debonding in Surface Flatness Specimens

4.3 NSM FRP Systems

In this section, first, the FE model for NSM FRP systems will be explained in detail. Then, model validation with the tests from both the present study and the literature will be presented. Subsequently the models will be used to explain the effect of the groove size tolerance. Finally, this section will be concluded with the results of the parametric study for both geometric and physical factors.

4.3.1 Generic Model Description

To save computational time and memory, only a quarter of the beams were modeled taking advantage of their symmetry. Figure 4.21 shows a typical FE mesh for the 9/16 in. square groove. The elements were typically of 1 in. size, except for the refined mesh around the groove, and the smooth transition area between the two regions. Smooth transition between the coarse and fine mesh regions produce better results. Assuming perfect bond, all coinciding nodes were merged together. Loading was applied as nodal displacements at the mid-span over an area with the same dimensions as the actual loading plate used in the experiments. Displacement control generally produces better results than the load control in traversing the bifurcation points, such as at concrete cracking and steel yielding. Symmetry boundary conditions and support restraints were also applied accordingly.

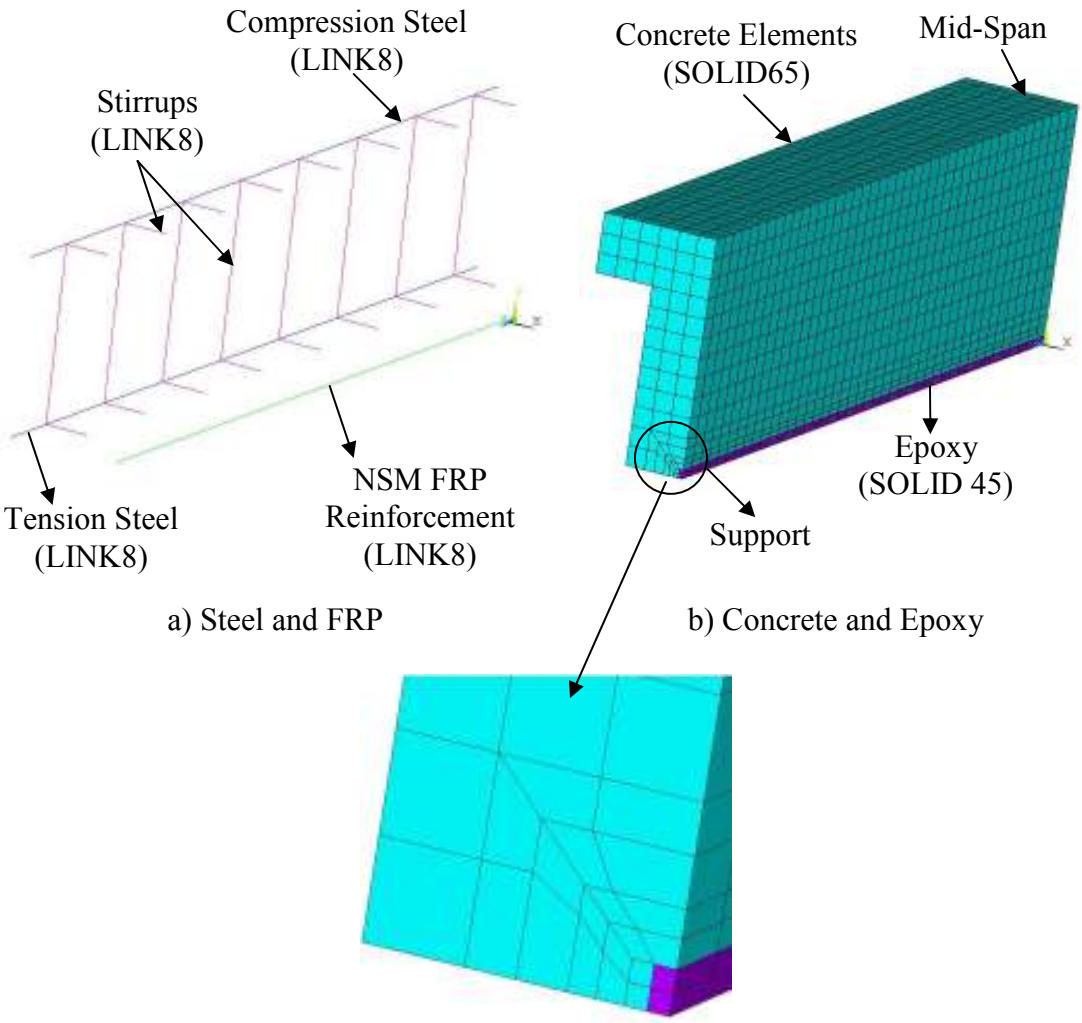

Figure 4.21 Finite Element Mesh

4.3.2 Model Validation

In order to validate the FE model, two test cases were analyzed; one from the present study and another from the literature. The test case from this study was the 7/16 in. square groove model with NSM FRP bar. Load-deflection responses of the test and predictions of the FE model are shown together in Figure 4.22.

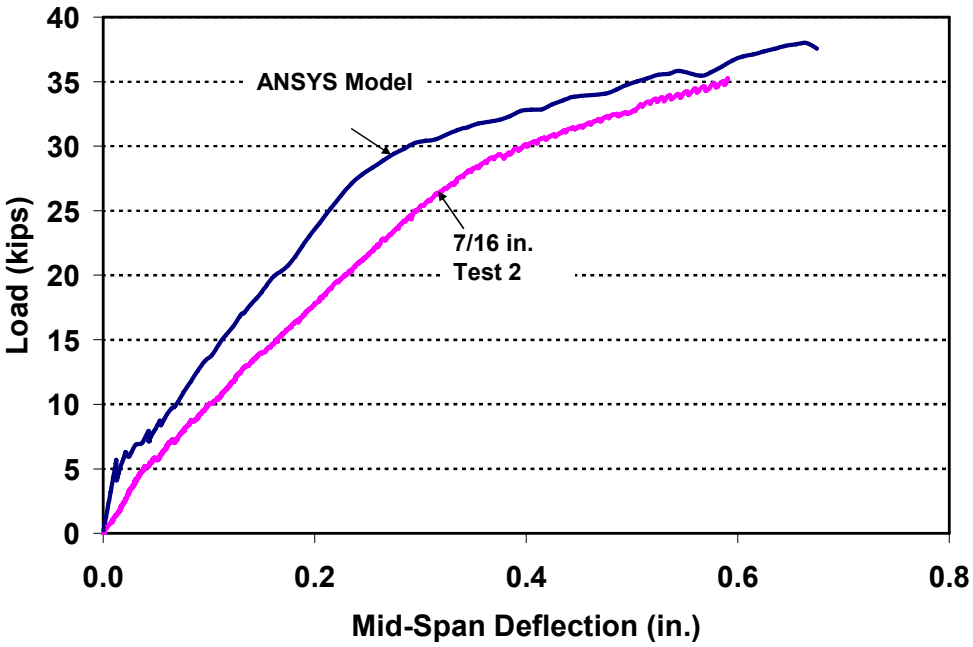

Figure 4.22 Model Validation with Present Study

In Figure 4.22, although the FE model response appears stiffer than the test results, there is adequate agreement to validate the model. Note that for the FE model, the reported material properties for steel, FRP and epoxy were used, which may differ from the actual values. Moreover, test results do not show a distinct cracking point which implies that the beam was already cracked before the test. The error in predicting the peak load, displacement at the peak load and post-yielding stiffness were 8%, 12% and 12%, respectively.

FE model was further verified using Specimen S1-NSM of Barros et al. (2007). Figure 4.23 shows the details of the specimen, which was a 39 in. long doubly reinforced rectangular concrete beam with a section depth of 6.7 in. and a width of 4.7 in. Two No. 5M and two No. 6.5M steel bars were provided as tension and compression reinforcement, respectively. Shear reinforcement consisted of No. 6M bars at 3.1 in. spacing on center. Concrete compressive strength was 8 ksi. Yield strength of steel used

was 114, 91 and 78 ksi for the tension, compression and shear reinforcement, respectively, as measured in the laboratory tests. The NSM FRP reinforcement was a single carbon FRP strip with 0.055 in. thickness and 0.378 in. width, a tensile strength of 397 ksi, and a modulus of elasticity of 23,032 ksi. Epoxy used for filing the grooves had an average tensile strength of 2.8 ksi and a Young's modulus of 725 ksi. The beam was tested under four-point bending with a constant moment zone of 11.8 in., and a clear flexural span of 35.4 in. Figure 4.24 shows the load-deflection response, as measured from the tests and predicted by ANSYS model.

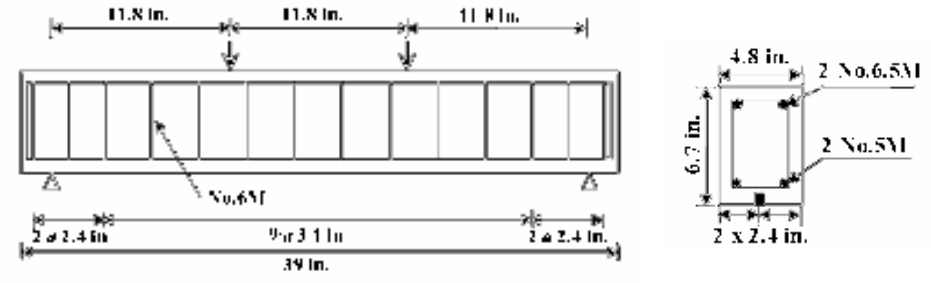

a) Elevation b) Cross Section

Figure 4.23 Details of Specimen S1-NSM (Barros et al. 2007)

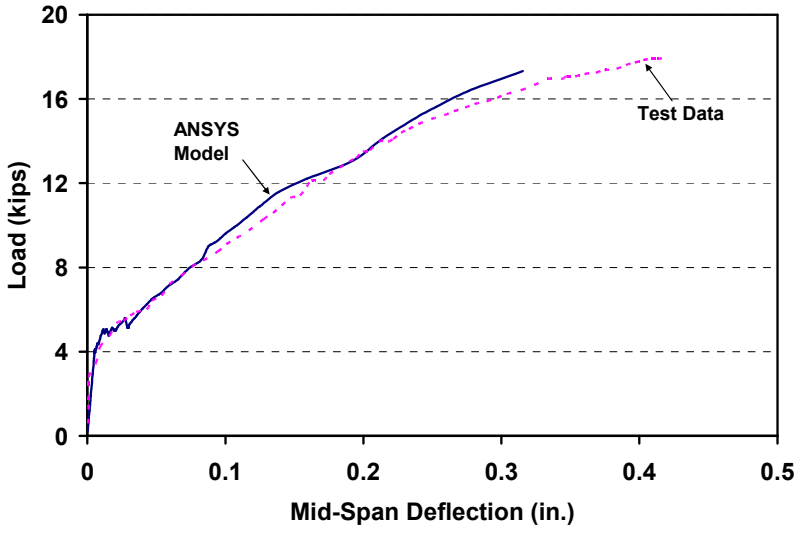

Figure 4.24 Model Validation for Specimen S1-NSM (Barros et al. 2007)

Considering the case of bond model with springs the error predicting the peak load, displacement at the peak load and post-cracking stiffness were 4%, 24% and 1%, respectively.

4.3.3 Groove Size Tolerance

The 7/16, 9/16 and 11/16 in. square groove specimens with NSM FRP bars were simulated using the FE model. Epoxy was modeled with linear SOLID45 elements and the NSM bar was modeled with LINK8 elements. Element size was constant at 1 in. beyond the transition area, and the coinciding nodes were merged together to ensure perfect bond. Figure 4.25 shows the load-deflection responses for the three models validating the findings of the experiments that the groove size in the range studied does not significantly affect the performance of the NSM FRP system. In order to test the sensitivity of the solution to the groove size, 1 in and 2 in. square models were also prepared. Results of the sensitivity analysis are shown in Figure 4.26, where, despite the great difference in groove sizes, there is little difference in the peak loads and corresponding mid-span deflections.

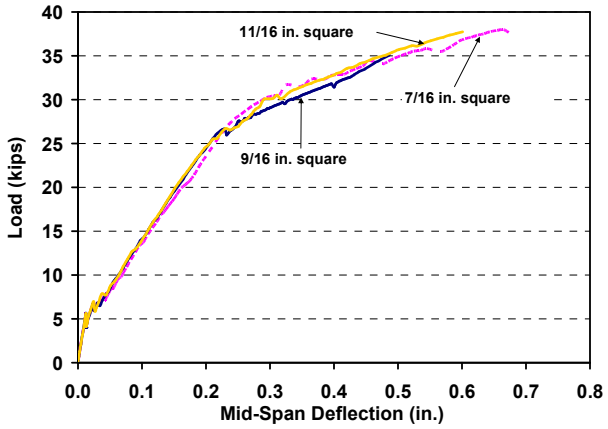

Figure 4.25 Load-Deflection Responses for FE Models with Different Groove Sizes

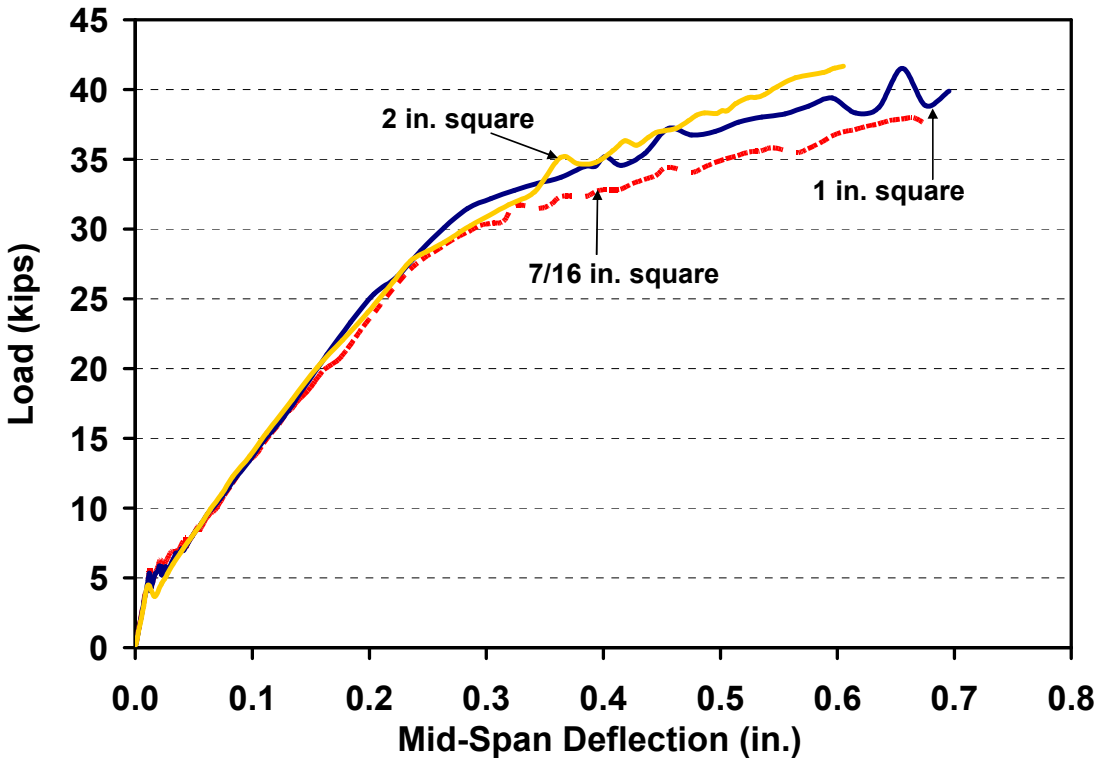

Figure 4.26 Sensitivity Analysis for NSM Grooves

4.3.4 Parametric Study

Effects of various geometric and physical parameters were investigated using the developed finite element model. Geometric parameters included the number of bars and the groove width and depth. Physical parameters were the compressive strength OF concrete and the modulus of elasticity of FRP and epoxy. Concrete compressive strengths were chosen such that low-, medium- and high-strength concretes were included. The Young's modulus of FRP reinforcement and epoxy paste were selected from the actual values for commercially available glass, aramid and carbon FRP bars, and low-, medim- and high-modulus adhesives, respectively. A benchmark model was created with a single FRP bar, and groove width and depth both as 1.5 times the FRP bar diameter, concrete

compressive strength of 4 ksi, FRP modulus of 18,000 ksi, and epoxy modulus of 435 ksi. Table 4.5 shows the test matrix for the parametric study.

Table 4.5 Test Matrix for Parametric Study

Number of bars	1, 2 and 3 bars
Groove Width[a]	1.2, 1.5, 1.8 and 2.2d[c]
Groove Depth[b]	1.2, 1.5, 1.8 and 2.2d[c]
Concrete Compressive Strength	4, 7 and 10 ksi
FRP Elastic Modulus	5,920, 7,687, 18,000 ksi
Epoxy Elastic Modulus	174, 435, 725 ksi

[a] Groove depth kept constant
[b] Groove width kept constant
[c] d: Bar diameter

In order to make comparisons, several response variables were identified, including load, mid-span deflection, compressive strain in concrete, and tensile strains in FRP and epoxy. For each model, all variables were recorded at concrete cracking, steel yielding, the common maximum load and the eventual failure. Cracking was identified as the first bifurcation point following the initial linear segment of the load-deflection curve. Yielding was noted as the first load at which steel bar reaches its yield strain. The common maximum load is the lowest maximum converged load for all models. Finally, the failure load is the maximum converged load of each model. The values at the common maximum load is believed to be more conclusive than the failure load, because the failure load is not necessarily the actual load which causes failure but rather is the load at which the finite element algorithm fails due to the convergence difficulties. Figures 4.27-4.31, 4.32-4.36 and 4.37-4.41 show the responses for the number of bars, the groove width and the groove depth, respectively.

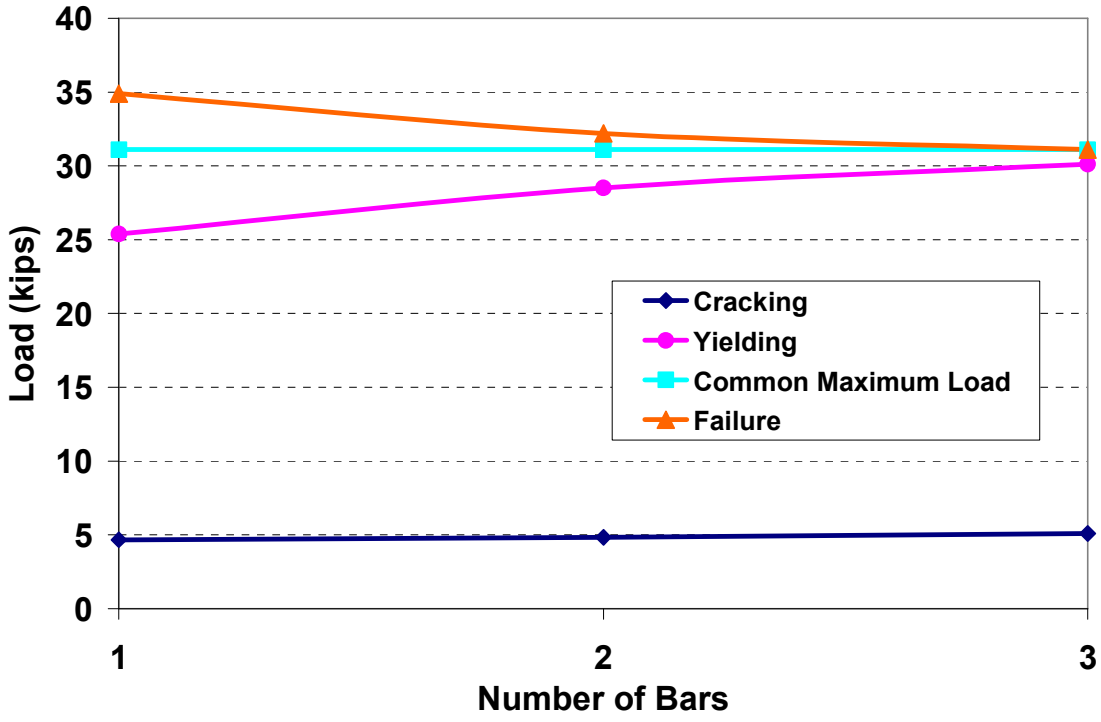

Figure 4.27 Load Versus Number of Bars

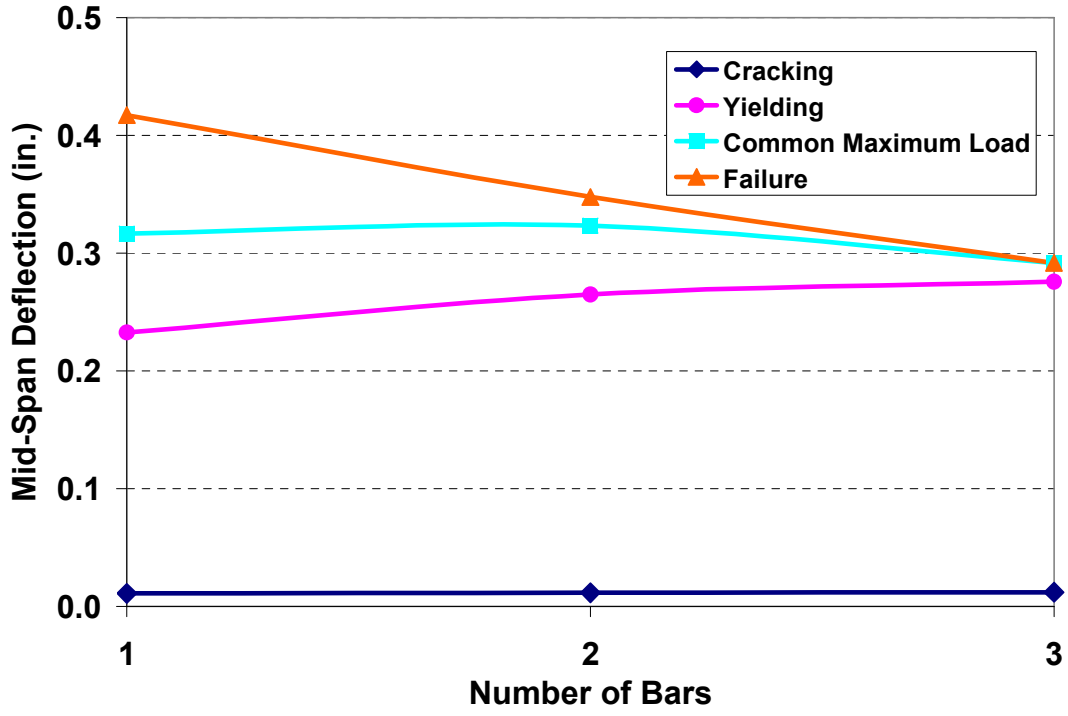

Figure 4.28 Mid-Span Deflection Versus Number of Bars

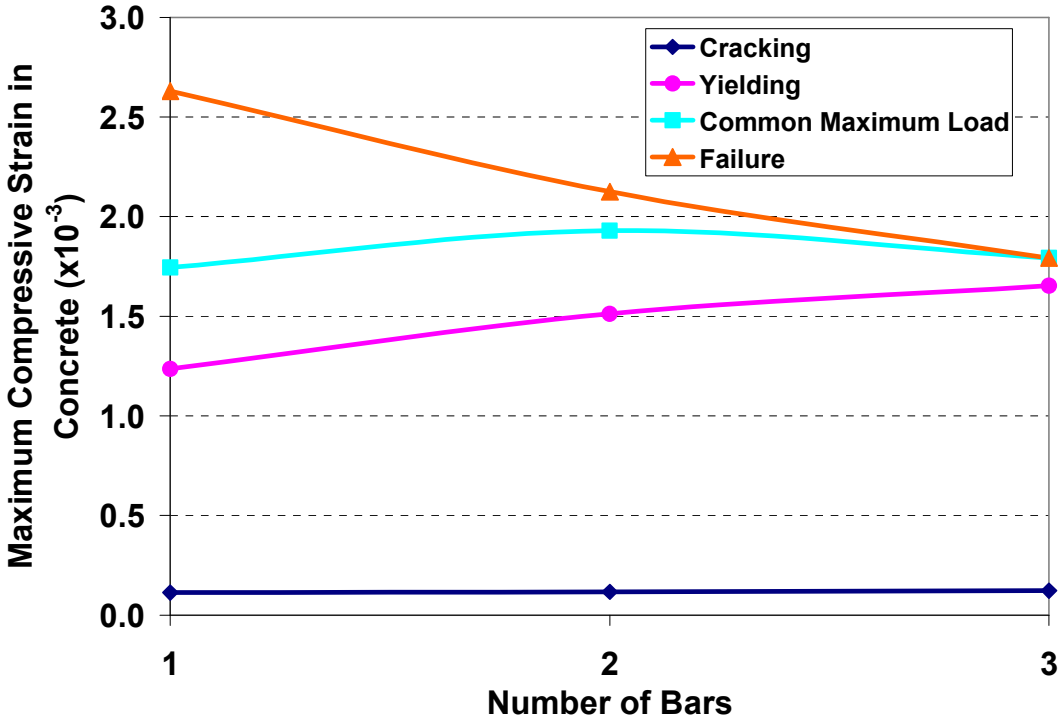

Figure 4.29 Maximum Compressive Strain in Concrete Versus Number of Bars

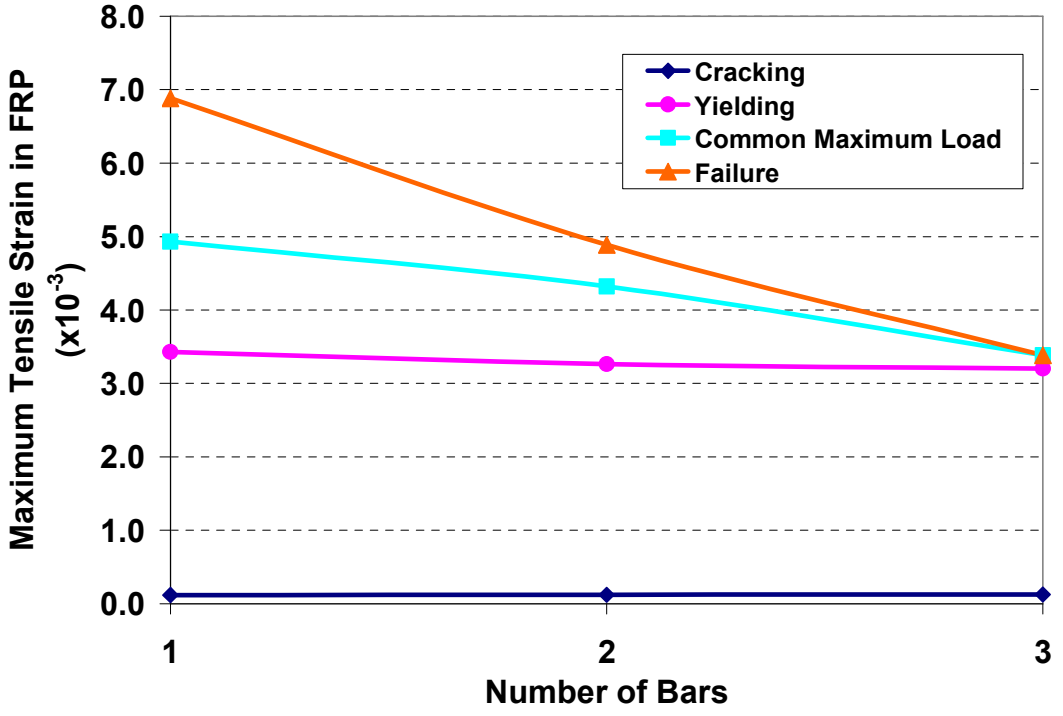

Figure 4.30 Maximum Tensile Strain in FRP Versus Number of Bars

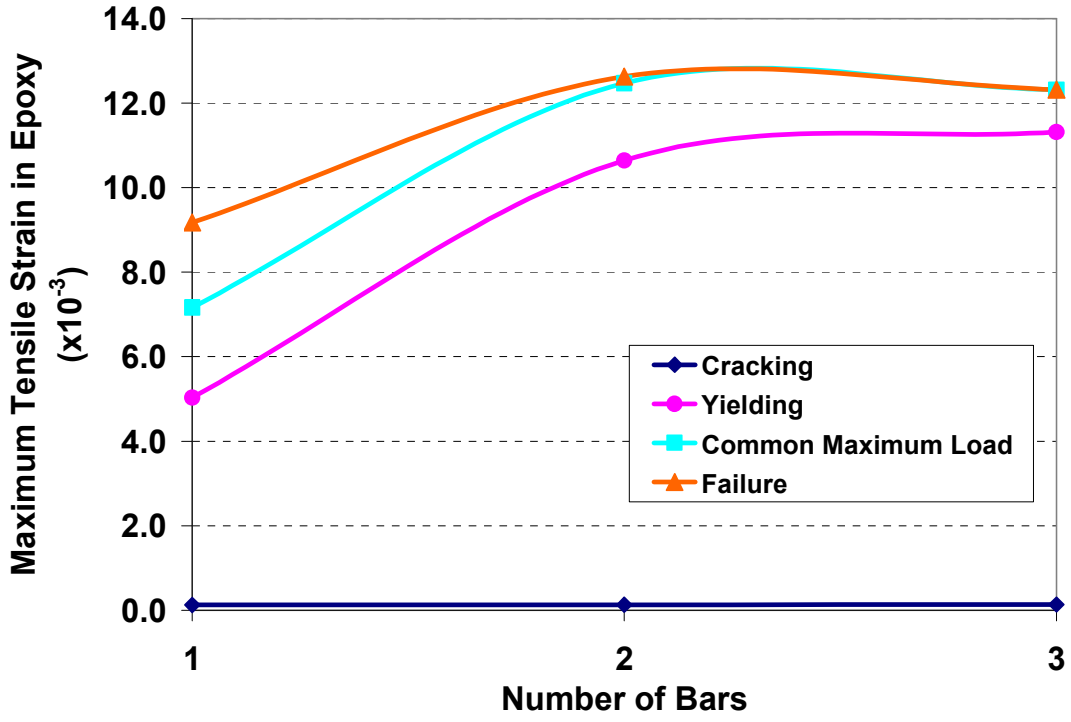

Figure 4.31 Maximum Tensile Strain in Epoxy Versus Number of Bars

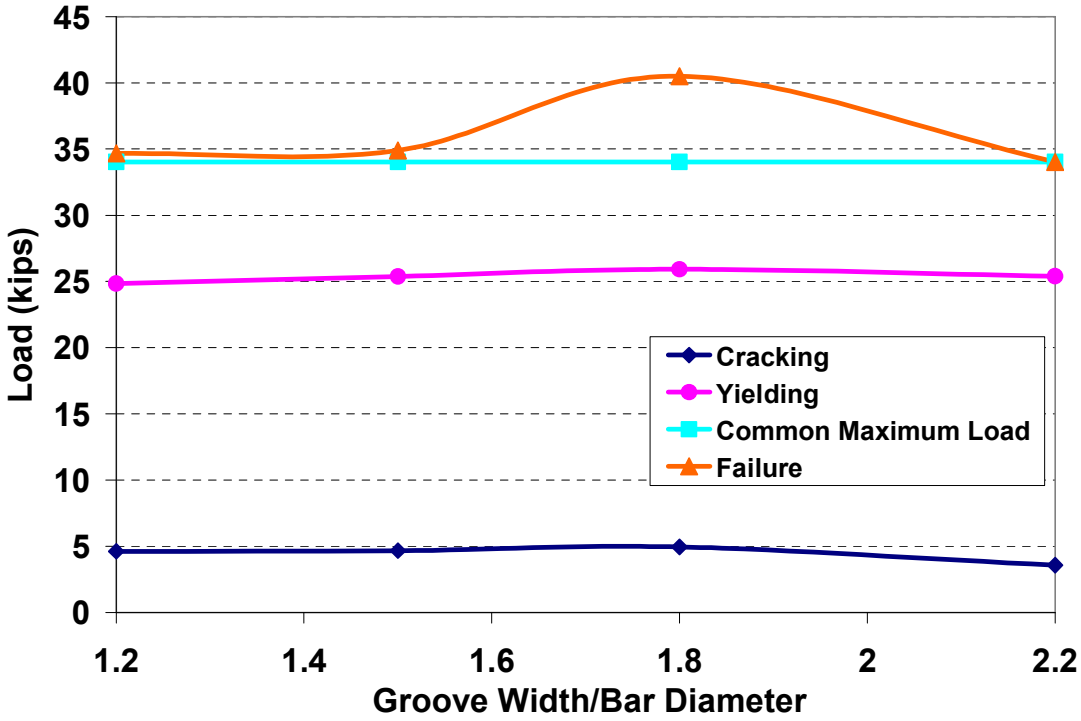

Figure 4.32 Load Versus Groove Width to Bar Diameter Ratio

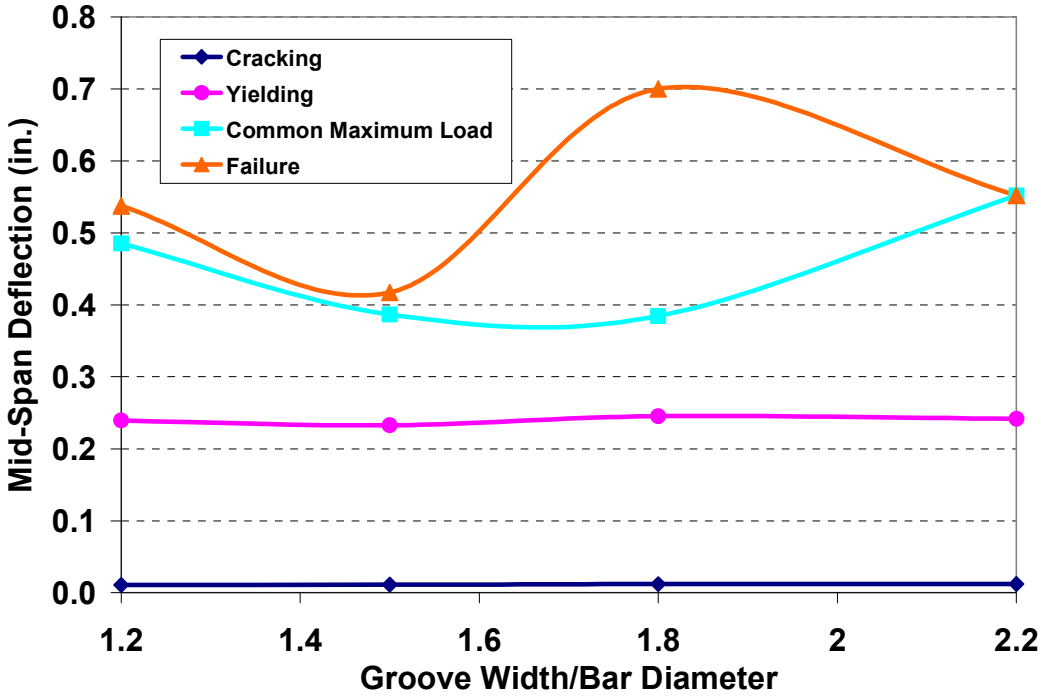

Figure 4.33 Mid-Span Deflection Versus Groove Width to Bar Diameter Ratio

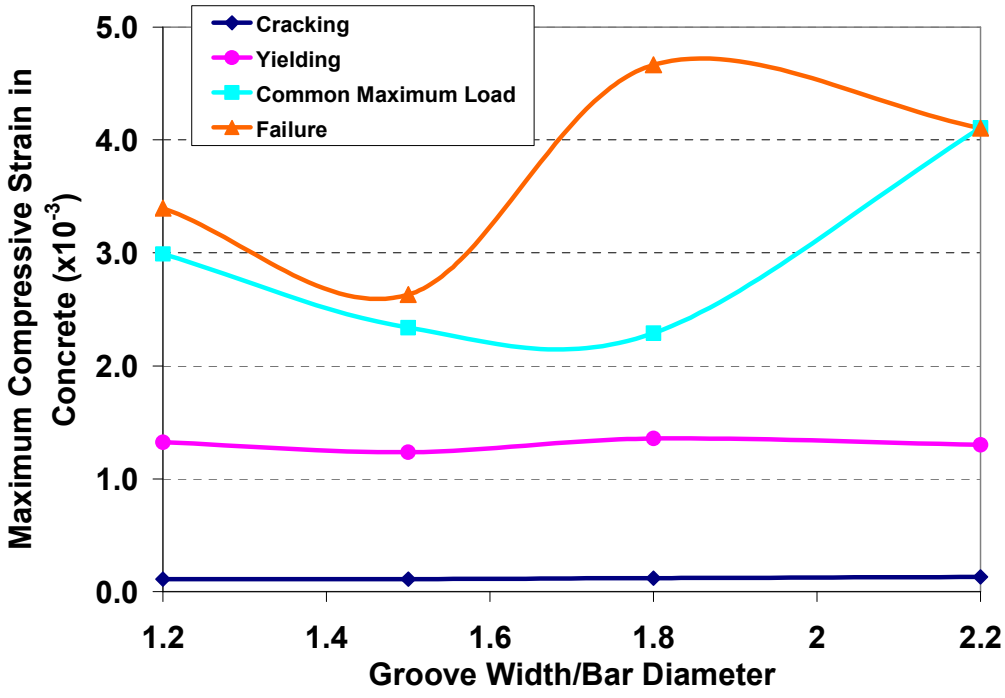

Figure 4.34 Maximum Compressive Strain in Concrete Versus Groove Width to Bar Diameter Ratio

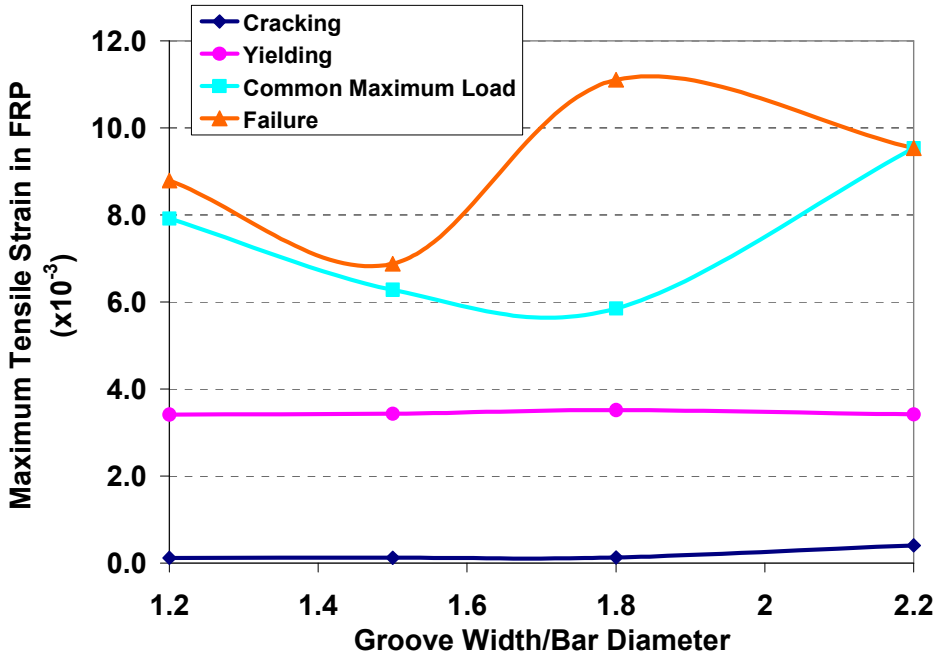

Figure 4.35 Maximum Tensile Strain in FRP Versus Groove Width to Bar Diameter Ratio

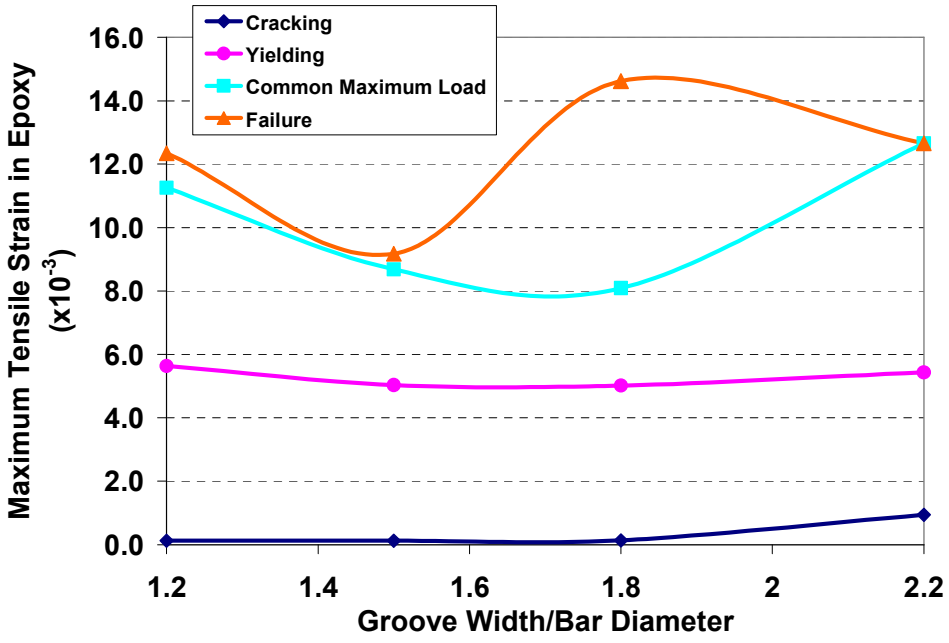

Figure 4.36 Maximum Tensile Strain in Epoxy Versus Groove Width to Bar Diameter Ratio

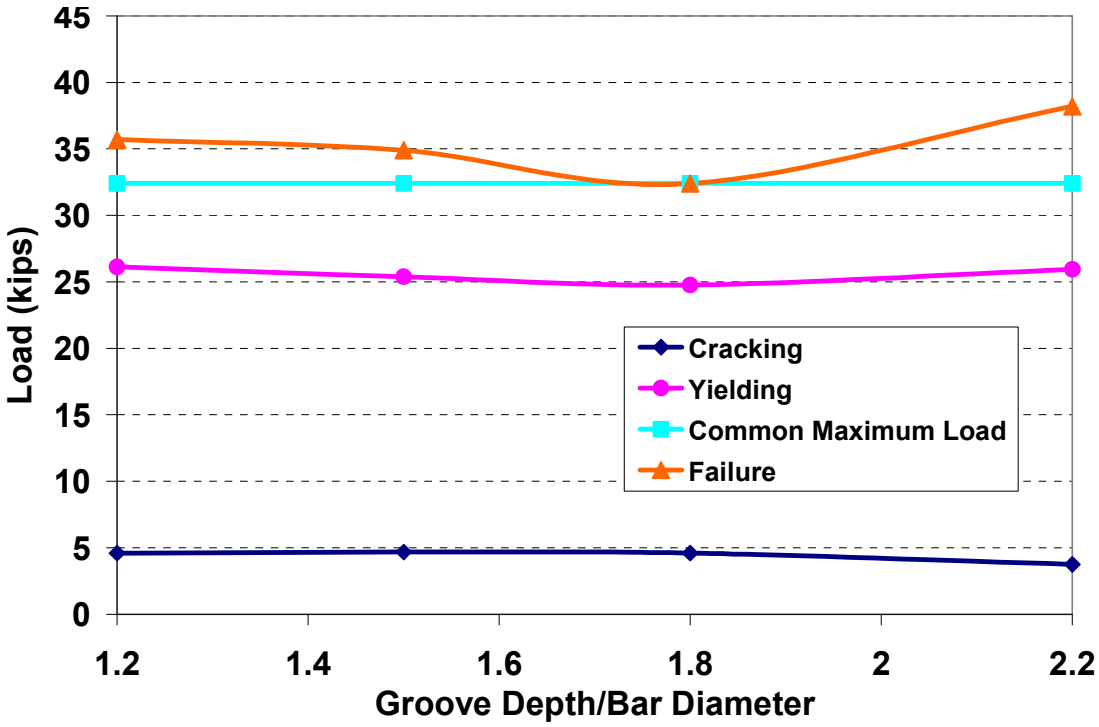

Figure 4.37 Load Versus Groove Depth to Bar Diameter Ratio

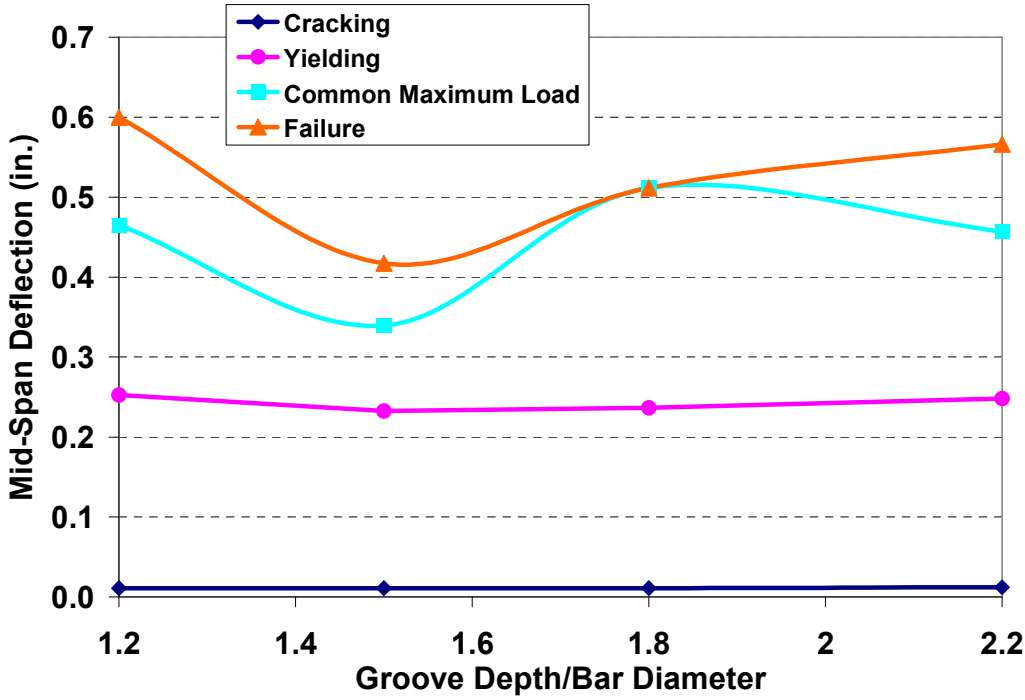

Figure 4.38 Mid-Span Deflection Versus Groove Depth to Bar Diameter Ratio

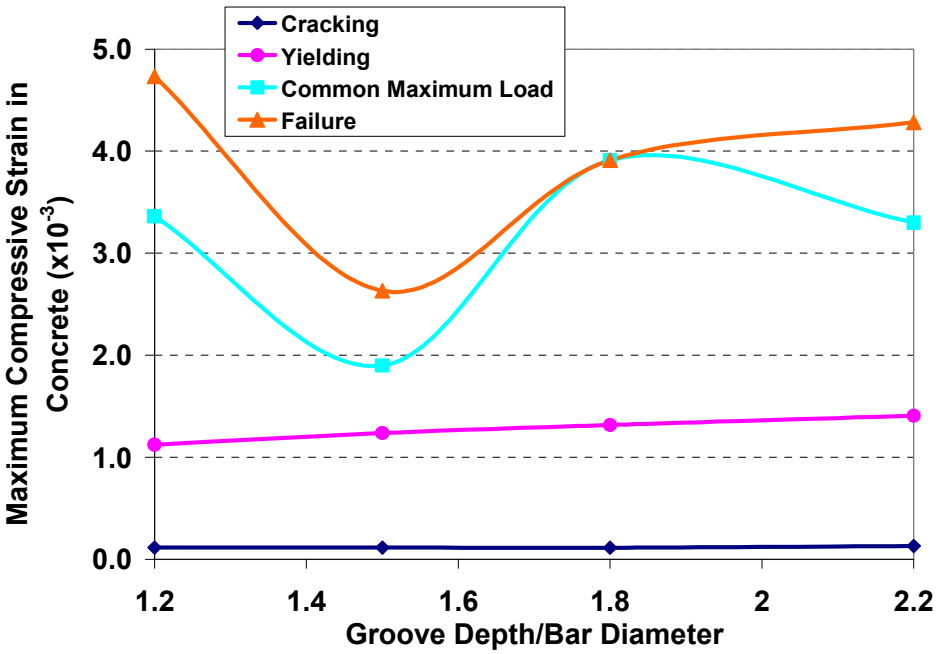

Figure 4.39 Maximum Compressive Strain in Concrete Versus Groove Depth to Bar Diameter Ratio

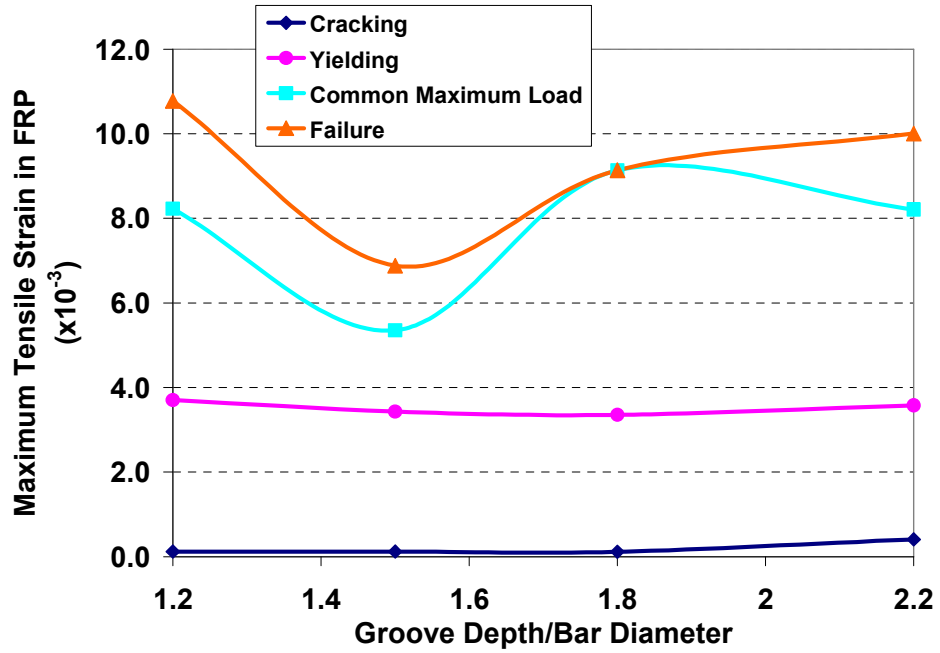

Figure 4.40 Maximum Tensile Strain in FRP Versus Groove Depth to Bar Diameter Ratio

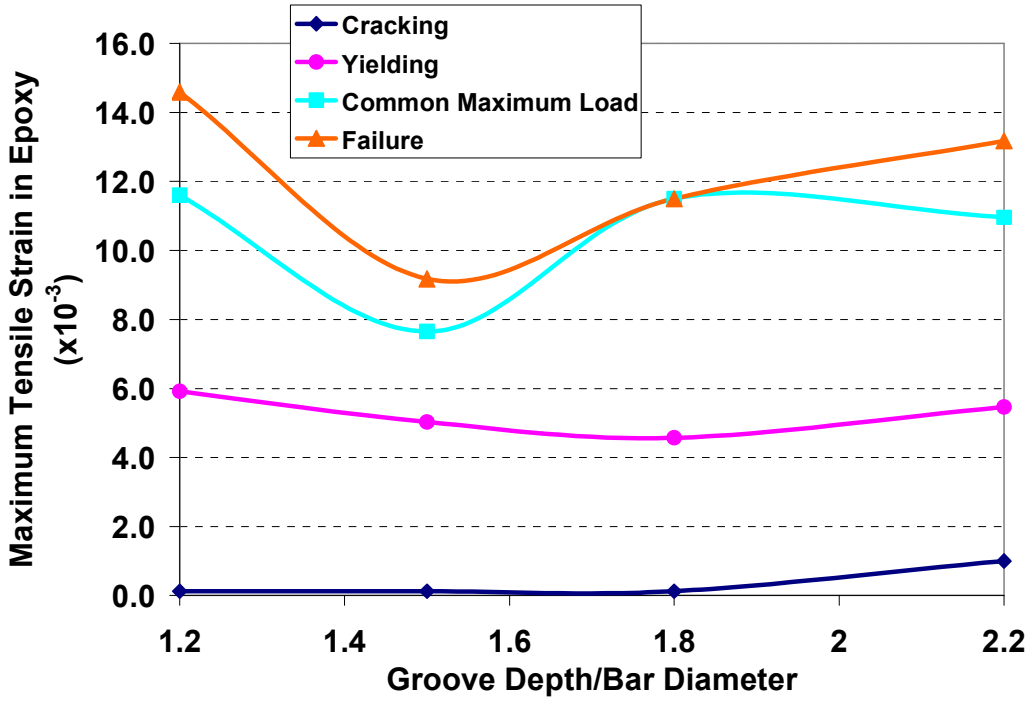

Figure 4.41 Maximum Tensile Strain in Epoxy Versus Groove Depth to Bar Diameter Ratio

Figures show identical responses at cracking for all cases and all variables, because the concrete compressive strength was kept constant. The mid-span deflection, load and maximum compressive strain in concrete at steel yielding tend to increase when the number of bars increases. Same response variables, however, remained almost unaffected at the common maximum load and tended to drop at failure with the increased number of bars. Maximum tensile strain in FRP remained unaffected by the number of bars at yielding, but decreased almost linearly at the common maximum load and at failure with the additional bars. Maximum tensile strain in epoxy increased when the bars were increased to 2, but remained constant afterwards. From these observations, it can be stated that as the number of bars increases, the failure load remains unaffected because

concrete controls the failure mode. Also, tensile strain in FRP decreases as apparent from simple mechanics that when the load is the same, the increased area results in lower strains. Finally, it is clear that addition of bars resulted in lower strains in the epoxy which may shift the failure mode from epoxy splitting to concrete splitting if delamination failure occurs. Note that when the number of bars increases, the distance between the bars and the distance from the edge of the outermost groove to the edge of the member decreases provided that the member dimensions are kept constant. Therefore, by analyzing the number of bars, the distance between the grooves and edge distance were also indirectly considered as parameters.

Figures 4.32-4.36 show response variables to be unaffected by the groove width at cracking and yielding as the concrete compressive strength was the same in all cases. At the common maximum load, all response variables exhibited a minimum value at some point between 1.5d and 1.8d. No clear trend could be traced for any of the response variables at the failure.

Figures 4.37-4.41 show no clear relationship between the response variables and the groove depth at any stage of loading.

Analytical results for concrete compressive strength, and FRP and epoxy moduli are shown in Figures 4.42 through 4.56. In Figure 4.42, the cracking load increased from 4.7 to 7.4 kips as the concrete compressive strength increased. However, the other response variables seemed to be unaffected. At steel yielding, mid-span deflection and maximum compressive strain in concrete decreased while load, maximum tensile strain in FRP and maximum tensile strain in epoxy remained almost constant, regardless of the increase in the concrete compressive strength. At the common maximum load, mid-span

deflection and load seemed to be indifferent to the concrete compressive strength. However, maximum tensile strains in FRP and epoxy increased initially and then remained unchanged. At failure, mid-span deflection, and maximum tensile strains in FRP and epoxy all exhibited a similar pattern with an initial ascending branch followed by a flat portion. Maximum compressive strain in concrete, on the other hand, followed an opposite path, starting with a flat segment followed by a descending portion. Finally, the failure load increased with increasing concrete compressive strength. From these observations, it can be concluded that an increase in the concrete compressive strength helps better utilization of FRP material. However, the effect diminishes for higher concrete compressive strengths. Strains in concrete drop but those in epoxy increase when higher strength concrete is used which may change the mode of failure from concrete splitting to epoxy splitting.

Selected FRP moduli of 5,920, 7,687 and 18,000 ksi in Figures 4.47-4.51 corresponded to commercially available glass, aramid and carbon FRP bars, respectively. Similar to the concrete strength parameter, at cracking and yielding, response variables were not affected by the FRP modulus. Load was also constant, regardless of the FRP type. The values for the other response variables decreased with increasing FRP modulus. These observations indicate that using high modulus FRP reinforcement does not necessarily improve the performance, as the failure is dictated by the concrete or the epoxy in most cases. When high-modulus FRP bars are used, strains in FRP, epoxy and concrete decrease. This implies that FRP modulus is not a significant parameter affecting the failure mode.

From Figures 4.52-4.56, comments can be made only at the common maximum load level, as for cracking and yielding the response variables are unaffected by the epoxy modulus. At the common maximum load level, however, curves for all response variables begin with a descending portion and then remain constant at higher levels. This may indicate that increasing the epoxy modulus increases the overall stiffness and lowers the strains in concrete, FRP and epoxy; therefore epoxy and concrete splitting failures may be prevented.

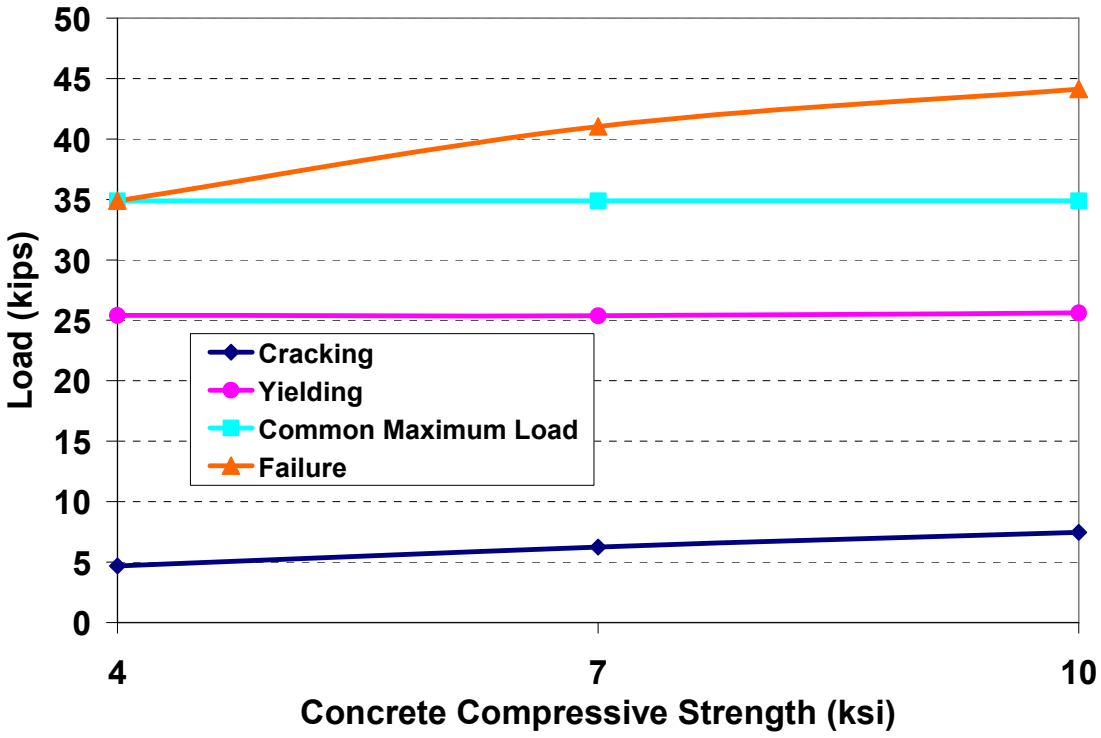

Figure 4.42 Load Versus Concrete Compressive Strength

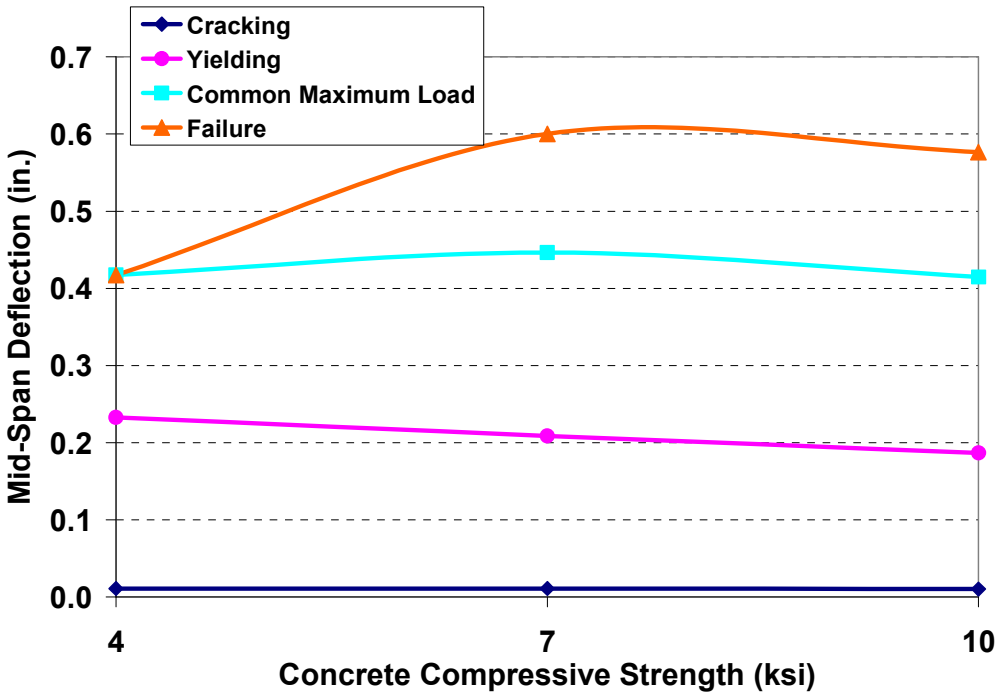

Figure 4.43 Mid-Span Deflection Versus Concrete Compressive Strength

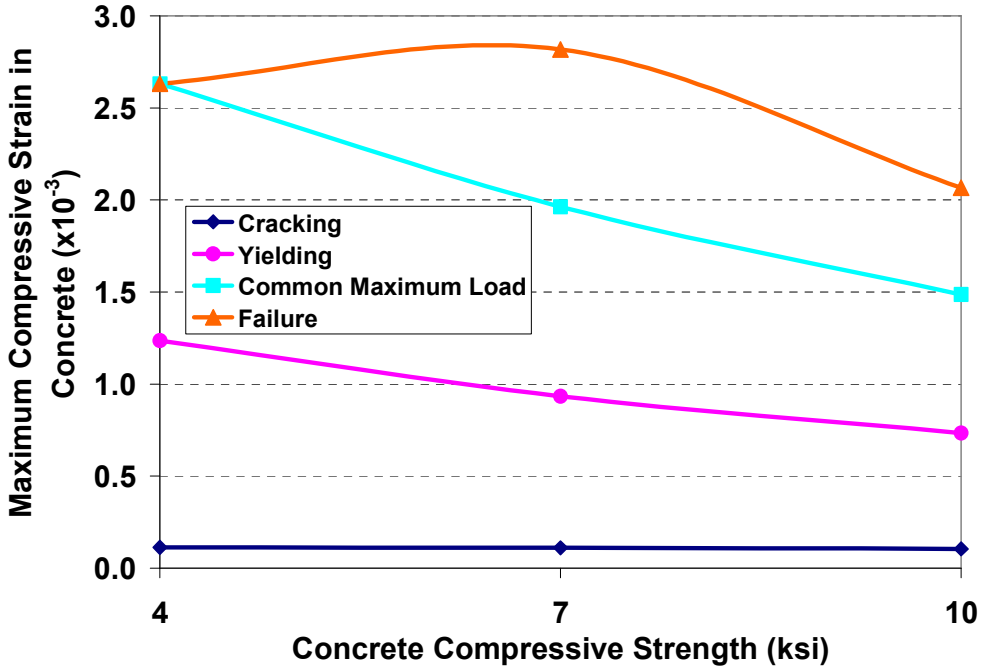

Figure 4.44 Maximum Compressive Strain in Concrete Versus Concrete Compressive Strength

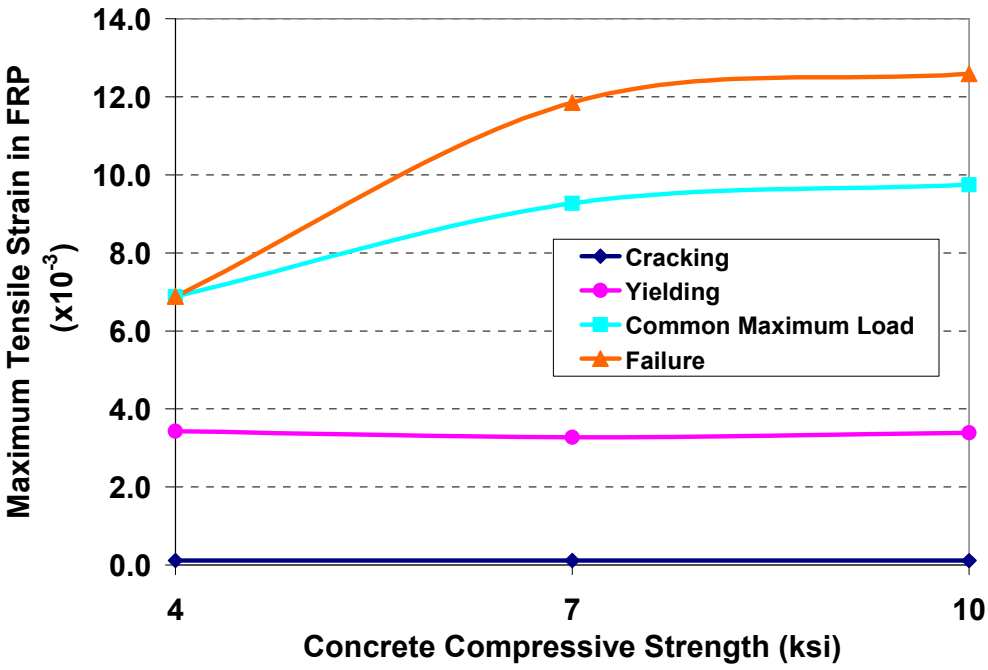

Figure 4.45 Maximum Tensile Strain in FRP Versus Concrete Compressive Strength

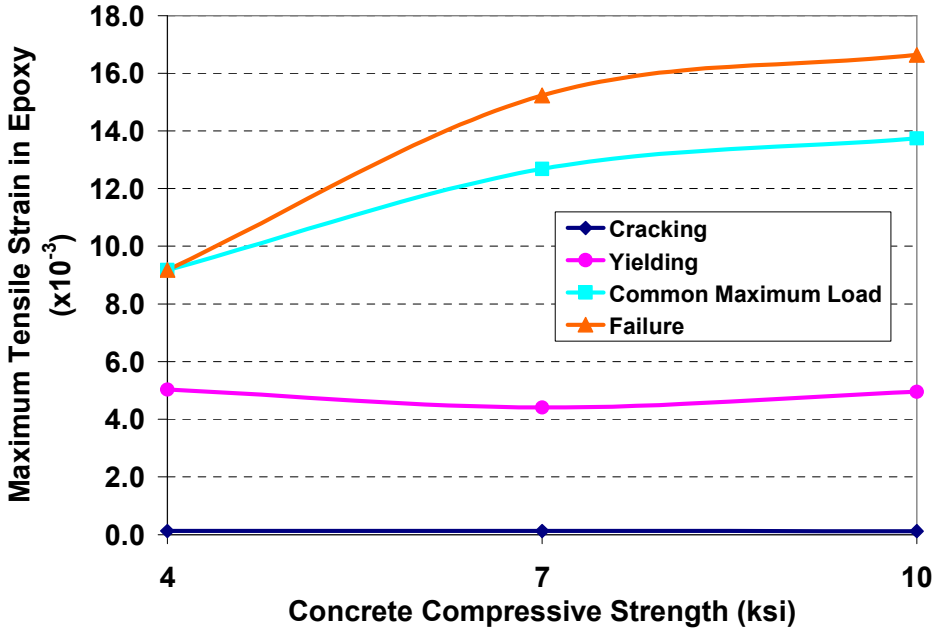

Figure 4.46 Maximum Tensile Strain in Epoxy Versus Concrete Compressive Strength

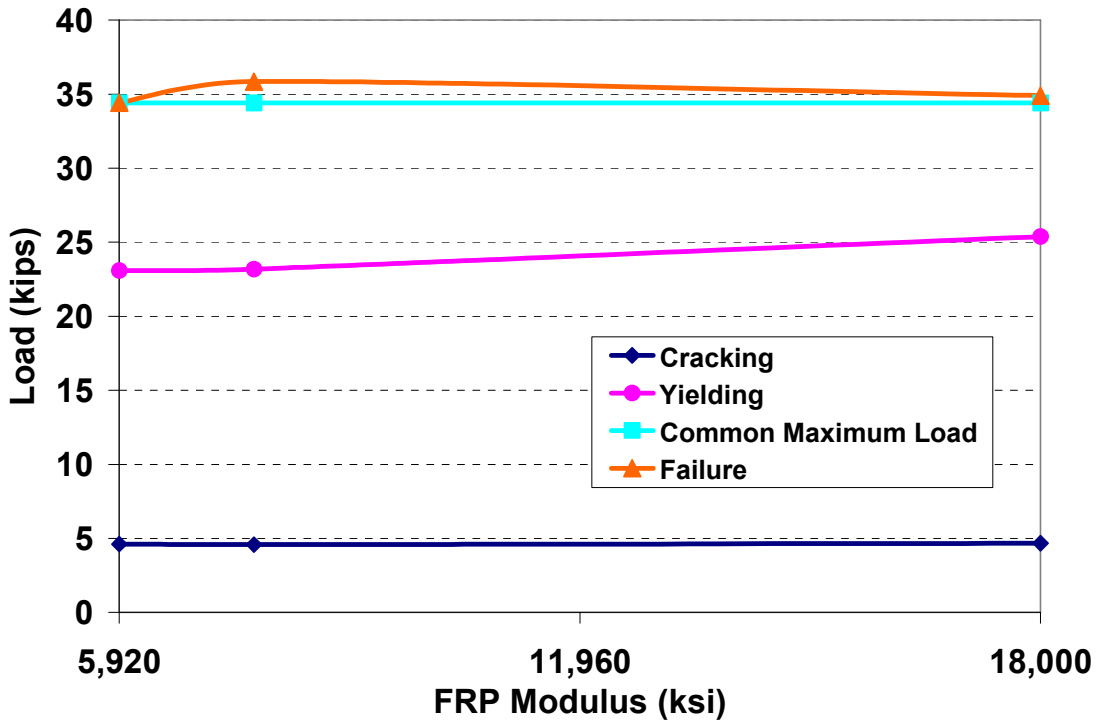

Figure 4.47 Load Versus FRP Modulus

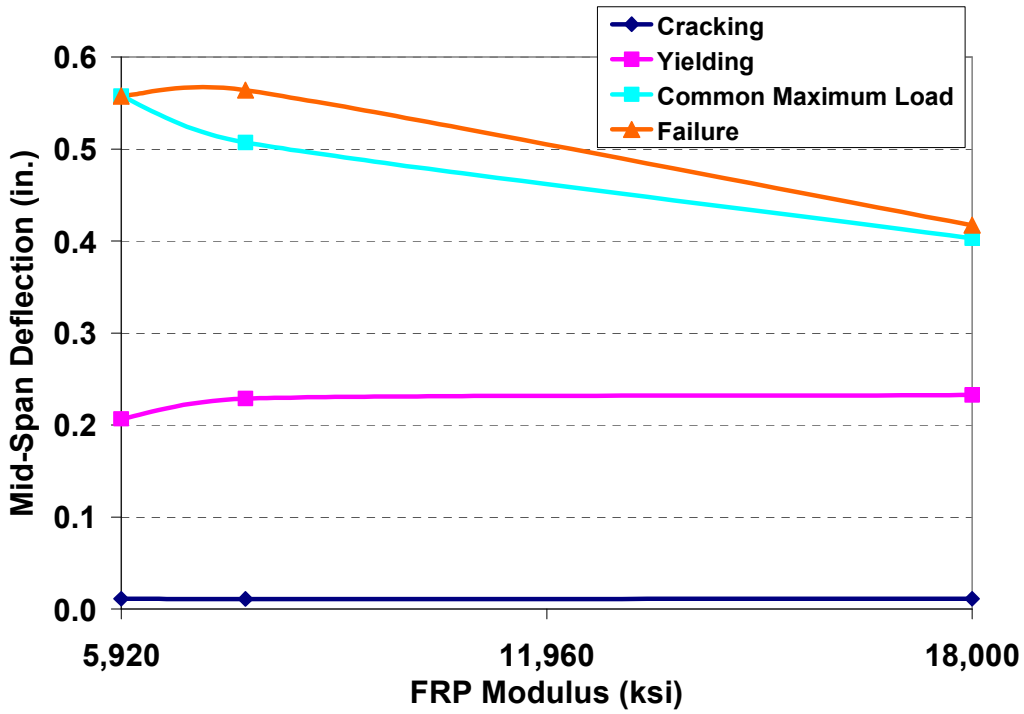

Figure 4.48 Mid-Span Deflection Versus FRP Modulus

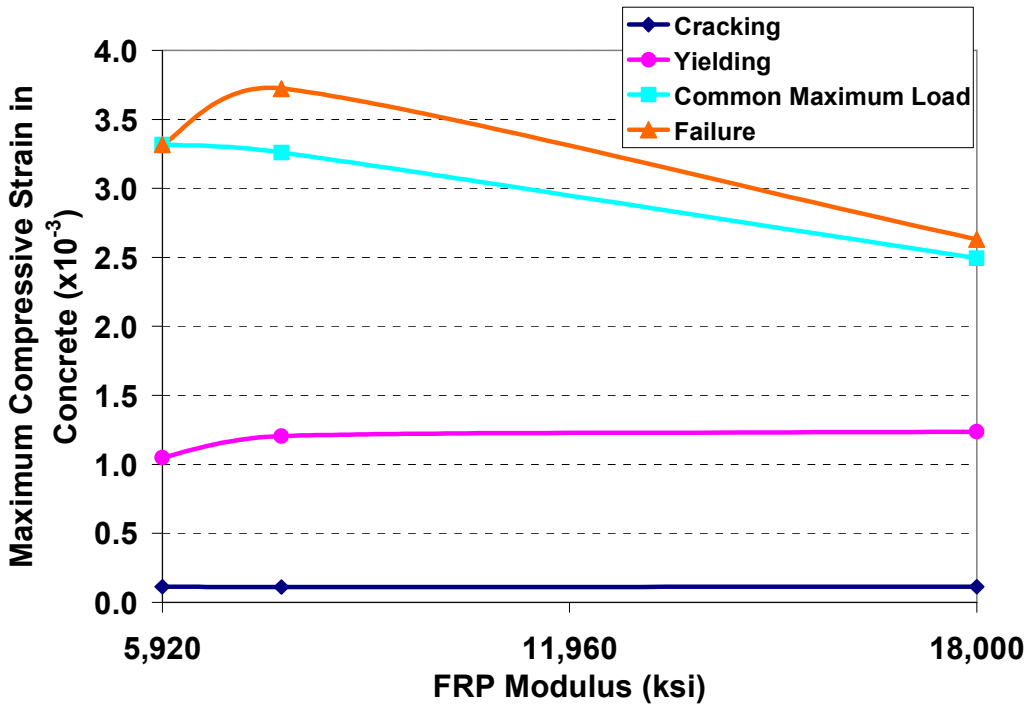

Figure 4.49 Maximum Compressive Strain in Concrete Versus FRP Modulus

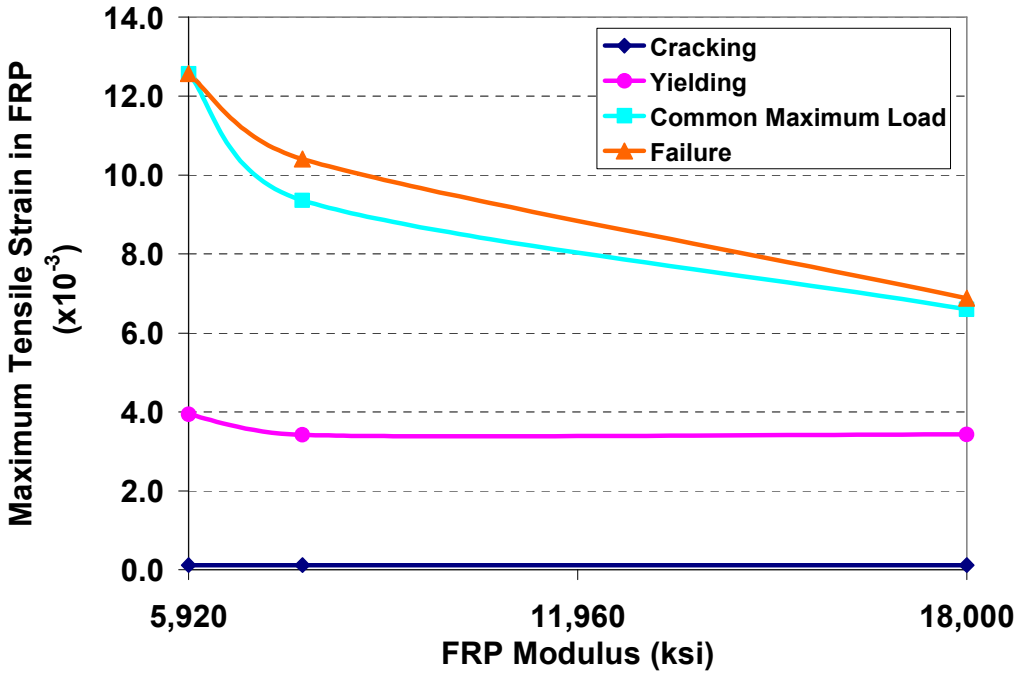

Figure 4.50 Maximum Tensile Strain in FRP Versus FRP Modulus

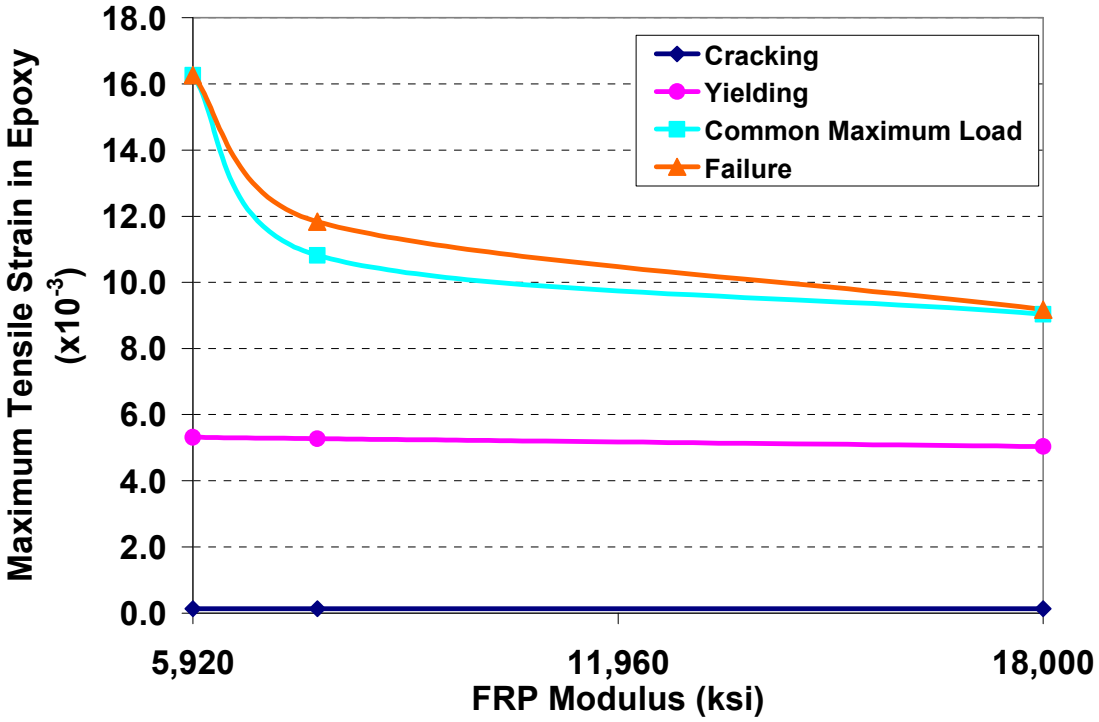

Figure 4.51 Maximum Strain in Epoxy Versus FRP Modulus

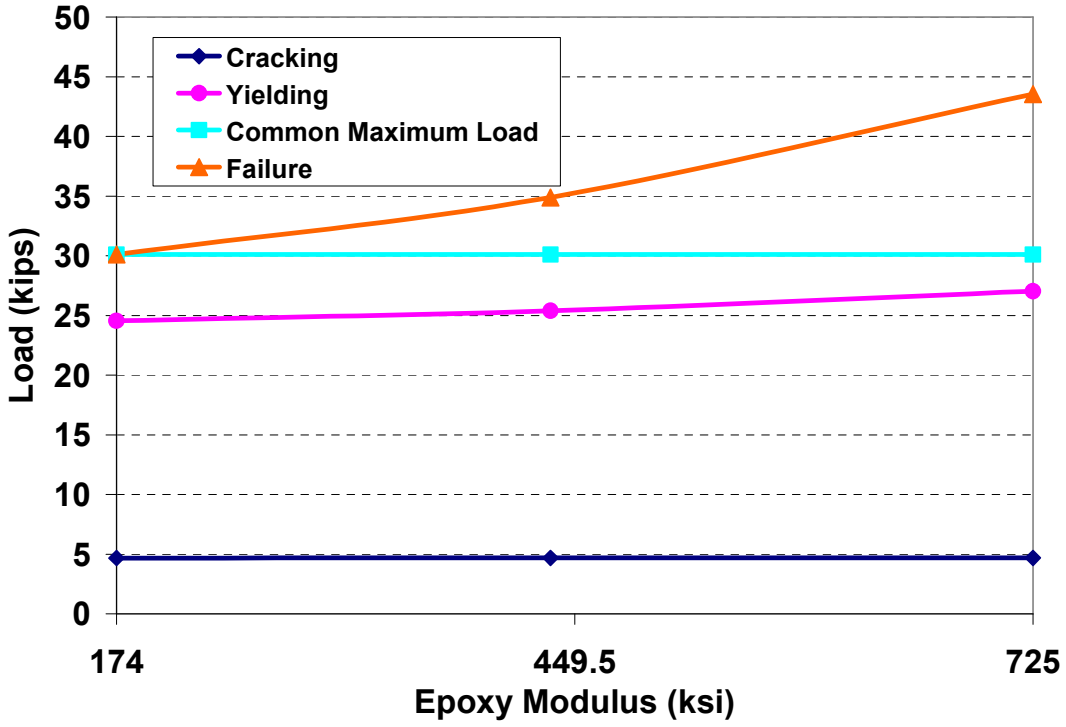

Figure 4.52 Load Versus Epoxy Modulus

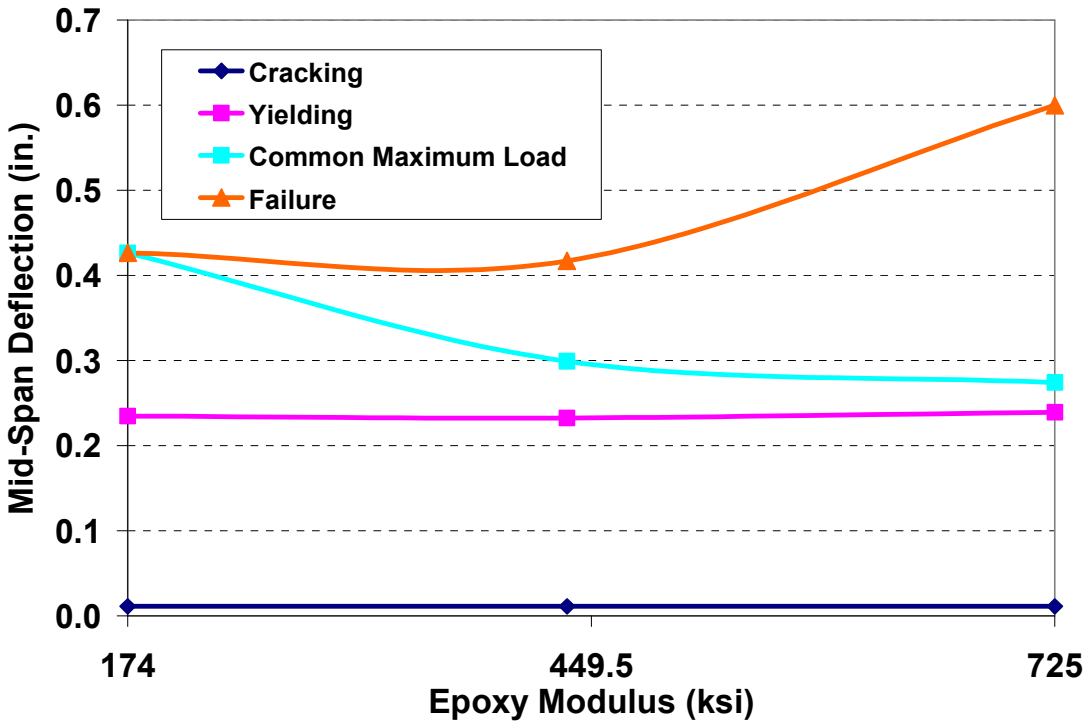

Figure 4.53 Mid-Span Deflection Versus Epoxy Modulus

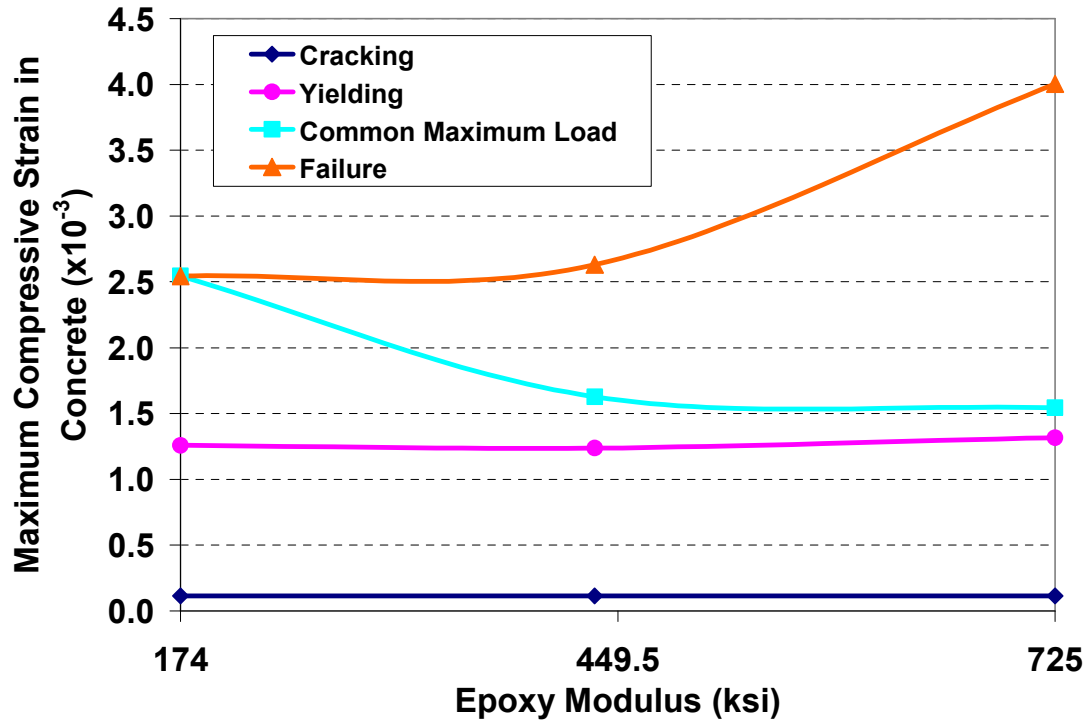

Figure 4.54 Maximum Compressive Strain in Concrete Versus Epoxy Modulus

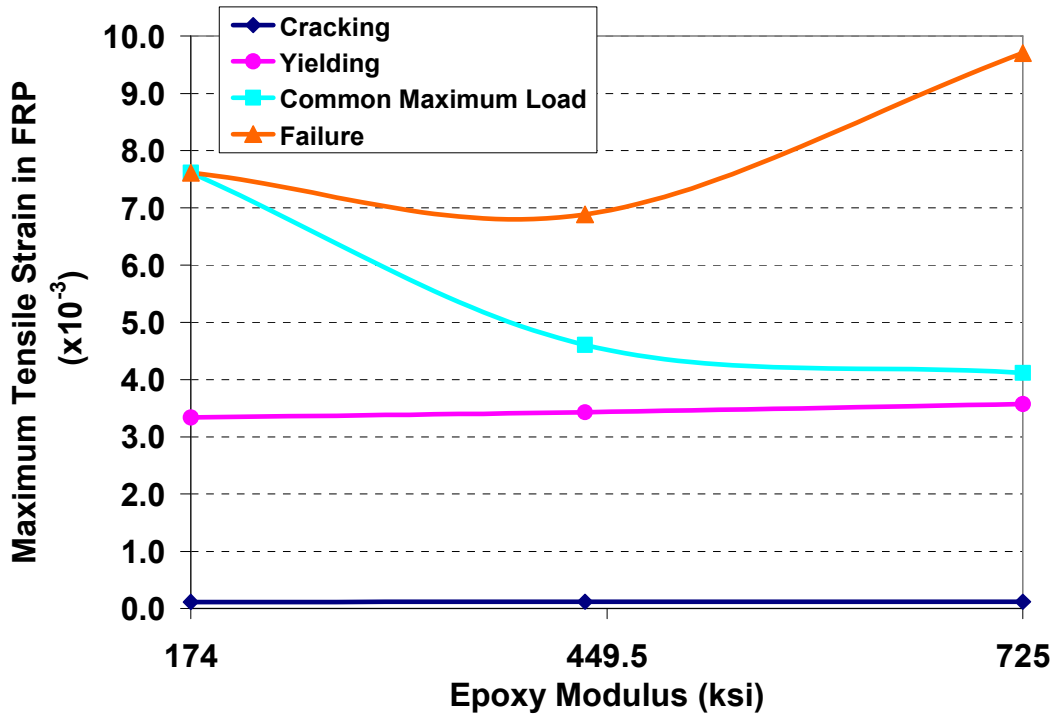

Figure 4.55 Maximum Tensile Strain in FRP Versus Epoxy Modulus

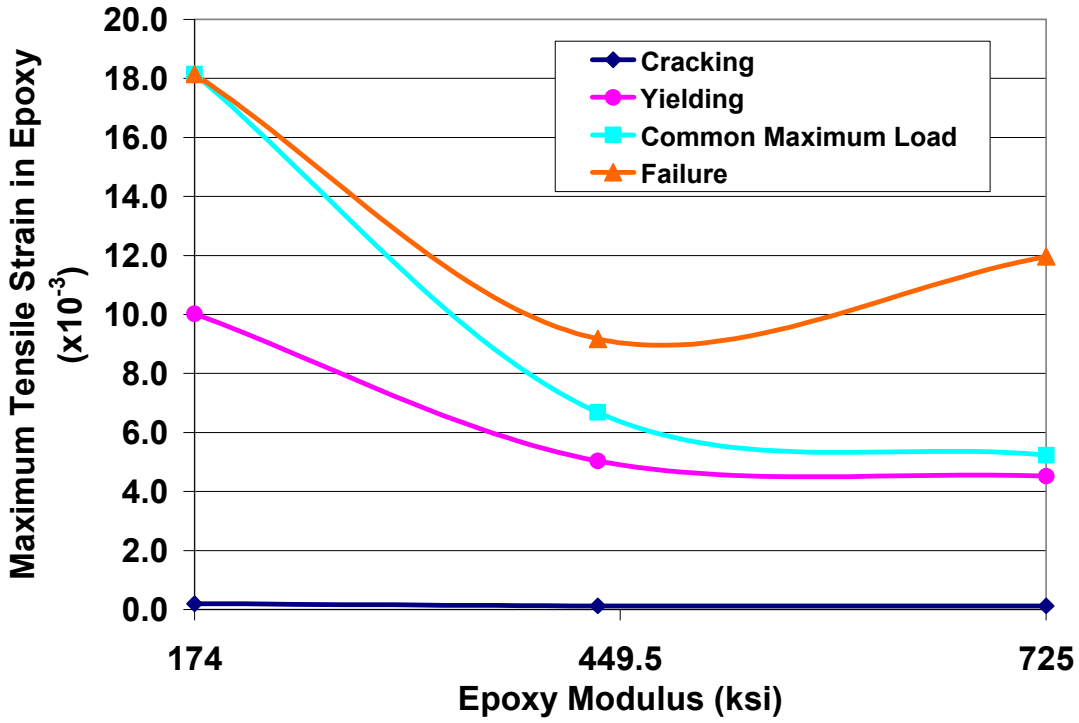

Figure 4.56 Maximum Tensile Strain in Epoxy Versus Epoxy Modulus

CHAPTER 5

CONCLUSIONS AND RECOMMENDATIONS

5.1 Summary

Current state of the art and practice of FRP strengthening of concrete structures lack scientifically-based thresholds for surface irregularities in the pre-cured externally bonded FRP systems and groove size tolerances for the NSM FRP systems. The following issues were the focus of this study:

- Effects of surface roughness, flatness, voids and cracks on pre-cured FRP systems; and
- Effects of groove size tolerance on NSM FRP systems.

A thorough experimental and analytical study was conducted on the above issues. The experimental component consisted of testing reinforced concrete beams with intentional surface irregularities and strengthened with FRP. The analytical component comprised of modeling surface flatness for the pre-cured section, and a parametric study involving various geometric and physical factors.

In the experimental program, six specimens were tested for each of the surface irregularities; roughness, flatness, cracks and voids. The parameters included concrete surface profile, surface out-of-flatness, void diameter and crack frequency. For the surface roughness study, three different surface profiles were used corresponding to ICRI/ACI (1999) concrete surface definitions of ICRI 1, ICRI 2-3 and ICRI 6-9. In the case of surface flatness, the validity of the threshold limit for the wet lay-up systems as

reported by Yalim (2008) was tested for the pre-cured systems. Both peak and valley specimens were prepared with out-of-flatness level of 1/16 in. over a length of 12 in. For surface voids, a constant void frequency of 5% and a constant void depth of 1/8 in. were considered with void diameters of 1/4, 3/8 and 1/2 in. For surface cracks, the frequency was varied by producing cuts on concrete surface at spacing of 1, 1.5 and 2 in.

In the NSM FRP part of the experimental program, a total of 12 beams were prepared, 6 each for FRP strips and bars. Groove widths for the strip specimens were 7/16, 9/16 and 11/16 in., while the groove depth was kept constant at 1 in. For the bars, 7/16, 9/16 and 11/16 in. square grooves were utilized. Moreover a database containing test results from different studies was compiled. Using the database, the effects of geometric properties on the performance of NSM FRP systems were evaluated.

The analytical program consisted of two parts; one dedicated to the pre-cured FRP and the other to the NSM FRP systems. ANSYS FE package was used for analytical modeling. For the pre-cured FRP systems, the FE model was validated using test results from the literature as well as the present study. A parametric study was then conducted, in which different surface out-of-flatness levels were considered for both the peaks and valleys. In the NSM FRP systems, first the FE model was validated using tests from the literature and the present study. Both the NSM strips tests and larger groove sizes were simulated. Moreover a parametric study was carried out involving geometric factors such as groove width and depth and number of grooves (and bars) and physical factors such as concrete compressive strength, FRP type (and modulus) and epoxy type (and modulus) was conducted.

5.2 Conclusions

The following conclusions can be drawn from this study:

1. Surface Roughness: Surface roughness did not seem to be a significant parameter affecting the structural performance of the pre-cured FRP systems. Even ICRI 1 surface profile seemed adequate for design strength. However based on the study by Yalim (2008) for the wet lay-up FRP systems, ICRI 2-3 may be recommended for the pre-cured FRP systems to ensure safety. All surface roughness specimens failed by FRP debonding, which is considered a premature failure mode.

2. Surface Flatness: Test results for surface flatness showed that the threshold of 1/16 in. set for the wet lay-up FRP systems (Yalim 2008) is also valid for the pre-cured FRP systems. Tests however did not consider the bigger out-of-flatness levels. In the analytical study, this issue was addressed, and it was noted that even 1/8 in. surface out-of-flatness in the form of peaks may provide the required strength. However, significant capacity drops were observed in the 1/4 and 1/2 in. peak specimens. In the valley specimens, no such trend was observed. Similar to the surface roughness specimens, surface flatness specimens failed by debonding.

3. Surface Voids: Within the void diameter range considered, and for a constant void frequency and depth; peak load, mid-span deflection and FRP strain decrease with increasing void diameter. Although the amount of disbond area is the same in all cases the larger void diameter result in the formation of weaker bond zones which may eventually adversely affect the load capacity and ductility.

4. Surface Cracks (Cuts): Both the surface voids and cracks are similar parameters as both can be considered as disbonds. Test results showed that as the crack frequency increases (i.e., cut spacing decreases), mid-span deflection and FRP strain corresponding to the peak load increase, whereas the peak load remains unaffected. This is an indication that the crack frequency affects the ductility rather than strength. All test specimens in this category failed by FRP debonding.

5. NSM FRP Systems: Tests on groove size tolerance showed that a groove size tolerance of ±1/8 in. did not have significant impact on NSM FRP system performance neither for the strips nor for the bars in the range of groove sizes studied. The FE simulations confirmed this conclusion. Furthermore, even for larger groove sizes the effect was negligible. Using the database comprised of test from the literature, it was shown that the most important parameter affecting the NSM FRP systems was the development length of the NSM FRP reinforcement. Failure mode for all tests in this category was either epoxy splitting or concrete splitting. The failure mode shifted from epoxy splitting to concrete splitting, as the groove size increased. Parameters such as the groove dimensions and other geometric factors were determined insignificant. Finally, the parametric study revealed that:

- Increasing the number of bars while keeping the concrete compressive strength the same does improve the performance, as the failure is controlled by the concrete strength.
- Groove width and depth do not significantly affect the system performance within the range studied.

- As the concrete compressive strength increases the strain in FRP also increases, implying better material utilization, which may lead to epoxy splitting instead of concrete splitting.
- Using high-modulus FRP does not improve the performance beyond a threshold, as the failure is governed by the weaker components.
- High-modulus epoxy on the other hand helps increase the overall stiffness and reduces the strains in both the concrete and epoxy.

5.3 Recommendations for Future Research

Only carbon FRP reinforcements were considered in this study. Aramid and Glass FRPs were not tested. The experimental program may be extended to other types of FRP materials. Different anchorage systems and arrangements may also be used, and their effects on the system may be evaluated. Additional analytical study maybe conducted on surface voids and cracks. Finally, tests on bundled NSM FRP bars may provide further data for practitioners.

LIST OF REFERENCES

Abdel Baky, H., Ebead, U. A., and Neale, K. W. (2007). "Flexural and Interfacial Behavior of FRP-Strengthened Reinforced Concrete Beams." *Journal of Composites for Construction*, ASCE, Vol. 11, No. 6, pp. 629-639.

ACI 440R-96 (1996). "State-of-the-Art Report on Fiber Reinforced Plastic Reinforcement for Concrete Structures." American Concrete Institute, Farmington Hills, MI.

ACI 440.2R-02. (2002). "Design and Construction of Externally Bonded FRP Systems for Strengthening Concrete Structures." American Concrete Institute, Farmington Hills, MI.

ACI 546R-96. (1996). "Concrete Repair Guide.", American Concrete Institute, Farmington Hills, MI.

Alemu, T., and Bhargava, P. (2007). "Numerical Simulation of Delamination Failure in RC Beams Laminated with FRP Plate." *8th Interational Symposium on Fiber-Reinforced Polymer Reinforcement for Concrete Structures, (FRPRCS-8)*, ACI, Patras, Greece, CD-ROM.

An, W., Saadatmanesh, H., and Ehsani, M. R. (1990). "RC Beams Strengthened with FRP Plates. II: Analysis and Parametric Study." *Journal of Structural Engineering*, ASCE, Vol. 117, No. 11, pp. 3434-3455.

ANSYS. (2007). Release 11.0, ANSYS, Inc.

Arduini, M., and Nanni, A. (1997). "Behavior of Precracked RC Beams Strengthened with Carbon FRP Sheets." *Journal of Composites for Construction*, ASCE, Vol.1, No.2, pp. 63-70.

Asplund, S. O., (1949). "Strengthening bridge slabs with grouted reinforcement." *ACI Journal*, Vol. 20, No. 6, pp. 397-406.

Barros, J. A. O., Dias, S. J. E., and Lima, J. L. T. (2007). "Efficacy of CFRP-Based Techniques for the Flexural and Shear Strengthening of Concrete Beams." *Cement and Concrete Composites*, Vol. 29, No. 3, pp. 203-217.

Bizindavyi, L. and Neale, and K.W. (1999). "Transfer Lengths and Bond Strengths for Composites Bonded to Concrete." *Journal of Composites for Construction*, ASCE, Vol. 3, No. 4, pp. 153-160

Brena, S.F., and Macri, B.M. (2004). "Effect of Carbon-Fiber-Reinforced Polymer Laminate Configuration on the Behavior of Strengthened Reinforced Concrete Beams." *Journal of Composites for Construction*, ASCE, Vol. 8, No. 3, pp. 229-240.

Buyukozturk, O., Gunes, O., and Karaca, E., (2004). "Progress on understanding debonding problems in reinforced concrete and steel members strengthened using FRP composites." *Construction and Building Materials*, Vol. 18, No. 1, pp. 9-19.

Chepur P.R. (2000). "Concrete Roughness Profiles Characterization Using Laser Profilometry for Improved Bond Strength with Fiber Reinforced Polymers." *M.S. Thesis*, University of Missouri, Rolla, MO.

Delaney, J.C., and Karbhari V.M. (2006). "The Assessment of Aspects Related to Defect Criticality in CFRP Strengthened Concrete Flexural Members." *Report No. SSRP 06/11*, Department of Structural Engineering, University of California – San Diego, La Jolla, CA.

De Lorenzis, L., Nanni, A., and La Tegola, A. (2000). "Strengthening of Reinforced Concrete Structures with Near Surface Mounted FRP Rods." *International Meeting on Composite Materials*, PLAST 2000, Milan, Italy.

De Lorenzis, L., Miller, B., and Nanni, A. (2001) "Bond of FRP Laminates to Concrete." Materials Journal, ACI, Vol. 98, No. 3, pp. 256-264.

De Lorenzis, L., and Nanni, A. (2002) "Bond Between Near Surface Mounted FRP Rods and Concrete in Structural Strengthening." *Structural Journal*, ACI, Vol. 99, No. 2, pp. 123-133.

De Lorenzis, L., Teng, J.G., and Zhang, L. (2006). "Interfacial Stresses in Curved Members Bonded with a Thin Plate." *International Journal of Solids and Structures*, Vol. 43, Issues 25-26, pp 7501-7517.

De Lorenzis, L., Teng, J. G., (2007). "Near-Surface Mounted FRP Reinforcement: An Emerging Technique for Strengthening Structures." *Composites Part B: Engineering*, Vol. 38, No. 2, pp. 119-143.

Ekenel, M., and Myers, J. (2004). "Nondestructive Testing of Dallas County Bridge." *16th World Conference on Nondestructive Testing*, Montreal, Canada, CD-ROM.

El-Mihilmy, M. T., and Tedesco, J. W., (2000). "Analysis of Reinforced Concrete Beams Strengthened with FRP Laminates." *Journal of Structural Engineering*, ASCE, Vol. 126, No. 6, pp. 684-691.

El-Mihilmy, M.T., and Tudesco, J.W., (2001). "Prediction of Anchorage Failure for Reinforced Concrete Beams Strengthened with Fiber-Reinforced Polymer Plates." *Structural Journal*, ACI, Vol. 98, No. 3, pp. 301-314.

Eshwar, N., Nanni, A., and Ibell, T.J. (2004). "Effectiveness of CFRP Strengthening on Curved Soffit RC Beams." *Advances in Structural Engineering*, Vol. 8, No.1, pp. 55-68.

FIB Bulletin 14. (2001). "Externally Bonded FRP Reinforcement for RC Structures." *Technical Report on the Design and Use of Externally Bonded Fiber Reinforced Polymer Reinforcement for Reinforced Concrete Structures,* International Federation for Structural Concrete, Lausanne, Switzerland.

Focacci, F., Nanni, A., and Bakis, C.E. (2000). "Local Bond-Slip Relationship for FRP Reinforcement in Concrete." *Journal of Composites for Construction*, ASCE, Vol. 4, No. 1, pp. 24-31.

Garden, H. N., and Hollaway, L. C., (1998). "An Experimental Study of the Influence of Plate End Anchorage of Crabon Fibre Composites Plates Used to Strengthen Reinforced Concrete Beams." *Composite Structures*, Vol. 42, No. 2, pp. 175-188.

GangaRao, H. V. S., and Vijay, P. V., (1998). "Bending Behavior of Concrete Beams Wrapped with Carbon Fabric." *Journal of Structural Engineering*, ASCE, Vol. 124, No. 1, pp. 3-10.

Hassan, T., and Rizkalla, S. (2003) "Investigation of Bond in Concrete Structures Strengthened with Near Surface Mounted Carbon Fiber Reinforced Polymer Strips." *Journal of Composites for Construction*, ASCE, Vol. 7, No. 3, pp. 248–257.

Hassan T., and Rizkalla, S. (2004). "Bond Mechanisms of NSM FRP Bars for Flexural Strengthening of Concrete Structures." *Structural Journal*, ACI, Vol. 101, No. 6, pp. 830-839.

Hognestad, E. (1951). "A Study of Combined Bending and Axial Load in Reinforced Concrete Members." *Bulletin Series No. 399*, University of Illinois, Engineering Experimental Station, Champaign, IL.

ICRI/ACI. (1999). *Concrete Repair Manual*. Joint publication by International Concrete Repair Institute and American Concrete Institute, Detroit, MI.

Jeffries, J.M. (2004). "Bond Behavior of Fiber Reinforced Polymer Laminates to Concrete Subjected to Varied Surface Preparation." *M.S. Thesis*, University of Missouri, Rolla, MO.

Kaiser, H. (2002). "Assessment of Defect Criticality and Non-destructive Monitoring of CFRP-Rehabilitated Civil Structures." *M.S. Thesis*, University of California – San Diego, La Jolla, CA.

Kaiser, H., and Karbhari V.M. (2003). "Identification of Potential Defects in the Rehabilitation of Concrete Structures with FRP Composites." Interscience Publishers, *International Journal of Materials and Product Technology*, Vol.19, No.6, pp. 498-520.

Khalifa, A., Gold, W. J., Nanni, A. and Aziz, A. (1998). "Contribution of Externally Bonded FRP to Shear Capacity of RC flexural Members." *Journal of Composites for Construction*, ASCE, Vol. 2, No. 4, pp. 195-203.

Kotynia, R. (2007). "Analysis of the Flexural Response of NSM FRP-Strengthened Concrete Beams." *8th Interational Symposium on Fiber-Reinforced Polymer Reinforcement for Concrete Structures, (FRPRCS-8)*, ACI, Patras, Greece, CD-ROM.

Larralde J., and Silva-Rodriguez R. (1993). "Bond and Slip of FRP Rebars in Concrete." *Journal of Materials in Civil Engineering*, ASCE, Vol. 5, No. 1, pp. 30-40.

Lu, X.Z., Teng, J.G., Ye, L.P., AND Jiang, J.J. (2005). "Bond-Slip Models for FRP Sheets/Plates Bonded to Concrete." *Engineering Structures*, Vol. 27, No. 6, pp. 920-937.

Maerz, N., Nanni. A, Myers, J., and Galecki, G. (2001) "Laser Profilometry for Concrete Substrate Characterization Prior to FRP Laminate Application." *Concrete Repair Bulletin*, May-June Issue, pp. 4-8.

Meier, U. (1987) "Bridge Repair with High Performance Composite Materials," *Material und Technik*, Vol. 4, pp. 125–128 (in German).

Meier, U., and Kaiser, H.P. (1991) "Strengthening of Structures with CFRP Laminates," *Proceedings of Advanced Composite Materials in Civil Engineering Structures*, American Society of Civil Engineers Specialty Conference, pp. 224–232.

Meier, U. (1995). "Strengthening of Structures Using Carbon Fiber/Epoxy Composites", *Construction and Building Materials*, Vol. 9, No.6, pp. 341-351.

Mirmiran A., Shahawy M., Nanni A., and Karbhari V. (2004). "Bonded Repair and Retrofit of Concrete Structures Using FRP Composites - Recommended Construction Specifications and Process Control Manual." *NCHRP Report 514*, National Cooperative Highway Research Program (NCHRP), Transportation Research Board, Washington, DC.

Mirmiran, A., Shahawy, M., Nanni, A., Karbhari, V., Yalim, B., and Kalayci, A.S. (2008). "Recommended Construction Specifications and Process Control Manual for Repair and Retrofit of Concrete Structures Using Bonded FRP Composites." *NCHRP*

Report 609, National Cooperative Highway Research Program (NCHRP), Transportation Research Board, Washington, DC.

Monti, M., Renzelli, M., and Luciani, P. (2003). "FRP Adhesion In Uncracked and Cracked Concrete Zones." *6th Interational Symposium on Fiber-Reinforced Polymer Reinforcement for Concrete Structures, (FRPRCS-8)*, ACI, Singapore, pp. 183-192.

Nakaba, K., Toshiyuki, K., Tomoki, F., and Hiroyuki Y. (2001). "Bond Behavior Between Fiber-Reinforced Polymer Laminates and Concrete." *Structural Journal*, ACI Vol. 98, No. 3, pp. 359-367.

Neale, K. W. (2000) "FRPs for Structural Rehabilitation: A Survey of Recent Progress." *Journal of Progress in Structural Engineering and Materials*, Vol. 2, No.2, pp. 133–138.

Neubauer, U., and Rostasy, F.S. (1999). "Bond failure of concrete fiber reinforced polymer plates at inclined cracks-experiments and fracture mechanics model." *4th Interational Symposium on Fiber-Reinforced Polymer Reinforcement for Concrete Structures, (FRPRCS-8)*, ACI, Farmington Hills, MI, pp. 369–82.

Niu, H., and Wu, Zhishen. (2006). "Effects of FRP-Concrete Interface Bond Properties on the Performance of RC Beams Strengthened in Flexure with Externally Bonded FRP Sheets." *Journal of Materials in Civil Engineering*, Vol. 18, No. 5, pp. 723-731.

Novidis, D.G., and Pantazopoulou, S.J. (2007). "Beam Tests on NSM – FRP Laminates in Concrete." *8th Interational Symposium on Fiber-Reinforced Polymer Reinforcement for Concrete Structures, (FRPRCS-8)*, ACI, Patras, Greece, CD-ROM.

Paretti, R., and Nanni, A., (2004). "Strengthening of RC Members Using Near-Surface Mounted FRP Composites: Design Overview." *Advances in Structural Engineering*, Vol. 7, No. 5, pp.1-15.

Porter, A. (2003). "The Effect of Surface Profile on Flexural Strengthening of RC Sections with FRP." *Structural Engineer Journal*, Vol. 81, No. 6, pp. 17-19.

Puliyadi, S. (2001). "Performance of CFRP Sheet Strengthened Reinforced Concrete Beams in the Presence of Delamination and Lap Splice." *M.S. Thesis*, University of Missouri, Rolla, MO.

Ritchie, P. A., Thomas, D. A., Lu, L. and Connelly, G.M. (1991). "External Reinforcement of Concrete Beams Using Fiber Reinforced Plastics." *Structural Journal*, ACI, Vol. 88, No. 4, pp. 490-500.

Ross, C. A., Jerome, D. M., Tedesco J. W., and Hughes, M. L., (1999) "Strengthening of Reinforced Concrete Beams with Externally Bonded Composite Laminates." *Structural Journal*, ACI, Vol. 96, No. 2, pp. 212-221.

Saadatmanesh, H. and Ehsani, M. R., (1991). "RC Beams Strengthened with GFRP Plates I: Experimental Study." *Journal of Structural Engineering*, ASCE, Vol. 117, No. 11, pp. 3417-3433.

Savioa, M., Farracuti, B., and Mazzotti, D. (2003). "Non-Linear Bond–Slip Law for FRP-Concrete Interface." *Prooceedings of the 6th International Symposium on FRP Reinforcement for Concrete Structures*, World Scientific Publications, Singapore, pp. 163-172.

Saxena, P., Toutanji, H., and Noumowe, A., (2008). "Failure Analysis of FRP-Strengthened RC Beams." *Journal of Composites for Construction*, ASCE, Vol. 12, No. 1, pp. 2-14.

Shahawy, M. A., Beitelman, T., Arockiasamy, M., and Sowrirajan, R., (1996). "Experimental Investigation on Structural Repair and Strengthening of Damaged Prestressed Concrete Slabs Utilizing Externally Bonded Carbon Laminates." *Composites Part B: Engineering*, Vol. 27B, No. 3, pp. 217-224.

Shen, H.S., Teng, J.G., and Yang, J. (2001). "Interfacial Stresses in Beams and Slabs Bonded with Thin Plate." *Journal of Engineering Mechanics*, ASCE, Vol. 127, No. 4, pp. 399-406.

Shen, X., Myers, J.J., Maerz, N., and Galecki, G. (2002). "Effect of Surface Roughness on the Bond Performance Between FRP Laminates and Concrete." *2nd International Conference on Durability of Fiber Reinforced Polymer (FRP) Composites for Construction*, B. Benmokrane, B., and El-Salakawy, E. (Eds.), Montreal, Canada, pp. 607–616.

Smith, S.T. and Teng, J.G. (2002) "FRP-Strengthened RC Beams. I: Review of Debonding Strength Models." Engineering Structures, Vol. 24, No. 4, pp. 385-395.

Telang N. M., Dumlao C., Mehrabi A.B., Ciolko A.T., and Gutierrez J. (2004). "Field Inspection of In-Service FRP Bridge Decks." *NCHRP Report 564*, National Cooperative Highway Research Program (NCHRP), Transportation Research Board, Washington, D.C.

Teng, J.G., Lu, X.Z., Ye, L.P., and Jiang, J.J., (2004). "Recent Research on Intermediate Crack Induced Debonding in FRP Strengthened Beams." *Proceedings of the 4th International Conference on Advanced Composite Materials for Bridges and Structures*, Calgary, Canada.

Toutanji, H., and Ortiz, G. (2001). "The Effect of Surface Preparation on the Bond Interface between FRP Sheets and Concrete Members." *Composite Structures*, Vol. 53, No. 4, pp. 457-462.

TR 55. (2004). "Externally Bonded FRP Reinforcement for RC Structures", *Technical Report No. 55,* Concrete Society, Berkshire, UK, pp. 40-55.

Ueda, T., and Dai, J. (2005). "Interface Bond Between FRP Sheets and Concrete Substrates: Properties, Numerical Modeling and Roles in Member Behavior." *Journal of Progress in Structural Engineering and Materials*, Vol. 7, No. 1, pp. 27-43.

Wolf, R., and Miessler, H. J. (1989). "Erfahrungen Mit Glasfaserverbundstaben." HLV-Spannglieder inder Praxis, Beton, Vol. 2, pp. 47-51.

Yalim, B. (2008). "Development of Thresholds for Surface Preparation in Repair Systems with Wet Lay-Up Fiber Reinforced Polymers." *Ph.D. Dissertation*, Florida International University, Miami, FL.

Yao, J., Teng, J.G., and Chen, J. F. (2005). "Experimental Study on FRP-to-Concrete Bonded Joints." *Composites Part B: Engineering*, Vol. 36, No. 2, pp. 99-113.

Yost, J. R., Gross, S. P., Dinehart, D. W., and Mildenberg, J.J. (2007). "Flexural Behavior of Concrete Beams Strengthened with Near-Surface Mounted CFRP Strips." *Structural Journal*, ACI, Vol. 104, No. 4, pp. 430-437.

VITA

AHMET SERHAT KALAYCI

February 28, 1981	Born, Ankara, Turkey
2002	B.S., Civil Engineering Middle East Technical University Ankara, Turkey
2005	M.S., Civil Engineering Middle East Technical University Ankara, Turkey
2003-2005	Planning and Survey Engineer General Directorate of Highways Ankara, Turkey
2005-2008	Teaching/Research Assistant Florida International University Miami, Florida